Fuzzy Based Smart Charging Station for Electric Vehicle Application to Mitigate Peak Power Demand

Kannan T.

Fuzzy Based Smart Charging Station for Electric Vehicle Application to Mitigate Peak Power Demand

A

Thesis submitted

for the award of the degree of

Doctor of Philosophy

By

Kannan T.

Department of Electronics and Electrical Engineering

Indian Institute of Technology Guwahati

Guwahati - 781 039, Assam, India

January 2014

Dedicated to

My Beloved Parents,
Punithamani T. and Thirugnanam A.;

My Teacher,
Dr. Praveen Kumar;

and

My Sisters,
Dr. Sumathi T., Dr. Gomathi T.,
Malathi T. and Lakshmi Prabha T.

Certificate

This is to certify that the thesis entitled "**Fuzzy Based Smart Charging Station for Electric Vehicle Application to Mitigate Peak Power Demand**", submitted by **Kannan T.** (09610215), a research scholar in the *Department of Electronics and Electrical Engineering, Indian Institute of Technology Guwahati*, for the award of the degree of **Doctor of Philosophy**, is a record of an original research work carried out by him under my supervision and guidance. The thesis has fulfilled all requirements as per the regulations of the institute and in my opinion has reached the standard needed for submission. The results embodied in this thesis have not been submitted to any other University or Institute for the award of any degree or diploma.

Date:

Place: Guwahati.

Dr. Praveen Kumar,

Assistant Professor,

Dept. of Electronics and Electrical Engg.,

Indian Institute of Technology Guwahati,

Guwahati - 781 039, Assam, India.

Acknowledgements

First and foremost, I feel it as a great privilege in expressing my deepest and most sincere gratitude to my supervisor Dr. Praveen Kumar, for his excellent guidance throughout my study. His kindness, dedication, hard work and attention to detail have been a great inspiration to me. My heartfelt thanks to you sir for the unlimited support and patience shown to me. I have no doubts that finishing my degree in a proper and timely manner was impossible without his helps, suggestions and advices.

I am also very thankful to my doctoral committee members Professor Sanjay Kumar Bose, Professor Somanath Majhi, Dr. Indrani Kar and Dr. Sisir Kumar Nayak for sparing their precious time to evaluate the progress of my work. I would also like to thank the Head of the Department and the other faculty members for their kind help in carrying out this work. I am also grateful to all the members of the research and technical staff of the department without whose help I could not have completed this thesis.

I express my heartfelt thanks to Professor Govinda Bol Shrestha, Dr. Praveen Tripathy and Dr. Deepak kumar M Fulwani for providing valuable suggestions on this work.

I express my heartfelt thanks to Ezhil Reena Joy .T . P for providing valuable suggestions on this thesis and her kind support. My work and stay in this IITG would have been impossible without her. Thank you very much my dear friend for your kind support and guidance.

I would also like to thank the Head of the Department and the other faculty members for their kind help in carrying out this work. I am also grateful to all the members of the research and technical staff of the department without whose help I could not have completed this thesis.

My special thanks to Mr. Sanjib Das for maintaining an excellent computing facility and various resources useful for the research work. Thanks also go out to all my friends at the Image and Signal Processing Laboratory. They have always been around to provide useful suggestions, companionship and created a peaceful research environment. They all contributed directly or indirectly to this thesis, be it academic help, proofreading and volunteering to be a test subject.

I am extremely thankful to Mr. Mohammed Nasir Ansari, Dr. Mukesh Singh and Mr. Ramesh Chandra Mishra for their kind support. My work and stay in this IITG would have been impossible

without them. Thank you very much for your kind support and guidance.

I have no words to express my thanks to my seniors, Dr. Shyam Anand, Dr. Senthil Kumar, Dr. Padam Priyal, Dr. AnanthaRaj, Dr. Anand Kumar, Dr. Sakthivel, N. Vinoth Kumar and P. Saravanan. My work in this remote place definitely would not be possible without their love and care that helped me to enjoy my new life in IITG.

I express my heartfelt thanks to my batch mates (2009-2013) for providing valuable suggestions and kind support.

I have no words to express my thanks to seven most important persons namely, Someswaran, Satheesh Kumar, Kanmani, Basker Naik, Mirdul, Ankit and Premavathi. My work in this place definitely would not be possible without their love and care that helped me to enjoy my new life in IITG.

I thank all my fellow research students and B Tech students especially Himanshu Saini, and Rajibh Das for their cooperation. During these five years at IITG I have had several friends that have helped me in several ways, I would like to say a big thank you to all of them for their friendship and support.

I thank all my fellow research students for their cooperation. During these five years at IITG I have had several friends that have helped me in several ways, I would like to say a big thank you to all of them for their friendship and support.

I also thanks my master degree class mates namely, Ms. Gomathy, Mr. Loganthan, Mr. Livingston, Mr. Abbas Kayasudeen, Mr. Senthil, Mr. Pugazhendhi and Mr. Jawahar Babu for their kind suggestions and support.

My deepest gratitude goes to my parents for their continuous love and support throughout my studies. The opportunities that they have given me and their unlimited sacrifices are the reasons where I am and what I have accomplished so far.

My relatives also played a great role in my PhD works and they are Dr. Sumathi, Dr. Gomathi, Ms. Malathi, my lovable sister Ms. Lakshimi Prabha, my lovable baby Vishalini, Anbu Selvan, Ranjith, Thendral and AmmuKutty. I am very grateful to them.

Finally, I believe this research experience will greatly benefit my career in the future.

Kannan Thirugnanam

Abstract

This thesis proposes a fuzzy based smart charging station (SCS) for electric vehicle's (EVs) application to mitigate the peak power demand of typical city. The SCS, as proposed in this thesis is a place where the EVs come together to charge (drawn power from grid) or discharge (support the grid) their batteries based on the distribution node (DN) voltage and the available energy in the EVs' batteries. The SCS has various charging points, which enables EVs of different battery ratings to charge and discharge. However, allowing the EVs to discharge or charge without any control may lead to voltage deviation in the DN. If multiple EVs can be discharged or charged in a controlled fashion, then they can act as distributed energy storage system (DESS). A proper implementation of controlled charging and discharging can mitigate the peak power demand of the DN by providing power to grid (peak shaving) or drawn power from the grid (valley filling).

In this thesis, the active power control strategies have been modeled for V2G system to enable peak shaving and valley filling. If EVs' batteries are intended to perform charging or discharging operations, it would get subjected to varying node voltage conditions. Such frequent charging/discharging operating conditions affect the internal circuit parameters due to change in state of charge, charge rate of the battery. Moreover, the capacity of EVs' batteries would decrease due to frequent charging/discharging process at different charge rate. Therefore, a precise model of EV battery is very much required, to predict the performance of EVs in real-time V2G interaction. Hence, an electric equivalent circuit based battery model and capacity fade/loss model suitable for EVs in V2G applications has been developed. By using the BM, the mathematical modeling and control of contactless based SCS in V2G scenario has been designed. Fuzzy logic controllers and aggregator have been used to control the power flow between the SCS and the grid.

The aggregator has been designed to distribute the reference power signal among the EVs' batteries present in the SCS during charging or discharging process. Finally, mathematical model for economic analysis of energy transfer between EVs' batteries and grid has been developed. Also, beneficiary calculation for EVs owners, grid operators and consumers has been proposed.

The major contributions of this thesis are as follows:

- Electric equivalent circuit based battery and capacity loss model has been developed for EVs' batteries to analyze the interaction between EVs' batteries and the grid.
- A smart charging station has been developed based on the fuzzy logic control, which the bidirectional power flow between EVs' batteries and grid during the peak hours, normal hours and off-peak hours.
- A mathematical model for the economic analysis of energy transfer between EVs and grid has been developed. In this work, the economic analysis has been done in such a way that the battery related liabilities do not become a financial burden to EVs owners.

Index Terms: Battery, contactless power transfer, distributed energy storage, electric vehicles, economic evaluation, fuzzy logic control, genetic algorithm, synchronization and vehicle-to-grid.

Contents

List of Figures

List of Tables

List of Acronyms

A	Ampere
Ah	Ampere hour
AC	Alternating current
BB	Buck-boost
BCCS	Bidirectional contactless charging system
BM	Battery model
B	Big
CB	Circuit breaker
CC	Contactless coil
CC-FLC	Current control - fuzzy logic controller
CCU	Central control unit
CCU-FLC	Central control unit - fuzzy logic controller
CFM	Capacity fade model
CL	Capacity loss/fade
CPT	Contactless power transfer
CS	Charging Station
DC	Direct current
DESS	Distributed energy storage system
DN	Distribution node/network
DOD	Depth-of-discharge
DOD_{cr}	Current DOD
DLV-FLC	Direct current link voltage - fuzzy logic controller
EEC	Electric equivalent circuit

EIG	Energy injection control
EOCV	End of charge voltage
EODV	End of discharge voltage
EVs	Electric vehicles
FLC	Fuzzy logic controller
GA	Genetic algorithm
G2V	Grid-to-vehicle
H	High
ICE	Internal combustion engine
IPT	Inductive power transfer
J	Joules
KVA	Kilovolt-ampere
kV	Kilovolt
kW	Kilo-watt
kWh	Kilo-watt hour
L	Low
LA-FLC	Load angle - fuzzy logic controller
LCL	Filter circuit
Li-ion	Lithium-ion
LPF	Low pass filter
M	Medium
MVA	Mega volt-ampere
MW	Mega watt
NB	Negative big
NH	Negative high
NL	Negative low
NM	Negative medium
NS	Negative small

PC	Polynomial coefficients
PEVs	Plug-in electric vehicle
PH	Positive high
PHEVs	Plug-in hybrid electric vehicle
PLL	Phase locked loop
PL	Positive low
PM	Positive medium
PS	Positive small
PB	Positive big
SPWM	Sine pulse width modulation
RES	Renewable energy source
S	Small
SCS	Smart charging station
SOC	State-of-charge
SOC_{cr}	Current SOC
SS	Secondary side
VB	Very big
V	Voltage
VL	Very low
VH	Very high
VS	Very small
V2G	Vehicle-to-grid
W	Watts
Wh	Watt hour
Z	Zero

List of Symbols

A	Total money to be paid for energy consumption
$abc - dq0$	Three phase to two phase transformation
$a_{m_{k,n}}$	n^{th} coefficient of the k^{th} solution set
AP_{cp}	Net cost price of the energy for EV owners
AP_{cg}	Total amount paid by the consumers to the grid operators during a complete day
AP_{evg}	Total amount paid by EV owner to grid operators during a complete day
AP_{gev}	Total amount paid by the grid operators to EV owner during a complete day
AP_{loss}	Total financial loss to the EV owners during V2G interaction
$a_1 - a_{31}$	Polynomial coefficients
c	Total quantity of energy supplied by the grid to the EV during the peak hours
c'	Total quantity of energy supplied by the grid to the battery during the off-peak hours
C	Battery capacitance
$C_{b1}C_{b2}$	Filter capacitance of the single ac to dc converter and buck-boost converter
C_{dc}	Filter capacitance
C_m	Compensation money for energy loss
M_e	Money equivalent of the capacity lost
C_r	Charge rate
C_r^{crt}	Current charge rate
C_r^{BCCS}	Charge/discharge rate of the individual BCCS unit
C_r^{lmt}	Charge rate limit
C_r^{min}	Minimum charge/discharge rate
C_r^{user}	User defined charge/discharge rate of the EVs
C_1, C_2	Compensation capacitance

D	Duration
D_n	Number of days the battery takes to depreciate its value to zero
D_r	Discharge rate
D_r^{crt}	Current discharge rate
D_r^{lmt}	Discharge rate limit
DOD_{cr}	Current depth-of-discharge
DOD_{max}	Maximum depth-of-discharge
$D_1 - D_{14}$	Diodes
δ	Power or load angle
δt_c	Difference in charging time
δt_d	Difference in discharging time
E_a	activation Energy
E_{avail}	Amount of available energy for discharging scenario
E_{bn}	n^{th} EV battery available or required energy to charge or discharge
E_{co}	Expected count
E_{ib}^G	input energy provided to the battery by the grid
$E_{off-peak}$	Total energy consumed during off-peak hour
E_l	Energy lost due to other reasons
E_{peak}	Total energy consumed during the peak hour
E_{pos}	Possible quantity of energy available in the battery that can be sold to the grid
E_q	Energy lost due to the capacity loss
E_{rem}	Energy remained in the battery after vehicle transportation
E_r, E_r'	Error rate
E_{sup}	Actual quantity of energy supplied by the EV battery to the grid
E_{stor}	Amount of stored energy for charging scenario
$E_{transpor}$	Energy used by EV for the transportation purpose
E_{trans}	Actual quantity of energy obtained by the grid from the EV
E_T/E_{total}	Total energy of the EVs batteries or CS/Total processed energy of the battery

$f(x)$	Difference between measured and calculated values of the C_r and D_r characteristics
$f'(x)$	Difference between measured and calculated values of the CL characteristics
$F(x)$	Fitness function of the charge and discharge rate characteristics
$F'(x)$	Fitness function of the capacity loss characteristics
$Freq$	Frequency
F_{avg}	Average fitness function value
f_s	System operating frequency
gen	Generation
gen_{max}	Maximum generation
I_{abc}	Three phase current
I_c	Charging current
I_d	Discharging current
I_{pc}	Primary current of the contactless coil
I_{ref}	Reference current
I_{sc}	Secondary current of the contactless coil
I^*	Reference signal for battery switch
I^*_{pre}	Previous reference current
k	Percentage of energy loss due to capacity loss
k'	Percentage of energy loss due to other reasons
L_b	Buck-Boost converter inductance
L_p	Self inductance of the primary side coil
L_r	Resonant inductance
L_s	Self inductance of the secondary side coil
M	Initial cost of purchasing the EV battery
M_{dep}	Depreciated monetary value of the battery after a particular number of cycles
n	Number of cycles that the battery has interacted with the grid
n'	Maximum number of cycles that the battery can charge/discharge in its life span
n''	Daily average number of cycles of battery-grid interaction

$n \times m$	Population matrix size
O_1, O_2	Off-string one and two
PE_c	Processed energy for charging scenario
PE_d	Processed energy for discharging scenario
P_c	Battery power for charging scenario
P_d	Battery power for discharging scenario
P_{co}	Crossover probability
P_{bn}	Distributed power to n^{th} EV battery
P_{es}	Probability of each selected string
P_{grid}	Total power transfer between EVs and grid during V2G or G2V operation
P_m	Mutation probability
P_{mea}	Measured power of the BCCS unit
P_1, P_2	Parents one and two
q	Total capacity loss of the battery
Q	Nominal battery capacity
Q_l	Capacity loss/fading
Q_r	Remaining battery capacity
$Q_{l_k}^C$	k^{th} calculated value of the capacity loss characteristics
$Q_{l_k}^M$	k^{th} measured value of the capacity loss characteristics
R	Gas constant
R_{peak}	Tariff of energy during the peak hour
$R'_{off-peak}$	Tariff of energy during the off-peak hour
$Rs.$	Monetary value is defined as per the Indian Currency
R_T	Total resistance
R_1R_2	Battery internal resistance
R', R''	Reference output of the fuzzy logic controller
s	Total quantity of energy obtained by the grid during the peak hours
s'	Total quantity of energy obtained by the grid during the off-peak hours

sin_cos	Unit vectors
SOC_{cr}	Current state-of-charge
SOC_{ini}	Initial state-of-charge
SOC_{max}	Maximum state-of-charge
S_n	Population size
SOC_{lt}	User define SOC/DOD limits
$S_1 - S_{14}$	Switches
t_c	Charging time
t_d	Discharging time
T	Temperature
T_s	Simulation Time
V_{abc}	Three phase voltage
$V_{c_i}^C$	i^{th} calculated value of the battery terminal voltage for charging scenario
$V_{c_i}^M$	i^{th} measured value of the battery terminal voltage for charging scenario
$V_{d_j}^C$	j^{th} calculated value of the battery terminal voltage for discharging scenario
$V_{d_j}^M$	j^{th} measured value of the battery terminal voltage for discharging scenario
V_{dc}^{mea}	dc measured voltage at primary side of three phase ac to dc converter
V_{dc}^{ref}	dc reference voltage of the DC link voltage controller
V_{dq0}	Direct and quadrature axis voltage
V_{node}	Node voltage
V_{max}	Maximum voltage
V_{min}	Minimum voltage
V_{pc}	Primary side contactless coil voltage
V_{prim}	Primary side voltage of the BCCS unit
V_{sc}	Secondary side contactless coil voltage
V_0	Open-circuit voltage
ωt	Angular frequency

x	Tariff paid by EV owner to grid per kWh during peak hour
x'	Tariff paid by EV owner to grid per kWh during off-peak hour
X_T	Total reactance of the system
x_1^L	Lower bit element of the sub-string
x_1^U	Upper bit element of the sub-string
x_1	Tariff paid by consumers to grid operators per kWh peak hour energy
x_1'	Tariff paid by consumers to grid operators per kWh off-peak hour energy
x_2	Tariff paid by grid operators to EV owner per kWh peak hour energy
x_2'	Tariff paid by grid operators to EV owner per kWh off-peak hour energy
z	Money charged by the EV owners to compensate for capacity loss.

Glossary

- ***ac to dc converter:*** Converts alternating current into direct current.
- ***Ancillary services:*** The ancillary services are necessary to support the distribution system and control the flow of active power in order to maintain power quality, reliability and stability of the distribution system.
- ***Charge/discharge rate (C_r/D_r):*** A common method for indicating the discharge, as well as the charge current of a battery.
- ***Current depth-of-discharge (DOD_{cr}):*** Depth-of-discharge is another method to indicate a batteries state-of-charge. The depth-of-discharge is the inverse of state of charge: as one increases, the other decreases. In other words, the Depth-of-discharge is usually defined as the amount of energy removed from a battery.
- ***Current state-of-charge (SOC_{cr})***: The state-of-charge is related to the electric charge stored by the battery at a given time. It is defined as the ratio between the available charge at a given time and the maximum capacity.
- ***Cycle life:*** The number of charge/discharge cycles the battery can experience before it fails to meet performance criteria. Cycle life is estimated for charge and discharge conditions. The actual operating life of the battery is affected by the rate, depth of cycles and by other conditions such as temperature.
- ***dc to ac converter:*** It receives dc voltage at input side and converts ac voltage at output side. The output voltage can controlled by varying the on and off time of the converter switch.

- ***dc to dc converter:*** Converts dc voltage to regulated dc voltage. Regulation can be achieved by controlling the duty ratio.

- ***Frequency regulation:*** The frequency regulation is required for reliable operation of the electric grid. To maintain grid frequency within permissible limits, electric vehicles (EVs) batteries are used to inject/support the power from/to grid. If load exceeds the generation, the frequency of the system decrease which indicates the grid required "regulation up" and vice versa. The EVs batteries can support/inject the power to/from grid for regulation up/down for matching the generation and load demand.

- ***Fuzzy logic:*** It is derived from fuzzy set theory which can deal with uncertainties in systems. Fuzzy logic incorporates a simple, IF-THEN rule based approach to solve a control problem rather than attempting to mathematically model a system.

- ***Grid-to-vehicle (G2V):*** The EVs' batteries are charged from the grid during the off-peak hours. During this operation the power flow from grid to EVs' batteries based on node voltage and available energy of the EVs' batteries.

- ***Internal resistance (R_1R_2)***: The internal resistance of battery is varying with respect to change in SOC_{cr}/DOD_{cr} and C_r/D_r.

- ***Open-circuit voltage (V_0):*** The open-circuit voltage is the voltage under a no-load condition, which is usually a close approximation to the battery terminal voltage.

- ***Smart grid:*** A smart grid is an electric network which is supply the electricity to consumers based on the digital technology. These digital systems control the electricity and improve the efficiency, reduce the energy consumption and cost.

- ***Terminal voltage ($V_{c_i}^C$ or $V_{d_i}^C$)***: It is defined as the voltage measured between the battery terminals under load condition. The terminal voltage varies with state of charge and the charge or discharge current.

- ***Vehicle-to-grid (V2G):*** EVs' batteries are used as a distributed energy storage system which can support the grid during peak hours or parking hours.

- ***Voltage regulation:*** To maintain system voltage within permissible limits at various points of the distribution system, reactive power compensation plays vital role. By inject/support the reactive power from/to the grid which impacts the distribution node voltage maintain within limits and also maintain system stability.

1

Introduction

Contents

1.1 Introduction

Electricity is a form of energy. It plays a very important role in everyday human life. The demand for this electrical energy is gradually increasing with the rising population. Electrical energy has led to development of society, its economic growth and high standard of living. The generation and consumption of electrical energy has been one of the most pressing challenges for the modern societies, due to ever increasing gap between the generation and consumption. Engineering efforts and solutions can address these challenges to bridge the gap.

In India, the installed power generation capacity is 229.133 Giga-watt (GW) [3,4]. About 57.18% of the electricity is generated from coal based power plants, 17.62% from hydroelectric power plants, 12.45% from renewable-energy sources, 9.03% from gas based power plants, 3.15% from nuclear power plants and 0.57%from oil based power plants [3]. The base load requirement is 861,291Megaunit (MU) against availability of 788,355MU which is a shortage of 8.5%. Due to population growth and economic development, the demand for energy has increased at a rate of 3.6% per annum over the past 30 years and the approximate energy consumption per capita is 96kWh in rural area and 288kWh in urban area [3–6]. During peak hours, the demand is 139.29GW against availability of 110.76GW which is a shortage of 20.48% [4]. The peak load energy shortage prevails in all regions of the country and varies from 5.98% in the North-Eastern region to 14.51% in the Southern region [3]. Due to shortage of electricity, power cuts are common throughout India and this has adversely affected the country's economic growth. Therefore, bridging the gap between the energy generation and its consumption becomes essential for the nation's development. The present energy generation in India from the various energy sources is shown in Fig. 1.1.

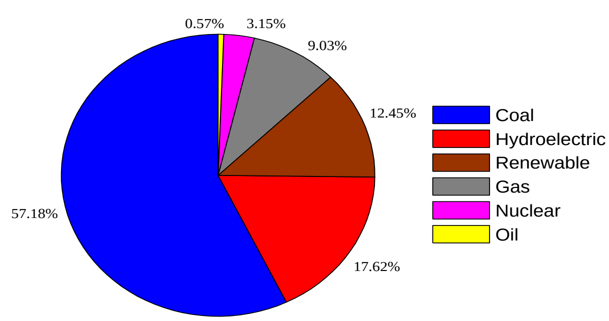

Figure 1.1: India's present power generation from various power plants.

The estimated total peak load demand for electricity in India is expected to cross 298GW by 2022 [3–5]. The peak load shortage would prevail in all the regions of the country and for North-Eastern region it would be 17.58GW. Assam which is a part of North-Eastern region will have peak power demand of 1.93GW [7]. The peak load demand for 132/33kV Sishugram substation in the city of Guwahati, Assam will be 0.62MW [8, 9]. From the power plant usage data it is seen that most of the power plants are underutilized during the off-peak hours. If some energy storage device can be used to store the energy during the off-peak hours, then an energy gap of 500kW during peak power demand can be met. Therefore, an energy storage system (ESS) is required to solve the issue of energy gap during peak hours. In order to handle the peak power demand, one possible solution can be to ramp-up the power generation capacity, but this option would require significant infrastructure cost of the power plants.

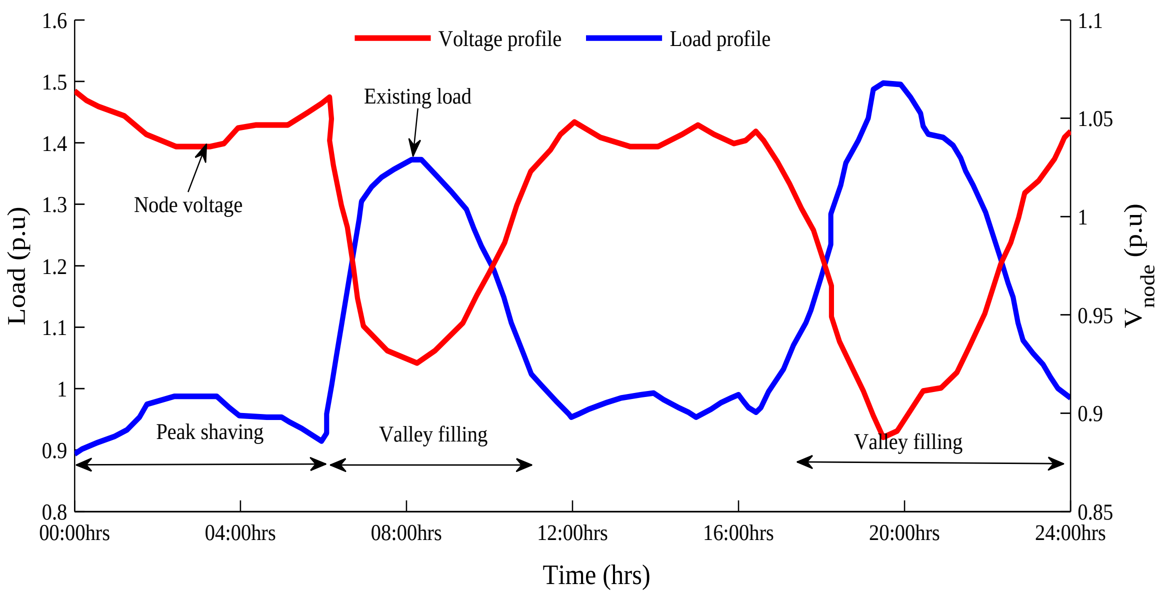

Figure 1.2: Grid load (p.u) and voltage profile of the Guwahati city, Sishugram 132/33kV Grid Substation.

The approximate overview of the grid load and voltage profile of Guwahati city, Assam is shown in Fig. 1.2 [10]. The energy demand is high during the peak hours from 07:00hrs to 10:00hrs and 18:00hrs to 22:00hrs. During these hours, power plants must ramp-up generation in order to meet up the demand. It is expensive to produce power in the peak hours because the increased generation usually comes from high cost fuel such natural gas. From Fig. 1.2, it can be seen that there is big difference between the peak power demand and off peak power demand. The gap between the peak and off-peak power demand can be reduced if ESS is used. During the off-peak hours the ESS can be charged and during peak hours the stored energy can be injected back to the grid.

There are different types of ESS available which is given in Fig. 1.3.

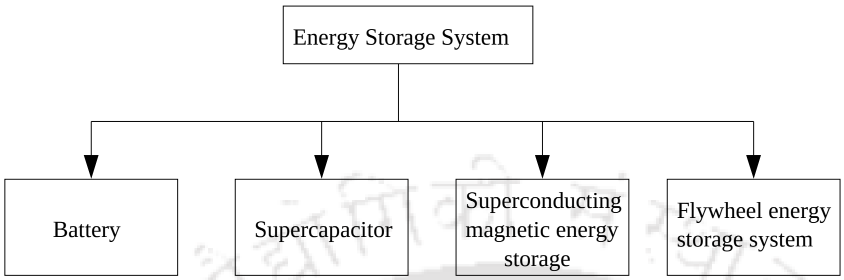

Figure 1.3: Types of energy storage system.

(i) Battery is electrochemical energy storage device which convert chemical energy to an electrical energy and vice versa [11]. The battery is generally expensive, has limited charge/discharge rate, has high energy density and low power density and has limited life cycle.

(ii) Supercapacitor (SC) is electrochemical energy storage device which stores the electrical energy in the form of on electric field in the electrochemical double layer [12]. The specific energy stored in an SC is relatively low due to limitations in the accessible specific surface area of the electrode the specific power is large due to the short time constant of double layer charging but the energy density, energy stored per unit of weight is less [13].

(iii) The Superconducting magnetic energy storage (SMES) device stores the energy in the form of magnetic field created by the flow of direct current (dc) in a superconducting coil [14]. The stored energy can be drawn from the SMES unit almost instantaneously and also can be delivered over a period ranging from fraction of seconds to several hours [15]. The SMES has high power, high efficiency and four-quadrant control [16, 17].

(iv) Flywheel energy storage system stores the electrical energy in a rotating mass [18, 19]. Depending upon the inertia and speed of rotating mass, the amount of kinetic energy is stored as a rotational energy [19]. The kinetic energy is transferred in and out of the flywheel with an electrical machine that can function either as a motor or generator depending on the load angle.

The flywheels have high power density, high energy density, ability to handle high power levels and need low recharge time [20].

The difference between daily peak and off-peak power demand is varying every year. In case the difference is small for a day, then the normal battery facilities become suitable. Since these normal battery energy storage facilities have not proven economical except in functional applications such as distributed energy storage system (DESS) upgrade a reasonable storage system is required to mitigate daily peak and off-peak power demand with less infrastructure cost.

The electric vehicles (EVs) can be used to mitigate the peak power demand because most of the time these vehicles are kept parked [21–24]. The batteries of EVs can be used as a DESS to support the electric grid when the power demand is high and store the excess amount of energy during the off-peak hours [22, 23, 25–37]. The EVs are idle most of the time and the batteries are expected to retain a significant amount of energy when the EVs are not in use [21–23, 34].

There are different types of batteries used in EVs such as lead acid, lithium-ion (Li-ion), alkaline battery etc. In the recent decades much attention has been given to the Li-ion batteries due to numerous advantages [38, 39]. The Li-ion batteries have high power (800-2000 W/kg), high specific energy (100-250Wh/kg), high working cell voltage, long life cycle, high power rate density (three time of the lead acid battery and one and half time of the alkaline battery), low self discharge rate and no memory effect [40]. Therefore, Li-ion batteries are most suitable for EVs and the higher energy density of these batteries makes them suitable as DESS. In the next section, mitigation of peak and off-peak hour power demand by using EVs is presented.

1.2 Electric Vehicles in Smart Grid

The EVs are driven only by the energy stored in rechargeable battery and use electric motors and controllers for propulsion. Charging/discharging characteristics of the EV depend on its range and its owner's driving patterns. EVs are plugged into a charging station (CS) or plug-in point to charge or discharge the battery. The energy required by a typical EV for driving 40 to 60 km using its battery energy is around 10 to 15 kWh [22], potentially making EVs one of the biggest energy consumers in future [41]. The time required to charge the battery of 10 to 15 kWh is about 2 to 3 hours [42].

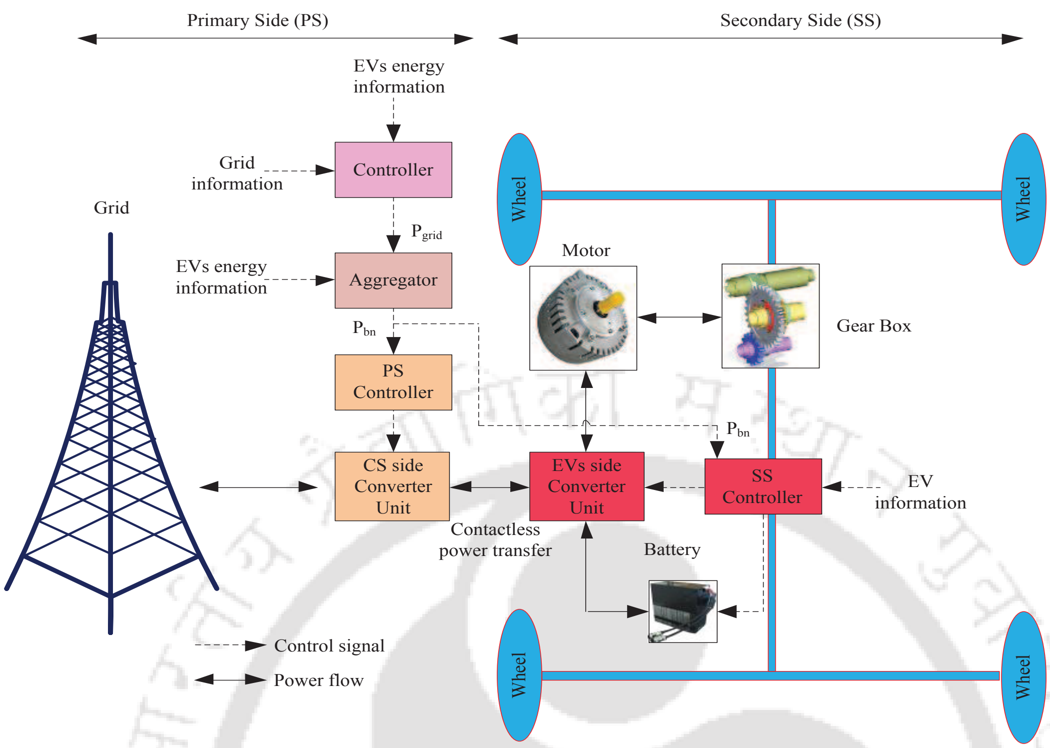

Figure 1.4: Vehicle-to-grid operation.

On an average a typical EVs travels only 3 to 6 hours a day and rest of the time these EVs are available in the parking bays [22]. The parked EVs can act as a load or source by storing the energy or feeding the energy back to grid. Therefore, the EVs' batteries can be used as a DESS for injecting its excess stored energy to the grid during peak hours and storing energy during the off-peak hours.

The Fig. 1.4 shows the block diagram representation of vehicle-to-grid operation. In contactless power transfer system, the primary side (PS) is on the CS and the secondary side (SS) is on the vehicle. To transfer the power in either direction, contactless coil has been used to eliminate direct contact. The controller and aggregator are used to control the power flow during peak and off-peak demand hours. The EV battery charge or discharge based on the grid voltage and the available energy in the EV. Similarly, multiple EVs are connected to the grid to solve the peak and off-peak hours power demand. If the grid voltage is high ($\geq$ 1 per-unit), then the controllers do not allow to discharge the EVs' batteries for grid support.

1.2.1 Vehicle to Grid

The EVs battery can be charged from the grid and support the grid during peak hours or parking hours. V2G interaction enables EVs to earn financial incentives while discharging the power to grid.

Thus, V2G interaction can facilitate the supply/demand balance by discharging during peak hours and charging during off-peak hours [24, 26, 28, 32, 43, 44]. One solution to mitigate the impact of EVs on the grid is to schedule their charging/discharging profiles based on node voltage conditions. This can be done by aggregating different sets of EVs for charging or discharging such that grid constraints (voltage and frequency limits) are maintained within the limit. The various types of services that can be provided by the EVs to grid interaction are shown in Fig. 1.5. These are mainly divided into two parts: unidirectional and bidirectional. The G2V implies that energy flows from the grid to the vehicle. It can be achieved with the help of scheduled charging (based on the node voltage) and voltage control (to keep node voltage and frequency stable).

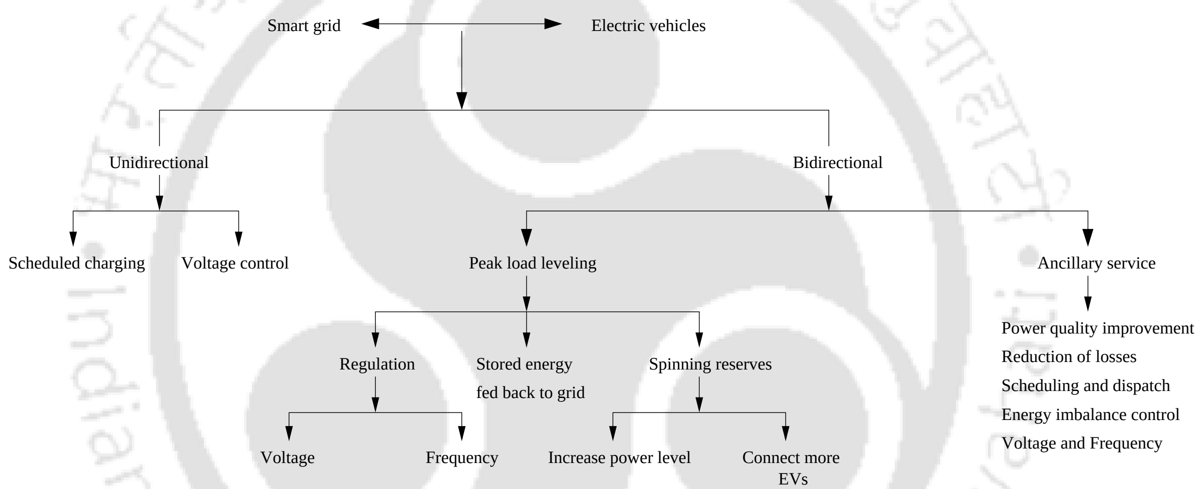

Figure 1.5: Electric vehicle-to-grid interaction with different type of power mitigation.

The bidirectional power flow can be divided into two parts: peak load leveling and the ancillary service. Peak load leveling is a method to balance the load and demand. It can be achieved with the help of regulation, stored energy fed back to the grid and spinning reserve. The regulation can be divided into two separate entities such as voltage and frequency regulation [45, 46]. The voltage regulation maintains the system voltage within permissible limits. This is required for proper operation of electrical equipment and to prevent it from failure [47]. With reduced system voltage, the current must increase to meet up the power demand. It further leads to the load consuming more reactive power and the system voltage getting reduced. If the current increases too much, the transmission lines goes off [48, 49]. Therefore, reactive power control improves the voltage imbalance. Hence, reactive power and voltage control are two aspects that can affect reliability of the grid [46, 47, 49].

The frequency regulation is a method to balance the generation and consumption which causes the system frequency to remain constant at the desired value [50]. For load demand greater than generation, the frequency decreases and in the reverse condition frequency increases. Therefore, frequency regulation is a real-time control which increases or decreases the output power level. Frequency regulation can also regulate the sudden fluctuations in the load demand. Another possible solution to maintain grid frequency within permissible limits is by using the EVs batteries to inject/draw the power to/from grid. In case the load exceeds the generation, the frequency of the system decrease, which indicates the grid requires " regulation up" and vice versa. The EVs batteries can inject/draw power to/from the grid for regulation up/down to match the generation and load demand. Apart from this, to mitigate the peak power demand, the stored energy in the EVs' batteries is used as a DESS which can support the grid during EVs parking hours. The spinning reserve is achieved by connecting additional generators or increase the power level to compensate the sudden increase or unpredicted load demand [51, 52]. These generators are already synchronized with the grid but these are not operating at rated power [51–53]. If suddenly the load increases or decreases, the reserve generators starts operating at rated power or reduced power level by increasing or decreasing the turbine rotation [54]. Spinning reserve maintains system frequency stability during emergency operating conditions and unpredicted load swings [54–56]. The EVs batteries are utilized for the ancillary services such as power quality improvement, reduction of power losses, scheduling and dispatch, energy imbalance control and voltage and frequency control. The ancillary services are necessary to support the distribution system and control the flow of active power in order to maintain power quality, reliability and stability of the distribution system [57]. Therefore, the EVs are used as a distributed energy sources which injects or draws the power to/from grid for solving the peak power demand. This method reduces the transmission and distribution losses, provide power for ancillary services and maintains voltage and frequency within the regulation.

1.2.2 Major Issues in V2G Interactions

From the above discussion, major issues in V2G interaction are given below:

(i) Uncoordinated charging methodology which can significantly stress the distribution system causing severe voltage fluctuations, performance degradations and over load to the grid.

(ii) Uncontrolled and random EV support to the grid can cause increased power losses and voltage fluctuations.

(iii) The load and economic considerations eventually impose the voltage and frequency fluctuations on distribution systems.

It is claimed by many researchers, that the EVs can provide energy to grid for voltage and frequency regulation, spinning reserve and ancillary services [21–23, 26, 27, 43, 44, 58–60]. The area has seen significant research activity in the last few years and several works have been done in order to support the utility grid. Among these, some of the important works are reported in the next section.

1.2.3 Literature Survey

Several works has been reported in the literature where the EVs are being used as a DESS to solve the peak power demand. In most of the work, an optimal charging station and control strategies has been developed which can store/support power from/to electric grid. Many researchers have developed a dynamic model and analyzed the power flow between the electric grid and system. The EVs and HEVs are becoming very popular these days. These vehicles are charged by plugging into electric outlets. Kempton *et al* has developed control strategies and business models for the implementation of V2G concept. In this work, the electric-drive vehicle (battery, fuel cell or hybrid) provides the power to electric markets [23]. In [21], the differences between three approaches by using dynamic model of EVs' batteries to grid application have been proposed. Tomic *et al* has proposed that the electric-drive vehicles can provide the power to the electric grid when they are parked or provide power to specific electricity market while they are not in use [22]. In [44], it is reported that the EVs can be used to supply the power to grid for stabilization and peak load shaving. They have also focused on the infrastructure and the implementation of V2G technology. Ekman *et al* has investigated the effects of different types of EV charging strategies on the balance between wind power generation and consumption [26]. They have developed a control algorithm to store the energy in the EV batteries when the power consumption is low on the grid. In [58], the intelligent solutions has been developed for monitoring and controlling the electrical grid when the PEVs and EVs are connected in distribution network.

In [27], the EVs have been used as a flexible DESS to charge their batteries. This work investigates the impacts of EVs with V2G capability to power system operation. Hedegaard *et al* has developed the EVs' batteries that are charged/discharged intelligently, it can also provide energy back to electric grid and reduce the need for new coal/natural gas power capacities [59].

The frequency regulation is considered as the most promising and practical challenges in V2G services [61]. It has focused, on amount of power that can be delivered from vehicle-to-grid based on the frequency regulation and the EVs are coordinated by using the aggregator. In [28], the different types of ESS are studied with a simple probabilistic method to predict the ability of energy storage to increase the penetration of intermittent renewable-energy generation on weak electricity grid. Kim *et al* has addressed dynamic modeling and control of grid connected hybrid generation system such as wind turbine, photovoltaic array and battery. In this work three types of control strategies has been used to control the power flow between grid and hybrid system [62]. In [37, 63], the design and simulation of a fast CS for PHEVs batteries has been developed. V2G algorithm has been developed to optimize energy scheduling, load regulation and spinning reserve [57]. This work focuses on the maximum profit to the aggregator and it also provides additional system flexibility, low costs of EV charging for the customer. An optimal scheduling scheme for charging and discharging the EV battery with the grid has been proposed in [64, 65]. In [66], the coordination of PHEVs and EVs charging methods are presented and its impact on the distribution network is analyzed in terms of voltage deviations and power losses. Lee *et al* has analyzed PHEVs behavior of charging and its impacts on the electric grid by using the daily driving schedule [40]. A real-time smart load management system has been proposed which can coordinate the multiple PHEVs and EVs charging and maintain the grid voltage in the stable region [24]. Li *et al* has developed a methodology of modeling and controlling the charging demand of PHEVs [67]. A sophisticated control methodology has been proposed for modeling and analyzing the load demand in a distribution system in [36]. In [68], a conceptual frame has been studied, successfully integrating the EVs to electric power system. The impacts of PHEVs charging on the distribution system using a case study based on a small residential distribution network has been comprehensively analyzed in [69, 70]. In [71], a bidirectional power flow between EV and grid has been reported by using the integrated traction machine and converter topology. The impact of the PHEVs charging on the distribution grid has been analyzed through a residential feeder of the distribution network in [72]. The preceding section has the detailed literature survey about the aggregator that has been used in the V2G integration, which distributes the power between the electric grid and the charging system.

1.2.3.1 Aggregator

An efficient optimal aggregator has been proposed for frequency regulation which can transfer the power between EVs and grid [73]. In [74], a large fleet of EVs supports the grid and charges its battery based on the grid condition. In this work, a fuzzy based control strategy has been used to control the power flow between grid and EVs' batteries. In [75], the PEVs charging rate has been controlled based on the charging behavior estimated from the graphical strategies data. They have studied different charging strategies and the impacts of PEVs charging on the DN by using standard load flow analysis. The application of aggregators to frequency regulation by making fair use of their energy storage capacity has been addressed in [50]. The coordinated charging control of a V2G aggregator has been discussed, which aims at minimizing the charging cost and reducing the power losses incurred by the fluctuating load [76].

An aggregator has been designed to predict the impacts of PHEVs on the electricity demand profile in a specific region [61]. In [34], a multi-charging station has been developed for EVs' battery charging during the off-peak hours and supports the grid during peak hours. They have proposed fuzzy based control scheme. An aggregator has been developed to estimate the required power to charge the EV battery or available power to support the grid and distribute the power to each charging station. An operating framework for aggregator of PEVs has been designed in [77, 78]. A minimum load scheduling algorithm has developed to determine the purchase of energy in a day-ahead market, based on the forecasted electricity and PEVs power demand. A dynamic dispatch algorithm has been developed, used for distributing the purchased energy to PEVs on the operating day in [77]. The major research work on the batteries or ESS is presented in the next section.

1.2.3.2 Energy Storage System or EVs Batteries

Dynamic Li-ion battery model has been developed to represent virtual prototyping of portable battery power systems in [79]. They have taken into account non-linearity, temperature, thermal effects and the transients. Dogger *et al* has proposed that Li-ion battery can used as a DES for grid support. They have developed an intelligent control algorithm which minimizes the degradation rate and maximize the financial benefits to EV battery owners [80]. An autonomous distributed V2G control scheme providing a distributed spinning reserve for the unexpected intermittency of RES has been discussed in [31]. In this work, large scale RES has been integrated to the power grid and the EV battery performs an important role of smoothing their natural intermittency and ensuring grid stability. In [38, 81], the possibility of extending the life cycle of PEVs batteries used for stationary application and the advantages of Li-ion battery has been discussed. In [35], EV battery has been used as an ESS that can be integrated with the distribution network of IEEE 30 node power system model. In this work, a decision making algorithm is established for the deployment of battery energy stored capacity, state of charge, time of day, electricity prices and vehicle charging requirements. In the next section, a detailed major research about the inductive power transfer between grid and EVs charging/discharging system is presented.

1.2.3.3 Inductive Power Transfer

The Inductive power transfer (IPT) or contactless power transfer (CPT) system overcomes the problem of failure in connection, sparking and the risk of electrical shock. Also, it is safe to operate, reliable and convenient to handle [82–85]. In vehicle applications, the IPT system was reported more than two decades back [67, 86–89], but till date there is only limited commercial development has taken place mainly due to the difficulties in transferring significant amount of power to a moving vehicle without improving the constraints on vehicle moments. Sallan *et al* has developed a detailed design procedure for IPT system with a 2kW prototype model [2]. The IPT system for EVs battery using neither of loosely nor tightly coupled contactless coils has been presented in [67, 87]. Bieler *et al* has developed the CPT system which can transfer the power from EVs battery to grid [90]. In [91], a bidirectional power flow capability has been reported by using the converter and chopper. An extensive closed loop control algorithm has been used to control the bidirectional power flow. In [92], the contactless charging systems are preferred for EVs application due to the elimination of direct electric contacts. They have developed IPT system for roadway vehicle minimizing each vehicle's on-board power pickup weight. Sophisticated and robust control strategies have been developed based on power frequency droop charging of IPT system [93]. In this work, regulation of the power flow in both directions has been studied without a communication link. In [82], an IPT system has been proposed using a direct ac-ac converter configuration that generates a high-frequency ac current for the contactless coil. A robust control strategy was developed for generating high-frequency in the primary side of the converter configuration. A general analysis has been proposed for the design of loosely coupled IPT system using net impedance or load seen by the source [87, 94]. In [95], the IPT system has been proposed that is suitable for EV battery charging system. In this work, a misalignment of the contactless coil and the possible combination of the compensation topologies (series, parallel, series-parallel and parallel-series) has been presented. The CPT system synchronizes with the electric grid and thus power flows in either of the directions. In the next section, literature review on the synchronization of the system with grid is explored.

1.2.3.4 Synchronization

A unidirectional and a bidirectional grid connected converter with IPT systems, requires sophisticated control strategies to control the power flow. The power flow is not guaranteed without synchronization of the system with grid [96]. In this work, a sophisticated control strategy has been developed for the synchronization technique in a bidirectional power flow between the grid and system. Yazdaniet *et al* has developed a new adaptive notch filtering approach for the synchronization of the converter connected to DESS [97, 98]. A sophisticated control algorithm has been developed for synchronization of grid connected converter and the advantage of this proposed system does not required phased locked loop (PLL). Grid synchronization with distributed generation using the PLL techniques has been reported in [87, 99–104]. In [105, 106], a sophisticated synchronization strategy has been reported for a single phase and a three-phase converter connected with the distributed generators. Due power transfer between EVs and grid, both the EV owners and grid operators earn incentives. In next section, the detail literature review of economic benefits to the EV and grid owners is presented.

1.2.3.5 Economic Impacts of EVs and Grid

Many researchers have investigated the economic benefits to EV owners and the electric grid. In [107], the effect of the PHEVs battery degradation and its effect on battery lifetime have been estimated under the driving and charging conditions. Quinn *et al* has studied the effects of battery state of charge limitations on V2G interaction and its economic benefits [25]. The economic and environmental benefits of EVs and HEVs have been compared with the conventional ICE based vehicles in [108]. In [109], an energy and economic evaluation is done for PHEVs interaction with the power grid and the energy market. The cost and benefits of PHEVs based on the comprehensive ownership cost model is studied in [110]. They have performed a sensitivity analysis to understand the total ownership cost, payback period to model parameters and modeled components of ownership costs. Dietz *et al* investigated a smart charging strategy and the economic benefits for the EVs owner against a zero intelligence charging strategy in a simulation based analysis [111]. The smart charging strategies reduce charging cost to the EVs owners by more than 50%. The researchers claim that EVs and PHEVs could provide energy to the ancillary services and to an electric grid. In [99], a simulation model has been proposed to analyze the economic and environmental performance of EVs operated under different conditions such as electricity generation mix, smart charging control strategies and real-time pricing mechanisms. In [112], the charge scheduling has been studied to provide the benefits to both the utility grid and the EVs owners. A cash flow model has been developed for different type of vehicle [113]. They have focused on ownership costs (capital investments, infrastructure and operating costs), potential revenue for ancillary services and specifically regulation services. In [114], various type of sources are used to evaluate the economic and environmental comparisons of the four types of vehicles such as conventional, hybrid, electric and hydrogen fuel cell. The power system integration with EVs and economic dispatch of PHEV to the electric grid is presented in [115]. They have discussed scheduling problem considering other renewable-energy resources and risk management of PHEVs penetration in power system. The detail reviews has been presented for V2G interaction requirements, economic costs, challenges and strategies for V2G interfaces [116].

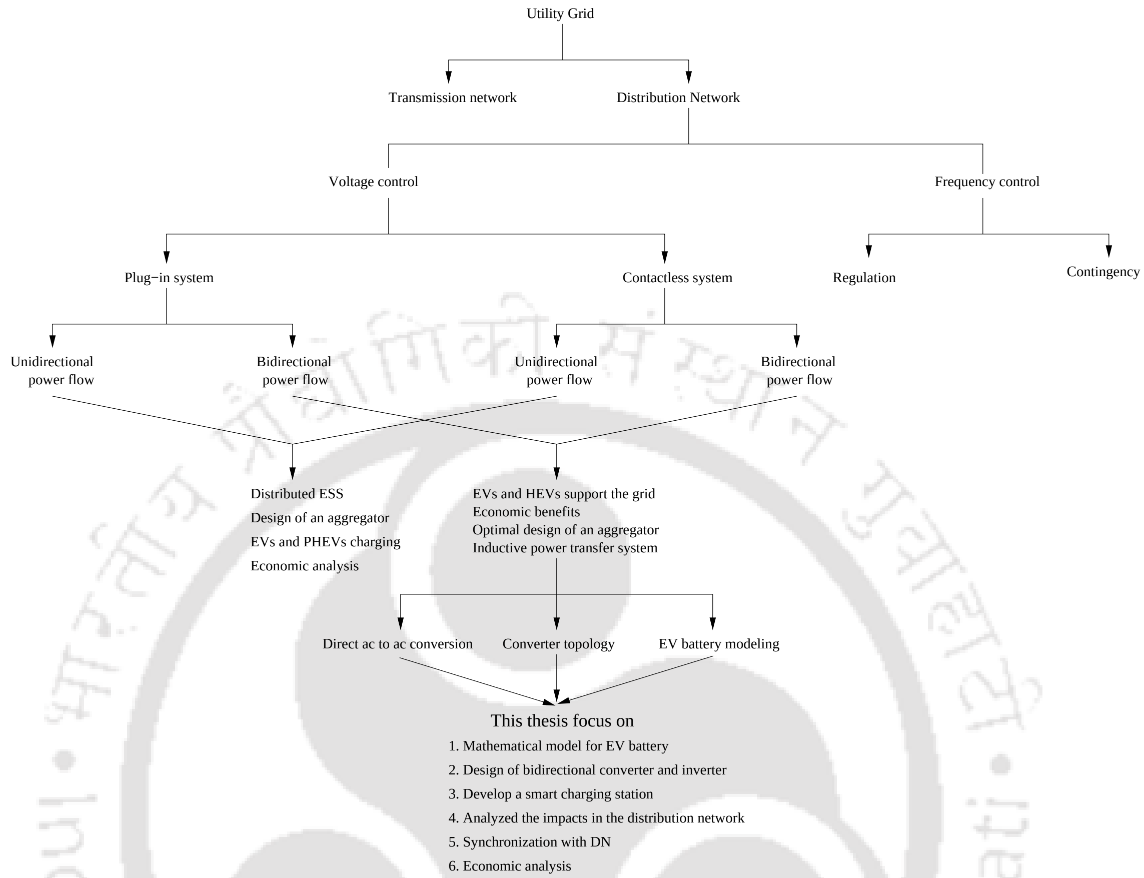

Figure 1.6: Layout of the literature review for grid connected system.

From the above literature it is evident that EVs batteries can act as distributed energy storage, which stores the excess amount of energy during the off-peak hours or peak shaving and supports the grid during peak hours or valley filling. Most of the time (an average of 95%) the EVs are available in the parking bay [22, 23], thus can be used for interacting with grid. The power transfer between EVs batteries and grid is based on the node voltage of the grid and energy status of the EVs batteries. However, the implementation of the EVs batteries drawing/injecting the power from/to grid with the converter unit, its control methodology and coordination of the multiple EVs still needs to analyzed. Fig. 1.6 shows the detailed literature review of the present research on V2G implementation based on the inductive power transfer. Many research works have discussed V2G system and the impact of charging system on the distribution node (DN). These studies have been done on the system level (converter and inverters are not designed) analysis and mainly focus on the voltage and frequency regulation. Most of the researchers have focused on the voltage regulation which draws power from the DN or support the DN using the DESS energy.

Numerous research works has been done for bidirectional power flow between grid and EVs' batteries with contactless system. The contactless charging systems are preferable for EVs applications due to the elimination of direct electric contacts [2, 92]. However, one of the works so far has discussed the converter configurations, control and coordination of the EVs batteries with the grid. Also, no literature has discussed the proper synchronization between the EVs batteries charging/discharging system and the grid. It is important to validate the peak power shaving and valley filling concepts in a coordinated manner, because the EVs are having different voltage and energy rating. This complex problem requires an exhaustive analysis and should be presented with the proper converter configuration and its control methodology. Moreover, none of the studies have attempted to analyze the economic impacts to the EV owners and grid operator. Therefore, the economic benefits for EVs owners and electric grid operator needs to be analyzed in detail.

1.2.4 Possible Solution Related to V2G Interactions

(i) The peak power demand is reduced by providing the stored energy back to grid.

(ii) Coordinated charging methodologies improve the voltage fluctuations and performance of the system.

(iii) Controlled and aggregated EVs' batteries energy can support the grid which reduce the power losses and improve the voltage fluctuations.

(iv) If the load exceeds the generation or vice versa, then the EVs' batteries will be able to regulate the grid frequency and voltage.

(v) The scheduled charging strategies provide the ancillary services to grid and improve the grid frequency.

(vi) The mathematical battery model is used to analyze the charge/discharge rate characteristics and capacity degradation.

1.3 Motivation and Reason to Adopt the Method

In literature, many researchers have validated the EVs and PEVs can be used as distributed energy storage system for grid support. They have implemented an extensive control strategy for scheduled charging/discharging of the EVs' batteries by controlling the charge/discharge rate. In few research papers, large scale renewable-energy source has been integrated with the power grid and it has been observed that the EVs' batteries play an important role for smoothening the natural intermittency and frequency stability. However, few researchers have analyzed the technical impacts of the distributed generators with ESS. Therefore, the EVs would support the grid during peak power demand and store the energy during off-peak hours. Several works has been developed to validate the V2G implementation. They have demonstrated various control algorithms to supply the power to electric grid for stabilization and peak load shaving. Tomic *et al* have demonstrated that the EVs can provide power to grid when they are parked in parking bay or not in use. Few research papers, they have focused on frequency regulation to coordinate multiple EVs with an optimal aggregator. They have designed an optimal scheduled charging methodology and an aggregator for multiple EVs coordination which can support the grid. Singh *et al* have designed an aggregated EVs energy system which can support the grid and charge their battery based on the grid condition. They have developed fuzzy based control strategy which can control the power in either direction. Moreover, they have analyzed system level control methodology for voltage regulation. They have not designed converter and inverter which can provide/take the power to/from grid [74]. Also, the aggregated V2G system minimizes the charging cost and reduces the power losses incurred by the fluctuating load. Lee *et al* have analyzed PHEVs charging behavior and its impacts on the electric grid by using the daily driving schedule. Some researchers have implemented sophisticated control methodology for modeling the system and analyzed load demand in a distribution system due to EV charging.

In most of the research work that have been reported, the V2G implementation with grid is as a plug-in or wired system. Only recently, contactless or inductive power transfer charging system is gaining attention for EVs and HEVs application due to elimination of direct electric contact. These charging systems overcomes the drawbacks of traditional wired charging systems such as heating of the sockets and cables, risk of fire, electrical injuries and cable breakage [2,92]. Many research works has been reported in literature to validate the IPT for V2G system. They have developed robust control methodology for controlling the power in either direction. Sallan *et al* has developed a detailed design procedure for IPT system with 2kW prototype model. Many researchers have modeled converter and inverter configuration for transferring the power. The power transfer takes place only when the charging system is synchronized with the grid. In other words, the power flow is not being guaranteed without synchronization of the system with grid. The PLL based synchronization technique is most suitable for DESS. In few papers, they have developed sophisticated control algorithm for the synchronization of grid connected with converter system. Numerous research works has analyzed the losses, economic burden and the impacts of DN while transferring the power. The economic burden to the EVs owners and the electric grid operator has been reported in few papers.

It can be concluded from the above literature that, to mitigate the peak power demand multiple EVs batteries are required to support the grid and store the energy during off-peak hours. However, coordination of multiple EVs for grid support requires an optimal aggregator. Therefore, a sophisticated charging station is required which provide aggregated energy for the grid support. EVs are charged at a place called as CS and this CS is situated near the DN in the parking bay. The parking bay can be a residential complex or an office complex or even a shopping complex. The EVs normally stay for longer duration in the parking bay and thus V2G concept can be achieved.

Sishugram power substation in Guwahati city has been considered for this analysis. The distribution network has been developed in MATLAB Simulink environment based on the data obtained from this substation. The multiple EVs are connected to the distribution node (11kV/440V) via ac bus. Therefore, the EVs can provide the power based on the DN status and energy availability of the CS.

If EVs' batteries are intended to perform V2G operation, it would get subjected to varying node voltage conditions. Also, during acceleration and regenerative breaking conditions, the EVs' batteries would get discharged and charged frequently. Such frequent charging/discharging operating conditions affect the internal circuit parameters due to change in state-of-charge or depth-of-discharge, charge rate or discharge rate of the battery. Moreover, the capacity of EVs' batteries would decrease due to frequent charging/discharging process at different charge/discharge rate. Therefore, a suitable

EV battery model is required to predict the V2G interaction. A mathematical model of EVs' batteries for different charge/discharge rate has been developed. Also, in this thesis a mathematical model for economic evaluation of V2G interaction is developed based on the capacity fading of EV battery at different charge/discharge rate. This model determines the optimal cost of electricity so that both the grid and the EVs owners are benefited.

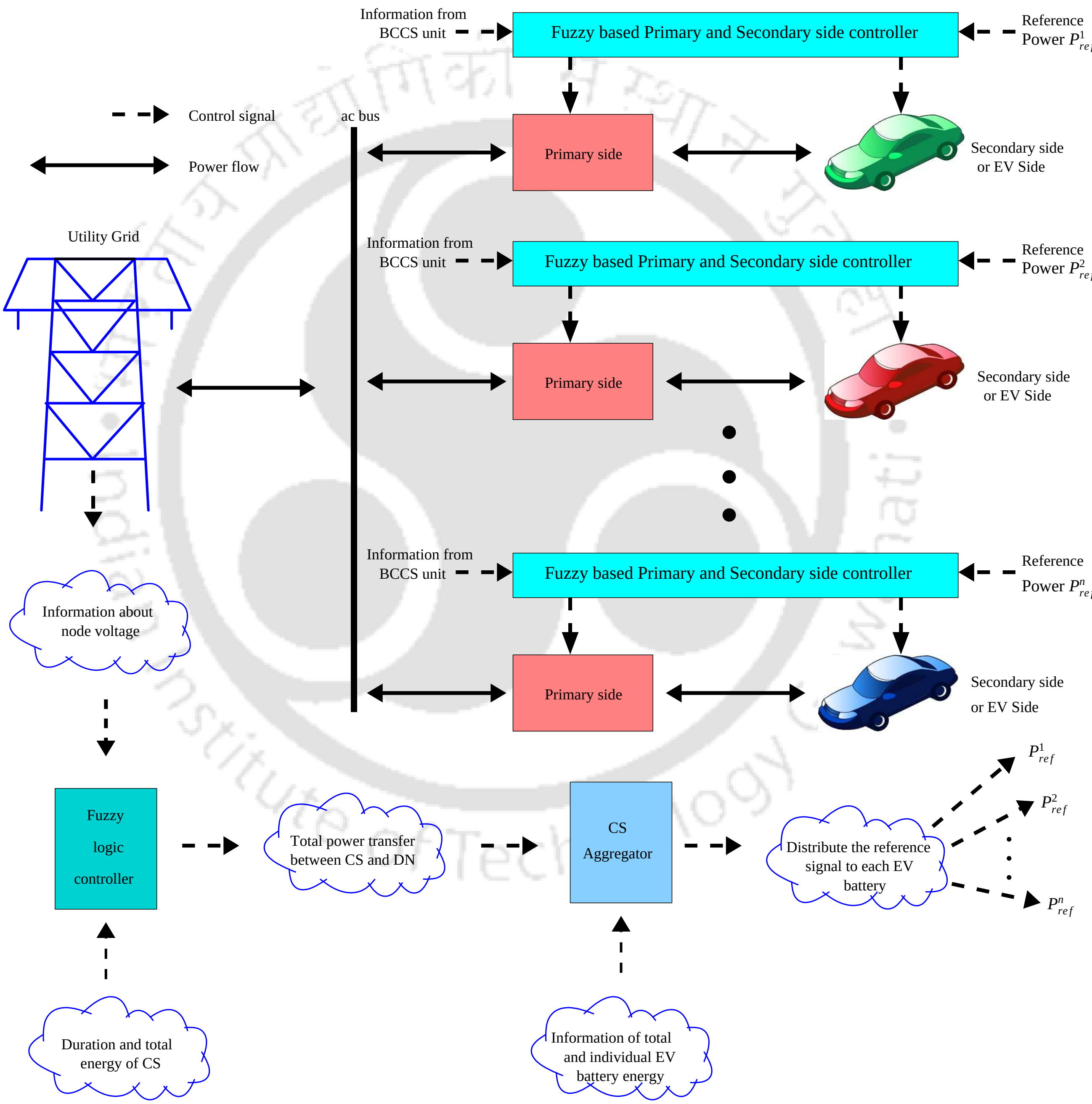

Figure 1.7: Illustration of smart charging station.

The schematic block diagram of the smart charging station (SCS) is shown in Fig. 1.7. It mainly consist of (a) utility grid, (b) fuzzy based central control unit (CCU), (c) CS aggregator,(d) primary side (PS) and secondary side (SS) converter units, (e) contactless coil coupled with the PS and SS converter unit and lastly (f) controller for the converter unit. Total power (P_{grid}) flow in either direction has been controlled by designing an extensive fuzzy based controller which decides the amount and direction of power flow. The fuzzy based CCU output could be positive or negative. The positive power implies that batteries getting charged and the negative power imply that batteries discharging for the grid support. The CCU decides the total power based on the node voltage (V_{node}), available/required energy (E_{avail}/E_{stor}) of the EVs batteries present in the CS and duration to support/inject the power from/to grid. Then, the CS aggregator gives the reference power (P_{bn}) signal to nth EV battery based on the P_{grid}, E_{avail}/E_{stor} and individual energy (E_{bn}) of the EV battery. The PS and SS controller would control the power flow based on the P_{bn}.

1.4 Aim of the Thesis

From the previous section, it can be concluded that coordination of multiple EVs can be achieved through proper design of mathematical model for EVs' batteries, charging station, controllers and CS aggregator. The primary objective of this thesis is to transfer the power between EVs' batteries and grid during off-peak and peak hours. The CS would transfer power based on the varying node voltage with respect to time. Hence, the charge/discharge current of the EV battery is varying based on the DN voltage. Therefore, a mathematical EV battery model is required to analyze the amount of power flow from/to EV battery. Based on these aspects, the main motivations of this work are given below:

(i) An electric equivalent circuit based battery model (BM) and capacity fade model (CFM) should be required to predict the performance characteristics at different charge and discharge rate for V2G applications.

(ii) The BM parameters should be in the form of polynomial equation with exponential function because the charge/discharge characteristics are exponentially increasing or decreasing.

(iii) The polynomial equations with exponential function have polynomial coefficients, which is optimized by using genetic algorithm (GA).

(iv) A control algorithm should be required to regulate the charge and discharge current. This will estimate processed energy for charging/discharging scenario, charge/discharge power, Current state-of-charge (SOC_{cr}) and depth-of-discharge (DOD_{cr}) of the battery, user defined SOD/DOD limits and charge/discharge rate.

(v) A complete capacity fade analysis should be carried out to quantify the capacity loss with respect to processed energy for charging/ discharging scenario and different charge/discharge rate.

(vi) The BM and CFM have to develop in MATLAB Simulink environment and it is compared with the different types of battery manufacturer's characteristics such as charge and discharge voltage, available and stored energy, battery power and capacity loss.

(vii) Validation of the proposed battery and capacity fade model will compare with four different types of battery manufacturers' catalogue.

The second objective of this thesis is to develop an smart charging station (SCS) by using the BM, bidirectional converter unit and associated controller to mitigate the peak power demand during peak hours or stored the energy into the EVs' battery during off-peak hours. The main features of this work are given below:

(i) An extensive SCS should be required to mitigate the peak and off-peak power demand.

(ii) An optimal charging station aggregator is necessary to coordinate the multiple EVs present in the SCS.

(iii) Sophisticated and robust control methodology should be required for power transfer between EVs' batteries and the grid.

(iv) The fuzzy logic controllers are used to control the power flow because it is well suited for uncertain situations of EVs arrival in the SCS.

(v) The converter and inverter unit should be to develop for EVs' batteries charging/discharging system.

(vi) Contactless or IPT system should be design to overcome the traditional wired charging system.

(vii) Fuzzy based synchronization controller should be required for the grid connected converter unit. Also, robust control strategies have to design for the primary side and secondary side converter units.

Finally, a mathematical model for economic evaluation of V2G integration should be required based on the energy transfer. In this work, a real-time model is formulated to calculate the economic benefits of V2G implementation. This mathematical model calculates beneficiary cost for grid operators while charging the EV battery and estimate the beneficiary cost for EV owners during the grid support. The main features are given below:

(i) Mathematical modeling for economic benefits of the EVs owners, grid operator and consumers have to analyze based on the different charge and discharge rate of the EV battery.

(ii) To determine the optimal cost of energy transfer between the EVs batteries and grid so that both the grid and the EVs owners are financially benefited.

1.5 Bidirectional Contactless Charging System for V2G Power Transfer

In the SCS, multiple EVs participate for the grid support and also to charge their batteries. To charge/discharge the EV battery from/to grid, a suitable charging system is essential. Fig. 1.8 shows the block diagram of bidirectional contactless charging system (BCCS). The PS and SS converter unit is called as the BCCS which enable the bidirectional power flow between EVs batteries and grid based on the CS aggregator command. It mainly consists of two parts; called bidirectional primary converter units (BPCU) and bidirectional secondary converter units (BSCU), which are separated by an air gap and magnetically coupled to each other. The power flow from either direction is through weak or loose magnetic coupling. Generally, controllers are employed on each side to regulate the power flow in either direction. The BPCU comprises of the bidirectional three-phase ac to dc and dc to high-frequency ac converter. This unit is connected to DN via circuit breaker (CB), transformer and LCL filter as shown in Fig. 1.8. The BSCU is connected to the EV battery through high-frequency ac to dc and dc to dc (buck-boost) converter.

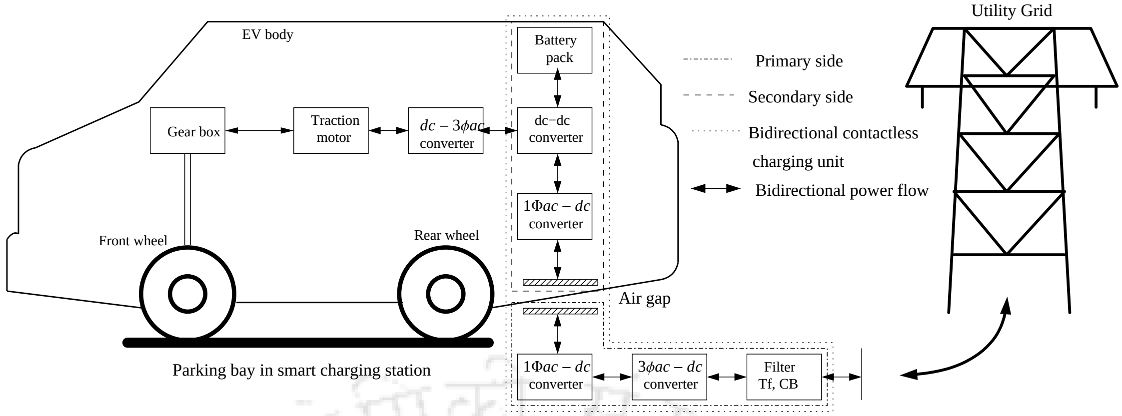

Figure 1.8: Block diagram of primary and secondary side converter with contactless charging system.

1.6 Main Contributions

The main contributions of this thesis are given below:

(i) Battery model has been developed for EVs batteries based on the polynomial equation with exponential function.

(ii) A new methodology has been developed for extracting the battery charge/discharge rate characteristics, capacity fading and total processed energy for charging and discharging scenarios.

(iii) The polynomial coefficients are optimized by using the GA.

(iv) A charging station has been developed based on the fuzzy logic control (FLC) and verified the bidirectional power flow between EV battery and distribution network during the peak hours, normal hours and off-peak hours.

(v) An FLC based synchronization methodology has been developed for grid connected bidirectional contactless charging system.

(vi) Fuzzy based control strategy has been developed for converter and inverter unit.

(vii) A mathematical model for the economic analysis of energy transfer between EVs and grid has been developed. In this work, the economic analysis has been done in such a way that the battery related liabilities do not become a financial burden to EV owners.

(viii) Finally, optimal cost of electricity has been determined such that the both the grid operators and EV owners are benefitted.

1.7 Thesis Organization

This thesis contains five (5) chapters presented as follows: An electric equivalent circuit (EEC) based battery model (BM) and capacity fade/loss model (CFM) suitable for EVs in V2G applications has been developed in Chapter 2. The circuit parameters of battery model is extracted using genetic algorithm based optimization method. A control algorithm has been developed for the battery, which calculates the processed energy, charge or discharge rate and state of charge limits of the battery in order to satisfy the future requirements of EVs. A complete capacity fade analysis has been carried out to quantify the capacity loss with respect to processed energy and cycling. The BM is tested by simulation and its characteristics such as charge and discharge voltage, available and stored energy, battery power and its capacity loss are extracted. The propriety of the proposed model is validated by superimposing the results with four typical manufacturers' data. The battery profiles of different manufacturers' like EIG, Sony, Panasonic, and Sanyo have been taken and its characteristics are compared with proposed models. The obtained battery characteristics are in close agreement with the measured (manufacturers' catalogue) characteristics.

In Chapter 3, the mathematical modeling and control of contactless based charging station in V2G scenario is presented. Various charging points, also called multi-point is present in a charging station. The SCS is a place where EVs of particular area comes to charge as well as to participate for the grid support. A multi-point bidirectional contactless based SCS with its control structure has been modeled in this chapter. A smart control algorithm is developed for the CS, which has the ability to decide the power flow between EVs and grid. The control algorithm modulates the charging/discharging rates of individual EV batteries by updating the power requirement and realizes a fast and synchronized response amongst multiple EVs. Each charging point is designed for a maximum peak power handling capacity of 50kW. The performance of the CS with its control system is investigated with multiple EVs of different battery ratings, connected under a single power distribution node of a grid. Simulation studies show that the CS can effectively perform scheduled charging/discharging based on the grid condition and EVs' batteries constraints.

In Chapter 4, mathematical model for economic analysis of energy transfer between EV battery and grid has been developed. The objective of this work is to develop a mathematical model for the integration of EVs to the grid. Integrating the EV with the grid would help in simultaneous charging of numerous EVs and also provide peak hour energy to the grid by the EVs. This bidirectional exchange of energy between the grid and EVs results in a complex financial calculations. A simple model has been proposed to meet up this issue. The energy provided by the EVs to the grid depends on the battery capacity and further battery capacity is affected by capacity loss (CL). The model includes the possible cases of CL, such as CL due to battery usage that is its discharge during vehicle transportation and CL due to the grid interaction.

Finally, the conclusions and future works are presented in chapter 5.

2

Mathematical Modeling of Li-Ion Battery Using Genetic Algorithm Approach for V2G Applications

Contents

2.1 Introduction

With the increased penetration of electric vehicles in the market, batteries are considered as one of the important components in the automobile industry [117, 118]. Among various available batteries, Lithium-ion batteries are more suitable for EV due to its long cycle life, less self discharge rate, high energy density, high efficiency, low maintenance and safe use [119].

EVs' batteries are charged from the distribution node and can be support the DN during parking hours or having excess amount of energy [120]. This concept is referred as grid-to-vehicle (G2V) and vehicle-to-grid (V2G) technology [121]. If EVs' batteries are intended to perform G2V and V2G operations, it would get subjected to varying node voltage conditions [120]. Also, during acceleration and regenerative breaking conditions, the EVs' batteries would get discharged and charged frequently. Such frequent charging/discharging operating conditions affect the internal circuit parameters due to change in state-of-charge (SOC) or depth-of-discharge (DOD), charge rate (C_r) or discharge rate (D_r) of the battery. Moreover, the capacity of EVs' batteries would decrease due to frequent charging/discharging process at different C_r/D_r [122, 123]. Therefore, a precise model of EV battery is very much required, to predict the performance of EVs in real-time V2G interaction. Capacity fade study is mainly required to predict batteries life time, which has been neglected in most battery models [124–126]. The capacity fade is proportional to charge or discharge rate and temperature of the battery [122, 123, 127].

An accurate battery model (BM) and capacity fade model (CFM) have three advantages as follows:

(i) It provides precise battery data for the simulation of EVs to predict the performance of the system.

(ii) To analyze the changes in circuit parameters according to SOC variations, for providing stable control in the system.

(iii) It is possible to analyze the capacity loss and hence to predict the lifetime of the battery.

In literature, there are four types of battery models such as experimental, electrochemical, mathematical and electric circuit models [121, 128–141] which is given in Fig. 2.1.

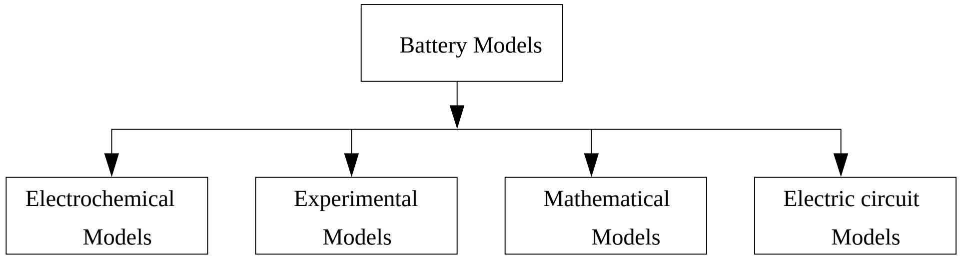

Figure 2.1: Types of battery Models.

The electrochemical models are the most accurate models, but they require complex nonlinear differential equations and detailed knowledge of the chemical reactions of the batteries [128, 142]. Experimental models require experimentation to determine the internal parameters of the battery [121, 129–131]. However, experimental and electrochemical models are not well suited to represent the cell dynamics for the purpose of SOC estimation of battery packs [132, 133]. The mathematical models are based on stochastic approaches to predict the efficiency and runtime of the batteries [134–136]. Due to high complexity and intensive computations, the above mentioned models are difficult to use in real-time power management and circuit simulations to predict the performance of the systems [137]. Electric circuit based battery model can be used to represent the electrical characteristics of the EVs' batteries [132, 137–141]. The simple common electric circuit model has a voltage source in series with an internal resistance [138]. However, this model does not take the account of battery SOC, C_r and D_r. There is another model based on an open circuit voltage in series with resistance and parallel *RC* circuit called as Warburg impedance [141]. The parameters of this model are identified using complicated impedance spectroscopy method [139,140,143]. From the literature, it is identified that the accurate estimation of internal battery parameters is a challenging task due to their nonlinear behavior.

Many soft computing and optimization techniques have been developed for battery parameter estimation [144–147]. Genetic algorithm (GA) is one of the best and robust kind of probability search algorithm, which has been used in this work [148]. In this Chapter, the GA is used to extract the battery parameters and gives optimum value. The C_r and D_r characteristics are calculated using the parameters of the BM which are obtained from the GA and it compared with the different types of battery manufacturers' data. The results from BM and data given by the different types of battery manufacturers' are in good agreement. Hence, it can be concluded that the GAs are able to extract the parameters of the BM effectively.

There are several other experimental works found in the literature, which have focused on capacity fade analysis of a particular manufacturers' battery [122, 123, 149–151]. However, performing experiments to determine the capacity fade of a battery for different C_r and D_r is a tedious as well as time consuming process [127]. Moreover, these studies are confined only for a particular type of battery. The results would differ for other battery types with different C_r and D_r, which cannot be performed experimentally every time. Therefore, there is a requirement of BM and CFM which can be used for any type of battery by reducing testing time and optimizing battery parameters for different C_r and D_r. Based on these aspects, the main motivations of this work are:

(i) To develop a simple circuit based BM and CFM, which can be used for any type of battery.

(ii) To extract the parameters of the model using GA approach.

(iii) To validate the developed model with different types of battery manufacturers' catalogue.

(iv) The model is computationally inexpensive and does not need experimentation.

This Chapter describes an electric circuit based BM and CFM which represents different type of battery manufacturers' C_r and D_r characteristics. The parameters of the BM is represented by a polynomial equation, which is optimized using GA approach. A control algorithm has been developed inside the battery, which calculates the processed energy, C_r/D_r, current SOC (SOC_{cr}) and DOD (DOD_{cr}) constraints of the battery. Simulations are performed with the developed BM and CFM. The validation of the models have been carried out by comparing the simulated results with the real-time battery data obtained from four manufacturers' data sheets such as EIG [1], Sony US18650 [127,152], Panasonic [153] and Sanyo [154]. Due to the unavailability of battery manufacturers' data, this work consider the low nominal voltage and Ampere-Hour ratings.

The Chapter is organized as follows. Section 2.2 describes the proposed battery model. The details of battery parameter extraction using GA approach is discussed in Section 2.3. Section 2.4 describes the capacity fade model. The model validation have been done in Section 2.5 by comparing the proposed model result with manufactures' data and summary of the present work is given in Section 2.6.

2.2 Battery Model

Fig. 2.2 shows the typical performance characteristics of EIG battery at different charge and discharge rate [1]. Energy extracted from the battery or stored into the battery is directly proportional to C_r for charging scenario and D_r for discharging scenario. It is concluded from the Fig. 2.2(a) and 2.2(b), behavior of the C_r and D_r characteristics are exponentially increasing and decreasing with respect to C_r and D_r. Therefore, polynomial equation with exponential function is the best way to represent the battery charge and discharge rate characteristics.

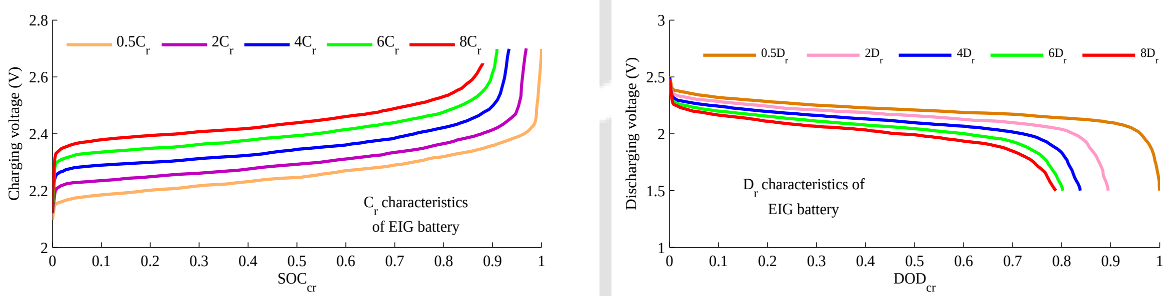

(a) (b)

Figure 2.2: Battery manufacturers' catalogue data (a) Charge rate characteristics of EIG battery (b) discharge rate characteristics of EIG battery [1].

An accurate, intuitive and simple electric circuit based BM is developed using an open circuit voltage (V_0) with a series resistance (R_1), and the parallel combination of resistance-capacitance (R_2C) as shown in Fig. 2.3. The V_0 is defined as the voltage between the terminals of battery in open circuit condition. The parameters of the battery are multi-variable functions of SOC_{cr}, DOD_{cr}, C_r, D_r, temperature and cycle number. The parameters V_0, R_1 in series with parallel R_2C characterizes the usable capacity, instantaneous voltage drop and self discharge energy. The R_2C network in the model is similar to Thevenins' model which simulates the transient response. The battery parameters R_1, R_2, V_0 and C have an exponential nature [155] and are approximated by polynomial functions. The general polynomial equations for the parameters are given in Eq. (2.1) - Eq. (2.4). The values of the battery parameters for charging and discharging scenarios are given in Appendix A.

$$R_1 = (a_1 + a_2x + a_3x^2)e^{-a_4y} + (a_5 + a_6x + a_7x^2) \tag{2.1}$$

$$R_2 = (a_8 + a_9x + a_{10}x^2)e^{-a_{11}y} + (a_{12} + a_{13}x + a_{14}x^2) \tag{2.2}$$

$$C = -(a_{15} + a_{16}x + a_{17}x^2)e^{-a_{18}y} + (a_{19} + a_{20}x + a_{21}x^2) \tag{2.3}$$

$$V_0 = (a_{22} + a_{23}x + a_{24}x^2)e^{-a_{25}y} + (a_{26} + a_{27}y + a_{28}y^2 + a_{29}y^3) - a_{30}x + a_{31}x^2 \tag{2.4}$$

In the above set of equations, R_1, R_2, C and V_0 are represented in terms of polynomial equations and there are 31 coefficients (from a_1 to a_{31}) in total. The detailed extraction method to find these polynomial coefficients has been explained in Section 2.3. The battery parameters for charging process can be derived by replacing x and y with C_r and SOC_{cr}, while for discharging process with D_r and $(1-DOD_{cr})$. Here, $(1-DOD_{cr})$ is chosen as V_0 decreases with increase in DOD_{cr} for discharging voltage. These equations are used for calculating battery terminal voltage for charging or discharging at different C_r and D_r. The terminal charge or discharge voltage of the battery ($V^C_{c_i}$ or $V^C_{d_j}$) changes with capacity of the battery, SOC_{cr}/DOD_{cr} levels and C_r/D_r. The parameters of non-linear relation of $V^C_{c_i}/V^C_{d_j}$ can also be represented in terms of polynomial equations, where i and j denotes i^{th} and j^{th} calculated value of the charging and discharging voltage. Therefore, under constant current the battery terminal voltage for charging and discharging scenario with respect to time is given in Eq. (2.5) and Eq. (2.6). In Appendix A, the calculated battery terminal voltage for charging and discharging scenarios has been mentioned.

$$V^C_{c_i} = \left(\left(\frac{Q_r}{C} + I_cR_2\right)\exp\left(-\frac{t_c}{R_2C}\right)\right) + V_0 - (I_c(R_1 + R_2)) \tag{2.5}$$

$$V^C_{d_j} = \left(\left(\frac{Q_r}{C} + I_dR_2\right)\exp\left(-\frac{t_d}{R_2C}\right)\right) + V_0 - (I_d(R_1 + R_2)) \tag{2.6}$$

where Q_r is the remaining capacity of the battery, t_c, I_c, t_d and I_d are charge time, charge current, discharge time and discharge current, respectively. Thus, Eq. (2.5) and Eq. (2.6) can accurately represent the behavior of any battery types, if the parameters are well defined. This equations capture the non-linear behavior of the battery which depends on the actual battery charge/discharge voltage. Fig. 2.3 shows the representation of electric circuit based battery model with its non-linear equations.

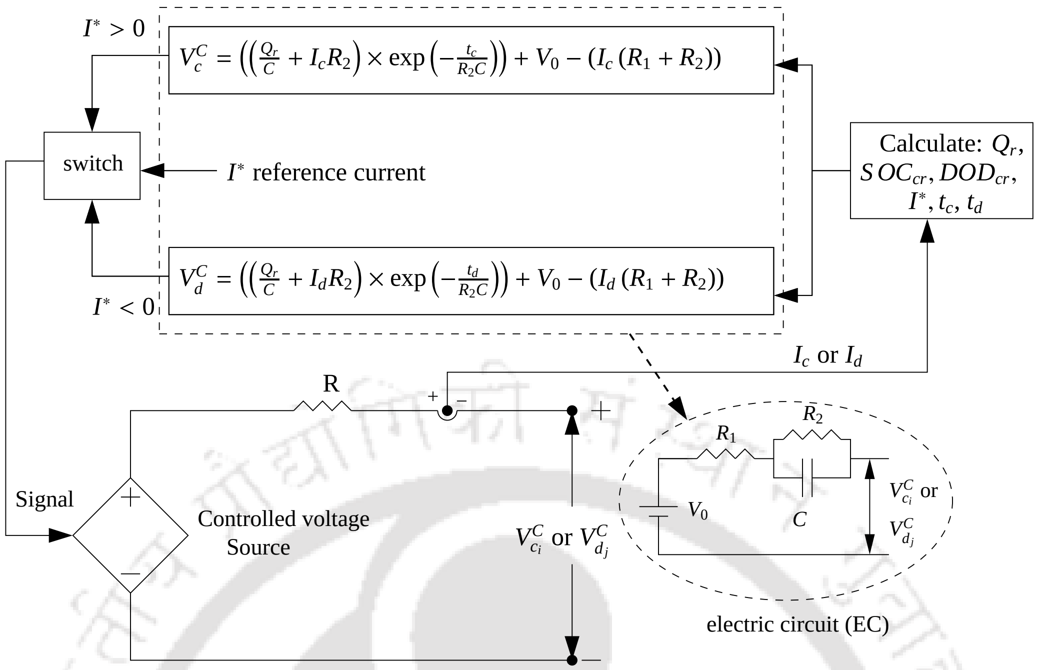

Figure 2.3: Non-linear battery model.

2.2.1 Charge/Discharge Rate and SOC Calculations

The charge or discharge rate algorithm is used to determine the amount of energy stored or extracted from the EV battery. The C_r and SOC_{cr} of the battery varies depending on the present condition of the battery.

Fig. 2.4 explains the calculation of C_r and SOC_{cr} for charging scenario. The control algorithm developed inside the battery checks the battery status and then calculates the current charge rate (C_r^{crt}) of the EV battery. It has also taken into account of user defined C_r limit (C_r^{lmt}) and initial battery SOC (SOC_{ini}). The C_r^{crt} and D_r^{crt} of the battery can be expressed as given in Eq. (2.7) - Eq. (2.8).

$$C_r = C_r^{crt} = \frac{I_c}{Q_r} \tag{2.7}$$

$$D_r = D_r^{crt} = \frac{I_d}{Q_r} \tag{2.8}$$

This is calculated based on current status of the battery, which is the ratio of current and remaining capacity of the battery. The algorithm chooses the minimum of charge rate based on the C_r^{lmt} and C_r^{crt} to regulate the charge current of the battery. Similar type of control algorithm is used for discharging scenario.

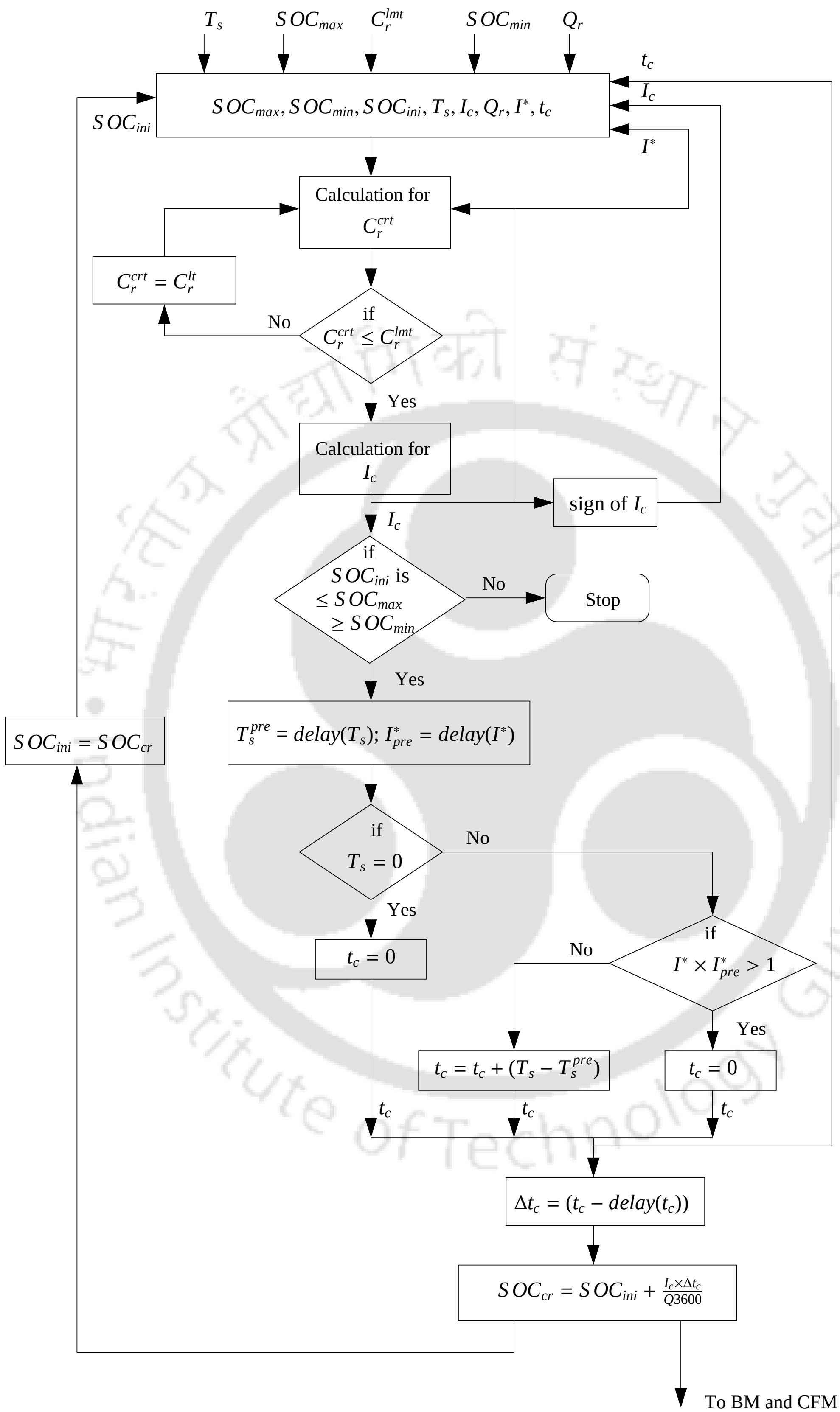

Figure 2.4: Functional flow chart for C_r and SOC_{cr}.

TH-1265_KANNANT

The SOC_{cr} and DOD_{cr} can be calculated from Eq. (2.9) - Eq. (2.10). The SOC_{cr} and t_c is estimated from the C_r control algorithm which is given in Fig. 2.4. Similarly, the DOD_{cr} and t_d is calculated for discharging scenario.

$$SOC_{cr} = SOC_{ini} + \left(\frac{I_c \Delta t_c}{Q_r 3600}\right) \tag{2.9}$$

$$DOD_{cr} = DOD_{ini} + \left(\frac{I_d \Delta t_d}{Q_r 3600}\right) \tag{2.10}$$

Here, SOC_{ini} is the initial SOC of the battery. The SOC_{max} and DOD_{max} are the maximum user defined SOC and DOD limits. If SOC_{cr} and DOD_{cr} of the battery reaches SOC_{max} and DOD_{max}, then the control algorithm should not allow to charge or discharge the battery to prevent over charging or discharging. The control algorithm used to charge/discharge the EVs' batteries from/to grid have been explained in Chapter 3. The sample calculation for SOC_{cr}, C_r, etc. has been given in Appendix A.

2.2.2 Battery Power and Processed Energy

The battery power for charging (P_c) and discharging (P_d) scenario is given in Eq. (2.11) - Eq. (2.12).

$$P_c = V_{c_i}^C \mathrm{I_c} \tag{2.11}$$

$$P_d = V_{d_j}^C \mathrm{I_d} \tag{2.12}$$

The amount of stored energy (E_{stor}) during charging process depends on increase in $V_{c_i}^C$ and SOC_{cr}, which is given in Eq. (2.13).

$$E_{stor} = V_{c_i}^C Q_r \Delta SOC_{cr} \tag{2.13}$$

where, ΔSOC_{cr} is the change in current SOC_{cr}. The processed energy (PE_c) for charging scenario is given in Eq. (2.14).

$$PE_c = \sum E_{stor} \tag{2.14}$$

The available energy (E_{avail}) in the battery during discharging process decreases $V_{d_i}^C$ with increase in DOD_{cr}, which can be calculated using Eq. (2.15).

$$E_{avail} = V_{d_j}^C Q_r \Delta DOD_{cr} \tag{2.15}$$

where, ΔDOD_{cr} is the change in current DOD_{cr}. The processed energy (PE_d) for discharging scenario is given in Eq. (2.16).

$$PE_d = \sum E_{avail} \tag{2.16}$$

The total processed energy (E_{total}) of the battery in a cycle is calculated using Eq. (2.17).

$$E_{total} = \sum (PE_c + PE_d) \tag{2.17}$$

Eq. (2.11) to Eq. (2.17) represents the real-time performance of the battery during charging and discharging process. Simulations are done based on these equations for the developed BM and has been validated with the manufacturers' catalogue which is discussed in Section 2.5. In Appendix A, battery power and processed energy calculation details has been mentioned.

2.3 Parameter Extraction Using Genetic Algorithm Approach

2.3.1 Genetic Algorithm

Finding the polynomial coefficients for battery model is a simple polynomial fit problem. In the direct methods, the initial iteration value of the battery coefficients should be very close to solution set. To overcome this problem, the GA has been used for finding the battery parameters at different charge and discharge rate. Genetic algorithm is a technique for stochastic search, learning and optimization. GA imitates the process of biological evolution, including selection, crossover and mutation based on the principle; good individuals survive and breed good individuals [147, 156]. Battery parameters are extracted using GA based optimization technique. Different types of manufacturers' data of Li-ion batteries are considered for extraction purpose. The main objective of GA is to optimize the battery parameters polynomial coefficients ($a_1 - a_{31}$) to evaluate the equations given from Eq. (2.1) to Eq. (2.6).

The main advantages of using GA to optimize the battery coefficients are given below:

(i) The purpose of using GA for battery parameter extraction problem lies in the fact that it requires only manufacturers C_r and D_r characteristics and gives consistent polynomial coefficient of battery model during relatively fewer iterations.

(ii) GA is more flexible in extracting the battery parameters with any initial values, while other numerical methods are incapable of obtaining satisfactory solution.

(iii) The algorithm is easy to understand and can be optimized using fitness function.

(iv) With its optimizing capability, GA steer the fitness function to be more representative and yields an accurate solution set even if the initial values are far from the solutions.

(v) GA encodes an optimum value based on simple chromosome.

(vi) By its evolutionary character, GA does not suffer from convergence problem and can be dealt with any number of coefficients in a defined boundary limits.

2.3.2 Parameter Extraction Process Using GA

The main objective is to find the battery parameters for the developed BM, which should exactly match the manufacturers' data. GA assigns random values and apply standard mutation and crossover operators without any impact on the periodic or continuous nature of the solution. The details of parameters extraction problem is given below.

2.3.2.1 Parameter Specifications

The charge or discharge rate characteristics of the battery model depends on polynomial coefficients ($a_1 - a_{31}$) which is given in Eq. (2.1) - Eq. (2.4). To perform GA based optimization, the population size (S_n) has been considered as a matrix size of 300×31. The length of the string is taken as 15. The crossover (P_c) and mutation probability (P_m) are taken to be 0.85 and 0.05. The measured (manufacturers' catalogue value) battery terminal voltage for charging ($V_{c_i}^M$) and discharging ($V_{d_i}^M$) scenarios are obtained from manufacturers' catalogue to optimize the polynomial coefficients.

2.3.2.2 Generation of Initial Solution Set

GA process begins with the generation of an initial random solution set to the problem. The entire solution set (300×31) is discretized and the variable is defined with a discrete binary set of strings ($a_{m_i,1}...a_{m_i,n}$). Each string is a combination of different representation of sub-strings ($a_{m_1,n}...a_{m_i,n}$). Let,

S_n is the random solution set of battery coefficient having m columns and n rows and is given in Eq. (2.18). Here, $a_{m_i,n}$ denotes n^{th} coefficient of i^{th} solution set. The initial random solution set has been mentioned in Appendix A.

$$S_n = \begin{pmatrix} a_{m_1,1} & \cdots & a_{m_1,n} \\ \vdots & \ddots & \vdots \\ a_{m_i,1} & \cdots & a_{m_i,n} \end{pmatrix} \tag{2.18}$$

Each n^{th} coefficients of i^{th} string in the solution set has a 15 bit number of a total of 465 bits. The 15 bit number in a single coefficient is denoted by Eq. (2.19).

$$a_{m_i,n} = (x_1 x_2 ... \mathrm{x_l}) \tag{2.19}$$

where x_1 and x_l is the lower and upper bit element in a single coefficient. The binary numbers in the strings are converted to real value, which will be manipulated with different genetic operators.

2.3.2.3 Coding

An important step in GA is to encode the vector ($a_{m_k,n}$) into binary string. Thus, the entire population vector is decritized and the variable is defined with a discrete binary set of sub-strings ($a_{m_k,1}...a_{m_k,n}$). Each string is a combination of different sub-strings ($a_{m_k,1}$), the length of the sub-string considered as 15. This process is referred as coding. The string in next generation is manipulated with different genetic operators. The genes of individual coded strings are represented with binary digits. The length of the string is determined according to the desired solution accuracy. Each variable is defined with a discrete set of binary set of strings. These group of strings can be called as population. Each string corresponds to a precision value of the corresponding actual value of the variable. The length of the string defines the accuracy in the solution. The strings are converted to decoded value (S_i) which is given in Eq. (2.20).

$$S_i = \sum_{i=1}^{l_i-1} 2^i a_{m_i,n} \tag{2.20}$$

where l_i is the length of the string which is 15, $a_{m_i,n} \in (0, 1)$ and string $a_{m_i,n}$ is represented by ($a_{l-1}a_{l-2}........a_2a_1a_0$). The decoded value should convert in to corresponding real or parameter value. The real value for the i^{th} polynomial coefficients is given in the Eq. (2.21).

$$a_i = {a_i}^L + \frac{{a_i}^U - {a_i}^L}{2^l - 1} \times S_i \tag{2.21}$$

where a_i^L and a_i^U are the lower and upper boundary limits of the parameter extraction problem. The sample calculation for string to decoded value and real value conversion for the parameter extraction problem has been given in Appendix A.

2.3.2.4 Fitness Function

The next requirement after generation of random solution set is the measure of quality of solution set. This can be achieved by establishing a fitness function ($F(x)$), which is rated by each solution according to its fitness. The function that has to be maximized ($F(x) = 1$) is called as fitness function. The difference between measured (catalogue value) ($V_{c_i}^M$ or $V_{d_j}^M$) and the calculated ($V_{c_i}^C$ or $V_{d_j}^C$) characteristics for charging or discharging case is determined as given in Eq. (2.5) or Eq. (2.6). Based on the calculated fitness value, the best list get updated and the lowest fitness is discarded. If $F(x)$ has to be maximized, then $f(x)$ should be minimized which is mathematically expressed as given in Eq. (2.22).

$$F(x) = \frac{1}{1 + f(x)} \tag{2.22}$$

Fitness function is followed by checking its optimal condition to know whether the solution set has reached the best fitness. Otherwards, the best fitness function is taken to be the parent for next generation based on Roulette-Wheel method [157]. The mathematical formulation of $f(x)$ for charging and discharging scenario is given in Eq. (2.23).

$$f(x) = \begin{cases} \sum_{i=0}^{n} \left| \left(V_{c_i}^M - V_{c_i}^C \right) \right| \\ \sum_{j=0}^{m} \left| \left(V_{d_j}^M - V_{d_j}^C \right) \right| \end{cases} \tag{2.23}$$

2.3.2.5 Selection

The individual having the highest fitness value is allowed to remain in the next generation as an elite individual. The selection operator is used to choose individual for evolution. Roulette-wheel method is used to select the best individuals based on the high value of $F(x)$. The bigger $f(x)$ value has worse quality of solution set. The selection of the fitness values for the next iteration can be obtained from Eq. (2.24) to Eq. (2.26). Here, F_{avg} is the average fitness function value, E_{co} is expected count and P_{es} is the probability of each string selected.

$$F_{avg} = \frac{\sum f(x)}{S_n} \tag{2.24}$$

$$E_{co} = \frac{F(x)}{F_{avg}} \tag{2.25}$$

$$P_{es} = \frac{E_{co}}{S_n} \tag{2.26}$$

Thus, the fitness values are arranged based on the maximum probability. The best solution set values are converted from real value to binary string of solution set. The string manipulation has been carried out using genetic operators such as reproduction, crossover and mutation.

2.3.2.6 Reproduction

This process rejects many worst $F(x)$ values and selects best values whose fitness is above F_{avg}. It picks the best fitness value from the current population and forms a mating pool. Multiple copies are inserted in the mating pool in a probabilistic manner. In order to choose the strings for next generation, a random numbers between 0's and 1's are generated. The cumulative probability is calculated based on the individual string probabilities. A string is chosen from the random number and is compared with the previous best solution set based on the cumulative probability. The string with higher fitness is selected and is copied to mating pool.

2.3.2.7 Crossover

After the next generation of solution set, the crossover genetic operators will be applied for the selected solution set. During crossover new strings are created by exchanging information among strings in the mating pool. A couple of parent (P_1 and P_2) strings are selected to perform crossover to get two new offspring strings. If the selected parents have the probability of $P_{co} \leq 0.85$, it performs crossover or else it is copied to the next generation.

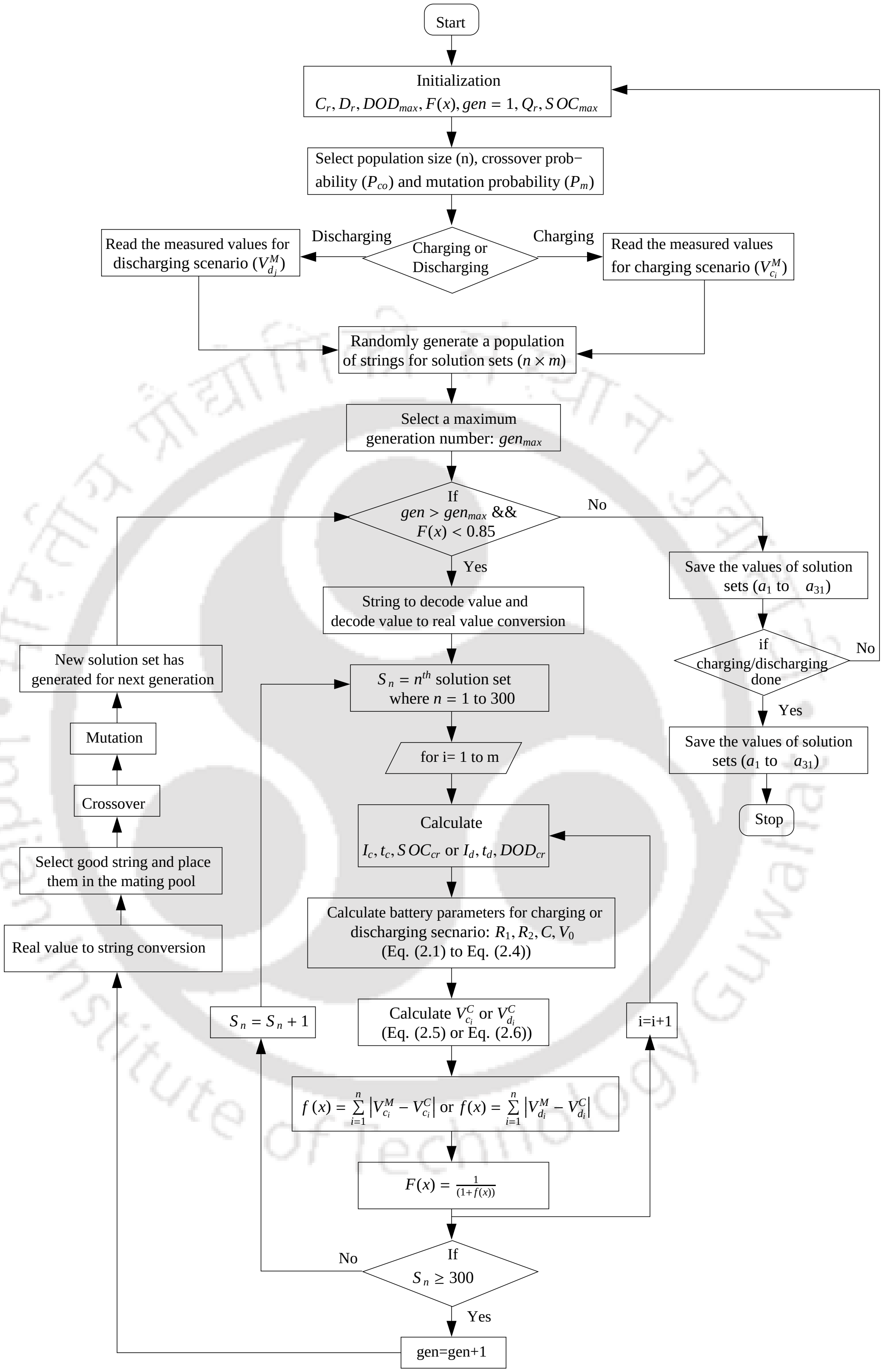

Figure 2.5: Flow chart for parameter extraction using genetic algorithm approach.

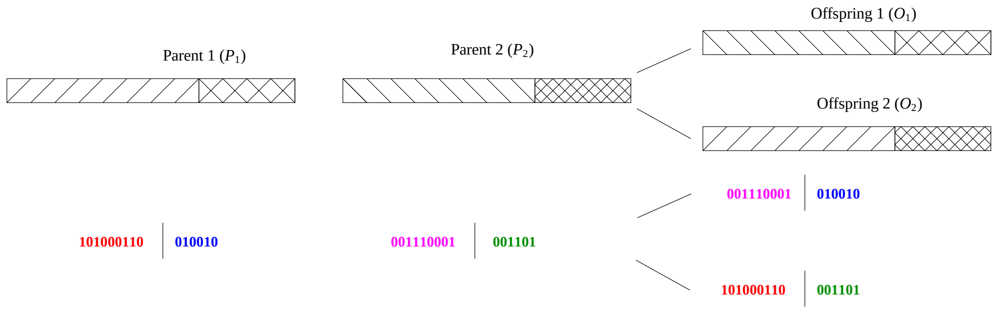

Figure 2.6: New offsprings (O_1 and O_2) generated from the parents (P_1 and P_2).

To illustrate this process, two parents P_1, P_2 are picked up from the mating pool. The crossover point is chosen to be 9 bit. Two offsprings O_1, O_2 are created by exchanging information among string in the matting pool as shown in Fig. 2.6. When reproduction happened between two intelligent genes, the probability to produce an intelligent gene is high. Good parent strings are combined to form a better child string, if an appropriate site is chosen. But good children strings may or may not be produced. This is not considered much because bad children strings would be discarded in the future mating pool based on their fitness.

2.3.2.8 Mutation

Mutation selects a particular offspring and randomly perform changes for one or more characters in the string by changing 0 to 1 or vice versa. The offspring selection is based on P_m which is evaluated from fitness. If the selected number is less than P_m, it performs mutation by altering the chosen string to create a better child string; otherwise it keeps the bit unaltered which is used for next generation. Fig. 2.7 shows the mutation process of the selected offspring.

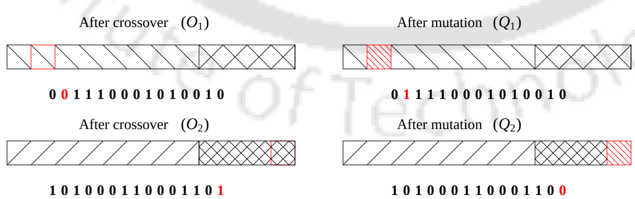

Figure 2.7: Mutation process for the n^{th} offspring.

After several generations, the algorithm converges the best individuals to represent the optimal solution. Fig. 2.5 shows the functional flow chart to obtain the polynomial coefficients of the battery. The obtained polynomial coefficients for charging and discharging scenario is given in Table 2.1.

Table 2.1: Polynomial Coefficients (PC) a_1 to a_{31} for charging and discharging scenario.

PC for charging scenario				PC for discharging scenario			
PC	Values	PC	Values	PC	Values	PC	Values
a_1	0.02109	a_{17}	0.028163	a_1	0.05256	a_{17}	0.004548
a_2	0.000579	a_{18}	0.668211	a_2	0.002547	a_{18}	15.90916
a_3	0.000064	a_{19}	5.235634	a_3	0.000587	a_{19}	134.2356
a_4	42.76495	a_{20}	0.110554	a_4	30.3548	a_{20}	0.012207
a_5	0.01246	a_{21}	0.063747	a_5	0.05215	a_{21}	0.002661
a_6	0.000396	a_{22}	0.012559	a_6	0.003147	a_{22}	1.01254
a_7	0.000033	a_{23}	42.78011	a_7	0.00032	a_{23}	20.2145
a_8	0.009526	a_{24}	2.146841	a_8	0.022546	a_{24}	2.5423
a_9	0.000238	a_{25}	0.188108	a_9	0.012547	a_{25}	0.22547
a_{10}	0.000003	a_{26}	0.024947	a_{10}	0.022657	a_{26}	0.1101
a_{11}	29.38634	a_{27}	0.002864	a_{11}	18.26547	a_{27}	0.02103
a_{12}	0.00687	a_{28}	0.162724	a_{12}	0.010001	a_{28}	0.00151
a_{13}	0.000324	a_{29}	0.015353	a_{13}	0.00088	a_{29}	0.0009
a_{14}	0.000025	a_{30}	0.011420	a_{14}	0.000023	a_{30}	1.42546
a_{15}	8.635732	a_{31}	0.00642	a_{15}	1.222364	a_{31}	0.00032
a_{16}	0.369508	-	-	a_{16}	0.010693	-	-

2.4 Capacity Fade Model

The energy storage capacity of battery decreases due to frequent charging or discharging. In this work, the capacity loss is calculated based on variable charge or discharge rate at an ambient temperature. The charge and discharge characteristics for a cycle is illustrated in Fig. 2.8. A cycle is defined as an interval during which the battery charges till SOC_{max} and discharges up to DOD_{max}. When the battery experiences different charge and discharge cycles, it fails to meet its performance thus reducing its life expectancy. Therefore, it is required to study the capacity fade to quantify the capacity loss with respect to number of cycles. The capacity fade calculation with an example has been mentioned in Appendix A.

Capacity fade of the battery can be quantified using Arrhenius equation for constant charge or discharge rate [122]. The mathematical model used to quantify the capacity fade is based on Arrhenius equation and is given in Eq. (2.27) [122, 123]. Here, A is pre-exponential factor, Q_l represents the capacity loss (Ah), E_a denotes the activation energy (J), R is the gas constant ($\frac{J}{molK}$), T is the temperature (K), t is the time and z is the adjustable factor.

$$Q_l = A \exp\left(-\frac{E_a}{RT}\right) t^z \tag{2.27}$$

Eq. (2.27) is used for calculating capacity fade under constant C_r. However, in real-time grid

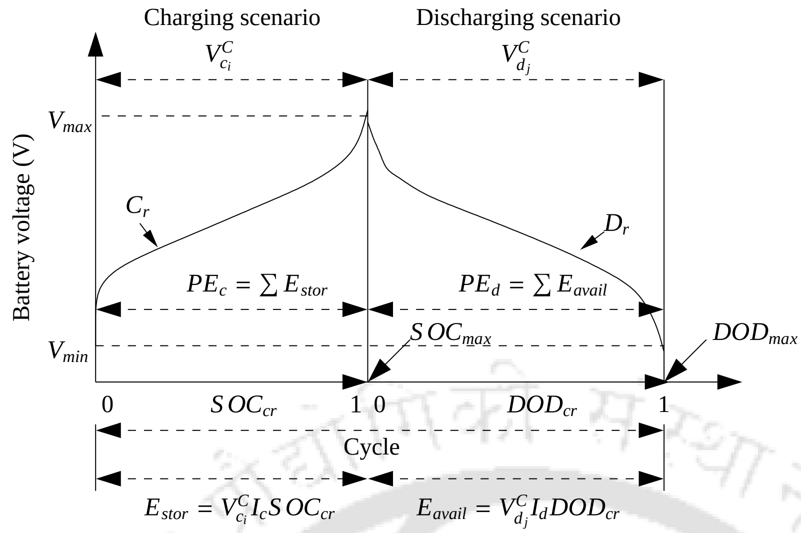

Figure 2.8: Battery performance characteristics for a cycle.

support, the charge or discharge rate of the battery would vary with respect to peak power demand and node voltage variations. This causes capacity loss of the battery. In real-time, the batteries charge or discharge rate varies with respect to variable node voltage conditions, SOC_{cr} or DOD_{cr} limits, temperature and also on the system constraints and user preferences. Due to this, the capacity fade changes with respect to the varying C_r, D_r SOC, DOD limits and temperature.

To account this loss, a mathematical model is developed in this work to predict the capacity fade at different charge and discharge rate. The total capacity fade can be quantified and written in terms of nominal capacity (Q), C_r, D_r, PE_c, PE_d, pre-exponential (A, B) and adjustable (C, D) factors, gas constant (R) and temperature (T) which is given in Eq. (2.28). In Eq. (2.28), $Q^C_{l_k}$ denotes calculated capacity loss and the remaining capacity of the battery can be calculated from Eq. (2.29).

$$Q^C_{l_k} = A \exp\left(-\frac{C\, PE_c\, Q_r\, C_r\, SOC_{cr}}{R\, T}\right) + B \exp\left(-\frac{D\, PE_d\, Q_r\, D_r\, DOD_{cr}}{R\, T}\right) \tag{2.28}$$

$$Q_r = Q - Q^C_{l_k} \tag{2.29}$$

where, Q_r is the remaining capacity of the battery which is updated value of the capacity loss at every cycle. The pre-exponential and adjustable factors are calculated based on trial and error method. The capacity loss characteristics is optimized by the fitness function ($F'(x)$). $F'(x)$ is maximized, when the difference between the measured (catalogue value) ($Q^M_{l_k}$) and calculated ($Q^C_{l_k}$) capacity loss is minimized. The mathematical representation of $F'(x)$ is given in Eq. (2.30), where n is the number

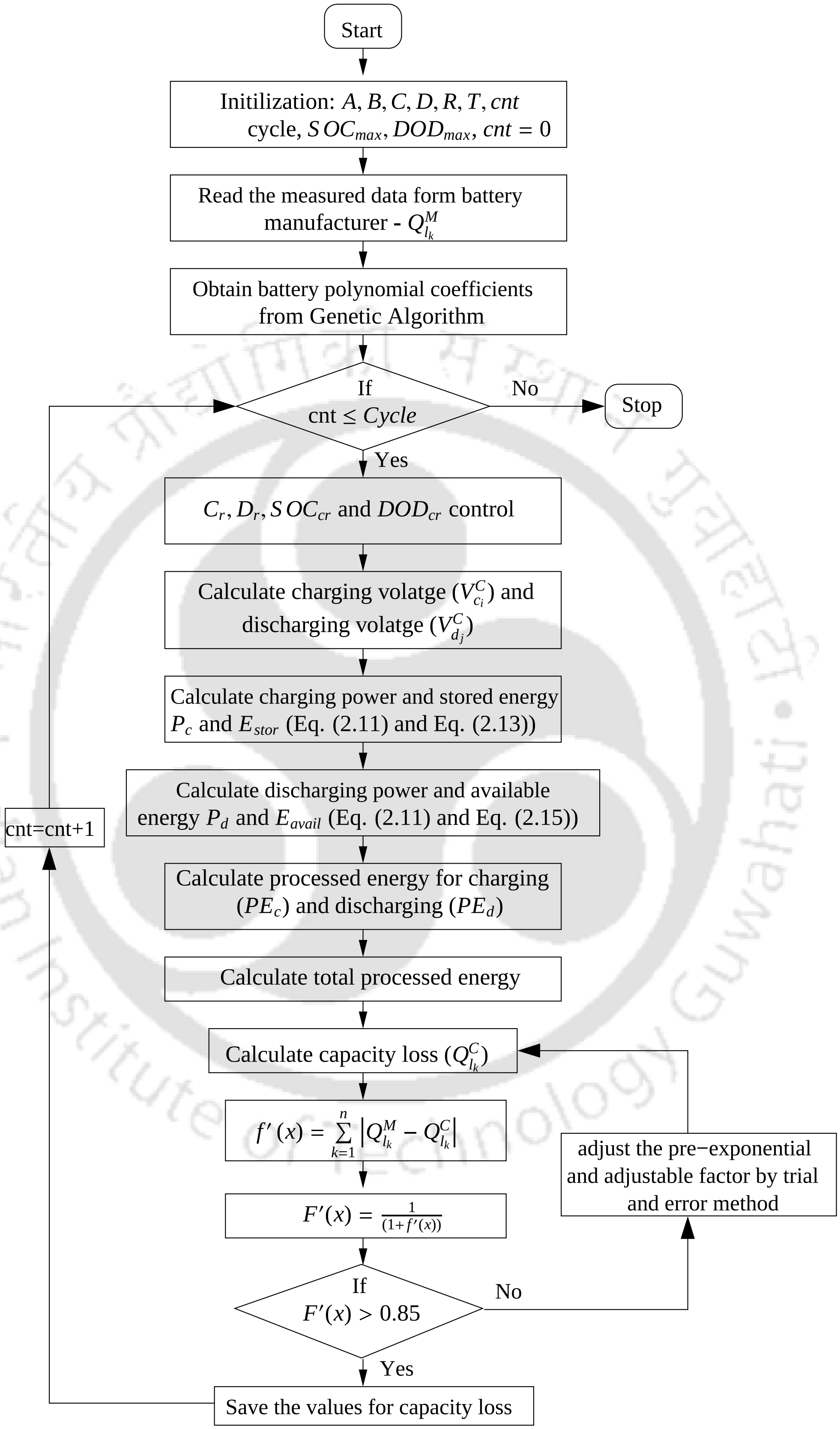

Figure 2.9: Functional flow chat for capacity loss.

of measured (catalogue value) and calculated values.

$$F'(x) = \frac{1}{1 + \sum_{k=1}^{n} \left(Q_{l_k}^{M} - Q_{l_k}^{C}\right)} \tag{2.30}$$

The functional flow chart for capacity loss calculation is shown in Fig. 2.9 has explained the complete process to calculate the capacity fade of the battery. Where, *cnt* denotes the number cycles involved in the calculation process. Table 2.2 shows the optimal values of pre-exponential and adjustable factors. Simulations are done to verify the developed capacity fade model and have been validated with different manufacturers' catalogue.

Table 2.2: Pre-exponential and adjustable factors

Pre-exponential factor		Adjustable factor	
A	B	C	D
0.01511	0.040144	7.8995	0.941e-4
0.09051	0.003873	1.295	1.442e-5
0.12053	0.000073	0.7961	1.9874e-4.4
0.00149	0.00993	1.4987	0.642e-2.2

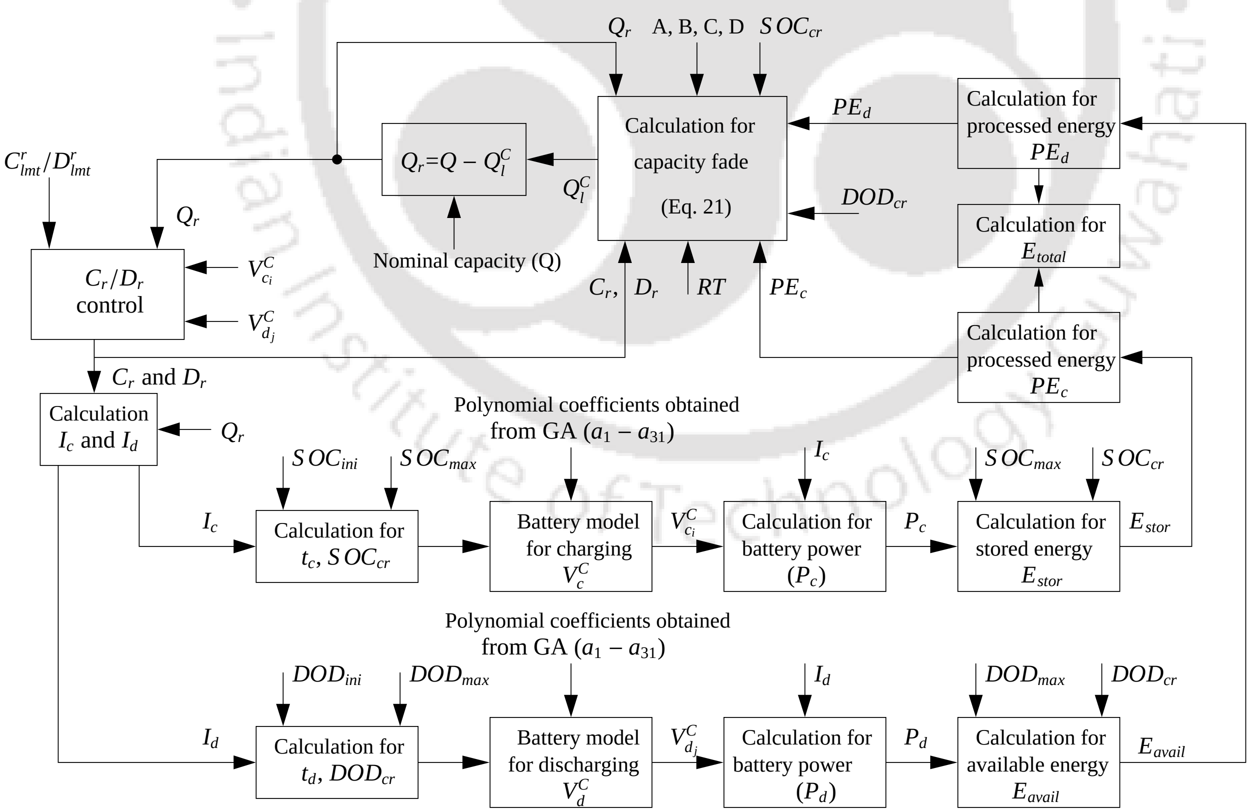

Figure 2.10: Block diagram of battery and capacity fade model.

Fig. 2.10 shows the detailed block diagram used to validate the proposed battery and capacity fade model. The battery manufacturers' charge/discharge rate characteristics have been extracted using the mathematical equations described in Section 2.2. Fig. 2.10 has two loops: the inner loop computes charging process and the outer loop computes discharging process. The control algorithm decides the amount of energy stored into the battery or extracted from the battery based on the current energy status and user defined C_r/D_r limit of the battery. The input of the control algorithm are: charge/discharge current, SOC/DOD limits and polynomial coefficients for charging/discharging scenario ($a_1 - a_{31}$). Based on these inputs, the BM calculates SOC_{cr}/DOD_{cr}, charge/discharge voltage ($V^C_{c_i}/V^C_{d_j}$), current (I_c/I_d), power (P_c/P_d) and energy (PE_c/PE_d). Capacity loss is calculated using energy of the battery, pre-exponential factor, gas constant, temperature and adjustable factor.

2.5 Model Validation

The battery and capacity fade models explained in section 2.2 and 2.4 have been compared with manufacturers' catalogue to validate its performance. An extensive simulation study has been performed with the proposed models. Comparison with four real-time batteries such as EIG, Sony US18650, Panasonic and Sanyo is provided to show the superiority of the models. The specifications of these batteries are given in Table 2.3. Due to unavailability of the manufacturer data, the models are compared with low voltage and ampere-hour ratings. The results have been discussed in two parts. In the first part, the validation of battery model has been carried out with four battery manufactures' data. The capacity fade results are analyzed in the second part.

Table 2.3: Specifications of batteries

Battery Name	Voltage(V)	Capacity(Ah)	C_r	D_r
EIG	2.5	8	1 & 4	1 & 4
Sony US18650	3.7	1.4	1 & 2	1 & 2
Panasonic	4.5	0.83	1 & 0.94	1 & 1.88
Sanyo	3.7	1.5	1 & 2	1 & 2

The performance of batteries from different manufacturers are analyzed separately. Comparison have been done for calculated and measured (catalogue value) characteristics of different batteries. The dotted line represents the measured (catalogue value) data from the battery manufacturers' catalogue and solid line denotes the proposed battery model characteristics.

2.5.1 Performance Characteristics of BM

Case (i) - EIG Battery: Fig. 2.11 shows the comparison of battery characteristics with 2.5V, 8Ah EIG battery at $1C_r/1D_r$. The charging and discharging voltage with respect to SOC_{cr} and DOD_{cr} are shown in Figs. 2.11 (a) and (b). The simulations are observed for different SOC_{cr} and DOD_{cr} values from 0-100% and 100%-0%. The end of charge value (EOCV) is 4.3V and end of discharge value (EODV) is 1.3V. It is observed from Figs. 2.11 (a) and (b), the end of charge and discharge voltages are higher and lower with respect to increase in SOC_{cr} and DOD_{cr}.

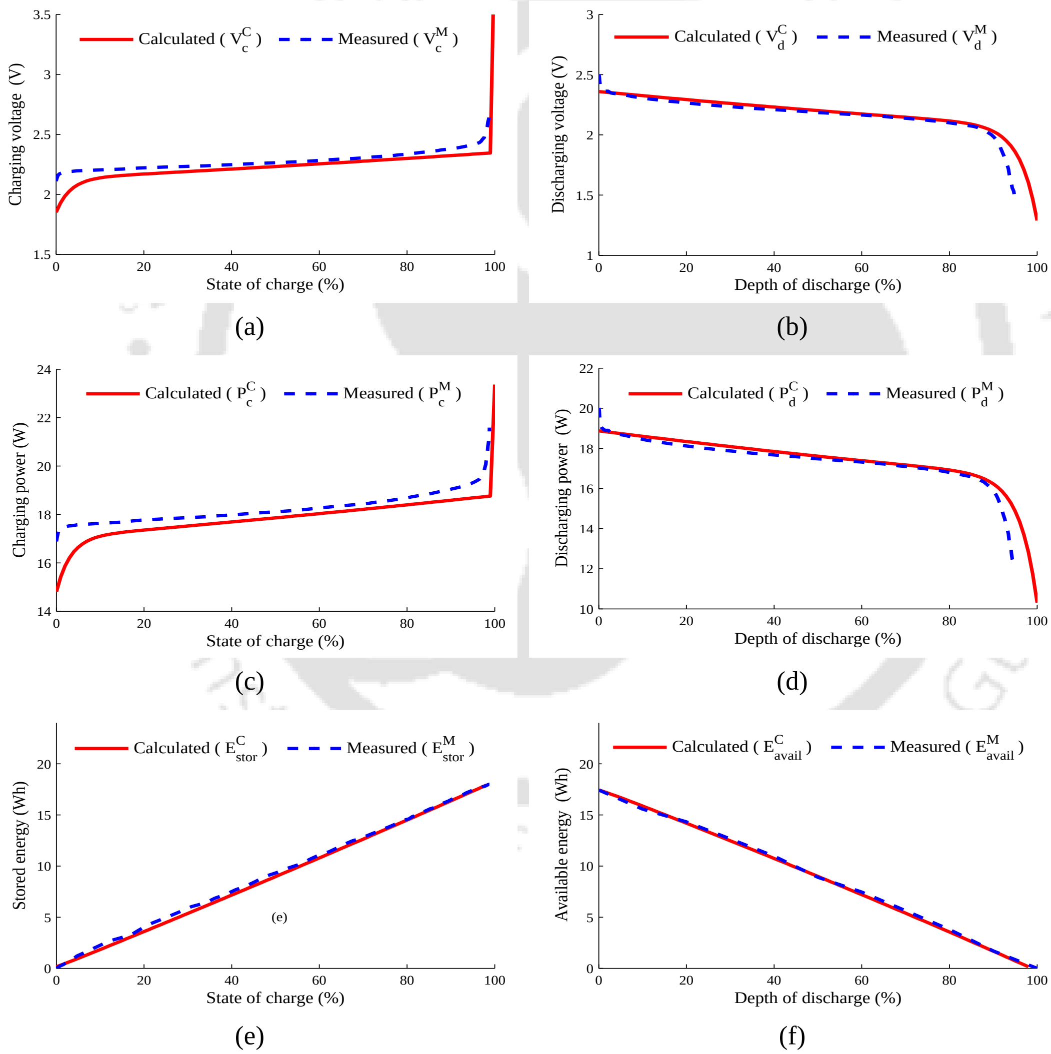

Figure 2.11: Comparison of proposed model result with EIG battery at $1C_r$ and $1D_r$.

It is observed from Figs. 2.11 (a) and (b), for large DOD_{cr} value the EODV is lower, while for large SOC_{cr} value the EOCV is higher. The initial portion of the curve is linear in fashion and after certain period it has varied. The comparison of charging (P_c) and discharging (P_d) power with respect to SOC_{cr} and DOD_{cr} are shown in Figs. 2.11 (c) and (d). Figs. 2.11 (e) and (f) show the comparison of charging (E_c) and discharging (E_d) energy with respect to SOC_{cr} and DOD_{cr}. It is clear from these plots that energy and power values are maximum at the end of SOC_{cr} and DOD_{cr} value.

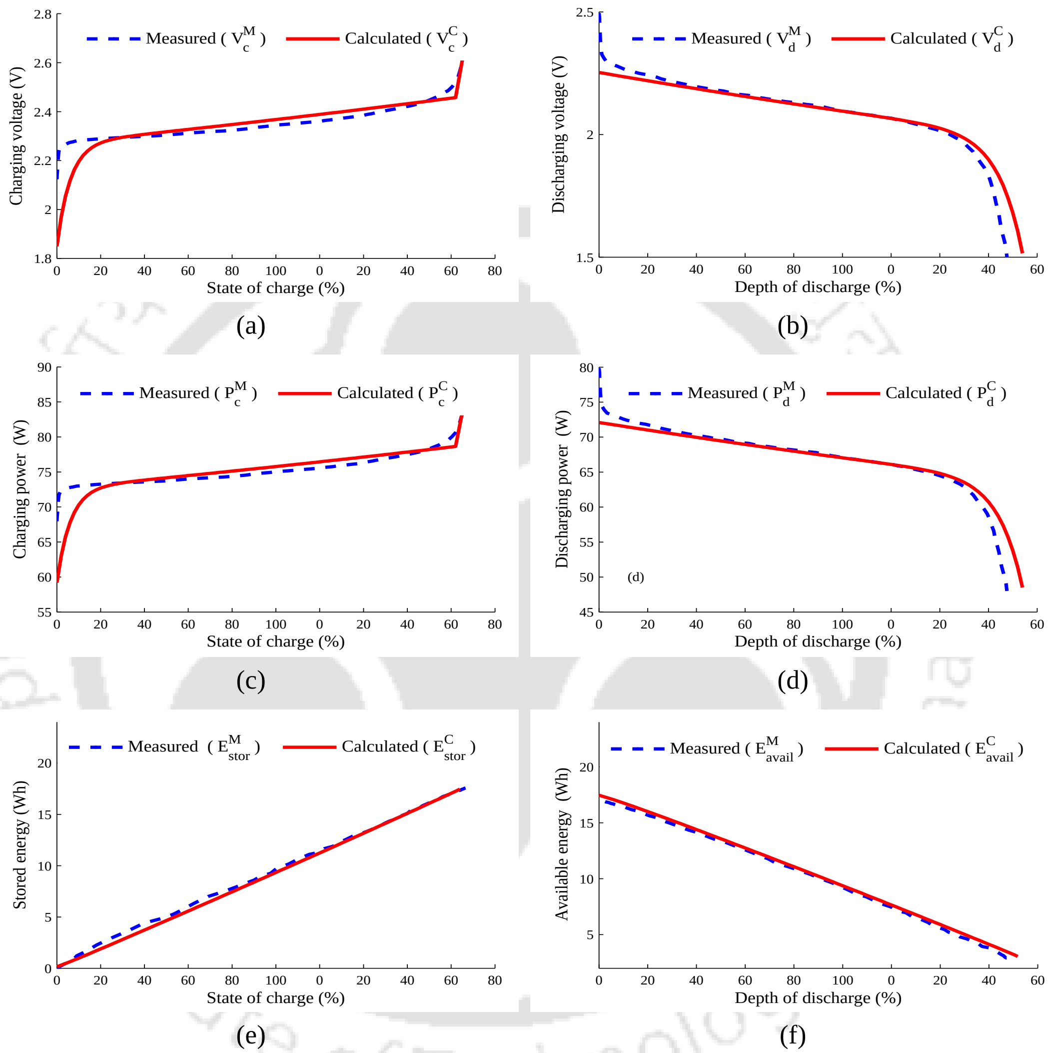

Figure 2.12: Comparison of proposed model result with EIG battery at $4C_r$ and $4D_r$.

Fig. 2.12 shows the comparison results of battery performance at $4C_r/4D_r$. The EOCV and EODV for this case is 2.75V and 1.5V. As can be seen in Fig. 2.11 (a) and Fig. 2.12 (a), for constant current charging the charging voltage is equal to the battery terminal voltage. However, in discharging case, it has an additional voltage drop. The comparison of P_c, P_d, E_{stor}, E_{avail} with respect to SOC_{cr} and DOD_{cr} at $4C_r$ and $4D_r$ are shown in Figs. 2.12 (c) - (f). It can be observed that the energy extracted from the battery is inversely proportional to D_r and directly proportional to battery voltage and current.

Notably for high C_r/D_r, the energy stored/extracted to/from the battery can be done in a short period of time, while for low C_r/D_r it takes long time. This affects the net energy stored/extracted from/to the battery. The time taken to charge or discharge the battery at $4C_r$ or $4D_r$ takes only $0.333hr$, while for $1C_r$ or $1D_r$ it requires 1hr.

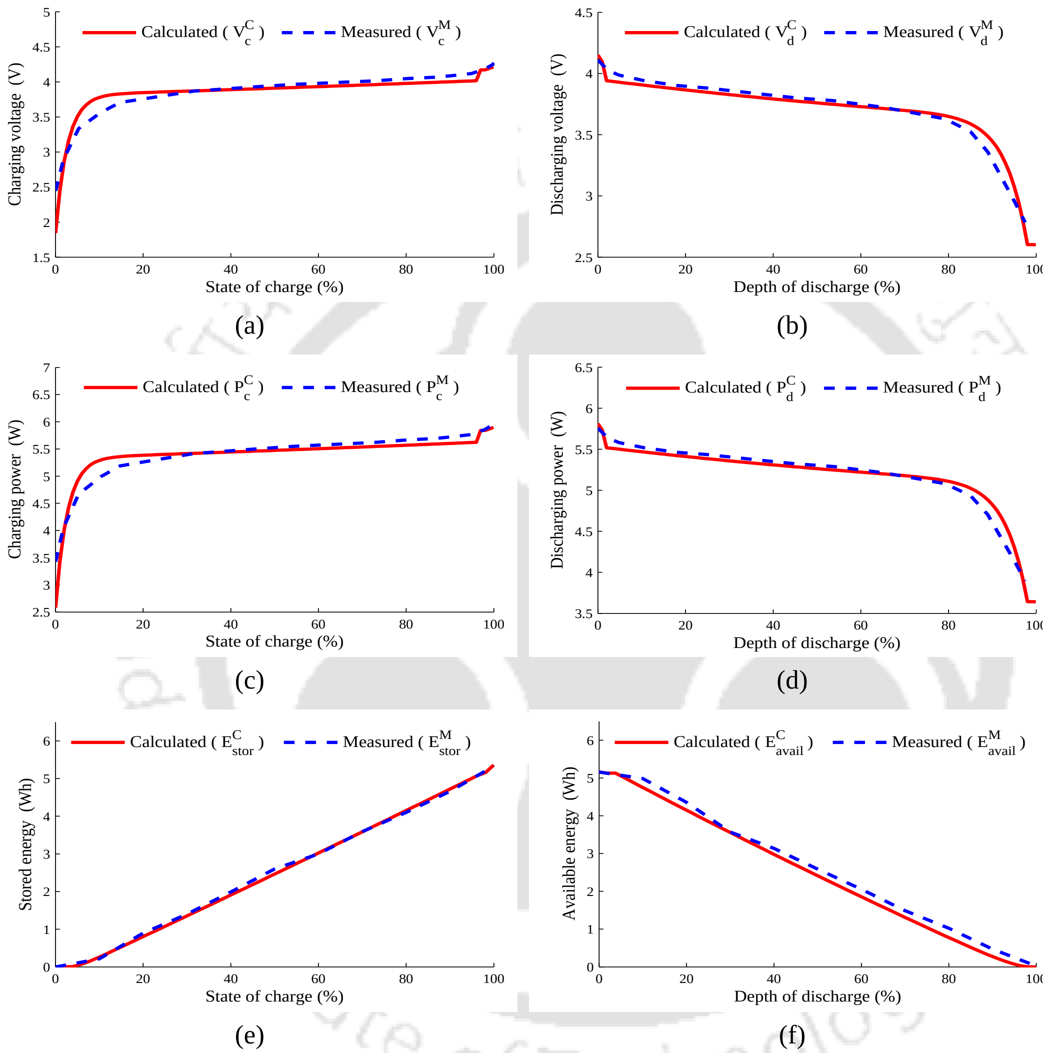

Figure 2.13: Comparison of proposed model result with Sony US18650 battery at $1C_r$ and $1D_r$.

Case (ii) - Sony US18650 Battery: Fig. 2.13 shows the comparison of battery characteristics with 3.7V, 1.4Ah Sony US18650 battery. Figs. 2.13 (a) and (b) show the simulated characteristics of terminal voltage plotted with SOC_{cr} and DOD_{cr}. It can be seen from these figures, EOCV and EODV for Sony battery are 4.1V and 2.7V. The results of battery power and energy shown in Figs. 2.13 (c) - (f) for charging and discharging cases are in good agrement. It is observed from Figs. 2.12 (e) the maximum stored energy is 17.46Wh, however in Figs. 2.12 (f) the initial extracted energy is only

17.32Wh due to capacity loss in the battery.

Fig. 2.14 shows the comparison of performance characteristics of Sony US18650 battery with $2C_r$ and $2D_r$ at 2.8A. The terminal voltage curves for charging and discharging scenarios are shown in Figs. 2.14 (a) and (b). The EOCV and EODV observed in this case are 4.42V and 2.5V. The comparison of battery power (P_c, P_d) and energy (E_{stor}, E_{avail}) with the manufacturers' data are shown in Figs. 2.14 (c) - (f). As it can be seen from Figs. 2.14 (e) - (f), the amount of energy stored into the battery and extracted (available) from the battery has reduced with respect to SOC_{cr} and DOD_{cr}.

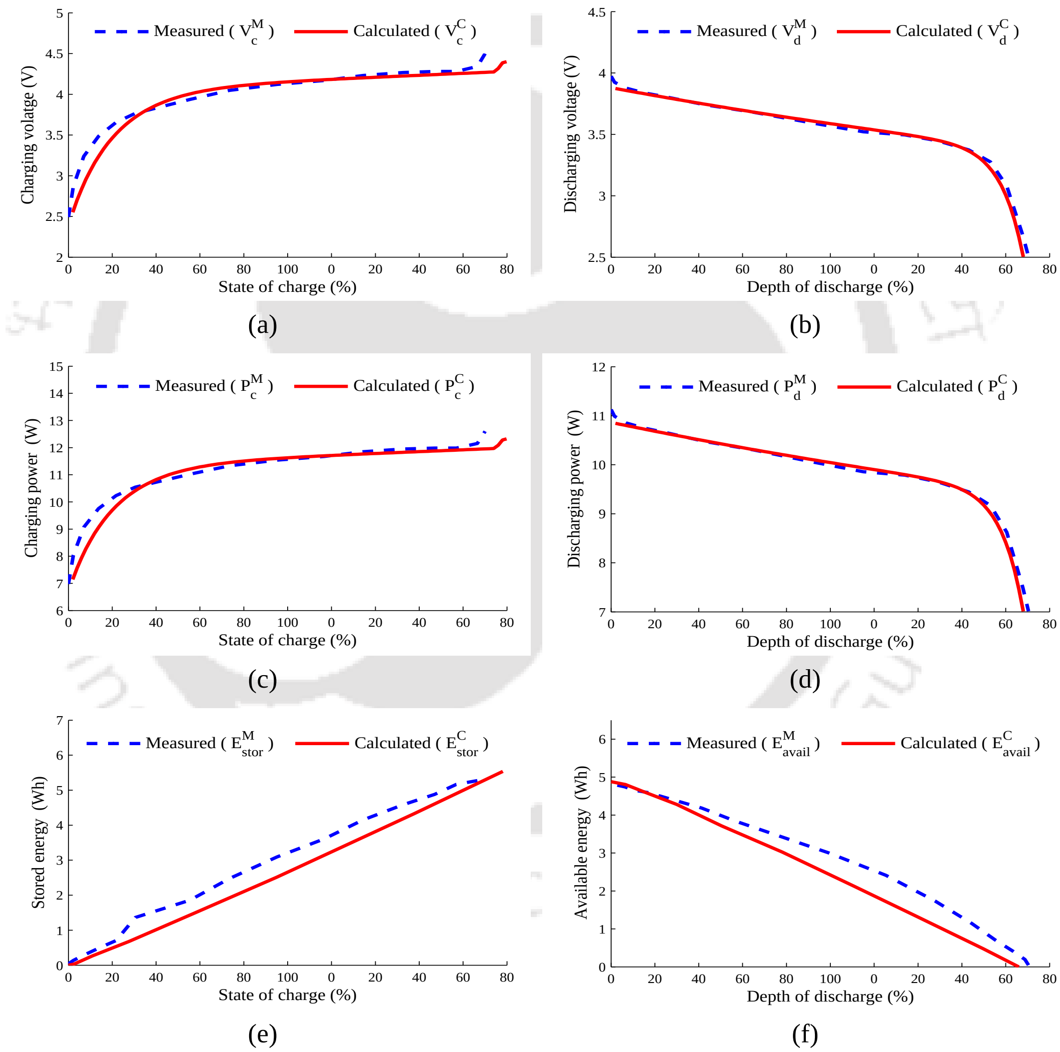

Figure 2.14: Comparison of proposed model result with Sony US18650 battery at $2C_r$ and $2D_r$.

Case (iii) - Panasonic Battery: Fig. 2.15 shows the comparison results with 4.5V, 0.83Ah Panasonic battery at $1C_r$ and $1D_r$. The terminal voltage characteristics with respect to SOC_{cr} and DOD_{cr} at $1C_r$ and $1D_r$ are shown in Figs. 2.15 (a) and (b). The EOCV and the EODV of this case are 4.3V and 3V. Figs. 2.15 (c) - (f) show the performance characteristics of battery power and energy. In all the cases, the measured (catalogue value) data agrees with the proposed data.

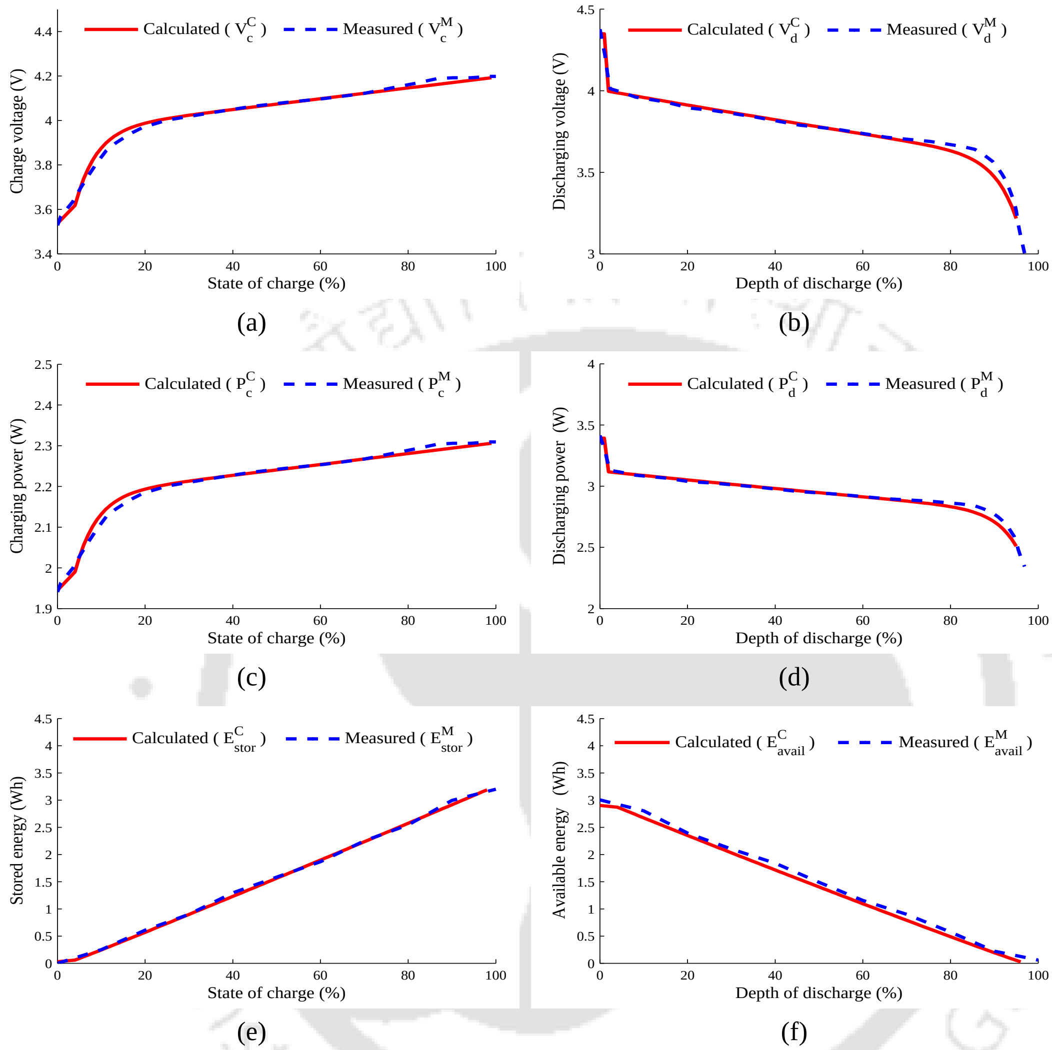

Figure 2.15: Comparison of proposed model result with Panasonic battery at $1C_r$ and $1D_r$.

The comparison of Panasonic battery with proposed model is shown in Fig. 2.16. Figs. 2.16 (a) and (b) show the comparison of terminal voltage characteristics with $0.9398C_r$ at 0.78A and $1.8795D_r$ at 1.56A. The charge and discharge voltage characteristics are shown in Figs. 2.16 (a) and (b). The EOCV and EODV observed in this case are 4.3V and 3V. Figs. 2.16 (c) and (d) show the performance of battery power. The amount of stored and available energy are shown in Figs. 2.16 (e) and (f).

Case (iv) - Sanyo Battery: The battery used in this case for comparison is Sanyo which has a nominal capacity 1.5Ah and a voltage of 3.7V. Here the battery is charged and discharged with a constant current of 1.5A. Figs. 2.17 (a) and (b) show the terminal voltage curves of charge and

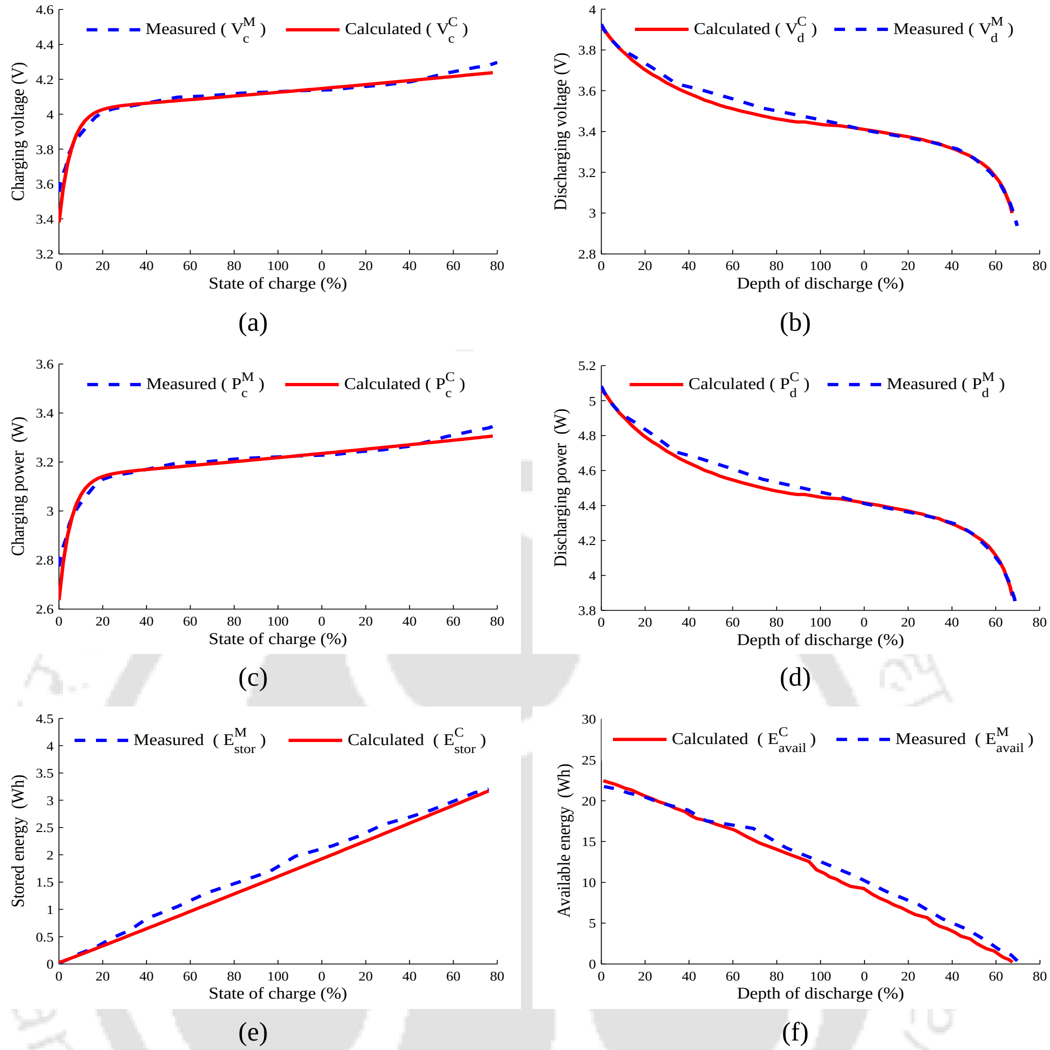

Figure 2.16: Comparison of proposed model result with Panasonic battery at $0.9398C_r$ and $1.8795D_r$.

discharge characteristics. As can be seen from the plots, the EOCV and EODV in this case are 4.3V and 2.5V. In this figures, the variation of SOC_{cr} and DOD_{cr} value has reflected in the charging and discharging voltage. The performance of power and energy characteristics are shown in Figs. 2.17 (c) - (f). The stored and extracted energy is maximum at very first cycle which is given in Fig. 2.17 (e) and Fig. 2.17 (f). The amount energy exchange is reduced after n_{th} cycle due to capacity fade which is given in Fig. 2.22 (a).

Fig. 2.18 shows the comparison of measured (catalogue value) and calculated characteristics of Sanyo battery of $2C_r/2D_r$ at 3A. The EOCV and EODV observed in this case are 4.02V and 2.5V. Figs. 2.18 (c) and (f) show the characteristics of charging and discharging battery power and energy (P_c, P_d, E_{avail} and E_{stor}) at $2C_r$ and $2D_r$. The t_c required to store the energy in the EV battery is

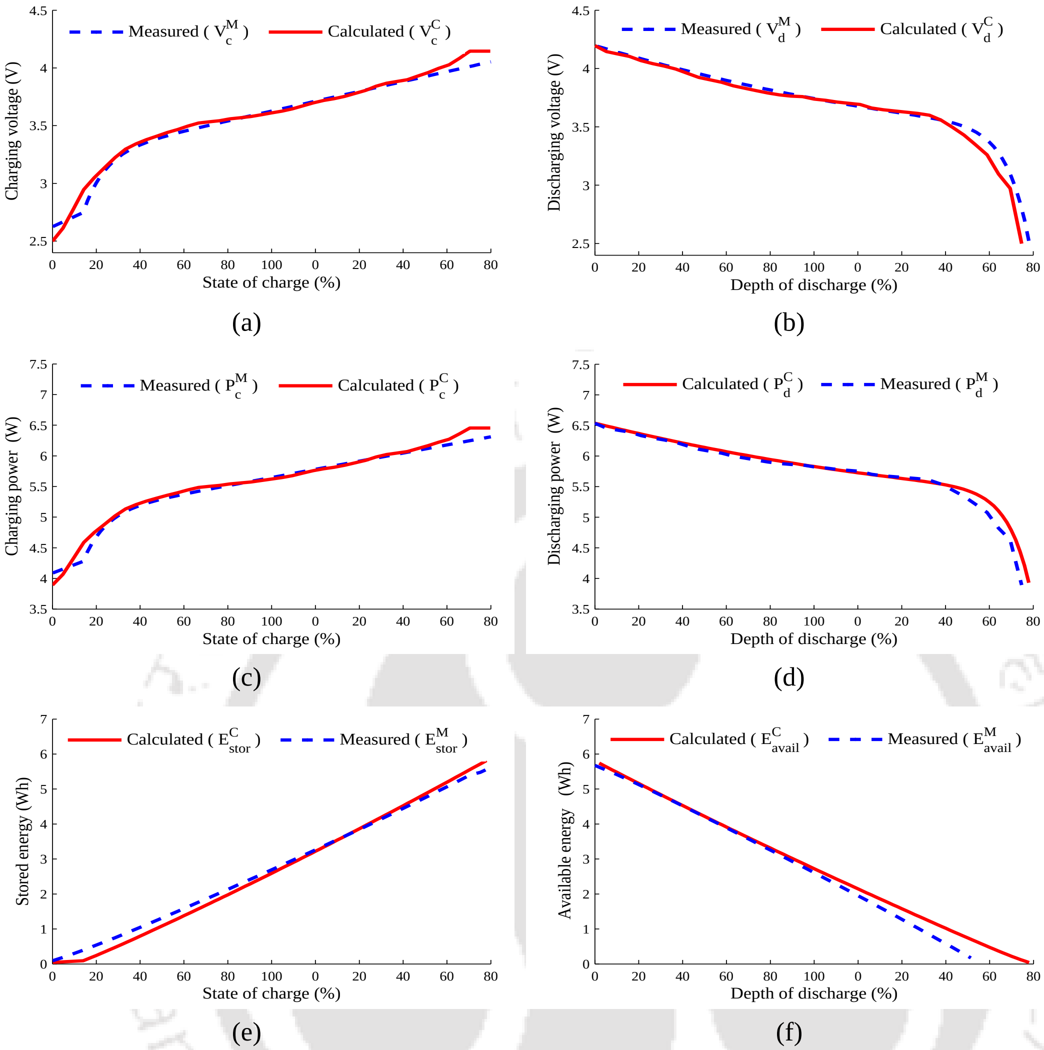

Figure 2.17: Comparison of proposed model result with Sanyo battery at $1C_r/1D_r$.

reduced due to high C_r which is shown in Fig 2.18 (e). It is observed from Fig. 2.18 (f) the energy extracted from the battery is reduced due to the high D_r.

Thus, it is observed from Fig. 2.11 to Fig. 2.18, the proposed battery model characteristics exactly fits the manufacturers' characteristics and in some cases it has an error less than 5%.

2.5.2 Capacity Fade Analysis

The validation of capacity fade study has also been carried out by comparing the proposed model with four manufacturers' data. The capacity loss data is taken from the battery catalogues provided by the battery manufacturers. However, due to limited availability of measured (catalogue value) data, the comparison has been done only for specified charge and discharge rate. Fig. 2.19 to Fig.

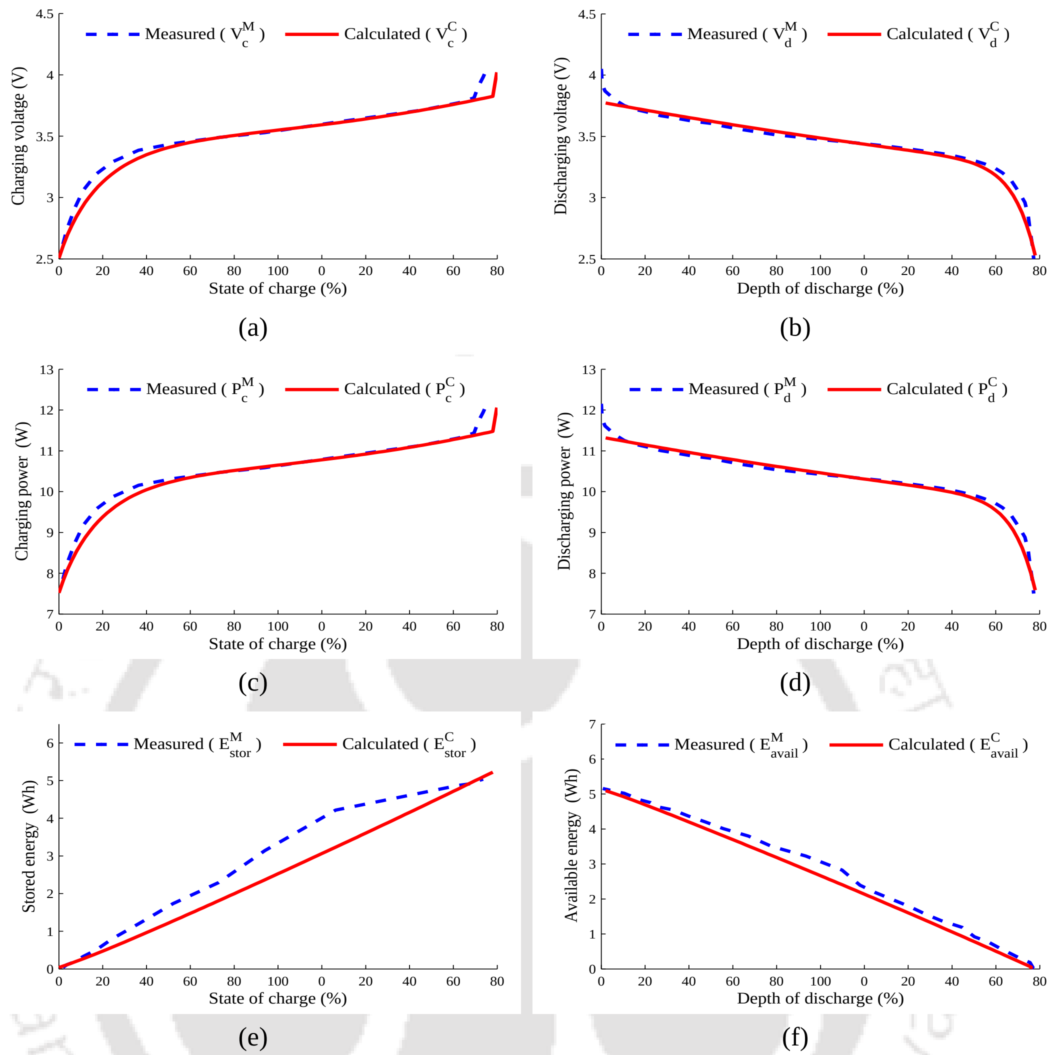

Figure 2.18: Comparison of proposed model result with Sanyo battery at $2C_r/2D_r$.

2.22 reports the results obtained from capacity fade study. The parameters of capacity fade analysis have been taken from the capacity loss data provided by the battery manufacturers' catalogue. Due to limited data, the capacity loss comparison only done for specified charge and discharge rate. Due to unavailability of the battery manufacturers' capacity loss data at different C_r and D_r, only specified C_r and D_r is discussed in this work. The results obtained after n number of cycle for each types of batteries are summarized from Table 2.4. The variation of capacity loss is shown with respect to cycle number and total processed energy. The remaining capacity of the battery has been given in each case to show the net processed energy.

Case (i) - EIG Battery: Fig. 2.19 shows the comparison of capacity fade characteristics of EIG battery. Figs. 2.19 (a) shows the capacity loss as a function of cycle number for EIG battery.

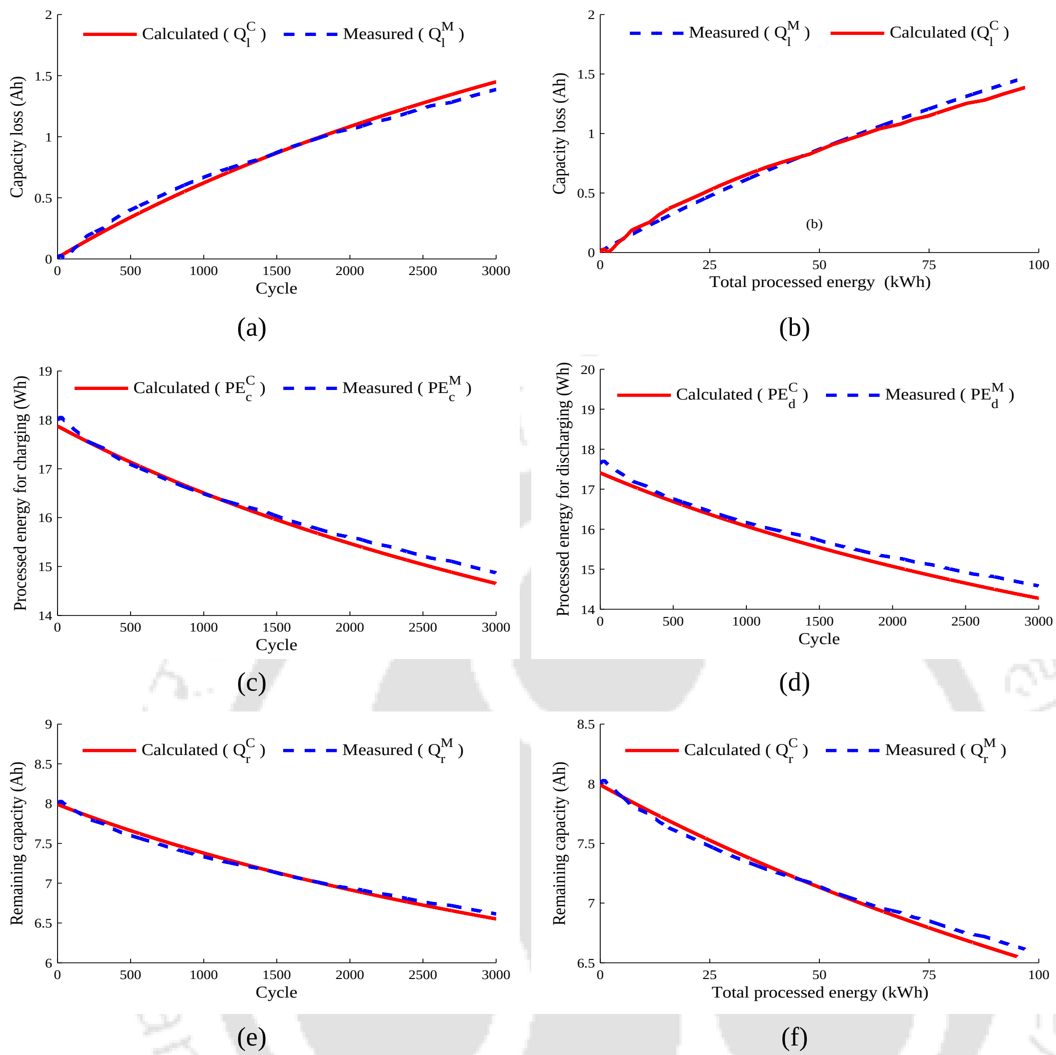

Figure 2.19: Capacity loss characteristics of EIG battery.

In Fig. 2.19 (b), the capacity loss is observed as a function of total processed energy. As it can be seen in Figs. 2.19 (a) and (b), the capacity loss as a function of cycle number and processed energy has a rising behavior. Figs. 2.19 (c) and (d) show the required and available energy plots with respect to cycle number. The observation is done till 3000 cycles to check the increase and degradation of charge and discharge energy. This results indicate, the charge and discharge rate plays a strong role in determining the capacity fade of batteries. Figs. 2.19 (e) and (f) show the remaining capacity curve as a function of cycle number and total processed energy.

Case (ii) - Sony US18650 Battery: The measured (catalogue value) and calculated capacity fade characteristics of Sony US 18650 is shown in Fig. 2.20. In this case, the capacity fade study has been observed for 300 cycles. The capacity fade as a function of cycle number and total processed energy are shown in Figs. 2.20 (a) and (b).

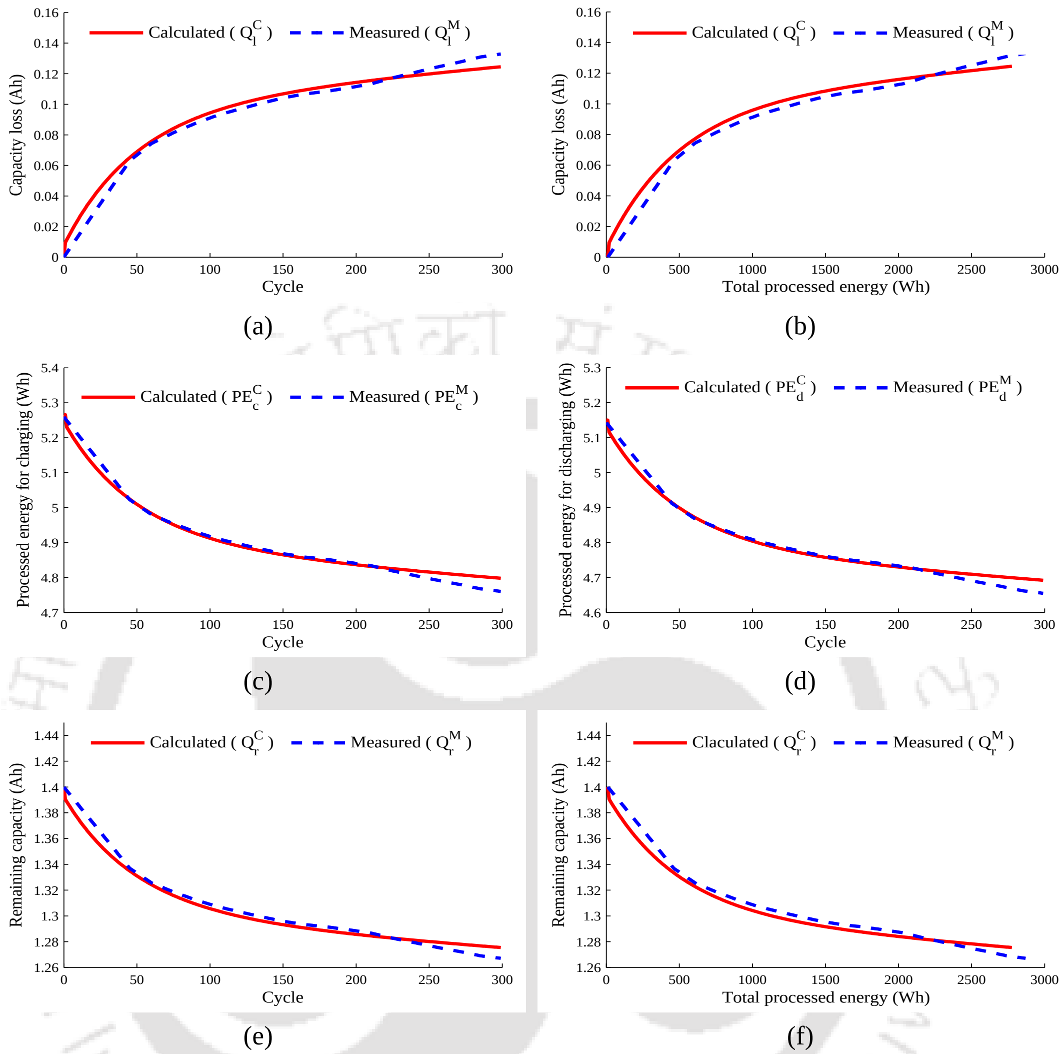

Figure 2.20: Capacity loss characteristics of Sony US18650 battery.

Figs. 2.20 (c) and (d) show the characteristics of charge and discharge energy as a function of cycle number, while the characteristics of remaining capacity and total processed energy are shown in Figs. 2.20 (e) and (f). It is noticed from the plots, the energy and remaining capacity of battery with increase in cycle has a falling behavior.

Case (iii) - Panasonic Battery: Fig. 2.21 shows the measured (catalogue value) and calculated characteristics of capacity fade for Panasonic battery. Here the study has been done till 500 cycles. Figs. 2.21 (a) and (b) show the capacity loss as a function of cycle number and energy. The capacity loss as a function of total processed energy is shown in Fig. 2.21 (b).

The characteristics of required and available energy as a function of cycle number are shown in Figs. 2.21 (c) and (d). It can be seen, the energy stored or extracted from or to the battery has decreased with increased in cycle number due to capacity loss. Figs. 2.21 (e) and (f) show the remaining capacity curve as a function of cycle number and total processed energy. As like previous cases, the energy and capacity loss characteristics have falling behavior with increase in cycle number and processed energy.

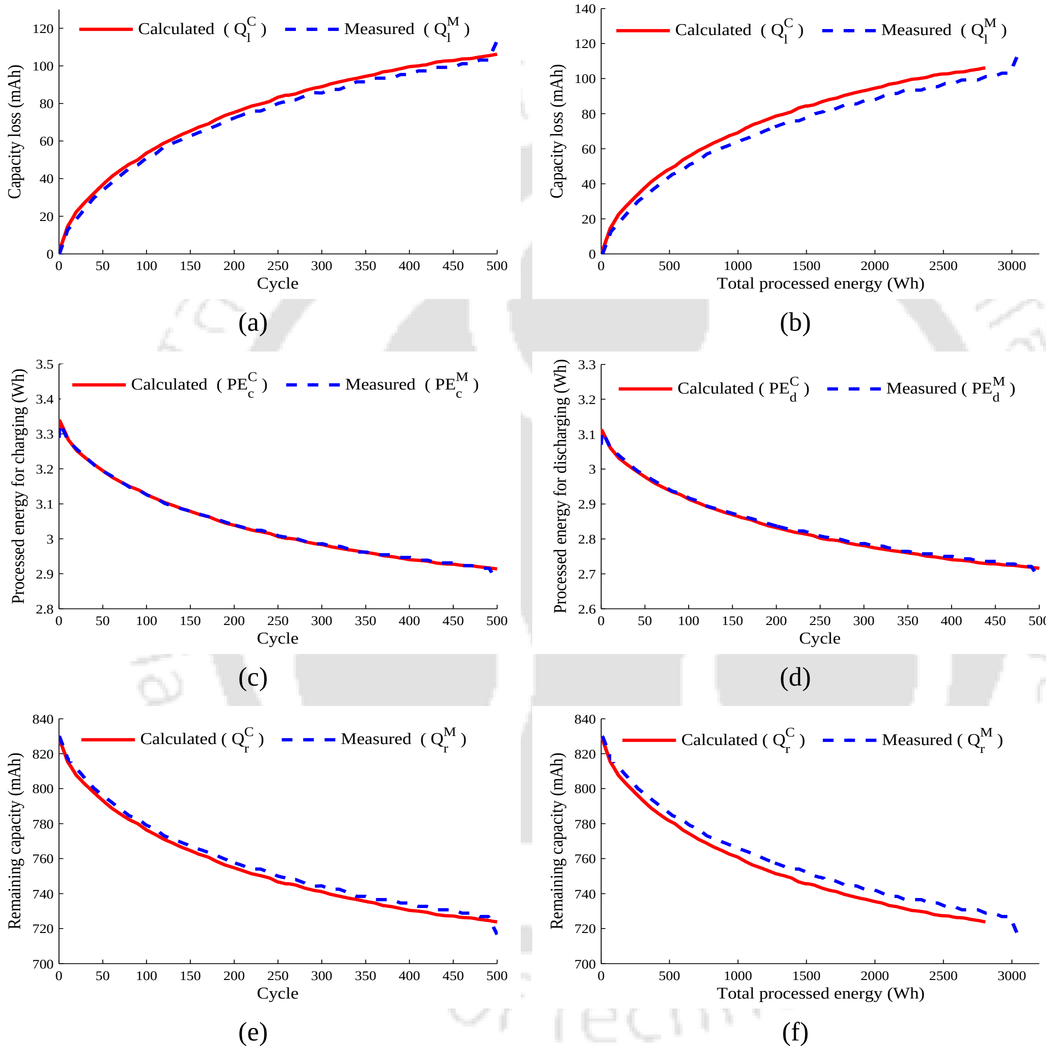

Figure 2.21: Capacity loss characteristics of Panasonic battery.

Case (iv) - Sanyo Battery: Fig. 2.22 shows the comparison of capacity fade profiles of Sanyo battery. The capacity loss as a function of cycle number and total processed energy are shown in Figs. 2.22 (a) and (b). As can be seen from these plots, the characteristics have rising behavior with respect to cycle and total processed energy.

Figs. 2.22 (c) and (d) show the characteristics of required and available energy as a function of

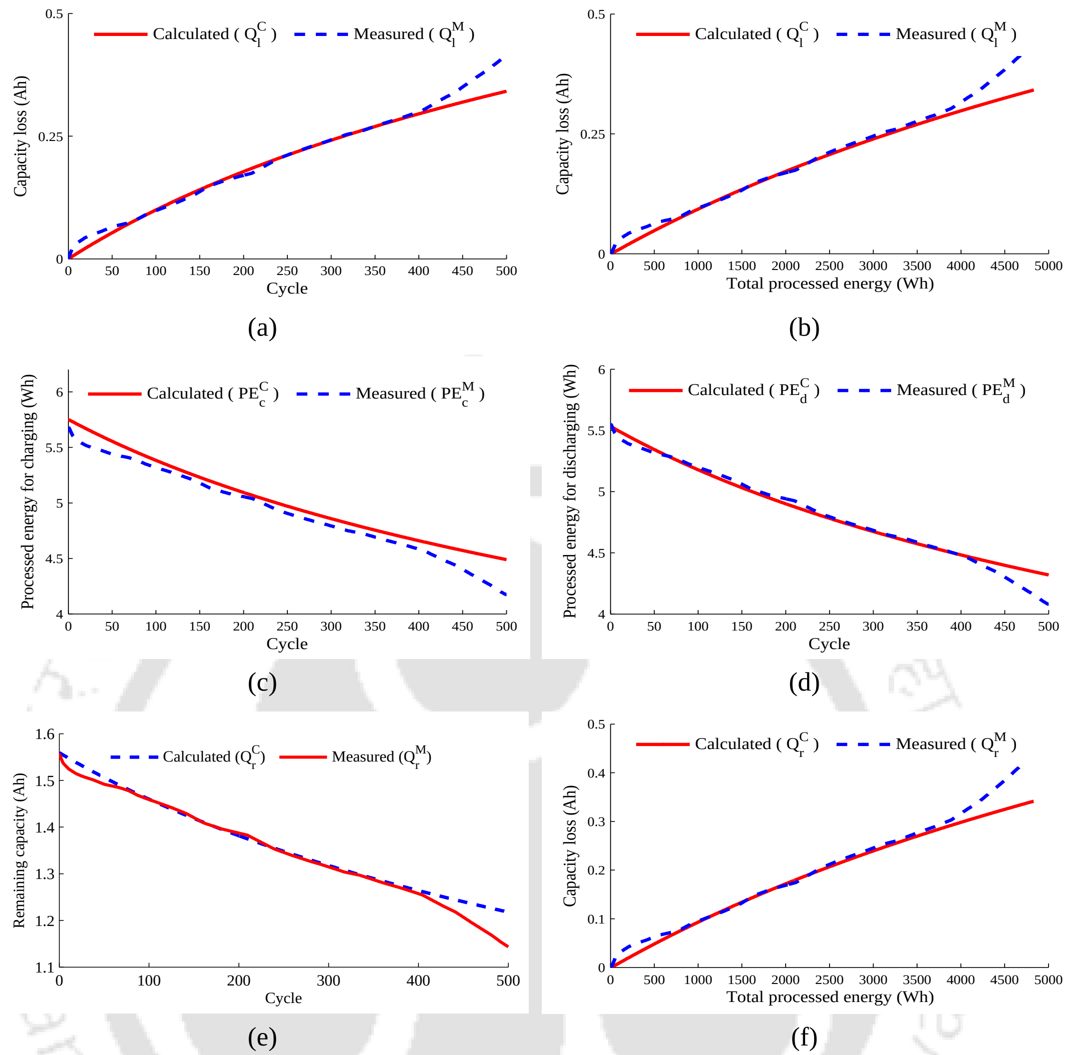

Figure 2.22: Capacity loss characteristics of Sanyo battery.

cycle number. The values are observed for 500 cycles to check its performance. The comparison of remaining capacity curve as a function of cycle number and total processed energy are shown in Figs. 2.22 (e) and (f).

Table 2.4: Results obtained from battery and capacity fade model.

Manufacturer →	EIG (2.5V, 8Ah)		Sony (3.7V, 1.4Ah)		Panasonic (4.5V, 0.83Ah)		Sanyo (3.7V, 1.5Ah)	
Parameter ↓	Measured	Calculated	Measured	Calculated	Measured	Calculated	Measured	Calculated
Q_r (Ah)	6.61	6.55	1.27	1.28	0.73	0.72	1.14	1.22
Q_l (Ah)	1.39	1.45	0.13	0.15	0.12	0.10	0.41	0.15
E_{total} (kWh)	94.98	95.12	2.87	2.78	3.04	2.81	4.67	4.83
E_{stor} (kWh)	14.87	14.65	4.76	4.79	2.88	2.9	4.18	4.49
E_{avail} (kWh)	14.58	14.27	4.65	4.69	2.69	2.72	4.08	4.32
1^{st} cycle E_{stor} (kWh)	17.99	17.89	5.33	5.36	3.19	3.19	5.55	5.81
1^{st} cycle E_{avail} (kWh)	17.53	17.43	5.15	5.16	3.01	2.95	5.67	5.74

It can be observed from Fig. 2.19 to Fig. 2.22, the capacity fade model characteristics exactly fits with the different battery manufacturers' curves. The typical simulation and measured (catalogue value) results of different battery types such as for EIG (till 3000 cycle), Sony (till 300 cycles), Panasonic (till 500 cycles) and Sanyo (till 500 cycles) are shown in Table 2.4.

2.6 Summary

- In this Chapter, an accurate electric circuit based battery and capacity fade model have been proposed.
- The battery parameters are extracted using genetic algorithm based optimization method which optimize the polynomial coefficients.
- Different performance characteristics like charge voltage, discharge voltage, power, energy, total processed energy and capacity loss are analyzed.
- Four different battery manufacturers' data are used for validating the result.
- The proposed battery and capacity models are simple and it accurately represents the measured (catalogue value) charge and discharge curves of the manufacturers' data sheets.
- The simulation and measured (catalogue value) results are in good agreement.
- BM and CFM has been developed to analyze the power flow between EVs' batteries and grid.

In the next Chapter, a charging station has been developed by using the battery model for grid support during the peak load demand and charge the EVs' batteries during the peak shaving hours. The charging station connected with the distribution node of the grid with bidirectional contactless charging system which enables the power transfer between the EVs' batteries and grid.

Note: This work, Mathematical Modeling of Li-Ion Battery Using Genetic Algorithm Approach for V2G Applications has been published in IEEE Transaction on Energy Conversion.

3

Modeling and Control of Contactless based Smart Charging Station in V2G Scenario

Contents

3.1 Introduction

Contactless charging systems are preferable for electric vehicle applications due to the elimination of direct electric contacts. These charging system overcomes the drawbacks of traditional wired charging systems such as heating of the sockets and cables, risk of fire and electrical injuries, cable breakage etc., [2, 92]. Indeed, EVs' batteries have enough potential to be used as distributed energy storage through multi-point bidirectional contactless charging system (BCCS), which are proven to be the most efficient and compatible technologies for an improved power system operation [82,158,159]. This bidirectional power flow functionality of BCCS module can be referred as grid-to-vehicle and vehicle-to-grid capability [159]. Many studies have been conducted on V2G system with most of the work focused on the impact of charging systems on the distribution network [66, 73, 160]. Some simulation studies have shown EVs acting as a smart storage and can provide fast and accurate response for frequency and spinning reserves [73, 160]. However, these studies have only done the system level analysis and are mainly focused on the frequency and voltage regulation. On the other hand, present area work on multi-point contactless systems are mainly focused on converter configurations, compensation circuits and control strategies of those systems [2, 82, 92, 158, 159]. These works have studied the component level description of BCCS systems. However, none of the studies have attempted to study the control and coordination of BCCS unit with multiple EVs in a charging station (CS) connected to a distribution node (DN) of the grid. To overcome the above shortcomings, the present work is mainly focussed on the following objectives:

(i) Developing a multi-point BCCS with its controllers to control the power flow during V2G and G2V operations.

(ii) Developing the controllers and CS aggregator, to obtain the control and coordination of large fleet of EVs with respect to the variations in the DN voltage.

In detail, this Chapter describes a multi-point BCCS unit present in a CS connected with the DN of the grid is investigated. A multi-point BCCS unit has various charging points, which are accessible to multiple EVs. However, a large fleet of EVs with different battery charging/discharging rates (in this Chapter the charge rate (C_r) and discharge rate (D_r) is referred as C_{rate} for simplicity) in BCCS units, distributed across a power grid network may stress the power system operation which results in extensive grid outages [66, 73, 74, 160]. In such case, the BCCS unit should necessarily have a controlled and coordinated smart charging station (SCS) as shown in Fig. 3.1.

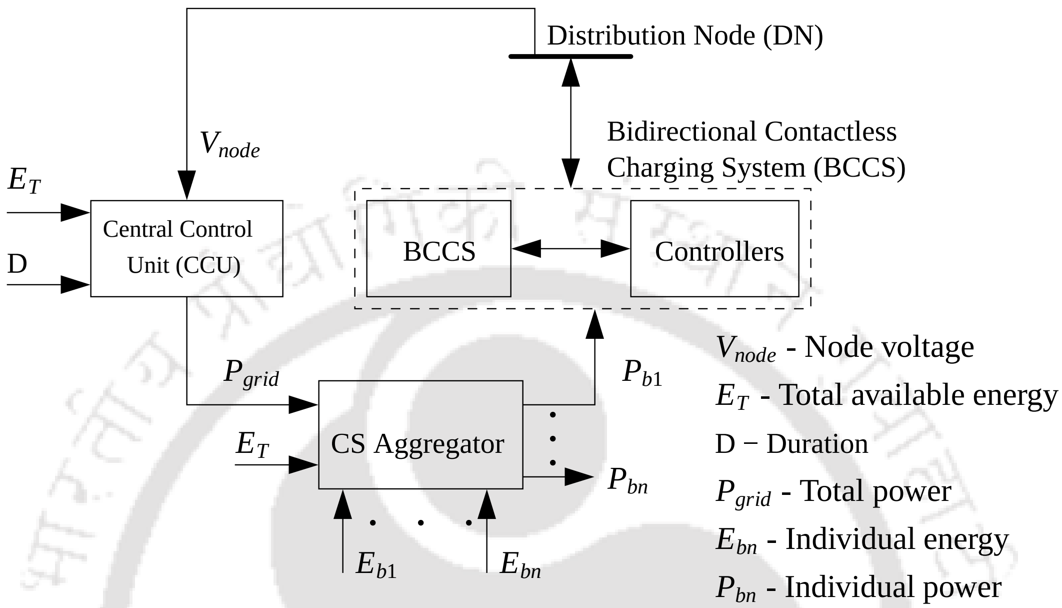

Figure 3.1: Smart charging station architecture.

The purpose of SCS is to distribute the power among different EVs, control the C_{rate} of EVs' batteries and to ensure grid voltage stability. In particular, the SCS will have the ability to receive and respond the charge/discharge instruction based on grid condition and the individual energy of EVs' batteries. The SCS developed has a main controller named as central control unit (CCU) and a Charging Station aggregator called as CS aggregator, which distributes the power requirement based on the energy demand and grid conditions. Apart from these controllers, a closed loop control strategy has been developed inside the BCCS module, which controls the power flow during charging/discharging operations based on CS aggregator output. The performance of the BCCS module and the control scheme is tested with multiple EVs of different battery ratings and are evaluated by simulation considering a practical distribution system of Guwahati city, Assam, India [74]. Although the present work is modeled for contactless based charging station but the proposed concept can be applied to any multi-point charging station as well.

The rest of the sections in the Chapter are organized as follows. Section 3.2 describes the modeling of multi-point SCS. Section 3.3 explains the details of problem formulation. An application scenario of multi-point SCS is presented in Section 3.4. Simulation results are discussed in Section 3.5. Finally, summary of the present work is given in Section 3.6.

3.2 Modeling of Multi-Point Smart Charging Stations

The EVs are consuming comparatively high power from the grid during charging. Therefore, uncoordinated charging of a large number of EVs gives an adverse impact in the grid [26,32]. One best possible solution can be to ramp-up the power generation but this will lead to significant infrastructure cost of the power plants. As an alternative cost-effective solution, grid allows EVs to coordinate their charging or discharging operations. This coordination amongst EVs facilitates avoiding grid overload and balancing supply/demand potential of the grid. Therefore, in this Chapter multi-point SCS has been modeled for coordinating multiple EVs present in the CS.

3.2.1 Distribution Network Model

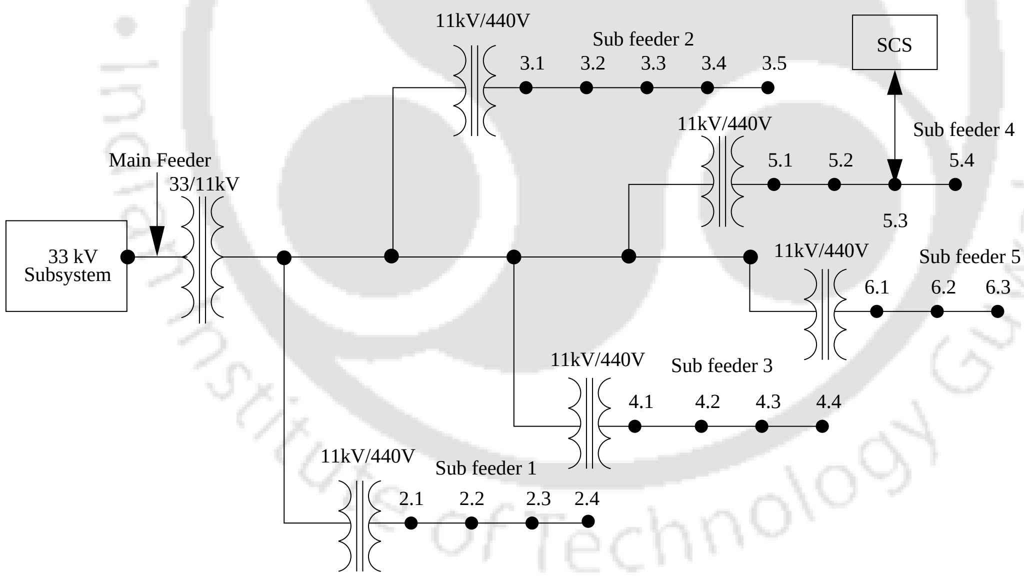

Figure 3.2: Radial distribution system of Guwahati city.

The practical grid data of typical network of Guwahati city has been taken in this work, which is shown in Fig. 3.2 [74]. This network is a reduced system of substation which consists of 33/11kV, 5MVA as the main feeder and the entire radial sub feeders have 11kV/440V, 500kVA transformers. The off-peak hour load was assumed to be 60% of peak hour load. The resistance and reactance of the lines are 0.0027p.u and 0.0024p.u, respectively. The location of SCS considered for test condition is connected in the distribution network at the node **5.3**, as shown in Fig. 3.2. Table 3.1 shows the existing peak hour load of substation at different nodes.

Table 3.1: Existing load profile of the substation.

Nodes	P (p.u.)	Q (p.u.)	Nodes	P (p.u.)	Q (p.u.)
2.1	0.50	0.22	4.2	0.63	0.38
2.2	0.47	0.23	4.3	0.67	0.23
2.3	1.13	0.64	4.4	0.53	0.37
2.4	0.27	0.15	5.1	0.45	0.39
3.1	0.42	0.29	5.2	0.23	0.13
3.2	0.94	0.43	5.3	0.84	0.46
3.3	0.13	0.09	5.4	-	-
3.4	-	-	6.1	0.37	0.18
3.5	0.25	0.17	6.2	0.23	0.13
4.1	0.23	0.13	6.3	0.73	0.45

3.2.2 Multi-Point Smart Charging Station(SCS)

The layout of contactless based multi-point SCS is shown in Fig. 3.3. The proposed SCS has multi-charging points, where EVs' batteries of different ratings are connected. The individual charging points are contactless, bidirectional and it is connected to the DN of the grid via ac bus. Hence, it is called as BCCS. The complete architecture of SCS is divided into three units: the central control unit, the CS aggregator and the multi-point BCCS unit.

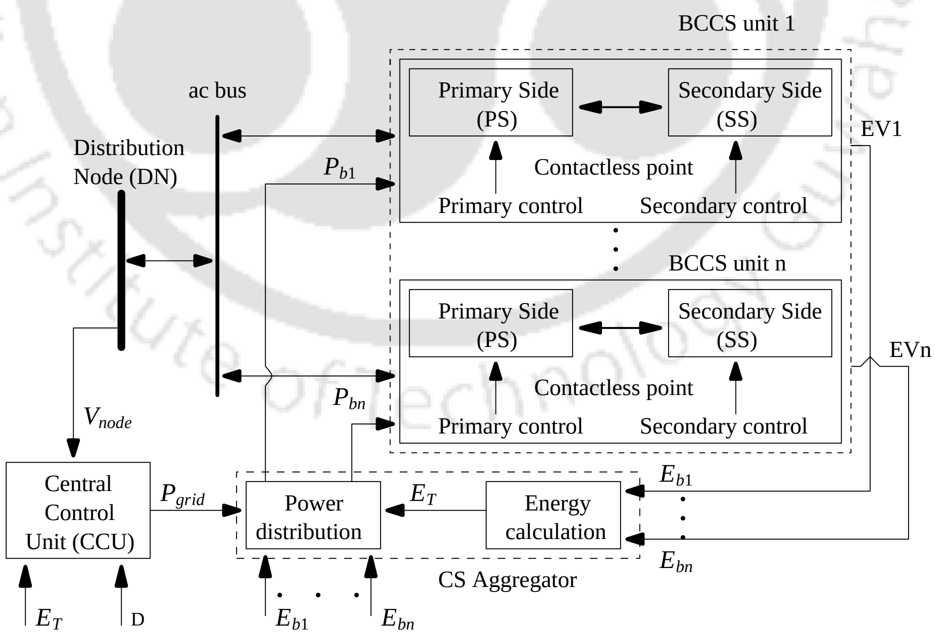

Figure 3.3: Layout of multi-point smart charging station.

The CCU decides the net power flow between the DN of the grid and the CS. The CS aggregator distributes the net power among the EVs' batteries. The CCU takes decisions of power flow (P_{grid})

based on three inputs: DN Voltage (V_{node}) of the grid, total energy availability (E_T) of SCS and duration in hours (D) to support the grid. The direction of P_{grid} can be either positive or negative. Positive power implies the CS will charge the EVs' batteries and negative power implies the CS has to support the grid. The P_{grid} obtained from CCU has to be distributed among the EVs by the CS aggregator. The CS aggregator takes individual energy available (E_{b1}, E_{b2},...E_{bn}) from each EVs' batteries, E_T of the SCS as well as P_{grid} and distributes the power among individual BCCS unit (P_{b1}, P_{b2}...P_{bn}). The distributed power can be either positive or negative depending upon the energy state of the batteries and P_{grid} as decided by CCU. The positive power allocated to the battery will get charged and the batteries with negative power will get discharged. The BCCS unit has two parts: the primary side and the secondary side (pick-up), which is separated by an air-gap and is magnetically coupled to each other. The power is transferred from the primary to the pick-up through weak magnetic coupling. Primary and secondary controllers are employed on either side of contactless coil, to control the power flow from G2V and V2G. Based on the information of power received from the CS aggregator, the controllers of the BCCS unit takes necessary action to control the C_{rate} of the battery. By this complete SCS arrangement, an EVs' batteries will be able to charge by absorbing power from the DN of the grid and supply the excess stored energy of EVs into the DN of the grid. The controllers present at the multi-point BCCS unit controls the power flow between individual EVs' batteries and DN of the grid.

3.2.3 EV Battery Model

Electric equivalent circuit (EEC) based battery model is used in this work for representing the real-time EVs' batteries, which is given in Fig. 2.3. The electrical parameters of EEC are represented by polynomial equation explained in Chapter 2 Section 2.2. The terminal voltage for charging/discharging scenario is given in Eq. (2.5) and Eq. (2.6). The EVs' batteries come to the SCS for both charging/ discharging operation. The batteries with excess energy (E_{avail}) would discharge and support the grid and EVs with less energy would charge (E_{stor}) by taking energy from the grid. The E_{stor} and E_{avail} are calculated from Eq. (2.13) and Eq. (2.14). The total energy (E_T) of SCS depends on the sum of stored energy into the battery and available energy to support the grid which is given in

Eq. (2.17).

3.3 Modeling of Smart Charging Station

The impact of EVs on DN and the quality of power in the node depends on the charging methodology adopted in EVs [161, 162]. Therefore, SCS is developed which can handle EVs' batteries of different capacity and can coordinate with the DN of the grid. In this SCS context, an entity called CCU and CS aggregator with multi-point BCCS unit would eventually play a vital role in coordinating the charging/discharging of large fleet of EVs. In view of this discussion, the main contributions of the present work are:

- Developing the controllers and CS aggregator for the SCS and its coordination with the DN. These controllers and CS aggregator would control the power flow between the DN and the EVs' batteries.
- In order to achieve the desired power flow, multi-point BCCS unit is modeled with its associated controllers. BCCS have many advantages including the convenience of being cordless and safety during high power charging/discharging [82, 158, 159].
- The entire CS has been controlled by using the fuzzy logic controller, which control and coordinate the EV's arriving at CS to drawn the power from grid or to support the grid during peak hours.

3.3.1 Central Control Unit (CCU) and CS Aggregator

In this section, the functioning of CCU and the CS aggregator are described. As explained in the previous section, the CCU receives information of V_{node}, E_T and D. Accordingly, it decides the P_{grid} which should flow between the DN and SCS. The CS aggregator allocates the power among different EVs' batteries.

The CCU is designed using a fuzzy logic controller (FLC). This FLC has three inputs (V_{node}, E_T and D) and one output (P_{grid}) as shown in Fig. 3.4. The P_{grid} obtained from CCU has to be distributed

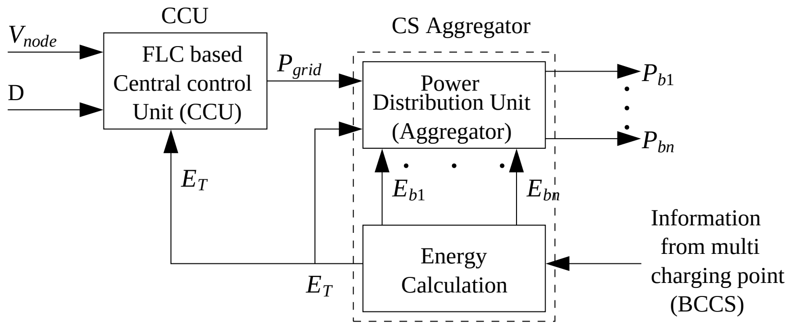

Figure 3.4: CCU and CS Aggregator.

among different EVs by the CS aggregator. The distribution of power (P_{bn}) for n^{th} EVs' batteries are calculated from Eq. (3.1).

$$P_{bn} = \frac{E_{bn}}{E_T} P_{grid} \tag{3.1}$$

The FLC has been used in the CCU because it is most suitable for this type of uncertain environments, which eliminates the need for complex mathematical models of the systems [34]. The control logic for CCU-FLC can be modeled by simple IF-THEN rules. Mamdani type inference is used here for the implication of rules. In order to achieve a fast and accurate result, center of gravity method is chosen for defuzzification process. Three fuzzy subsets such as low (L), medium (M) and high (H) have been chosen for the input variables. negative high (NH), negative medium (NM), negative Low(NL), positive low (PL), positive medium (PM) and positive high (PH) are chosen as output in order to obtain the required control action. Triangular membership function is used as it is simpler and easier to implement as shown in Fig. 3.5. The rule base for CCU-FLC is given in Table 3.2. The Fuzzification and defuzzification example for the CCU-FLC has been demonstrated in the Appendix B.

The detail sample calculation of CS aggregator has been given in Appendix D. The main feature of the fuzzy based cental control unit and the CS aggregator is given below:

- It estimates the total energy availability of the CS and individual EVs available/required energy.
- The fuzzy based CCU decides the amount and direction of power flow based on the node voltage, total energy availability of the CS and duration to support the grid.
- The power distribution unit estimate the required power to BCCS unit or EVs' batteries.

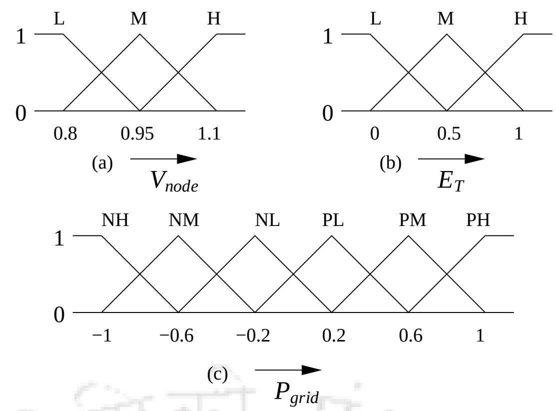

Figure 3.5: Fuzzy based CCU control structure in p.u (a) input: V_{node}, (b) input: E_T, D (c) output: P_{grid}.

Table 3.2: Rule base for CCU-FLC.

V_{node}	E_T	D	P_{grid}	V_{node}	E_T	D	P_{grid}
L	L	L	NH	M	M	H	NL
L	L	M	NM	M	H	L	NH
L	L	H	NL	M	H	M	NM
L	M	L	NH	M	H	H	NL
L	M	M	NM	H	L	L	PH
L	M	H	NL	H	L	M	PM
L	H	L	NH	H	L	H	PL
L	H	M	NM	H	M	L	PH
L	H	H	NL	H	M	M	PM
M	L	L	PL	H	M	H	PL
M	L	M	PL	H	H	L	PH
M	L	H	PL	H	H	M	PM
M	M	L	NH	H	H	H	PL
M	M	M	NM	-	-	-	-

3.3.2 Synchronization Mechanism

When EVs arrive at the CS, the BCCS unit will get connected with the DN and when it leaves the CS, the BCCS unit will get disconnected. However, in the cases of charging/discharging operation of EVs, the initial synchronization process with the grid is necessary without which the real power transfer in any direction cannot be controlled. The importance of synchronization of any power converters connected to the grid is explained in [163] and synchronization of BCCS unit has been described in detail in references [96]. The synchronization between the DN and the BCCS unit can be described by a simple system consisting of two interconnected sources as shown in Fig. 3.6.

The V_{prim} represents the transformer terminal voltage of BCCS unit, R_T is the total resistance and X_T represents total reactance of the system which includes transformer reactance, grid impedance and a third order LCL filter. The LCL filter is designed based on the standard level determined by

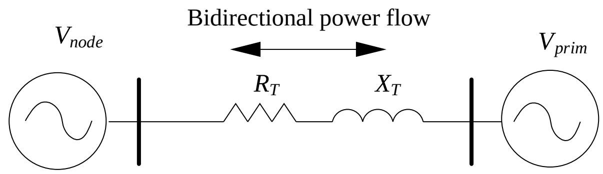

Figure 3.6: Synchronization mechanism between DN and BCCS unit.

IEEE519 for harmonic limits, which considers the level of current harmonics injected into the grid network [164]. The power transferred between the terminals of BCCS unit and DN is given in Eq. (3.2).

$$P_{bn} = \frac{V_{node}V_{prim}}{X_T}\sin(\delta) \tag{3.2}$$

Here, δ denotes power angle between V_{node} and V_{prim}. This power is equal to the distributed power from the CS aggregator. The real power control between EV batteries and the DN is regulated by controlling the δ. The value of δ can be derived from Eq. (3.2).

$$\delta = \sin^{-1}\left(\frac{P_{bn}X_T}{V_{node}V_{prim}}\right) \tag{3.3}$$

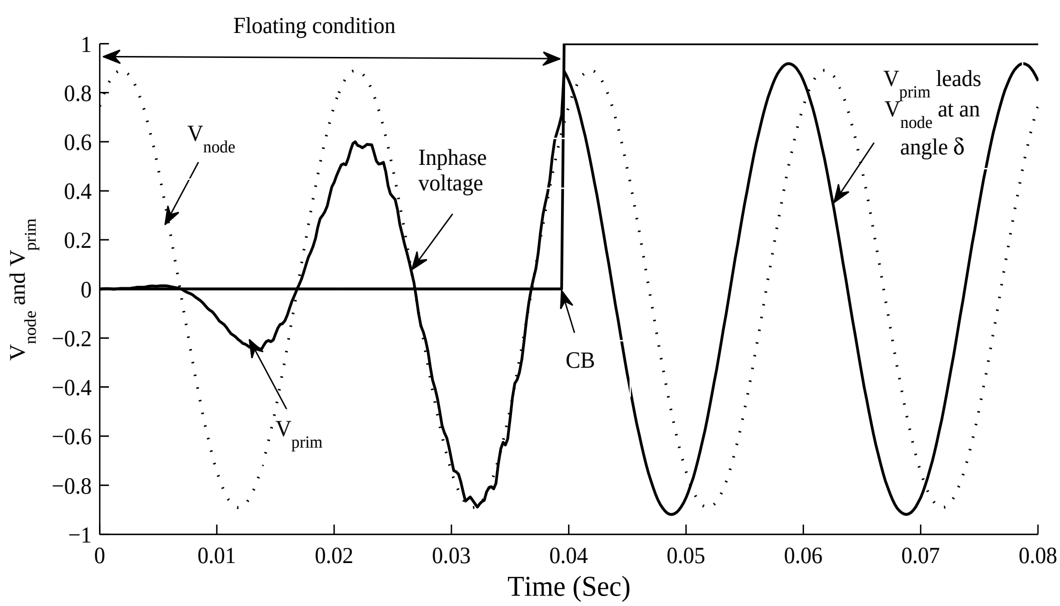

Figure 3.7: Synchronization waveform.

For the discussion of power flow, voltage waveform for V_{node} and V_{prim} is shown in Fig. 3.7. For example, let us consider that the Root-Mean-Square (RMS) value of the V_{node} and V_{prim} is 440V, the P_{b1} is 9.8077kW and reactance (X_T) of the system is given in Table 3.8. Therefore, $\delta = -8.43°$

required to transfer the power (P_{b1}) from BCCS unit to DN. In Appendix D, the detail calculation of power angle has been mentioned.

The BCCS unit and the DN will be in floating condition till the system gets synchronized with the DN. When the system gets synchronized with the DN, the circuit breaker (CB) closes and the angle δ determines the power flow between the BCCS unit and the DN.

To achieve this synchronization operation and to control the real power, load/power angle control have been used in Fig. 3.8.

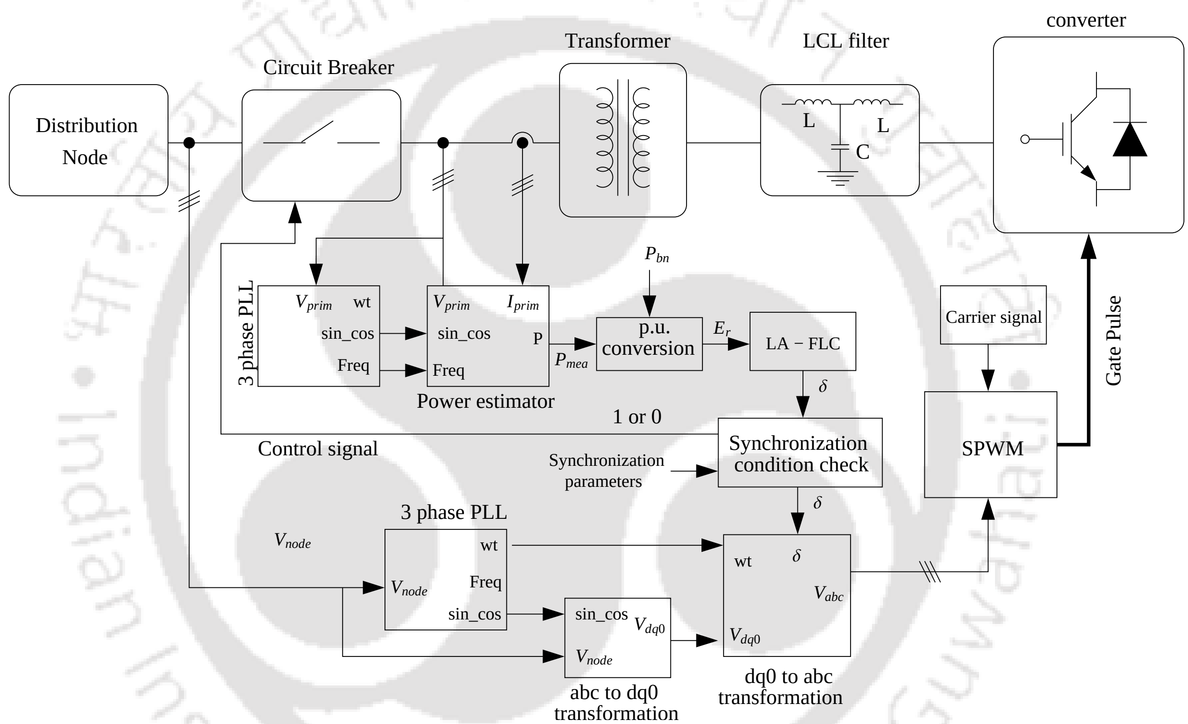

Figure 3.8: Load angle control.

The load angle control has used enhanced fuzzy based phase locked loop (PLL) based synchronization technique, which takes DN voltage as reference and estimates the frequency and phase sequence components of the grid to synchronize the BCCS unit with the DN. Besides, the converter voltage (V_{prim}) and current (I_{prim}) of BCCS unit is given as input to the power estimator block and P_{meas} is obtained. Based on P_{meas} and P_{bn} from aggregator, the Load Angle FLC (LA-FLC) generates the required δ as shown in Fig. 3.8. The amount and direction of real power transfer takes place, when the voltage produced by the BCCS unit leads or lags the voltage of the DN. A leading phase of BCCS voltage constitutes power transfer from V2G and lagging phase enables power transfer from

G2V. The brief overview of the load angle controller is given below:

- The three-phase phase locked loop (PLL) estimate the unit vectors ($sin\theta$ and $cos\theta$), frequency and angular time of the BCCS unit and grid.
- The measured power has been calculated from the power estimator unit based on the BCCS unit three-phase voltage and current, unit vectors and frequency of the system.
- The fuzzy based load angle controller decide the power angle based on the P_{mea} and the P_{bn} which is obtained from the CS aggregtor.
- The park transformation has been used to convert the three-phase (abc) to two phase ($dq0$) transformation.
- The required power angle has been added with the two phase quantities and then it converted into three-phase transformation.
- The three-phase voltage is the reference signal for sine pulse width modulation (SPWM).

Fig. 3.8 mainly consists of discrete three-phase PLL units, which extract the synchronization parameters (frequency and phase sequence) of the node and converter voltage, three-phase to two phase transformation and vice versa, FLC based load angle controller (LAC-FLC) and power estimator. Three-phases V_{node} is the input for $abc - dq0$ transformation unit and discrete three-phases PLL. The $abc - dq0$ transformation unit converts the three-phase (abc) stationary components of the V_{node} to two phase ($dq0$) reference frame [99]. The three-phase DN voltage can be represented by Eq. (3.4).

$$V_{node} = V_{abc} = V_m \left| \sin(\omega t) \quad \sin\left(\omega t - \frac{2\pi}{3}\right) \quad \sin\left(\omega t + \frac{2\pi}{3}\right) \right|^T \tag{3.4}$$

where V_m is the peak voltage. The three-phase to two phase transformation is given in Eq. (3.5) [165].

$$\begin{bmatrix} V_d \\ V_q \\ V_0 \end{bmatrix} = \frac{2}{3} \begin{bmatrix} \cos\omega t & \cos\left(\omega t - \frac{2\pi}{3}\right) & \cos\left(\omega t + \frac{2\pi}{3}\right) \\ \sin(\omega t) & \sin\left(\omega t - \frac{2\pi}{3}\right) & \sin\left(\omega t + \frac{2\pi}{3}\right) \\ \frac{1}{2} & \frac{1}{2} & \frac{1}{2} \end{bmatrix} \begin{bmatrix} V_a \\ V_b \\ V_c \end{bmatrix} \tag{3.5}$$

The three-phase discrete PLL extracts the frequency and the unit vector components of V_{node} and feeds to $abc - dq0$ transformation unit and $dq0 - abc$ transformation unit (phase shift (30^o) between primary and secondary side voltage of the transformer also considered). The frequency, unit vector components (sin_cos) and converter measured voltage (V_{conv}) and current (I_{conv}) are input for power estimator which calculate the actual bidirectional power flow between BCCS unit to DN. The LAC-FLC decide the load angle (δ) between DN and converter voltage. The range of the δ for LAC-FLC has chosen based on the impedance of the BCCS unit and DN. The δ can be either positive or negative, if the positive values of the δ represents the V_{conv} lagging with respect to V_{grid} and negative value of the δ denotes the V_{conv} leading with respect to V_{grid}. The inverse transformation $V_{dq0} - V_{abc}$ is performed to generate a reference voltages (V_{abc}^*) delayed with δ, which is given in Eq. (3.6) [165]. The V_{abc}^* compared with the carrier signal to generate the gate pulse for the converter.

$$\begin{bmatrix} V_a \\ V_b \\ V_c \end{bmatrix} = \frac{2}{3} \begin{bmatrix} \cos\left(\omega t + \frac{\pi}{6} \pm \delta\right) & \sin\left(\omega t + \frac{\pi}{6} \pm \delta\right) & 1 \\ \cos\left(\omega t - \frac{\pi}{2} \pm \delta\right) & \sin\left(\omega t - \frac{\pi}{2} \pm \delta\right) & 1 \\ \cos\left(\omega t + \frac{5\pi}{6} \pm \delta\right) & \sin\left(\omega t + \frac{5\pi}{6} \pm \delta\right) & 1 \end{bmatrix} \begin{bmatrix} V_d \\ V_q \\ V_0 \end{bmatrix} \tag{3.6}$$

Further the SPWM generates switching pulses for the three-phase convertor unit considering the regenerated sinusoidal wave V_{abc}^* as a reference signal. The converter work as a inverter for V2G and rectifier for G2V operating mode, respectively. The operation of the synchronization controller can be explained by considering the switching operation of CB.

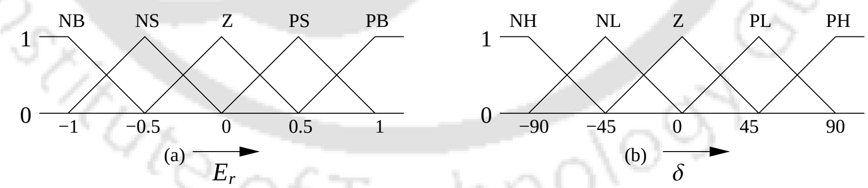

Figure 3.9: Fuzzy membership function for LA-FLC control (a) input: E_r (b) output: δ.

The input and output membership function of LA-FLC is given in Fig. 3.9. Table 3.3 shows the rule base for LA-FLC. The control parameters used in the BCCS unit are shown in Table 3.4.

Table 3.3: Rule base for LA-FLC.

E_r	NB	NS	Z	PS	PB
δ	VS	S	M	B	VB

For example, let us suppose that error is -0.198 p.u. This means, the measured power (P_{mea}) is grater than the reference power (P_{bn}). The load angle controller will decides the required power angle to transfer the power between BCCS unit and gird. The LA-FLC decide the power angle is 10.25° but required δ to transfer the power is 8.43° which is theoretically calculated from Eq. (3.3). This power angle information will be updated every instant of time and the LA-FLC minimize the error. If the error is minimum, then the P_{mea} follow the P_{bn} which is distributed from the CS aggregator.

3.3.3 Multi-Point BCCS Unit

In this part, the multi-point BCCS unit is explained. The circuit topology of individual BCCS unit is shown in Fig. 3.10. The primary side connected to the DN is the CS and the secondary side is the EV battery system.

Table 3.4: Control parameters

Parameters	Descriptions	Parameters	Descriptions
$V^{C}_{c_i/d_i}$, I_c	Charge/discharge battery terminal voltage and current (SS)	V_{prim}, I_{prim}	Transformer terminal voltage and current (PS)
E_r	Error input of fuzzy (SS)	V_{node}	DN Voltage (PS)
P_{bn}	n^{th} distributed power of the CS aggregator (PS)	V_{dcmeas}	dc measured voltage at inverter input (PS)

The primary side (PS) comprises of bidirectional three-phase ac to dc and dc to high-frequency ac converter. The secondary side (SS) has a bidirectional high-frequency ac to dc converter and a buck-boost (BB) converter with EV battery pack connected. Compensation capacitors (C_1,C_2) are generally used on either side of contactless coil to compensate the leakage inductance between the coils [166]. The detailed design procedure of BCCS unit of rectangular with planar coil distribution has already been discussed and their specifications are given in Table 3.8. The charging and discharging states of EV batteries are controlled by the power converters. The controllers present at the multi-point BCCS unit plays a vital role in controlling the power flow from individual EV battery and the DN. Thus, the BCCS unit is fully controlled and it uses direct control signal from the aggregator. Depending upon the power distribution from the CS aggregator to each BCCS unit, G2V and V2G operations are performed. As already mentioned in Section II.B, positive power implies G2V operation and negative power implies V2G operation. P_{bn} from the aggregator is the main control signal for the BCCS unit, which is fed into the load angle control (LA-FLC), which determines the amount and

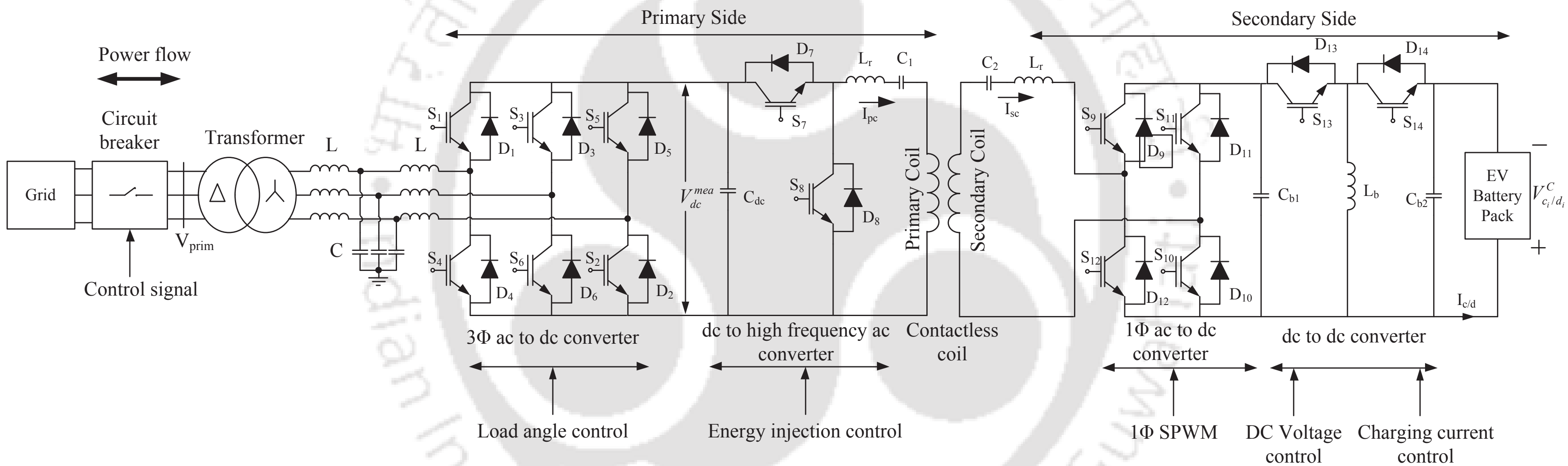

Figure 3.10: Circuit topology of individual BCCS unit

direction of power flow from/to the DN as shown in Fig. 3.8 for both G2V and V2G operation. As it is not desired to deplete or overcharge the battery, an algorithm has been used to control the power flow of the EV battery which calculates the C_{rate}; and the energy status is calculated by considering the SOC limits (Chapter 3, Section 3.3, 3.3.4). Based on this, P_{bn} is also fed into the controller of buck boost converter in the battery side; which determines the reference current signal. The detailed control process and controllers involved for both G2V and V2G operations is explained below. Load angle control, energy injection control and charging current control is used for G2V operation and load angle control, sine pulse width modulation (SPWM) technique and DC link voltage control is utilized for V2G operation.

3.3.3.1 G2V Operation

The detailed circuit diagram for V2G operation is shown in Fig. 3.11. In Fig. 3.11, the primary side (PS) controlled rectifiers are used to convert three-phase ac to dc using bidirectional switches ($S_1 - S_6$). These switches are controlled based on SPWM using load angle control taking DN voltage as reference. The amount of power supplied to the battery is controlled based on δ. Then the inverter switches ($S_7 - S_8$) converts dc to high-frequency ac using energy injection control [67, 167] which is given in Fig. 3.14. In the secondary side (SS), the diodes ($D_9 - D_{12}$) convert high-frequency ac to dc. Diode rectification is used here, as the system employs tight magnetic coupling. Obviously, controlled rectifiers can be used, if the system has a special requirement to control the misalignments between the PS and SS. Further, the buck boost converter (S_{13}, D_{14}) controls the charging current of the battery. The buck-boost converter is required in this case because the sudden flow of high current may damage the EVs' batteries. P_{bn} from the aggregator is fed into the charging current controller of the buck boost converter. Fig. 3.12. shows the charging current control, P_{bn} and the battery terminal voltage generates the reference current (I_{ref}) for the controller. For convenience, the controller is normalized in per unit ($p.u$) values. Error (E_r') is obtained from Eq. (3.7).

$$E_r' = \left(1 - \frac{V_{c_i}^C I_c}{P_{bn}}\right) \tag{3.7}$$

The E_r is given as input to charging current FLC (CC-FLC), which generate the required duty ratio

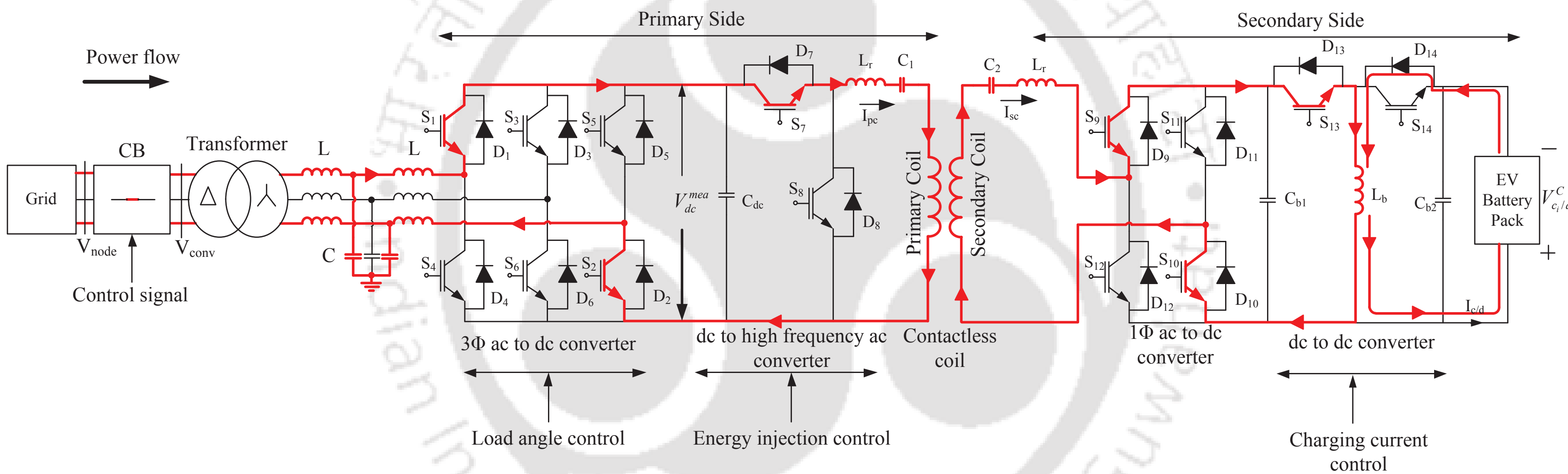

Figure 3.11: Circuit topology for G2V operating mode.

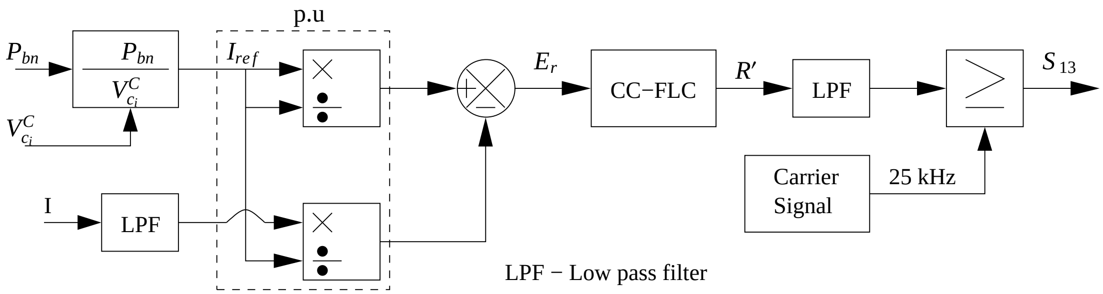

Figure 3.12: Charging current control.

for pulse generation. Low pass filters (LPF) is used in the output of CC-FLC, to obtain oscillation free output. The rule base and membership function used for CC-FLC is given in Fig. 3.13 and Table 3.5. The triangular membership function has been used for both input and output which is shown in Fig. 3.13. Five fuzzy subsets are chosen as input variable (E_r): negative high (NH), negative low (NL), zero (Z), positive low (PL) and positive high (PH). The fuzzy subsets chosen for reference (R) output: very low (VL), low (L), medium (M), high (H) and very high (VH).

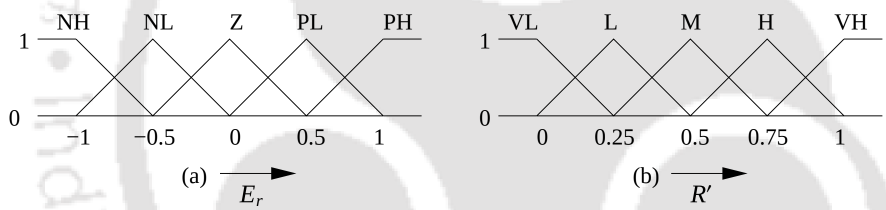

Figure 3.13: Fuzzy membership function for CC-FLC control (a) input: E_r' (b) output: D'.

Table 3.5: Rule base for CC-FLC.

E_r'	NH	NL	Z	PL	PH
D’	VL	L	M	H	VH

For example, let us suppose that P_{b1} is 12.52kW, the measured battery terminal voltage ($V_{c_i}^C$) is 258V and the charging current (I_c) is 20.45A. The reference current (I_{ref}) has been calculated from the ratio between the P_{b1} and the $V_{c_i}^C$, it is 48.53A. Then the error (E_r') sinal is 0.5786 p.u. This means, the I_c is much less than I_{ref}. Therefore, the charging current controller is increase the duty ratio (D') of the BB converter. If the D' is increased with respect to the E_r', then the BB converter switching time (t_{on}) has been increased. Therefore, the energy stored in the inductor (L_b) will increase. This information will be updated every instant of time and the CCC maintain the battery I_c is equal to the I_{ref} by increasing the D'.

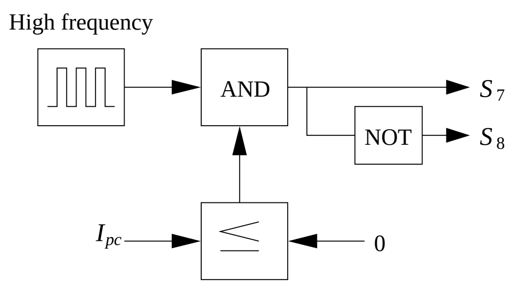

Figure 3.14: Energy injection control.

The block diagram of energy injection control is given in Fig. 3.14. The primary side current is compared with the zero, then the gate pulse is generated for switches S_7 and S_8 which converts dc current to high-frequency ac current.

3.3.3.2 V2G Operation

The detailed circuit diagram for V2G operation is shown in Fig. 3.15. In V2G operation, the EVs' batteries supplies power to the DN. The BCCS unit should maintain the line-line peak voltage of the node (625V) for supporting the grid. This is achieved by controlling the secondary side dc-dc converter (S_{14}, D_{13}) using DC link voltage based FLC (DLV-FLC) which is shown in Fig. 3.16. Further, the dc voltage is converted to high-frequency ac (S_9-S_{12}) using SPWM technique [168]. In the PS, the diodes (D_7 and D_8) convert high-frequency ac to dc and inversion operation is performed by the switches (S_1-S_6) using load angle control as shown in Fig. 3.8. The amount of power supplied to the grid is based on the power signal obtained from the aggregator. The Error (E_r'') for DC link voltage controller is calculated from the equation given below.

$$E_r'' = \left(1 - \frac{V_{dc}^{mea}}{V_{dc}^{ref}}\right) \tag{3.8}$$

The membership function of DLV-FLC is shown in Fig. 3.17. Five fuzzy subsets are chosen as input variables for E_r'' and $\Delta E_r''$: negative big (NB), negative small (NS), zero (Z), positive small (PS) and positive big (PB). The output reference (D'') is given by very small (VS), small (S), medium (M), big (B) and very big (VB). The rule base for DLV-FLC is given in Table 3.6.

For example, let us consider that V_{dc}^{mea} is 600V and V_{dc}^{ref} is 625V. The E_r'' is 0.04 p.u and the $\Delta E_r''$ is 0.008 p.u. This means, the V_{dc}^{mea} is almost equal to the V_{dc}^{ref}. Therefore, the DLV-FLC will increase the duty ratio (D'') of the BB converter. If the D'' is increased with respect to the E_r'' and $\Delta E_r''$, then

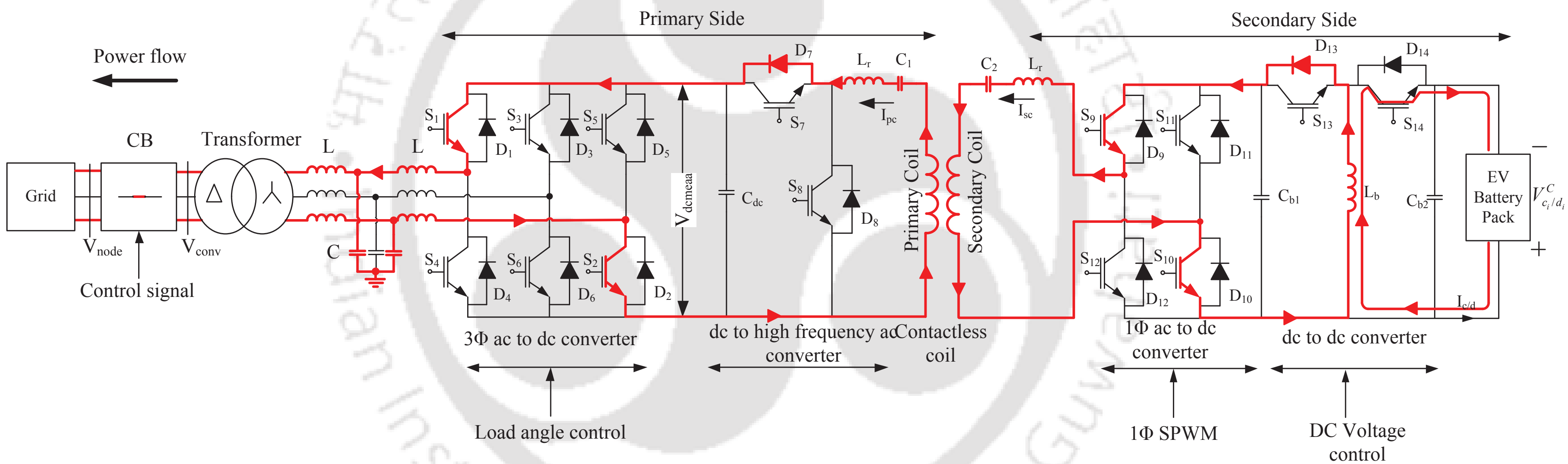

Figure 3.15: Circuit topology for V2G operating mode.

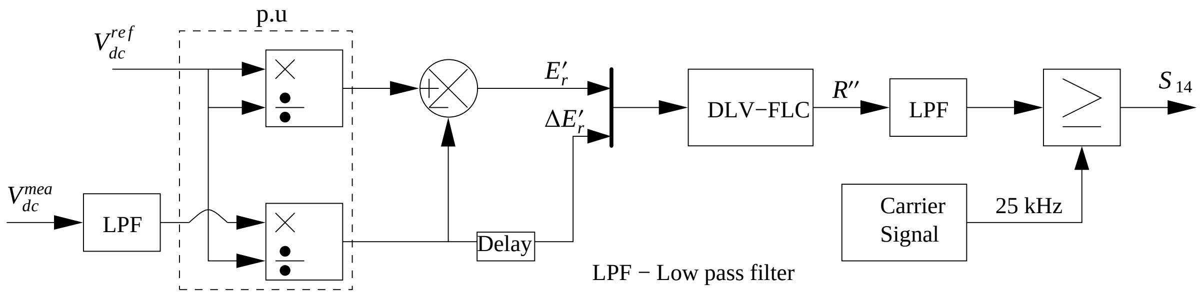

Figure 3.16: DC link voltage control.

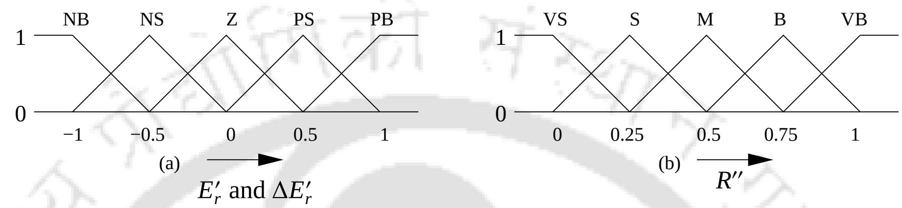

Figure 3.17: Fuzzy membership function for DLV-FLC (a) inputs: E_r'' and $\Delta E_r''$ (b) output: D''.

Table 3.6: Rule base for DLV-FLC.

E_r''	$\Delta E_r''$	D''	E_r''	$\Delta E_r''$	D''
PB	NB	M	Z	PS	B
PB	NS	B	Z	PB	B
PB	Z	B	NS	NB	VS
PB	PS	VB	NS	NS	S
PB	BP	VB	NS	Z	S
PS	NB	S	NS	PS	M
PS	NS	M	NS	PB	B
PS	Z	B	NB	NB	VS
PS	PS	B	NB	NS	VS
PS	PB	VB	NB	Z	S
Z	NB	S	NB	PS	S
Z	NS	S	NB	PB	M
Z	Z	M	-	-	-

the BB converter t_{on} has been increased. This information will be updated every instant of time and the DLV-FLC maintain the V_{dc}^{mea} is equal to the V_{dc}^{ref} by increasing the D''.

3.3.4 C_{rate} and SOC Calculation

As it is not desired to deplete or overcharge the battery, the C_{rate} and SOC (in this Chapter SOC denotes both SOC_{cr} and DOD_{cr} for simplicity) of the batteries are monitored. The capacity fading of the EVs' batteries is not considered in this work. An algorithm is used to control the charging/discharging of EVs' batteries by changing the C_{rate} of EVs' batteries. The C_{rate} of BCCS unit is calculated from Eq. (3.9).

$$C_{rate}^{BCCS} = \frac{P_{\max}}{V_{c_i/d_i}^{C} Q} \tag{3.9}$$

where, P_{max} is the maximum peak power handling capability of charging point. The algorithm has also taken into account of user defined C_{rate} (C_{rate}^{user}) and the current C_{rate} (C_{rate}^{crt}) of the battery. The C_{rate}^{crt} calculated from the equation given below.

$$C_{rate}^{crt} = \frac{P_{bn}}{V_{c_i/d_i}^{C} Q} \tag{3.10}$$

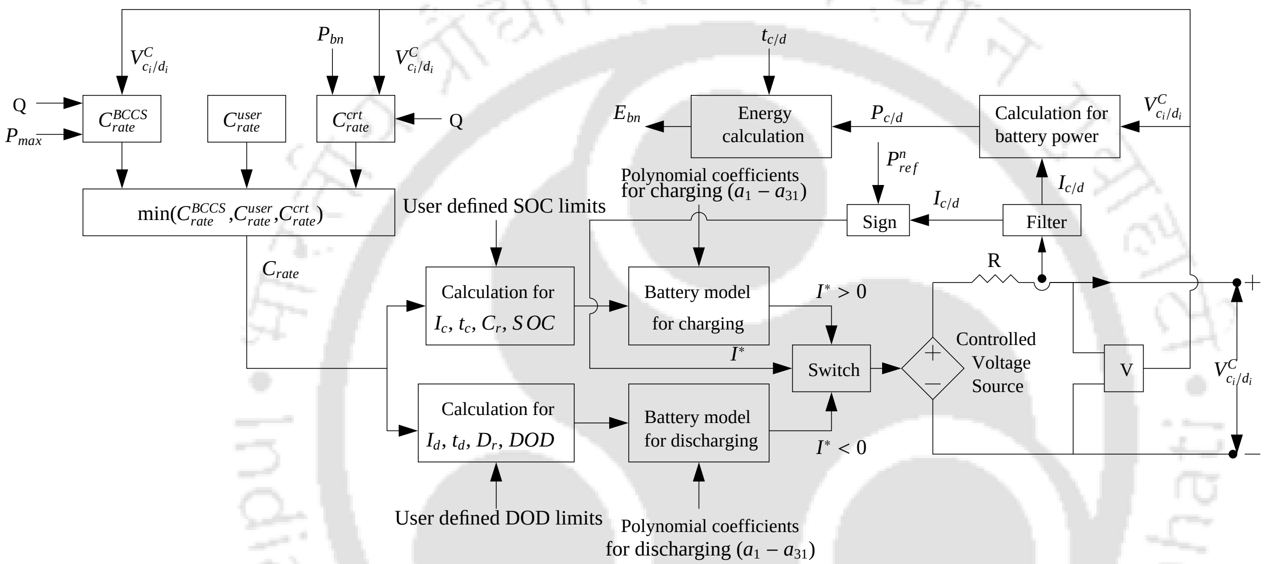

Figure 3.18: C_{rate} and SOC calculation.

The control algorithm chooses the minimum of the C_{rate} (C_{rate}^{BCCS},C_{rate}^{crt} and C_{rate}^{user}) to regulate the current flows of individual EV battery. The minimum of the C_{rate} (C_{rate}^{min}) will be the processed C_{rate} of the charging point. Besides, the SOC limits of vehicle owners are also considered in this work. When the SOC is near to full (empty), a high power charging or discharging should not be allowed for preventing over charge (over discharge). Therefore, SOC_{min} and SOC_{max} of the EVs' batteries are taken into account. Based on these limits, the control algorithm is implemented using Eq. (2.13) and Eq. (2.14). Fig. 3.18 shows the block diagram of C_{rate} and SOC evaluation used in EV batteries of SCS.

The main features of the charge rate control is given below.

- Control the minimum C_{rate} to regulate the battery current based on the user define C_{rate}, BCCS unit C_{rate} and current C_{rate} of the battery.

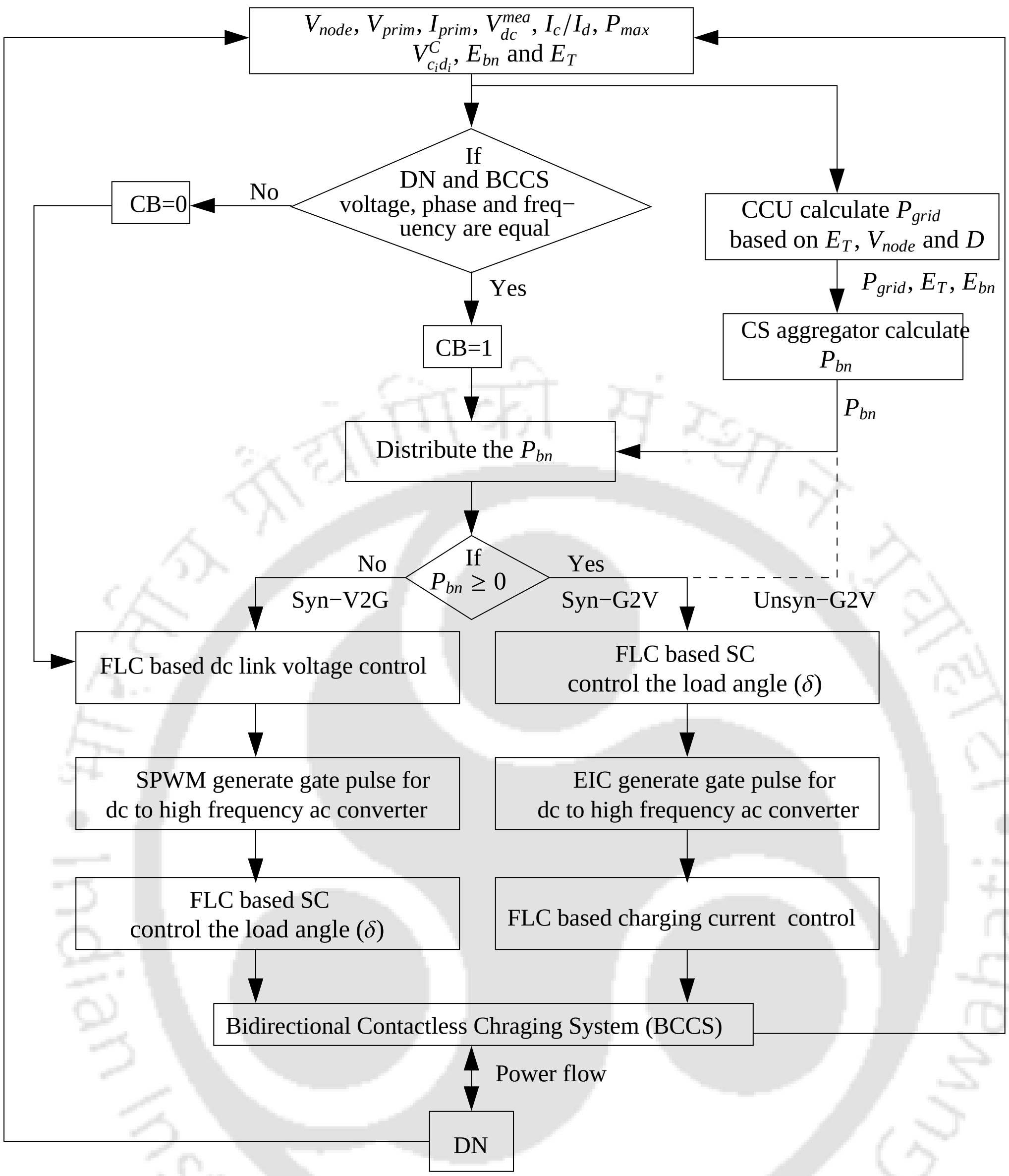

Figure 3.19: Flow chart for energy transfer in V2G and G2V operations based on DNC command.

- Estimate the I_c, t_c, SOC and $V_{c_i}^C$ for charging scenario and I_d, t_d and $V_{d_i}^C$ for discharging scenario.
- Calculate the battery power and availability/required energy of the individual EVs.
- The battery model work based on the reference current $I^\star$. If $I^\star > 0$ for charging scenario and $I^\star < 0$ for discharging scenario.

For example, let as consider that P_{max} is 50kW, Q_r is 32Ah, $V_{c_i}^C$ is 258V, P_{b1} is 9.81kW and the C_{rate}^{user} is 2.5. The C_{rate} of the BCCS is 6.056. The C_{rate}^{crt} of the battery is 1.188. The control algorithm chooses the minimum of the C_{rate} to regulate the battery charging current flow to the EV battery. The minimum C_{rate} is 1.188. For the ease of analysis, the flow chart for V2G, G2V with synchronization operation is given in Fig. 3.19. The detail explanation is already discussed in the previous section.

3.4 Application Scenario of Multi-Point SCS

The proposed SCS is connected to a node **5.3** of the typical distribution network as shown in Fig. 3.2 [74]. Simulations are performed considering 10 EVs' batteries of different ratings. The specifications of EVs' batteries are given in Table 3.7. For ease of analysis, EVs' batteries are divided into five groups based on the terminal voltage (V), energy (kWh), nominal capacity (Ah), SOC limits and C_{rate}.

Table 3.7: Specifications of EV batteries.

Voltage (V)	Energy (kWh)	Q (Ah)	SOC_{lt}		SOC_{cr}			C_{rate}^{user}
			SOC_{max}	SOC_{min}	Case i	Case ii	Case iii	
250	8	32	100	25	20	70	70	3
250	10	40	90	30	30	50	30	3
400	16	40	85	45	40	85	40	2.5
400	20	50	95	30	35	60	60	2.5
500	24	48	80	25	20	80	70	2

In order to examine the real-time situations, the following three cases of EVs present in the SCS are considered:

(i) EVs' batteries with low SOC connected during off-peak hours (23:00hrs to 06:00hrs).

(ii) EVs' batteries with high SOC connected during peak hours (07:00hrs to 10:00hrs) and (17:00hrs to 22:00hrs).

(iii) EVs' batteries with both high and low SOC connected during normal hours (11:00hrs to 17:00hrs).

(iv) Impacts of the distribution node.

These cases are considered for testing the behavior of SCS because there is a large variation of node voltage during off-peak and peak hours and marginal variation in normal hours. The value of SOC_{cr} is assumed to be different for these three cases, which is given in Table 3.7. The controller in the SCS decides the magnitude and direction of power flow depending on the node voltage variations.

EVs' batteries will not charge, if the node voltage is low (peak hours) and batteries will not discharge when the node voltage is high (off-peak hours). However, if the voltage is within the specified limit (0.95 to 1.05 p.u), some batteries would charge and some would discharge depending on the energy availability or requirement of the individual battery.

The following assumptions have been made in this work:

- Each BCCS unit of the SCS is designed for maximum peak power handling capacity of 50 kW.
- The EV batteries are not allowed to discharge below the SOC_{min} and the batteries are not allowed to charge above SOC_{max}.

Fig. 3.10 shows the circuit topology of individual BCCS unit and its specifications of parameters are given in Table 3.8. The battery parameters (R_1, R_2, C, and V_o) depends on the status of SOC. In Table 3.8, the battery parameter is mentioned for a single EV battery having the rating of 250V, 8kWh and SOC level of 70%.

Table 3.8: Specifications of BCCS unit.

Parameter	Descriptions	Values	Parameter	Descriptions	Values
LCL	3 Φ filter (PS)	0.6mH, 0.08mF, 0.8mH	C_1, C_2	PS and SS compensation capacitance	1.17F, 1.17F
C_{dc}	dc link capacitor (PS)	10mF	M	Mutual inductance	8.83μH
L_p, L_s, L_r	inductance of PS, SS, resonant	34.8μH, 34.8μH, 30μH	L_b, C_{b1}, C_{b2}	BB inductance, capacitance	0.48mH, 5.47mF
R_1, R_2, C, V_o	Battery parameters	0.0407Ω, 0.0102Ω, 1.5027F, 275.19V	X_T, f_s	Total reactance, system operating frequency	2.894Ω, 25kHz

3.5 Results and Discussion

In this section, SCS behavior is analyzed for three cases (off-peak, peak, normal hours of a day) as discussed. To avoid the repetition of similar graphs, only five EVs batteries results are shown throughout this section.

Case I: EVs' batteries with low SOC connected during off-peak hours. In this case, the SCS is tested during off-peak hours, where the node voltage (V_{node}) is generally high (1.05p.u to 1.1p.u).

Also, it is considered that during off-peak hours, EVs batteries arrive at the SCS have low value of SOC as mentioned in Table 3.7. In this case, CCU-FLC at the grid side decides a total of 180kW of power which is required to charge the EVs' batteries and it is shown in Table 3.9. The summary of individual energy, total available energy of SCS, division of power from CS aggregator and the minimum C_{rate} ($C_{rate}^{\min}$) chosen by the proposed SCS are summarized in Table 3.9.

Table 3.9: Summary of power and required energy of case I.

Parameter	Energy (kWh)		Parameter	Power (kW)	C_{rate}^{min}
	E_{stor}	E_{avail}			
E_{b1}-E_{b2}	6.4	-	P_{b1}-P_{b2}	12.63	1.58
E_{b3}-E_{b4}	6.0	-	P_{b3}-P_{b4}	11.84	1.18
E_{b5}-E_{b6}	8.0	-	P_{b5}-P_{b6}	15.79	0.99
E_{b7}-E_{b8}	12.0	-	P_{b7}-P_{b8}	23.68	1.18
E_{b9}-E_{b10}	13.2	-	P_{b9}-P_{b10}	26.06	1.08
E_T	45.6 ×2=91.2		P_{grid}	90×2=180	

Fig. 3.20 shows the power distributed across the terminals of ac bus of each BCCS unit of SCS. The individual BCCS units are operated at resonant state to decrease the conduction loss of the system. When the system operates at resonance condition, maximum power is transferred in the system and the power factor (pf) of the system is maintained to unity or near to unity [169]. The pf of the proposed SCS lies between 0.99 to 1 as shown in Fig. 3.21.

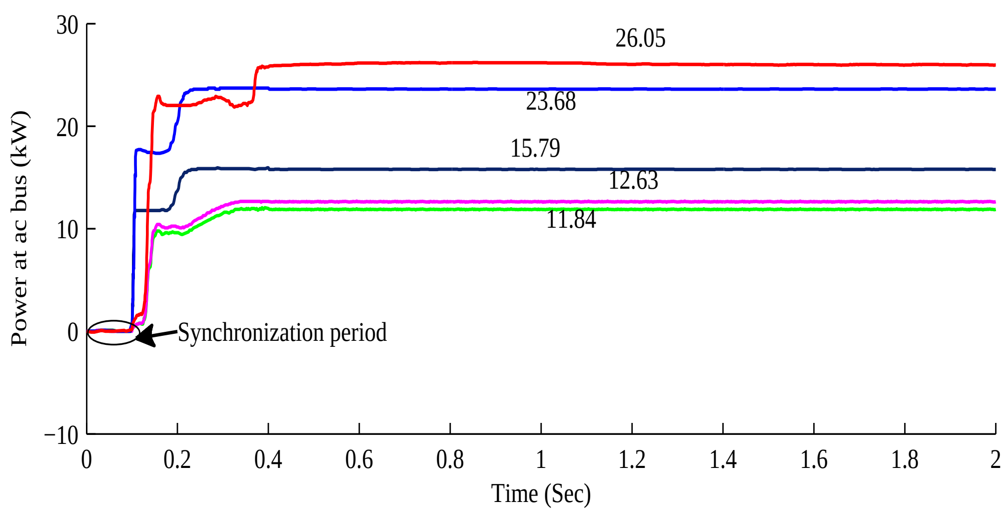

Figure 3.20: Power at each terminal of BCCS unit.

The charging current controller controls the charging current of individual EV battery. It is evident from Fig. 3.22, the EVs' batteries are charging at constant current, which shows the effectiveness of

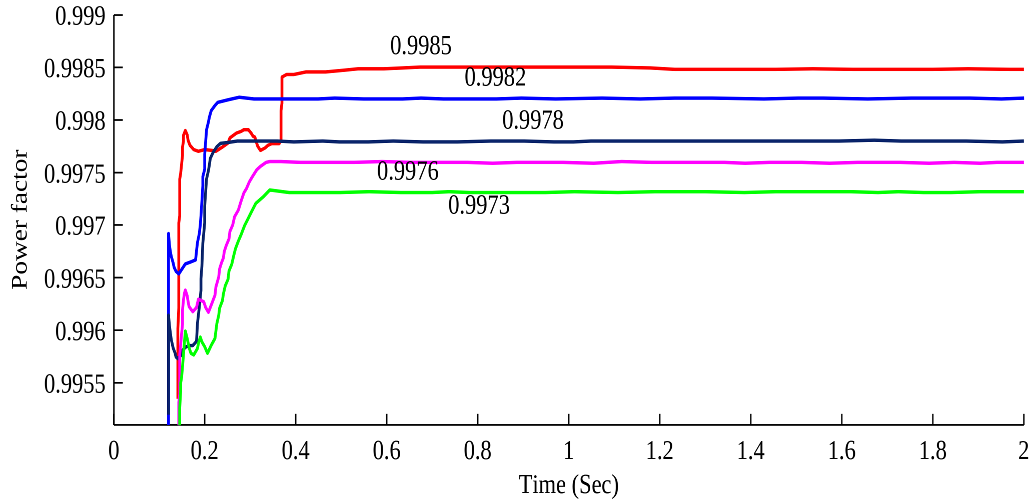

Figure 3.21: Power factor of the BCCS unit.

the controller. There will be a small negative flow of current during synchronization period. Actually during synchronization period, the system is controlled and there is no power transfer between DN and EVs' batteries. This is because, the EVs' arrive at the CS will make a closed path through converters switches having low resistance and there is some initial current flow through LCL filter and this consumes very less power. This can be seen from Fig. 3.20 and Fig. 3.23. Fig. 3.20 shows the power distributed at each terminal of BCCS (i.e., near to ac bus at grid side), there is no power transfer during synchronization. However, Fig. 3.23 shows the battery power there is some initial negative power flow at the time of synchronization. The detailed circuit topology of individual BCCS unit with current flow direction during the synchronization period is given in Fig. 3.15.

Fig. 3.23. shows the power delivered by each battery. The efficiency of the system is calculated based on the ratio of the EV battery power and the distributed power from CS aggregator (P_{bn}). The efficiency of this case lies between 86% to 94%, with reduced losses of around 0.6kW to 0.8kW. After synchronization operation, the direction of power transfer is decided. This must be satisfied for all EVs in the charging station arriving with high and low values of SOC. The buck-boost converter present in the EV battery system handles this operation. The duty ratio of the buck-boost converter is controlled and does the necessary operation and maintains the voltage level in the grid side. Initially, the EVs' batteries have to discharge its energy to perform the synchronization operation.

Fig. 3.24. shows the initial and final SOC values of five groups of EVs' batteries. It is clear from

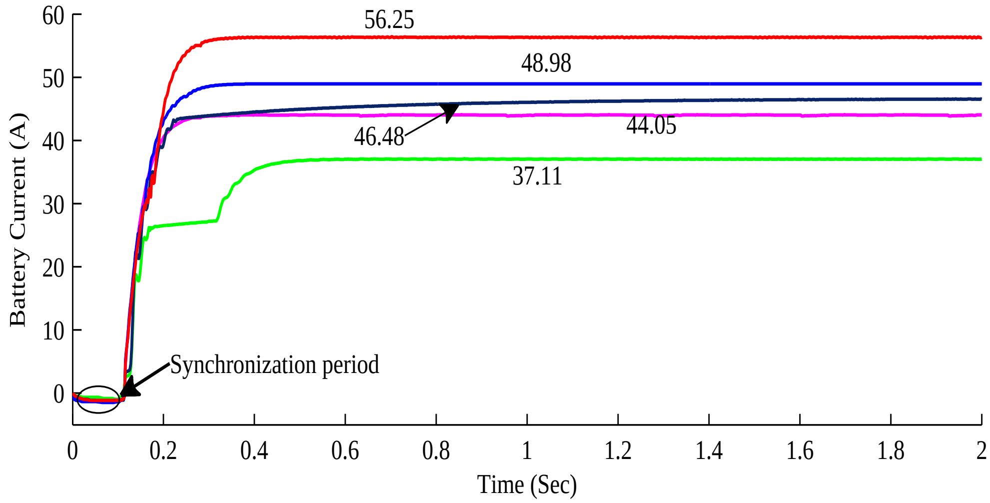

Figure 3.22: Charging currents of individual EVs' batteries.

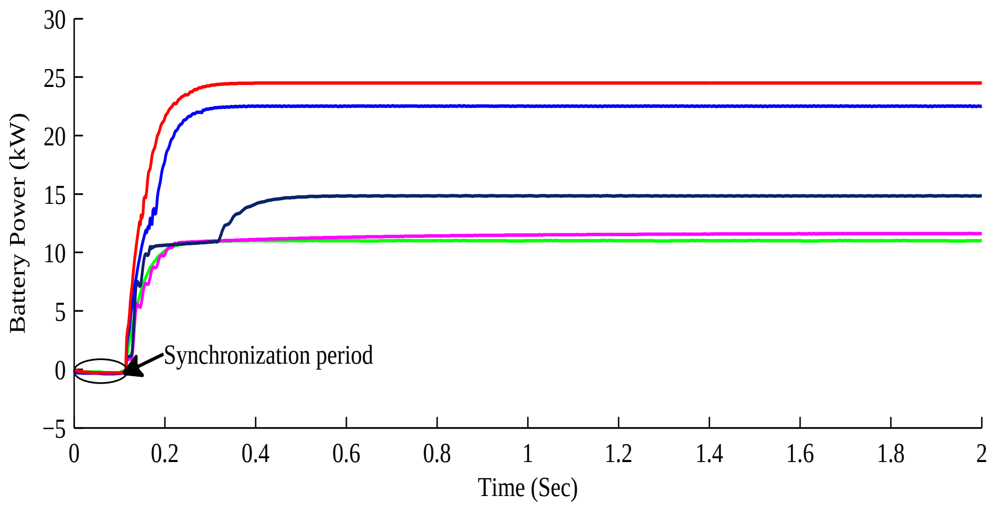

Figure 3.23: Power at each terminal of EVs' batteries.

the Figure that EVs batteries have not crossed the SOC limit as mentioned in Table 3.15.

The Total harmonic distortion (THD) and the pf of the BCCS unit is give in Table 3.10. The THD of the BCCS unit is found in the range of 1.897% to 2.939% and the power factor of the BCCS unit is found in the range of 0.9982 to 0.9982. The THD and power factors are allowable as per the IEEE standard 519-1992 [170].

Case II: EVs' batteries with high SOC connected during peak hours. The V2G operation has been considered for the negative value of P^{n}_{ref}. Power flow from EV's batteries to DN will take place in proportion with δ. All the BCCS units connected at the CS together supplies P_{grid} to the DN.

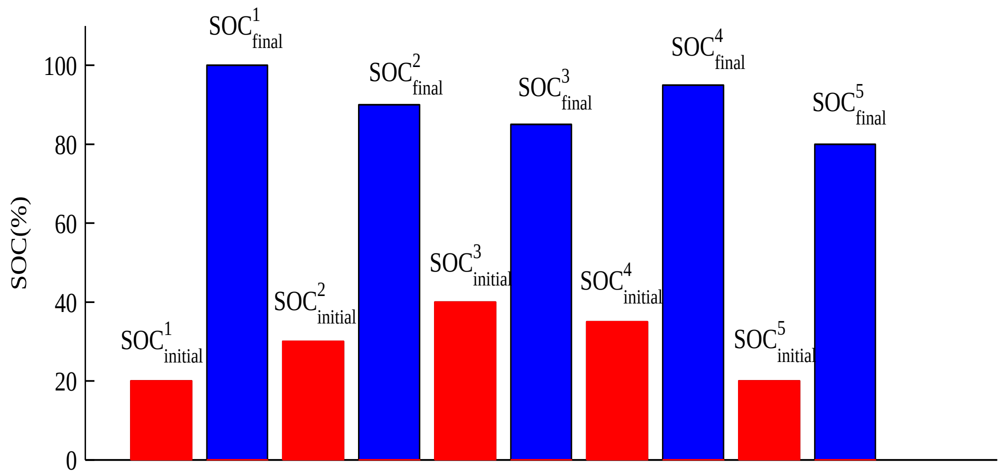

Figure 3.24: Initial and final SOC of the EVs' batteries

Table 3.10: THD and power factor of the BCCS unit during the G2V operating mode.

Sl. No	THD (%)	Power factor
1.	2.939	0.9976
2.	1.897	0.9973
3.	1.897	0.9978
4.	2.028	0.9982
5.	2.545	0.9985

Voltage profile of the DN improved due to support the DN in the peak hours. The node voltage varies with respect to the magnitude of P_{total} drawn from the node. The graphical results for battery power and current, ac bus power, P_{total} and V_{node} for V2G operating mode has been presented. In this case, all 10 EVs arrive at SCS with high energy. The CCU-FLC at the grid side decides to draw -170kW of power for supporting the grid as given in Table 3.11. During peak hours, V_{node} is generally low (0.95p.u to 0.97p.u). The controllers in the SCS allow the EVs' batteries to discharge its energy. The EV batteries discharge based on the SOC limit prescribed by the EV owner.

Table 3.11: Summary of power and available energy of case II.

Parameter	Energy (kWh)		Parameter	Power (kW)	C_{rate}
	E_{stor}	E_{avail}			
E_{b1}-E_{b2}	-	3.6	P_{b1}-P_{b2}	-9.81	1.23
E_{b3}-E_{b4}	-	2.0	P_{b3}-P_{b4}	-5.44	0.55
E_{b5}-E_{b6}	-	6.4	P_{b5}-P_{b6}	-17.45	1.09
E_{b7}-E_{b8}	-	6.0	P_{b7}-P_{b8}	-16.35	0.82
E_{b9}-E_{b10}	-	13.2	P_{b9}-P_{b10}	-35.95	1.49
E_T	31.2 × 2=62.4		P_{grid}	-85×2=-170	

Fig. 3.25-3.26 shows the discharging current of EVs' batteries and the power supplied from each

group of EVs' batteries to the DN. Because of the power losses in contactless system, the power supplied from the EVs' batteries are found to be lower than the power demanded. The power demanded by the CCU is -170kW, but the total powers delivered from the EVs' batteries are found to be around -165kW. The efficiency of this case lies between 85% to 92%.

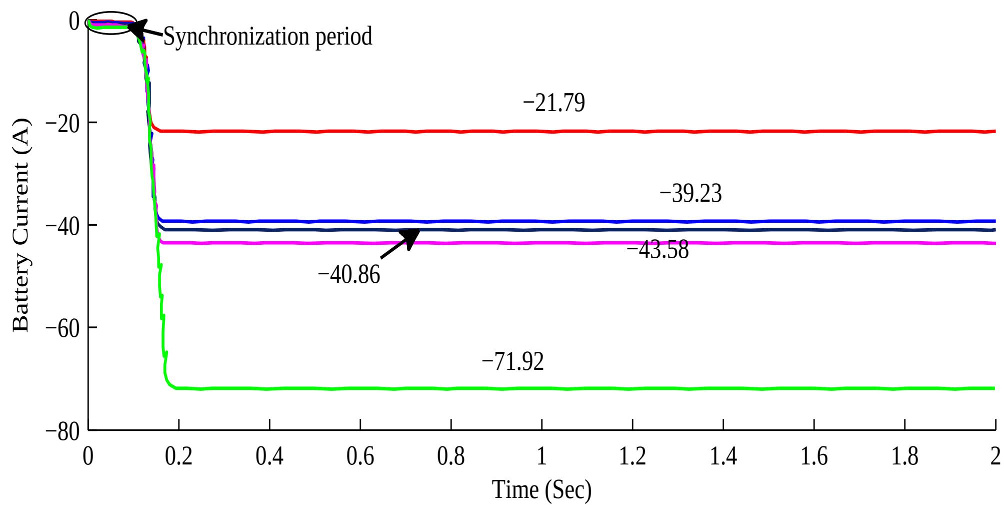

Figure 3.25: Discharging current of EVs' batteries.

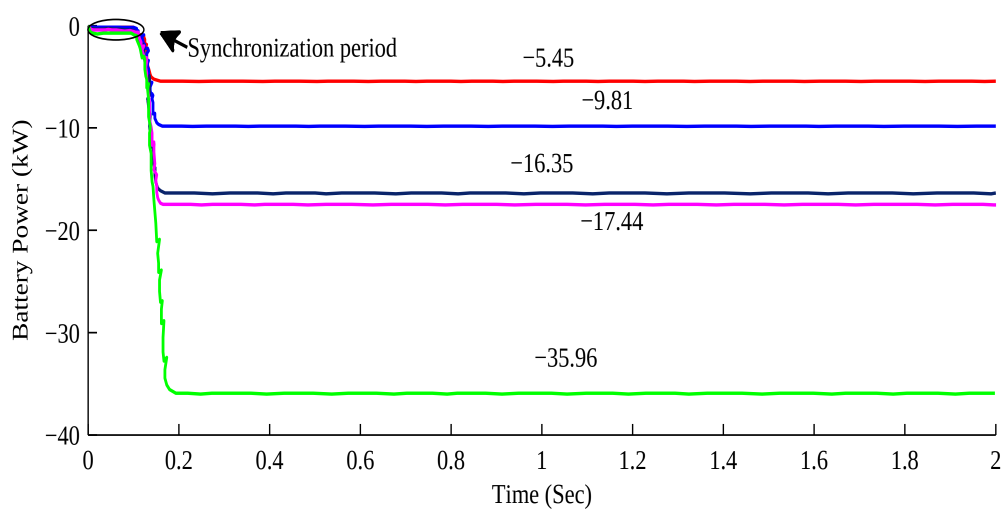

Figure 3.26: Power supplied from the EV battery.

Fig. 3.27 shows the power at the terminals of the primary side inverter at each BCCS unit, while supplying power to the DN.

Fig. 3.28 shows the pf of the BCCS unit. The BCCS unit is operated at resonant state and the pf is maintained near to unity, which is an acceptable pf to transfer maximum power in the system.

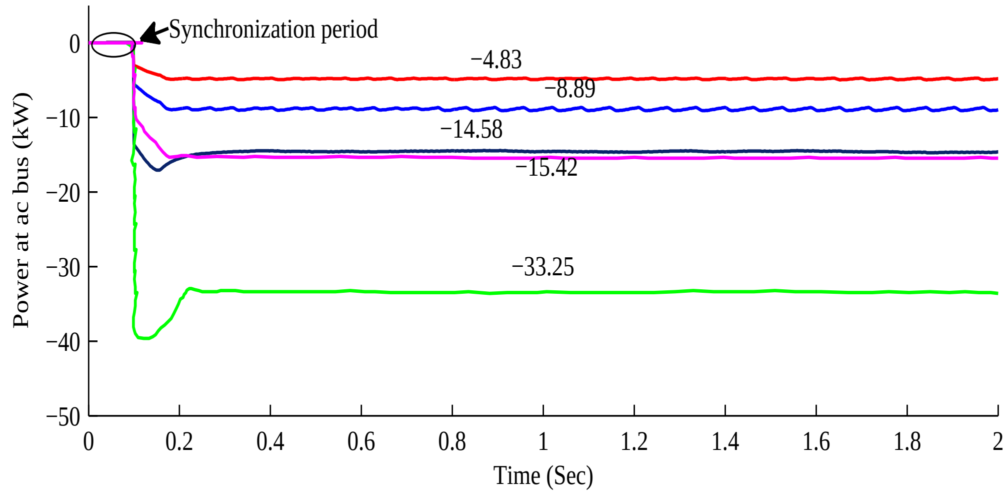

Figure 3.27: Power at the terminals of inverter of individual EVs.

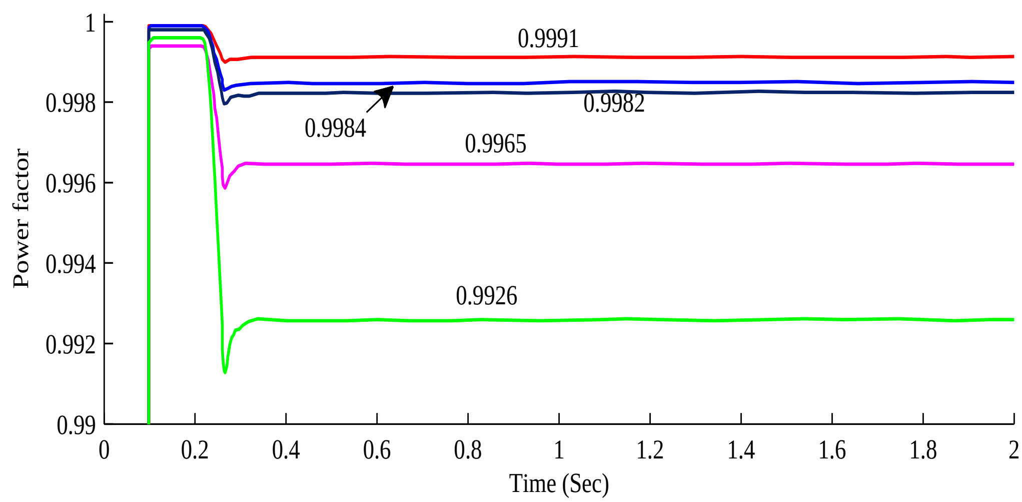

Figure 3.28: Power factor of the BCCS unit.

The DC link voltage controller controls the DC link voltage input of three-phase inverter at the primary side of BCCS unit, which is shown in Fig. 3.29. This control action is necessary to maintain the voltage level to make the circuit in synchronized condition to cause the power flow.

Fig. 3.30 shows the initial and final SOC of EVs' batteries of this case. It is observed from the figure, the EV batteries are not discharged beyond the SOC limit preferred by the owner.

The THD and the pf of the BCCS unit for V2G operating mode is give in Table 3.12. The THD of the BCCS unit is found in the range of 1.95391% to 3.08595% and the pf of the BCCS unit is found in the range of 0.9982 to 0.9991. The THD and power factors are allowable as per the IEEE standard

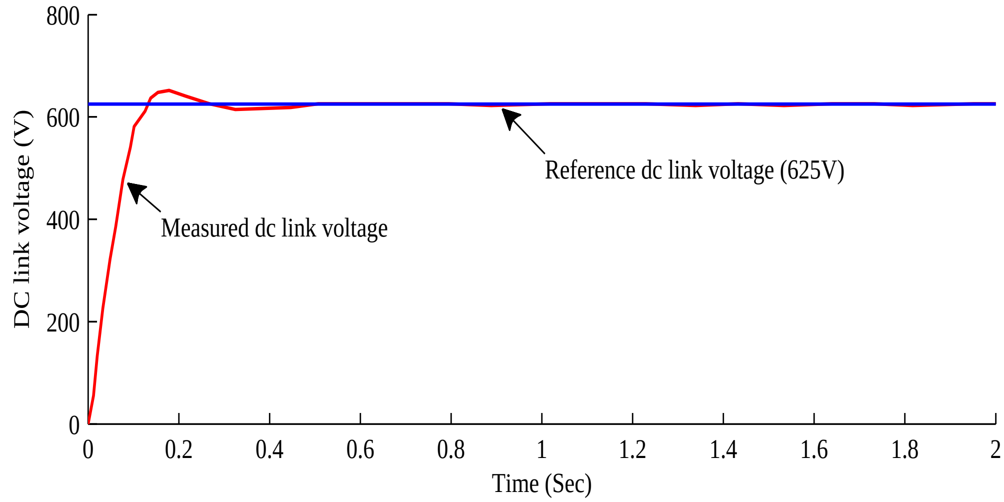

Figure 3.29: DC link reference voltage at the primary side.

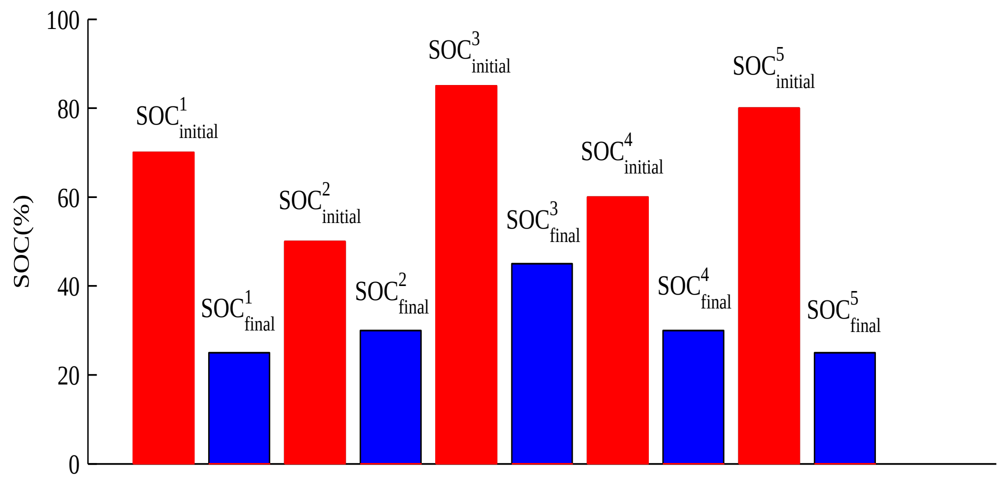

Figure 3.30: Initial and final SOC of the EVs' batteries

519-1992 [170].

Table 3.12: THD and pf of the BCCS unit during the V2G operating mode.

Sl. No	THD (%)	Power factor
1.	2.939	0.9965
2.	2.5959	0.9926
3.	2.10912	0.9982
4.	1.95391	0.9984
5.	3.08595	0.9991

Case III: EVs' batteries with low SOC and remaining batteries with high SOC connected during normal hours. In this case, few EVs arrive at SCS with low energy and others with high energy. The V_{node} is assumed to be low (0.95p.u to 0.97p.u). The FLC decided to draw -130kW of power for supporting the node. However, it is observed from Table 3.13, EVs' batteries are not able to give the demanded power to the grid. This is because few EVs come to SCS with low energy batteries.

Table 3.13: Summary of power and required/available energy of case III.

Parameter	Energy (kWh)		Parameter	Power (kW)	C_{rate}
	E_{stor}	E_{avail}			
E_{b1}-E_{b2}	-	3.6	P_{b1}-P_{b2}	-9.81	1.23
E_{b3}-E_{b4}	6.0	-	P_{b3}-P_{b4}	5.45	0.55
E_{b5}-E_{b6}	7.2	-	P_{b5}-P_{b6}	17.44	1.09
E_{b7}-E_{b8}	-	6.0	P_{b7}-P_{b8}	-16.35	0.82
E_{b9}-E_{b10}	-	13.2	P_{b9}-P_{b10}	-35.96	1.49
E_T	9.6×2=19.2		P_{grid}	-39.23×2 = -78.46	

Fig. 3.31-3.32 shows the battery current and power for both charging and discharging cases of EVs' batteries. In this case, the total available energy of EVs' batteries is 45.6kWh and the total energy required for charging the EVs' batteries are 26.4kWh. The grid demands -130 kW power but the SCS could provide only -78.46kW of power to the grid. This is due to the redistribution of power for low energy EVs' batteries.

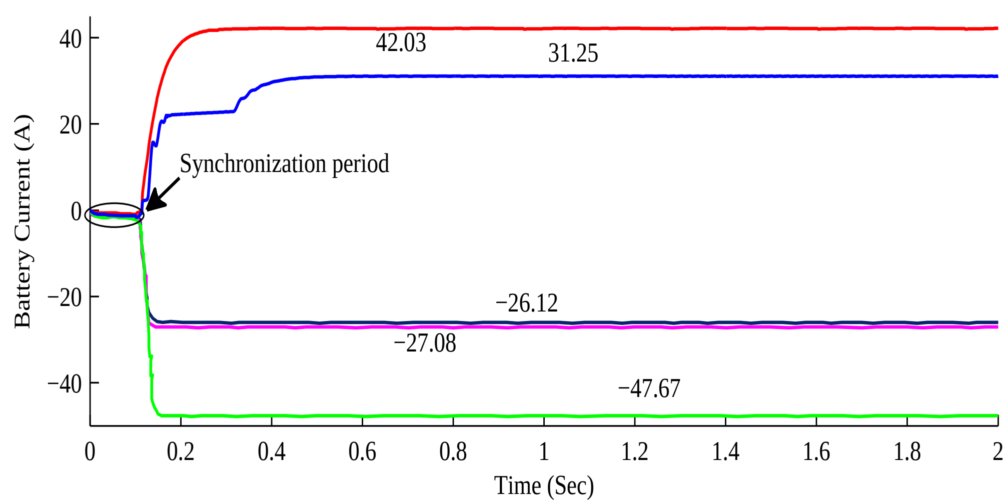

Figure 3.31: Battery current for charging and discharging case.

Fig. 3.33-3.34 shows the inverter power and the power factor of the BCCS unit. The initial and final SOC set by the vehicle owners for five group of EVs' batteries are given in Table 3.15. It is observed from the Table 3.15, EVs' batteries have not crossed the user defined SOC limits as mentioned in Table 3.7. EVs' batteries are not charged above the maximum limit (SOC_{max}) and it is not discharged beyond the minimum limit (SOC_{min}) set by the vehicle owner. Besides, the variation

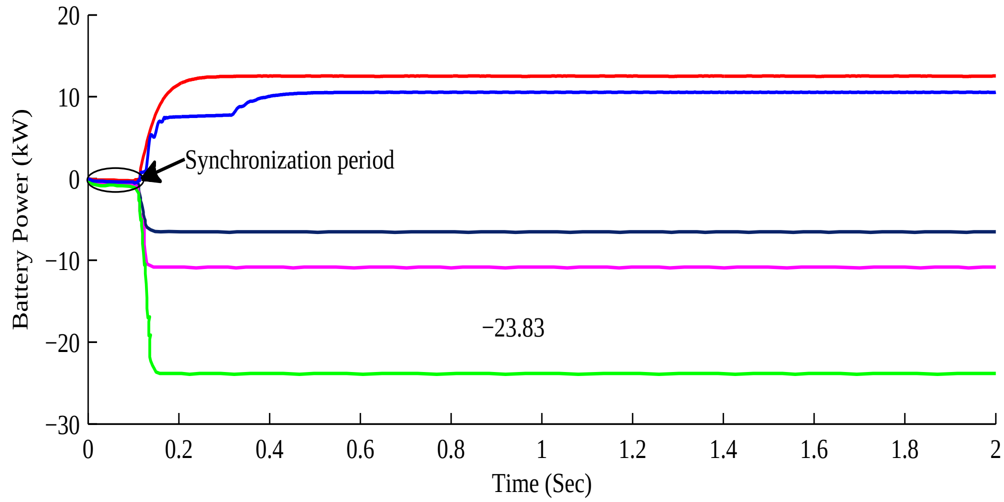

Figure 3.32: Power supplied/drawn from/to the grid.

in the node voltages are also observed for three cases of the proposed SCS. The V_{node} of case I and case II varies from 1.053 p.u to 1.03 p.u and 0.98 p.u to 1.01 p.u. While, for case III their is only a marginal variation between 0.95 p.u to 1.05 p.u and 0.96 p.u to 1.03 p.u, respectively.

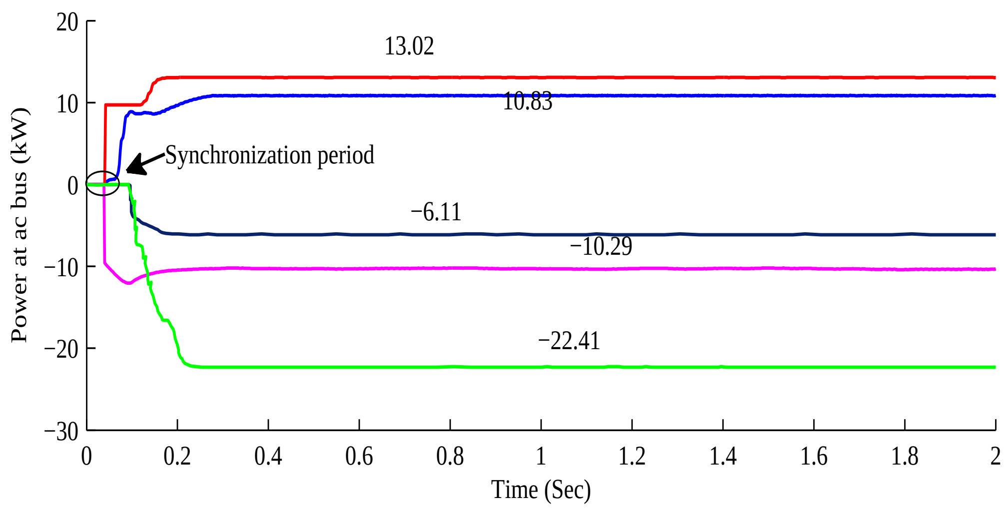

Figure 3.33: Inverter power at the primary side.

Fig. 3.35 shows the initial and final SOC of EVs' batteries of this case.

An EV battery of 8kWh with an initial SOC of 20% (SOC_{cr}) starts charging during off-peak hours and reaches 90%. At 17:00hrs, the node voltage fall below 1p.u and the battery discharges to the grid in peak hours. At 21:00hrs the battery reaches to 40% SOC. It is observed from the figure, the SOC of the EV battery increases due to charging of the EV battery (G2V) and SOC level decreases due to

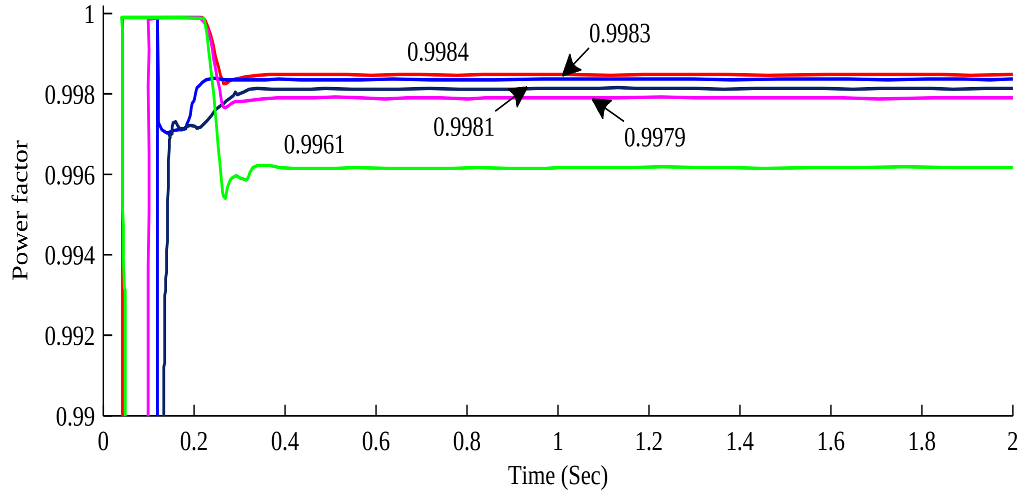

Figure 3.34: Power factor of BCCS unit.

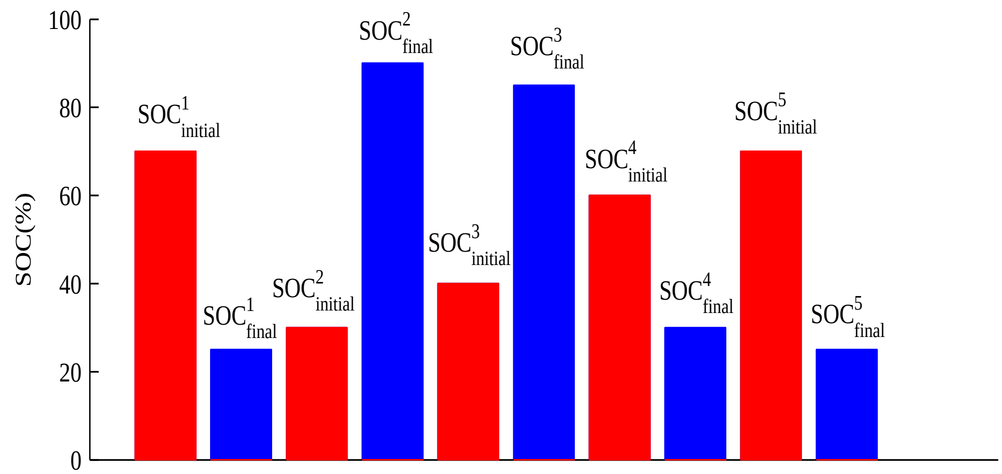

Figure 3.35: Initial and final SOC of the EVs' batteries

discharging of the EV battery (V2G).

Fig. 3.36 shows the change of SOC against the node voltage variation. An EV battery of 8kWh with an initial SOC of 20% (SOC_{cr}) starts charging during off-peak hours and reaches 90%. At 17:00hrs, the node voltage fall below 1p.u and the battery discharges to the grid in peak hours. At 21:00hrs the battery reaches to 40% SOC. It is observed from the figure, the SOC of the EV battery increases due to charging of the EV battery (G2V) and SOC level decreases due to discharging of the EV battery (V2G). Node voltage variation has been observed for bulk charging and discharging of EVs.

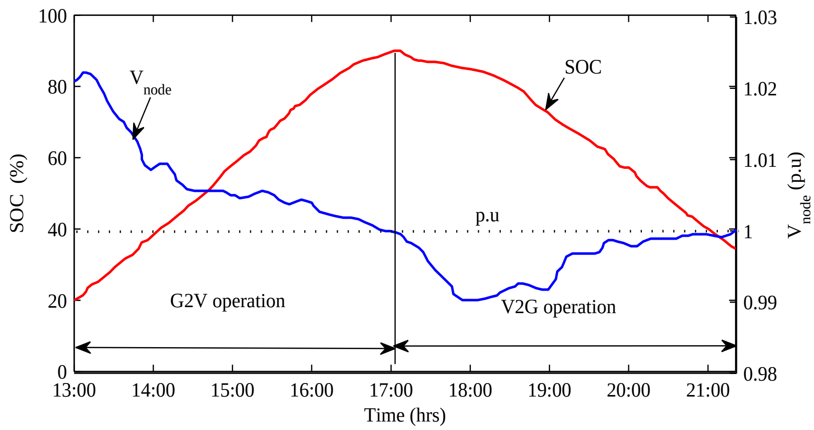

Figure 3.36: Changing the SOC level of the EV battery (8kWh, 250V) with respect to the V_{node}.

The THD and the pf of the BCCS unit for combined G2V and V2G operating mode is give in Table 3.14. The THD of the BCCS unit is found in the range of 1.88604% to 2.79205% and the pf of the BCCS unit is found in the range of 0.9961 to 0.9984. The THD and power factors are allowable as per the IEEE standard 519-1992 [170].

Table 3.14: THD and pf of the BCCS unit during the G2V and V2G operating mode.

Sl. No	THD (%)	Power factor
1.	1.88604	0.997
2.	2.01082	0.9961
3.	2.7486	0.9981
4.	1.98975	0.9983
5.	2.79205	0.9984

Table 3.15 shows the summary of the SOC variation of EVs' batteries. In Case I, the batteries SOC are increased because the EVs are charging during the off-peak hours. The EVs' batteries SOC levels are decreasing in Case II due to grid support. The peak power demand has been mitigated by using the EVs as a DESS to supporting the grid. In Case III, the EVs' batteries are charging as well as discharging due to low and high SOC level of the EVs' batteries.

Case IV: Impacts on the Distribution Node. Special case has been consider to analyze the impacts in the distribution node during the G2V operation. In this case, the BCCS units are not synchronization with distribution network which means the power flow from grid to BCCS unit after a random time interval. Unsynchronized V2G operation has not been considered, as the power flow from EV

Table 3.15: Summary of SOC for EVs' batteries.

	Case I		Case II		Case III	
	SOC_{cr}	SOC_{max}	SOC_{cr}	SOC_{min}	SOC_{cr}	$SOC_{min/max}$
EV1-EV2	20	100	70	25	70	25
EV3-EV4	30	90	50	30	30	90
EV5-EV6	40	85	85	45	40	85
EV7-EV8	35	95	60	30	60	30
EV9-EV10	20	80	80	25	70	25

battery to DN cannot taken place without the synchronization. The charging operation of EVs' batteries without synchronization of BCCS unit to DN has been assessed in this unsynchronized G2V operating mode. The *CB* is switched on after a random time interval without considering the phase sequence, frequency and the node voltage to show the impacts in the DN.

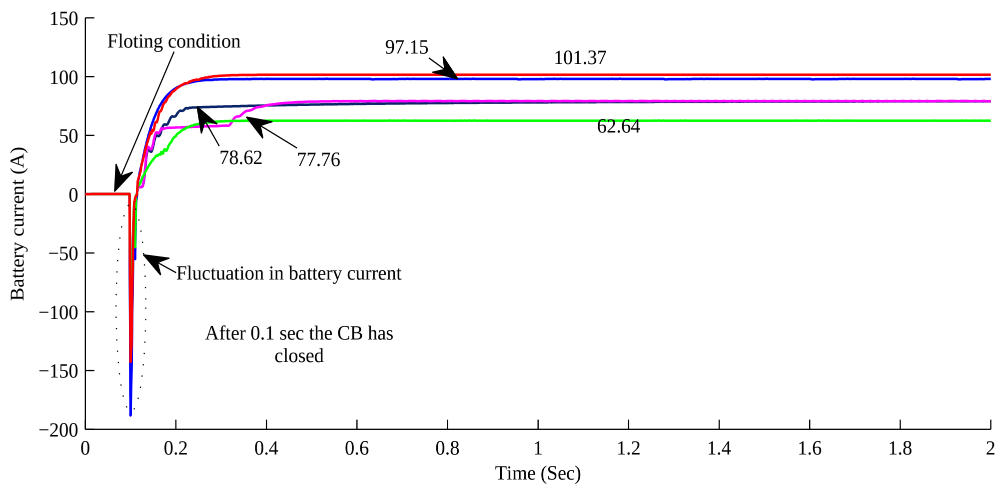

Figure 3.37: Battery current in unsynchronized G2V operating mode.

Fig. 3.37-3.40 shows various graphical results obtained in this mode. It is observed in the Fig. 3.37, that large current is fluctuating in the EVs' batteries for a very short time interval and it may damage the EV battery, PS and SS converter unit.

The node voltage suddenly increases due to without synchronization of the BCCS unit and DN, which results in the undesired sharp peak of 1.013 p.u. magnitude as shown in Fig. 3.39. The V_{node} is suddenly increased due to proper coordination between the BCCS unit and DN. Therefore, the BCCS unit must synchronize with DN for power flow in either direction.

Graphical results for the total power drawn from the node by the entire BCCS unit in unsynchronized G2V operating mode have been shown in Fig. 3.40. Form this figure, the total of 120kW power

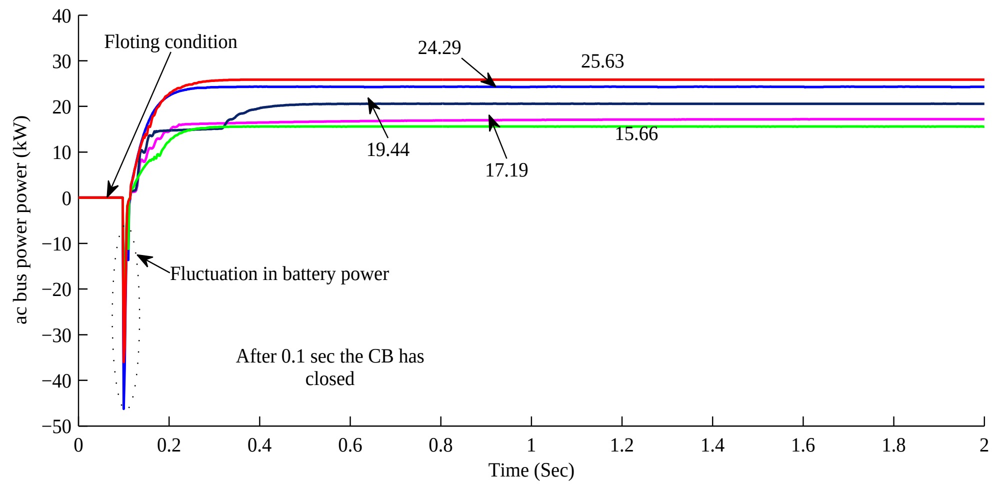

Figure 3.38: Battery power in unsynchronized G2V operating mode.

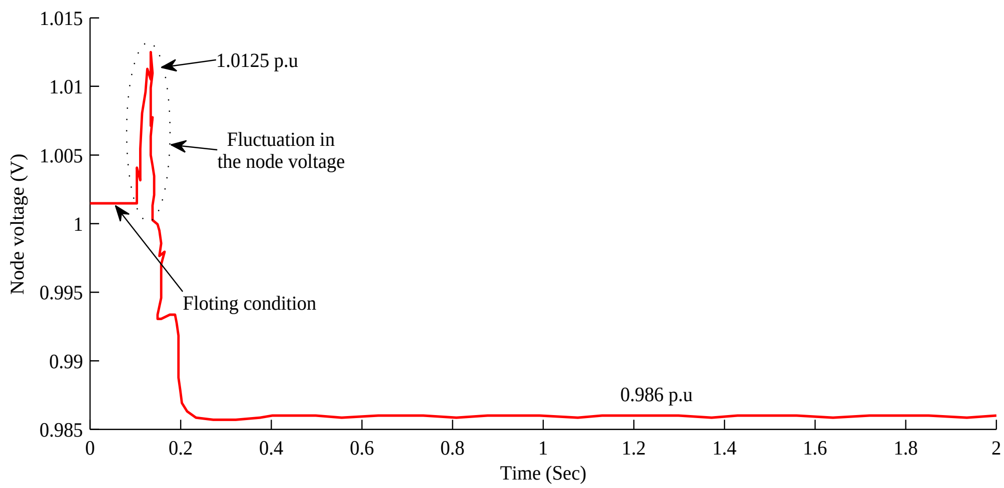

Figure 3.39: Node voltage in unsynchronized G2V operating mode.

has been drawn by the node as soon as the *CB* is switched on, which is settled to 113.7 kW in 0.4 seconds.

It is evident from Fig. 3.37 to Fig. 3.40, the power should flow between grid and BCCS unit after the synchronization of BCCS unit.

Table 3.16 shows the summary of node voltage before and after supporting the distribution node.

Table 3.16: Summary of node voltage before and after supporting

	V_{node}	V_{node}
Case I	1.05	1.053
Case II	0.98	1.01
Case III	0.95 - 1.05	0.96 - 1.03

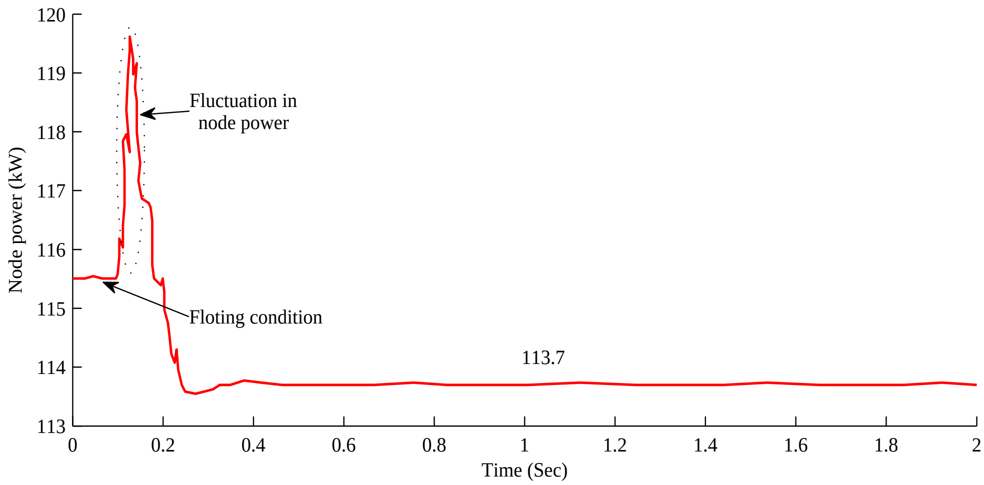

Figure 3.40: Power drawn from the node in unsynchronized G2V operating mode.

It is evident from Fig. 3.20-3.36, that the proposed multi-point SCS can handle the charging/discharging operation individually and simultaneously by ensuring grid voltage stability. The C_{rate} and SOC limit of EVs have been maintained as per the limit set by the vehicle owner. The individual BCCS unit power factor for V2G and G2V operating mode is lies between the range of 0.95 to 0.88. The THD lies between the range of 1.897% to 2.939% which allowable as per the IEEE standard 519-1992 [170]. Therefore, this CS has been more suitable for gird support during peak power demand and also store the energy during off-peak hours.

3.6 Summary

- In this Chapter, the multi-point smart charging station has been proposed which is connected in the distribution node of Guwahati city.

- The SCS has three main units such ac CCU, the CS aggregator and the BCCS unit.

  - The CCU decides the power flow between BCCS unit and DN based on node voltage of the grid, total energy availability of SCS and duration to support the grid.

  - The CS aggregator have the ability to distribute the reference power signal to EVs' batteries.

  - The BCCS unit provide the power based on the CCU and CS aggregator control signal.

Further, the BCCS unit has three main units such as primary side, secondary side and contactless coil.

  * The primary side and the secondary side, which is separated by an air-gap and is magnetically coupled to each other. The power is transferred from the primary to the secondary side through weak or loose magnetic coupling.
  * Primary and secondary controllers are employed on either side of contactless coil to control the power flow.

- The BCCS unit modeled has 10 charging points, which is accessible for EVs of different battery ratings. Each charging points of BCCS unit are designed for a maximum peak power handling capacity of 50kW.
- The complete multi-point SCS and real-time grid data of Guwahati city has been implemented in MATLAB Simulink environment.
- The EVs' batteries are not charged/discharged beyond the SOC limits and maximum C_{rate} defined by the EV owner.
- The SCS has been used for grid support during peak power demand and store the energy during off-peak hours.

In the next Chapter, the economic burdens (beneficiary calculation) to EVs owners and grid operator while transferring the energy in either direction (from grid to EVs or vice versa) have been presented. Also, the economics beneficiary calculation has been analyzed based on the capacity loss in the EVs' batteries.

Note: This work, Modeling and Control of Contactless based Smart Charging Station in V2G Scenario has been published in IEEE Transaction on Smart Grid.

4

Mathematical Modeling For Economic Evaluation Of Electric Vehicle To Smart Grid Interaction

Contents

4.1 Introduction

Conventional internal combustion engine vehicle depends on oil based energy sources. Along with it, the environmental issue and the regular hike in the fuel price has prompted to look for alternatives. Electric vehicles have emerged as an alternative to the ICE vehicles [171]. Presently researchers are trying to integrate the EVs with the recently developed technologies.

The EV's higher fuel efficiency, lower per km cost, eco-friendly are some of the advantages. EV's disadvantages are mainly in the form of limited driving range, higher refueling time (battery recharge time), higher purchasing cost (due to high cost of the battery), bulky battery size and weight [172]. The EV's named disadvantages are mainly related to the battery. Numerous research work is being carried out to neutralize all such battery related problems. Though there is increasing demand for EVs, but its large scale implementation remains a challenge. EV's untimely charging pattern will create a major problem to the grid operators [173, 174].

Simultaneous charging of a large number of vehicles can lead to grid instability. This can be avoided, if the EVs are integrated with the grid. For grid, this will provide an option to minimize peak power demand [22, 175, 176]. Researchers are evaluating the technical feasibility of the scheme and finding the solutions to the problems [32]. In a different approach, optimal scheduling for charging and discharging of EVs in V2G scenario has been developed [64]. In V2G scheme, the peak hour energy supplied by the EV to the grid depends on the battery capacity. The battery capacity represents the maximum amount of energy that can be extracted from the battery. The battery capacity is affected by capacity fade (CF) or capacity loss (CL). Capacity fade is directly proportional to C_r and D_r [177, 178]. The capacity of the battery also decreases with its usage and with time (due to its self-reacting chemicals).

Though the above paragraph has established the technical advantages of V2G, but to practically implement the scheme it has to be checked on the scale of its financial feasibility. The economic aspects of V2G have been reported in various literatures [77, 179]. Coordinating V2G services for energy trading has been discussed in [179].

Integrating the EV to the grid results in capacity loss of the battery, which mainly depends on C_r. This capacity fade results in energy loss. Battery capability is mainly affected due to the CL during

V2G interaction [9, 68, 74, 174, 177, 180–184]. This loss is dependent on the chemical structure of the battery. Hence, this is a characteristic loss which can never be eliminated. The CL results in financial loss to the EV owners. Also while replacing the battery, its high cost becomes a burden to the EV owners. For the EV's to sustain, EV owners should never lose money specially due to V2G interaction. The vehicle owners will cooperate with the grid operators only if they are financially benefited. The grid operators also have some constraints on the amount of money it can charge from consumers and the amount with which it purchases energy from the EV owners [8]. In this work, a method has been described for the grid to minimize peak hour energy demand by considering the EV as an distributed storage source. Further the energy transfer between the grid and the EV has been discussed at different C_r, D_r and some of the important financial results have been analyzed.

The main features of the model have been summarized below:

(i) For the bidirectional flow of energy between the EV and grid, the monetary calculation for per km transportation becomes complex. This Chapter has made this complex calculation into a fairly simple calculation using a set of equations.

(ii) As integration of the EVs to the grid is arguably profitable, this work compares the per km transportation cost for the EV with and without integration to the grid. It has found that due to peak hour transfer of energy between the EVs and the grid, the per km cost for the EV integrated to the grid is higher.

(iii) Capacity loss has been determined for the integration of the EV's to the grid. Based on the capacity loss, all the major financial calculation have been done, i.e., the economics related to the capacity loss has been analyzed.

(iv) The capacity losses in the integration of the EVs to the grid for different charge/discharge rate have been calculated.

This Chapter is organized as follows: Section 4.2 presents the capacity loss model of Li-Ion battery. The mathematical model for economic evaluation of the V2G has been formulated in Section 4.3. In this section the process of bidirectional energy transfer between the EVs and the grid has been identified and analyzed. In section 4.4, a scenario has been analyzed where the EV is not integrated to the grid. The cost benefit related calculations for energy transferred from grid-to-vehicle (G2V) and vehicle-to-grid (V2G) are discussed in Section 4.5. In this section the energy flow from V2G and G2V is analyzed at different C_r and D_r. Section 4.6 summary of the present work.

4.2 Capacity Fade/Loss Model

In this section, mathematical model for capacity loss of the EV battery is presented. The electric equivalent circuit (EEC) for EV battery is given in Fig. 2.3. The EEC model has three parameters: an open circuit voltage (V_0), internal resistances (R_1 and R_2) and capacitance (C). This model is used to determine the circuit parameters for different C_r and D_r. The battery parameter values are different for the different charge or discharge rate. The battery parameters are determined using the measured value of the battery manufacturer's characteristics data. If the charge or discharge rate is constant, the electrical equivalent circuit parameters (R_1, R_2, C and V_0) are approximately constant from 20% SOC to 100% SOC, but changes exponentially from 0% SOC to 20% SOC. This is due to the electrochemical reaction inside the battery [39]. The variation of small parameters among the curves for different charge or discharge rate indicate that these parameters are approximately independent of charge or discharge currents. The mathematical representations for R_1, R_2, C and V_0 under constant current charging conditions are given in Chapter 2, Section 2.2.

The terminal voltage ($V^C_{c_i/d_j}$) of charging/discharging scenario is given in Eq. (2.5) and Eq. (2.6). The terminal voltage of the battery equivalent circuit depends on the parameters of the polynomial equation. The quantity of energy stored (E_{stor}) to charge the EV battery depends on the SOC of the battery which is given in Eq. (2.13). The total processed energy (PE_c) for charging scenario is given in Eq. 2.14. The energy available (E_{avail}) from the EV battery can be calculated from Eq. (2.15). The processed energy (PE_d) for discharging scenario is given in Eq. 2.16. Using Eq. (2.15) and Eq. (2.16), the total processed energy (E_{total}) of the EV battery is defined as the sum of processed energy for charge and discharging scenarios.

It should be noted here that the total processed energy is not equal to the energy that can be processed. The total processed energy is the sum of the energy that has been injected and extracted from the battery. For example, assuming a 20kWh battery, if 5kWh is extracted from it and 5kWh is injected back into it, then the total processed energy is 10kWh. Whereas the total energy that can be processed is 40kWh, i.e. if the battery is new and has 100% SOC then 20kWh can be extracted from it and once its SOC is 0% then 20kWh can be injected into it.

The amount of energy that can be extracted from the battery or stored in the battery decreases rapidly due to the CL in the EV battery. The CL mainly depends on total processed energy during charging/discharging, C_r, D_r and temperature [180]. C_r and D_r varies with respect to the grid condition [185]. Therefore, a mathematical model is required to predict the CL at different C_r and D_r. The battery capacity depends on certain specified conditions such as C_r, D_r, SOC and temperature [181]. In this work, room temperature has been consider. The mathematical model for CL at different C_r and D_r is given in Eq. (2.28).

4.3 Mathematical Model for Economic Evaluation

Due to the bidirectional energy transfer between the grid and the EV, determination of the amount of money that the consumers (who uses the EV for transportation) have to pay becomes complex. Normally, the electricity tariff is based on peak and off-peak hours demand [186]. However, due to the bidirectional energy transfer, the current tariff structure is not suitable for the immediate future. Therefore, a model should be formulated such that large scale implementation of EVs does not result in a complex financial calculation. This section discusses such a possible model for V2G.

4.3.1 Notations

While doing the mathematical modeling we need to define few notations and they are as follows:

- q is the total capacity loss of the EV battery in Ah. Using Eq. (2.28), q can be mathematically represented as:

$$q = \sum Q_{l_k}^{C} \tag{4.1}$$

4.3.2 Assumptions

The following assumptions have been made.

- Peak hour is that period of the day when the demand for the electrical energy is maximum. On an average, the duration of peak hour is assumed to be $\frac{1}{3}$ of the day i.e 8 hours [187]. So the duration of off-peak hour is 16 hours. Therefore, the total energy consumed by EV in a day can be mathematically represented as:

$$E_{total} = E_{peak} + E_{off-peak} \tag{4.2}$$

where, E_{total} is the total energy consumed in kWh, E_{peak} is the total energy consumed during peak hours in kWh and $E_{off-peak}$ is the total energy consumed during off-peak hours in kWh. Using Eq. (4.2), the monetary equivalent of energy consumed can be represented as:

$$A = R_{peak}E_{peak} + R'_{off-peak}E_{off-peak} \tag{4.3}$$

where, A is the total money to be paid for energy consumption ($Rs.$), R_{peak} is the tariff of energy during the peak hours (($Rs.$)/kWh) and $R'_{off-peak}$ is the tariff of energy during the off-peak hours (($Rs.$)/kWh).

- EV owners are the proprietor of the EVs. The consumers are the people who use the EV for transportation only. In terms of EV to grid coordination, EV owners are the participants in V2G and G2V scheme. Consumers are participants only in the G2V scheme.

- When the EV owner uses the EV, the owner itself becomes its customer as it (the EV owner) pays for the cost incurred for transportation. The EV owners and the consumers are the different entity for the same EV.

- Efficiency of the EV battery has been assumed 90%. This lower efficiency is due factors such as heat, faulty electrical components, etc [188].

- Scheduling of peaks hours power plant is very costly as well as complex. Also the cost of the battery is very high. So whenever energy is required by the grid, if the EVs supply it then it gets money. So, it's economically beneficial for both the EVs and the grid operators.

- For ease of calculation, all the financial and energy transactions are calculated on per day basis.

The sample calculation has been demonstrated in the Appendix E. The next subsection discusses about the energy required by the EV battery.

4.3.3 Energy Required by EV Battery

To supply the energy, the battery has to charge itself (store energy). For a battery with 90% efficiency (assumed), 10% of the energy supplied to it by the grid is always lost. Therefore, 90% input energy to the battery should be equal to the energy required by the battery. Mathematically, this can be represented as:

$$\begin{aligned}\left(\frac{90}{100}\right) E_{ib}^{G} &= E_{stor} \\ E_{ib}^{G} &= E_{stor} \times \left(\frac{100}{90}\right)\end{aligned} \tag{4.4}$$

where, E_{ib}^{G} is the input energy to the battery provided by the grid. The grid operators will charge the EV owners depending upon the total quantity of energy consumed by the battery. Using Eq. (4.3), the amount paid by EV owner to grid operators is given by the following equation:

$$AP_{evg} = \mathrm{cx} + \mathrm{c'x'} \tag{4.5}$$

where, AP_{evg} is the total amount of money paid by the EV owners to the grid operators during a complete day, c is the total quantity of energy supplied by the grid to the EV battery during peak hours, c' is the total quantity of energy supplied by the grid to the EV battery during the off-peak hours, x is the tariff paid by EV owner to grid operators per kWh during peak hour ($Rs.$) and x' is the tariff paid by EV owner to grid operators per kWh during off-peak hour ($Rs.$).

Using Eq. (4.5), the total energy supplied by the grid is equal to $c+c'$. Assuming grid transmission lines to be lossless, this energy is also the input energy to the battery. Therefore, this energy is equal to E_{ib}^{G}. Mathematically, this can be represented as:

$$\begin{aligned}c + c' &= E_{ib}^{G} \\ \Rightarrow c + c' &= \frac{E_{stor}}{0.9}\end{aligned} \tag{4.6}$$

The EV battery has been charged with E_{ib}^{G}, the energy that can be extracted from EV battery which is less than E_{stor}. Using Eq. (2.15), E_{avail} is the energy that can be extracted from the EV battery. The next subsection describes the possible quantity of energy that the EV can supply to the grid during stress.

4.3.4 Peak Hour Energy Supplied to Grid

During the V2G interaction the battery exchanges energy with the grid. This also results in capacity fade. The total capacity loss is calculated using the CFM which is mentioned in Eq. (4.1). This equation provides a easier method to calculate capacity loss.

If the EV has sufficient energy after its transportation use, then only the EV can support the grid. For a battery with nominal capacity Q, the minimum level up to which the battery is usable for grid interactions and its daily requirements for transportation purposes is $\frac{Q}{3}$. The value of $\frac{Q}{3}$ chosen for transportation requirements is user defined. It has been chosen so that the initial energy that the EV can give to the grid, after the losses, is at least 50% of the initial energy that the EVs has extracted to charge its battery. The EV owner invests in a battery that can store 3 times the energy due to the following reasons:

- EVs can support the grid during stress.
- To match performance of the conventional vehicles, EVs requires a large battery.
- EVs can sustain itself in sudden requirement of long distance travel. Fuel engine based vehicle has the option to instantaneously refill itself, at present the EVs does not enjoy such facility.

The EV has remaining energy $\left(\frac{2Q}{3}\right)$, which also includes the losses. Mathematically,

$$E_{transpor} = \frac{E_{avail}}{3} \tag{4.7}$$

$$E_{rem} = \frac{2E_{avail}}{3} \tag{4.8}$$

$$E_q = k\left(E_{rem}\right) = \frac{2kE_{avail}}{3} \tag{4.9}$$

$$E_l = k'\left(E_{rem}\right) = \frac{2k'E_{avail}}{3} \tag{4.10}$$

where, $E_{transpor}$ is the energy used by EV for the transportation purpose, E_{rem} is the energy remained in the system after its usage for the transportation purpose, k is the percentage of energy loss due to CL, k' is the percentage of energy loss due to other reasons, E_l is the energy loss due to other reasons such as faulty circuits, components, etc and E_q is the energy lost due to capacity loss. This CL is due to grid interaction and as well as transportation.

The EVs are available in the parking bay [22, 23], thus can be used for interacting with grid. The battery energy that can be sold back to grid during peak hours. It is equal to remaining energy in the EV battery minus losses. Mathematically,

$$E_{pos} = E_{rem} - E_q - E_l \tag{4.11}$$

where, E_{pos} is the possible amount of energy available in the battery that can be sold to the grid. Substitute Eq. (4.8), Eq. (4.9) and Eq. (4.10) in Eq. (4.11).

$$E_{pos} = \frac{2E_{avail}}{3}(1 - k - k') \tag{4.12}$$

It must be noted here that the energy sold by the EV owner to the grid operators may be different from the possible amount of energy available in the battery. It is the EV owners who decides and supplies the amount of energy to the grid. The above scenario is validated with the assumption that the grid obtains as much peak hour energy as provided to them. The quantity of energy received by the grid depends on the discharging efficiency of the battery. For a 90% efficient battery (assumed), the energy obtained by the grid can be mathematically represented as:

$$E_{trans} = \left(\frac{90}{100}\right) E_{\text{sup}} \tag{4.13}$$

where, E_{trans} is the actual amount of energy that the grid obtains from the EV and E_{sup} is the amount of energy supplied by the EV battery to the grid. The supplied energy (E_{sup}) is equal to the possible energy (P_{pos}) available for grid support. Therefore, substitute Eq. (4.12) in Eq. (4.13).

$$E_{trans} = \left(\frac{90}{100}\right) E_{pos} \tag{4.14}$$

The grid operators pay for the quantity of energy actually received from the EV. Using Eq. (4.3), the amount paid by the grid operators to EV owner is given by the following mathematical equation:

$$AP_{gev} = \mathrm{sx_2} + \mathrm{s'x_2'} \tag{4.15}$$

where, AP_{gev} is the total amount of money paid by the grid operators to the EV owners during a complete day, s is the total energy obtained by the grid during the peak hours, s' is the total energy obtained by the grid during the off-peak hours, x_2 is the tariff paid by grid operators to EV owner per kWh during peak hour energy ($Rs.$) and x_2' is the tariff paid by grid operators to EV owner per kWh during off-peak hour energy ($Rs.$). Using Eq. (4.15), the total energy obtained by the grid is equal to $s + s'$. Mathematically, this can be represented as:

$$\begin{aligned} & s + s' = E_{trans} \\ \Rightarrow\ & s + s' = \left(\frac{90}{100}\right) E_{pos} \end{aligned} \tag{4.16}$$

4.3.5 Capacity Loss Compensation

For a battery, charging is the process of accumulation of energy and discharging is the process of dissipation of energy. The process of charging and discharging for one time completes one battery life cycle. Due to natural limitations, the usage of a battery is limited to a fixed number of cycles, after which the battery is of no use to the EV owner. Let, M_{dep} be the depreciated value of the battery after n number of cycles of V2G interaction. The battery is expected to last n' number of cycles. The average per unit cost of the battery in terms of number of V2G cycle is $\frac{M}{n'}$. So after n number of V2G interactions, the depreciated value is given by the following mathematical equation:

$$M_{dep} = \frac{n}{n'} M \tag{4.17}$$

where, M is the initial cost of the battery and M_{dep} is the depreciated value of the battery after n number of cycles. The energy loss (E_q) due to capacity loss is estimated by running the iteration of CL model n times and assuming that only E_p amount of energy is being exchanged from the battery. This is an additional loss to the EV owners. Therefore, they should be compensated for this loss. The sum of compensation money charged by the EV owners should be greater than or equal to the monetary equivalent of the energy lost due to degradation of capacity of the battery. This will ensure that the EV owners are beneficiary participants. Mathematically,

$$C_m \geq M_e \tag{4.18}$$

where, C_m is the compensation money for energy loss and M_e is the money equivalent of the capacity lost. The capacity loss mainly depends on the number of cycles of V2G interaction and the energy associated with it [180]. In this work, the SOC limit has been assumed from 20% SOC to 100% SOC for charging scenario and 100% SOC to 20% SOC for discharging scenario. If the SOC limit is interrupted, then the amount of energy processed for charging and discharging scenarios will change. As the capacity losses also depends on the processed energy for charging and discharging scenario, the capacity losses will have different value if the SOC limit is interrupted. The compensation money is calculated using the above mentioned factors. Mathematically, it can be denoted as:

$$\begin{gathered} C_m \propto nPE_{c/d} \\ or \\ C_m = znPE_{c/d} \end{gathered} \tag{4.19}$$

where, z is the compensation money charged by the EV owners for capacity loss and $PE_{c/d}$ is the processed energy for charging (PE_c) and discharging (PE_c) scenarios. With time and usage, the battery does not provide the energy it had provided in the very first cycle. This generates a loss of energy as well as loss of money. Therefore, the capacity loss should be compensated. As capacity loss is a permanent loss, it can only be compensated in terms of money. Hence, the capacity loss is compensated, then the financial losses for the EV owner are taken care off. The maximum energy available from the battery is E_{avail}. So the cost of per unit of battery is $\frac{M}{E_{avail}}$. This per unit battery cost is true only when the total energy can be used. For transportation purpose, the maximum energy that the battery can use is up to $\frac{E_{avail}}{3}$. The remaining energy is $\frac{2E_{avail}}{3}$, which also includes the losses (capacity and other loss). The capacity loss depends on the number of cycles of V2G interaction, so z is calculated using the depreciated value of the battery. Therefore, the per unit energy cost which also includes the losses of the battery is $\frac{M_{dep}}{\frac{2E_{avail}}{3}}$. Hence, the monetary equivalent of the capacity loss of the battery can be mathematically represented as:

$$M_e = \frac{3M_{dep}}{2E_{avail}} E_q \tag{4.20}$$

Using Eq. (4.17) to Eq. (4.20) the above condition is formulated as:

$$nzPE_{c/d} \geq \frac{3M_{dep}}{2E_{avail}} E_q \tag{4.21}$$

$$z \geq \frac{3M_{dep}E_q}{2E_{avail}nPE_{c/d}} \tag{4.22}$$

Using Eq. (4.21) and Eq. (4.22), the value of z can be determined. It should be noted that the EV's CL is due to grid support during peak hour. Therefore, gird operators provide compensation money to EV owners for capacity loss. Eventually the grid recover this cost from the consumers while selling the energy in peak hours. The next subsection presents the amount of money that has to be paid by the grid operators (for peak hour energy) to the EV owners.

4.3.6 Determination of Tariff for Grid Operators

The high cost of battery (M) and the capacity loss of the battery are the major financial liabilities to the EV owners. For EV owners, these liabilities can be attributed as losses. Mathematically,

$$T_{loss} = z + M_{dep} \tag{4.23}$$

where, T_{loss} is the total losses to the EV owners during V2G interaction. The total cost price of energy for the EV owners is the sum of the money paid to the grid operators to charge the EV battery and the loss incurred during V2G interaction. Mathematically,

$$\begin{aligned} AP_{cp} &= AP_{evg} + T_{loss} \\ &= AP_{evg} + z + M_{dep} \\ \Rightarrow AP_{cp} &= cx + c'x' + z + \left(\frac{nM}{n'}\right) \end{aligned} \tag{4.24}$$

where, AP_{cp} is net cost price of the energy for the EV owners. In Eq. (4.24), z and M_{dep} are dependent on the full battery discharge. It may take days or months or years for the battery to discharge completely. Therefore, Eq. (4.24) has to be normalized. Mathematically,

$$A_{cp} = cx + c'x' + \frac{z + \frac{nM}{n'}}{D_n} \tag{4.25}$$

where, D_n is the number of days the battery takes to depreciate its value to zero. D' can be mathematically represented as

$$D_n = \frac{n'}{n''} \tag{4.26}$$

where, n' is the maximum number of cycles that the battery can charge/discharge in its life span (this value is fixed by the manufacturer) and n'' is the average number of cycles of daily G2V interaction. From the economic point of view, this cost price has to be raised by selling energy to the grid operators. Mathematically,

$$\begin{aligned} & AP_{cp} = AP_{gev} \\ & \Rightarrow \mathrm{cx} + \mathrm{c'x'} + \frac{z+\frac{nM}{n'}}{D_n} = \mathrm{sx_2} + \mathrm{s'x_2}' \end{aligned} \tag{4.27}$$

EV owners to get profit, tariff paid by grid operators to EV owner per kWh during peak hour (x_2) should be greater than tariff paid by EV owner to grid per kWh during peak hour (x) and tariff paid by grid operators to EV owner per kWh during off-peak hour (x_2') greater than tariff paid by EV owner to grid per kWh during off-peak hour (x'). Mathematically,

$$\begin{aligned} & \mathrm{x_2} \geq \mathrm{x} \\ & \mathrm{x_2}' \geq \mathrm{x}' \end{aligned} \tag{4.28}$$

The cost of per kWh energy charged by the EV during selling is more than the money it had paid to buy the energy. The cost charge by the EV also includes the battery cost and the capacity loss. As the result EV always gains money, whenever they sell energy to the grid. While the cost of battery is very high, but participation of EVs in V2G can be safely assumed. To meet the peak hour demand, the grid may install extra generators. Functioning of these generators are very economically costly and also very complex. So buying energy from the EVs to meet the peak hour energy demand is economical more beneficial for the grid. So by participating the EV owners also can obtain the battery cost from the grid. So this is also beneficial for the EV owners. The next subsection determines the amount the consumers (passengers) have to pay for EV transportation service.

4.3.7 Determination of Tariff for Consumers

The grid had supplied energy $\left(\frac{E_{stor}}{0.9}\right)$ to the EV. The EV pays for it and the grid operators obtain its cost price. When the EV sells back the energy $\left(0.9E_{\mathrm{sup}}\right)$ to the grid, the EV gets its money including its battery price. So if the consumers pay for $\left(0.9E_{\mathrm{sup}}\right)$, then the total quantity of energy exchanged during the complete process is financially accounted. Using Eq. (4.3), the amount paid by the consumers to grid operators is given by the following mathematical equation:

$$A_{cg} = \mathrm{sx_1} + \mathrm{s'x_1}' \tag{4.29}$$

where, A_{cg} is the total amount of money paid by the consumers to the grid operators during a complete day, x_1 is the tariff paid by consumers to grid operators per kWh peak hour energy (Rs.) and x_1' is the tariff paid by consumers to grid operators per kWh off-peak hour energy (*Rs.*).

Grid operators to get profit, tariff paid by consumers to grid operators per kWh peak hour energy (x_1') greater than tariff paid by grid operators to EV owner per kWh during peak hour (x_2) and tariff paid by consumers to grid operators per kWh during off-peak hour (x_1') greater than tariff paid by grid operators to EV owner per kWh during off-peak hour (x_2'). Mathematically,

$$\begin{aligned} x_1 &\geq x_2 \\ x_1' &\geq x_2' \end{aligned} \tag{4.30}$$

The next section presents the scenario where EV uses its complete energy for transportation without supporting the grid.

4.4 Electric Vehicle Without Supporting the Grid

This section presents the scenario where EV is not supporting the grid during peak hours. The EV uses its complete energy for transportation. An EV with a battery of 80% SOC, nominal capacity 100 Ah, constant terminal voltage 400 V and 90% efficiency has been considered in this Section. The capacity of the battery for the complete life cycle for different C_r and D_r is shown in Fig. 4.1.

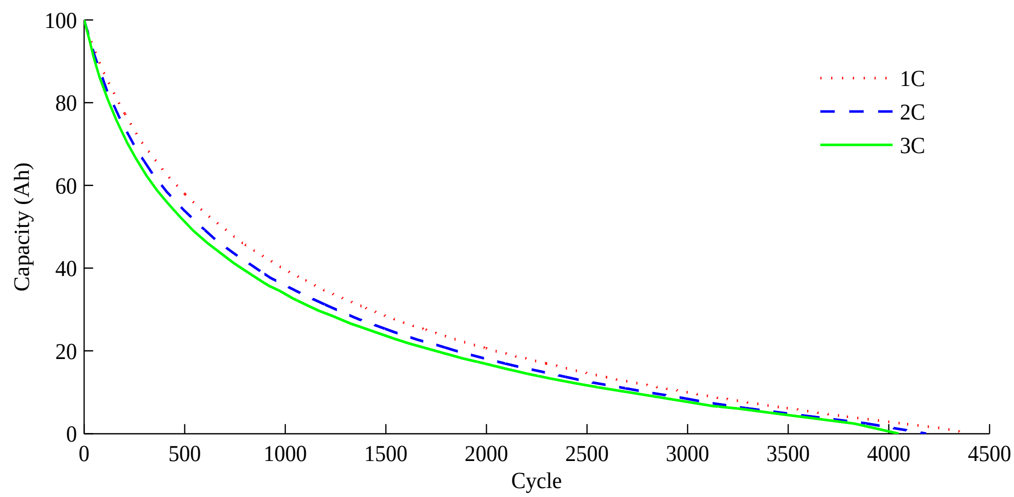

Figure 4.1: Capacity loss for a 40 kWh battery without grid-interaction.

The critical level (or value) has been chosen based on the battery capacity. When the battery capacity is reduced to 46.65 Ah, the corresponding cycle number is called critical value. Using Eq. (4.4) and Eq. (4.5), the financial parameters are calculated and are listed in Table 4.1. It is observed that the average per km transportation cost for 1C_r-1D_r to 3C_r-3D_r is almost same. This is due to the fact that the per unit battery cost is almost same for all the C_r-D_r .

Table 4.1: Average financial value for a normal EV

	$1C_r$-$1D_r$	$2C_r$-$2D_r$	$3C_r$-$3D_r$
Battery reaches its critical level	2664^{th} cycle	2461^{th} cycle	2352^{th} cycle
Consumer pay to Grid ($Rs.$)	254.84	264.13	269.78
Cost/Per km ($Rs.$)	1.13	1.17	1.20

The next section presents the cost benefit related calculations for a model where EV is supporting the grid during peak hour. This section discusses the financial aspects of V2G and G2V.

4.5 Analysis of Energy Trading Scenario Under Different Charging/Discharging Rates

Among the present types of batteries, Li-ion battery has a low self-discharging rate. Also Li-ion battery has better energy density, long durability, low cost and intrinsic safety when compared to other battery types [189]. Therefore, Li-ion battery has been considered for this model. Nowadays the Li-ion battery is widely used in the EV. Generally the EV uses battery which ranges from 20kWh to 55kWh [190, 191]. In this work, a 40 kWh battery system has been considered.

For a 40 kWh battery system, the voltage and current associated with it must be high. With high current, the I^2R loss increases. Therefore, a nominal value of current is desired to minimize this loss. For the present work, a battery with nominal capacity 100 Ah and constant terminal voltage of 400 V is considered [192].

The total CL is mathematically calculated using Eq. (4.1). At present, the parameters required in Eq. (4.1) are not available for the required battery. Hence, the parameters of a chosen battery are theoretically (by simulation) expanded to meet the desired condition. Here a SONY 18650 US battery has been used to produce the required data. It should be noted that the battery parameters and its associated characteristics varies with respect to the type of battery and its manufacturer.

Assuming SOC of the battery to be 80%, the maximum energy that can be extracted from the battery is 32 kWh. After complete discharge, the battery has to be charged with 32 kWh of energy. Out of this, 10.67 kWh ($\frac{32kWh}{3}$) is used for transportation and 21.33 kWh ($\frac{2}{3}(32kWh)$) is the remained energy that can be used for grid support. This 21.33 kWh also includes the losses. The energy required for EV's transportation is constant, but the energy supplied by the EV to grid during peak hour decreases as capacity of the battery decreases. Mathematically,

$$\begin{aligned} E_{stor} &= 32kWh \\ E_{rem} &= \tfrac{2}{3}(32kWh) = 21.33kWh \\ E_{rem} &= \tfrac{2}{3}(32kWh) = 21.33kWh \end{aligned} \tag{4.31}$$

The CL of the battery results in its lower energy storing capability. The battery can be used till it supplies sufficient energy for EV's transportation. Therefore, the battery is useful till it can store and supply 10.66 kWh. Hence, the useful energy that the battery supplies for supporting the grid is 21.34 kWh (32 kWh - 10.66 kWh). The constant terminal voltage is 400 V. Therefore, the useful nominal capacity range is 53.35 Ah (21.34 kWh/400 V). Hence, the battery is useful till its nominal capacity has reached 46.65 Ah (100 Ah - 53.35 Ah). The i^{th} cycle, until which the battery is useful, is said to be the critical point of the battery. In this model, n is the critical point and it is the maximum number of cycle of possible G2V and V2G interaction.

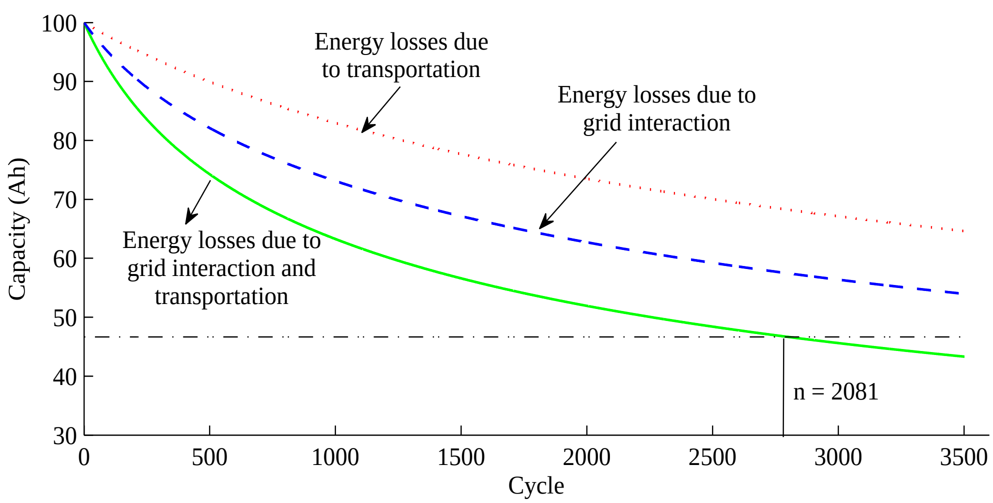

Figure 4.2: Capacity loss for 53.33 kWh energy interactions of a 40 kWh battery ($1C_r/1D_r$).

The capacity of the battery during the complete life cycle under different C_r and D_r are shown in Fig. 4.2 to Fig. 4.4. The graphs are expectedly similarly decreasing in nature, as it represent the capacity of the battery. This decreasing in the capacity is due to the capacity loss. The graphs obtained are linear in nature. It has been claimed by some of the manufacturers that the capacity loss are linear in nature. In this work the capacity loss are calculated using base values (data) provided by the manufacturers. In the above graph the only difference lies in the number of cycles required to reach the critical value (n). As the CL is directly proportional to the C_r and D_r, higher C_r or D_r degrades the battery very quickly. This can be seen in Fig. 4.2 to Fig. 4.4. While 3C_r-3D_r takes 2041 cycles to reach its critical state, 2C_r-2D_r takes 2544 cycles and 1C_r-1D_r takes 2801 cycles to reach its respective critical state.

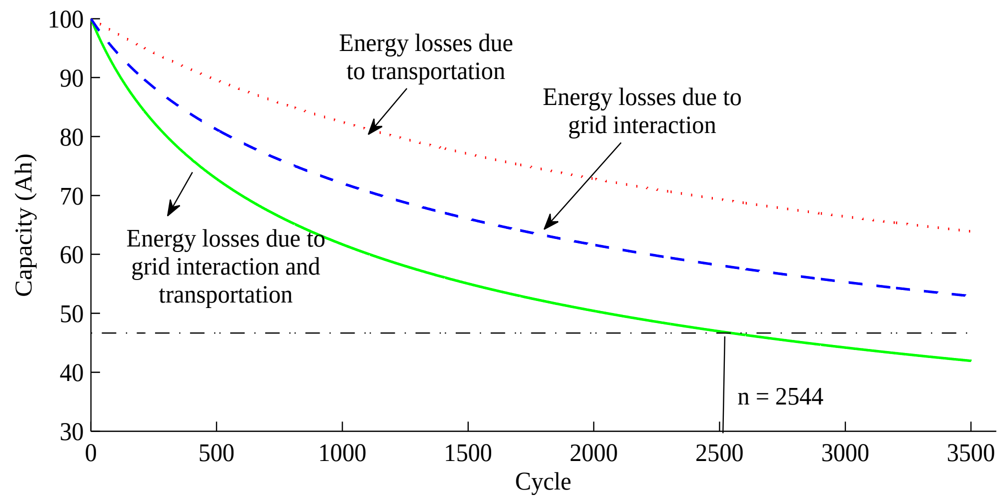

Figure 4.3: Capacity loss for 53.33 kWh energy interactions of a 40 kWh battery (2C_r/2D_r).

To calculate the monetary equivalent of the energy losses, the cost of the battery is required. The optimum cost of a high energy Li-ion battery is approximated to be 7,500 ($Rs.$)/kWh, so the total cost of purchasing the 40 kWh battery, (M) comes out to be 3,00,000 ($Rs.$) [193].

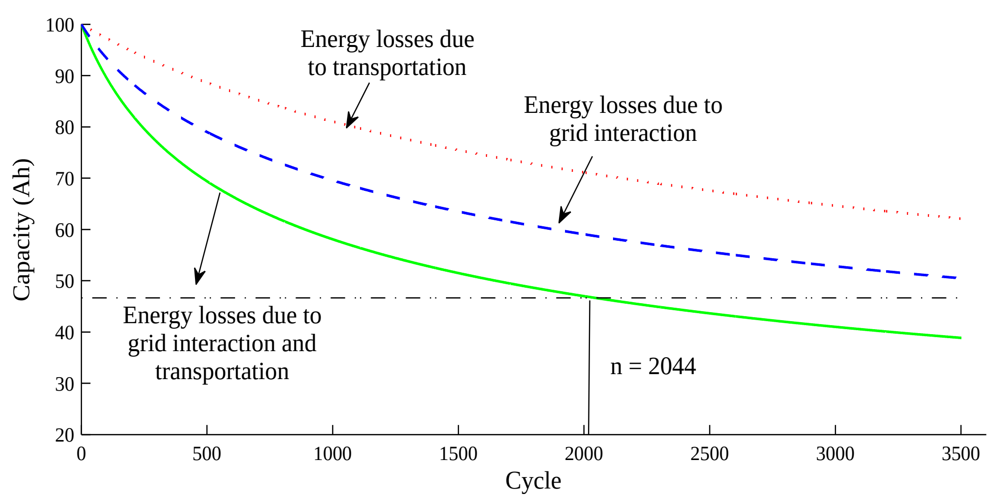

Figure 4.4: Capacity loss for 53.33 kWh energy interactions of a 40 kWh battery (3C_r/3D_r).

For mathematical calculation, certain parameters are assumed and they are as follows:

- The EV charge their battery during the off-peak hours. Using Eq. (4.6), $c = 0$ and $c' = \frac{E_{stor}}{0.9}$.
- The EV supports the grid during peak hours. Using Eq. (4.16), $s = 0.9E_{\text{sup}}$ and $s' = 0$
- The peak rate of energy consumption (x_i) is assumed to be 40% higher than the off-peak consumption rate (x_i'). $\mathrm{x_i} = 1.4(\mathrm{x_i}')$
- The off-peak hour electrical tariff in Assam, India is 4 ($Rs.$)/kWh [8]. During charging, the EVs are consumer to the Grid. Therefore, $x = 5.6$ ($Rs.$) and $x' = 4$ ($Rs.$).
- The EV will charge itself during the off-peak hours and support the grid in the peak hours. This process will take a complete day. Therefore, the average number of daily grid interactions can be assumed to be 1. Mathematically it will represent as $n'' = 1$.
- Using Eq. (4.26), the number of days, required by the battery to completely discharge is shown below: $D_n = \frac{n'}{n''} = \frac{n'}{1} = n'$
- An EV with 40kWh battery is expected to give a mileage of 225 km per charge [194].
- Let the profit percentage be p. Using Eq. (4.30), x_1 can be mathematically represented as:

$$\mathrm{x}_1 = \mathrm{x}_2\left(1 + \frac{p}{100}\right) \tag{4.32}$$

  In this model p has been assumed to be 0.1% such that x_1 remains as low as possible.

Using Eq. (2.15), Eq. (2.17), Eq. (4.7) - Eq. (4.10), Eq. (4.17) and Eq. (4.24), the compensation money for capacity loss for $1C_r$-$1D_r$, $2C_r$-$2D_r$ and $3C_r$-$3D_r$ is shown in Fig. 4.5. The compensation money is highest for $3C_r$-$3D_r$, when the battery discharges comparatively faster than $1C_r$-$1D_r$ and $2C_r$-$2D_r$. This is due to the fact that per cycle battery cost is highest in $3C_r$-$3D_r$. So, $3C_r$-$3D_r$ is the favorable case for the EV owners. It can be observed from the graph that the z is lower than expected. With capacity loss the ratio $\frac{M_{dep}}{E_{avail}}$ increases, but the ratio $\frac{E_q}{E_p}$ decreases very quickly, as E_p increases with each cycle. Also n in the denominator further normalizes the compensation money. These factors contribute to the low compensation money for capacity loss. In the work, the total processed energy has been considered for calculating the compensation money for capacity losses. This can be replaced by the processed energy during discharging process, whenever required.

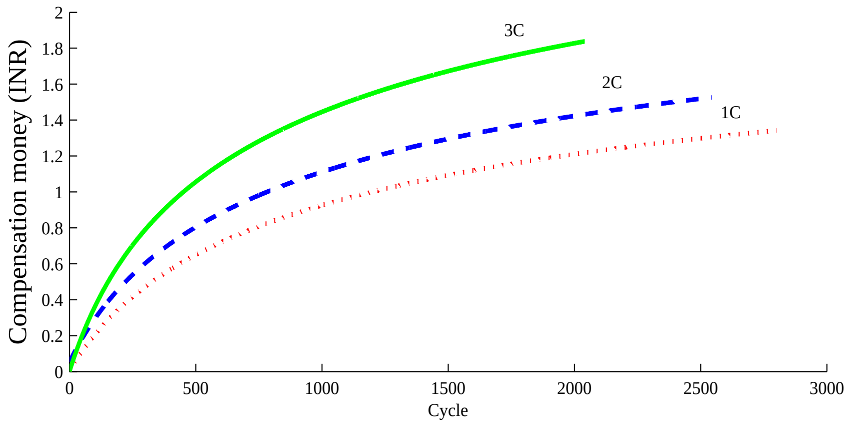

Figure 4.5: Compensation money charged by the EV owners for capacity loss of the battery.

Using Eq. (4.11) and Eq. (4.14) the net energy obtained by the grid during V2G interaction is shown in Fig. 4.6. Maximum energy is transferred during the first cycle and least during the last. The per cycle average transferred energy is same for $1C_r$-$1D_r$, $2C_r$-$2D_r$ and $3C_r$-$3D_r$. As n is more for $1C_r$-$1D_r$, maximum quantity of energy is transferred in this case. Hence, $1C_r$-$1D_r$ is the most useful case for the grid as it gets the maximum possible energy.

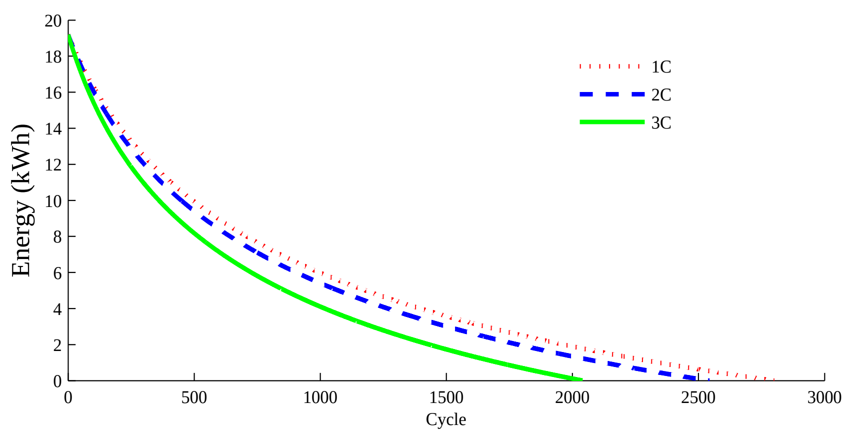

Figure 4.6: Energy obtained by the grid in kWh during V2G interaction.

Using Eq. (4.21), Eq. (4.26) and Eq. (4.27), the tariff paid by grid operators to EV owner per kWh energy (x_2) is shown in Fig. 4.7. x_2 is linearly increasing upto 1401 cycles. Therefore, only the linear part of x_2 has been shown in the graph. Since the EV deals in money only with the grid operators, this is the only way to generate profit for them. The EV accommodates its financial liabilities by charging a higher tariff for the peak hour energy (from grid operators). With decreasing capacity of the battery, the energy supplied to the grid goes on decreasing and its tariff goes on increasing. This scenario is due to the fact that the cost of energy for the EV remains the same, but the quantity of its extra energy for selling becomes less. So to recover the money, the EV charges a higher tariff. The tariff is inversely proportional to the quantity of energy sold by the EV to grid. x_2 is maximum at the critical point.

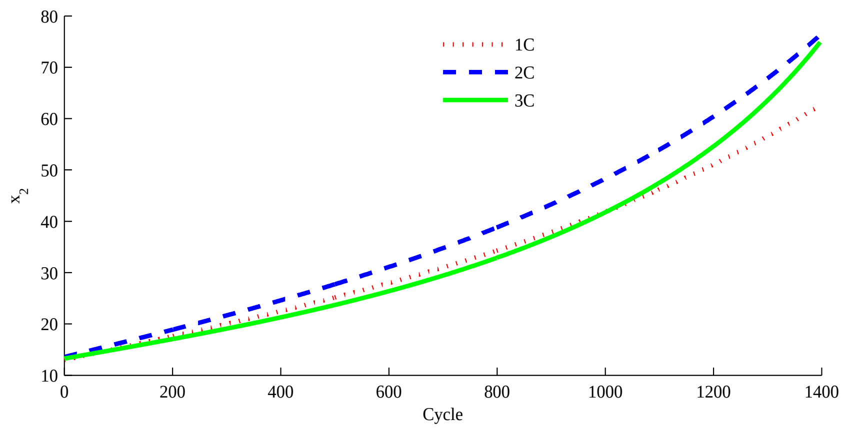

Figure 4.7: Tariff paid by grid operators to EV owner per kWh energy.

Using Eq. (4.11) to Eq. (4.15), the money paid by the grid operators for grid stress energy to the EV is shown in Fig. 4.8.

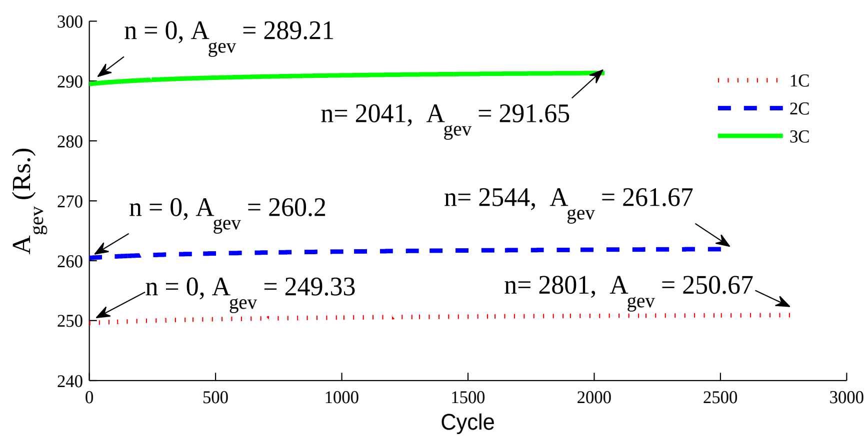

Figure 4.8: Money paid by the grid operators to the EV for the grid stress energy.

Using Eq. (4.16), Eq. (4.29) and Eq. (4.30), the money paid by the consumers (for transportation usage) to the grid operators is shown in Fig. 4.9.

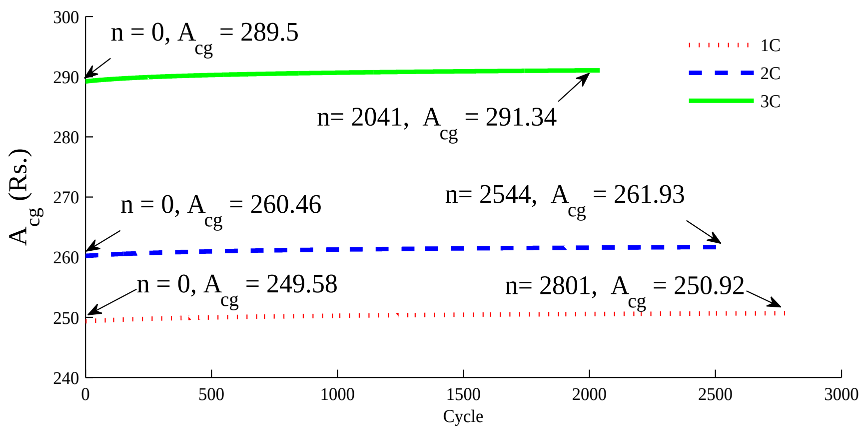

Figure 4.9: Money paid by the consumers to the grid operators for the energy used by EV for transportation.

As the variation in the compensation money for the CL is very low, A^{p}_{gev} and A_{cg} is almost constant for the complete battery cycles. The money paid in 1C_r-1D_r in both cases is lower when compared to 2C_r-2D_r and 3C_r-3D_r. This is due to the fact that in 1C_r-1D_r the per cycle battery cost is lower when compared to 2C_r-2D_r and 3C_r-3D_r. Hence, the average cost price of energy for the EV is lower in 1C_r-1D_r.

The grid operators and the EV should benefit for their service. For the EV owners, cost price is the money paid for obtaining the energy to recharge the battery and revenue is the money obtained by providing grid services. Mathematically, the EV's profit and grid operators's profit can be denoted as:

$$profit = revenue - costprice \tag{4.33}$$

$$EV_{profit} = AP_{gev} - AP_{cp} \tag{4.34}$$

For the grid operators, cost price is the money paid for obtaining the energy from the power generation set-up and the EV owners (during grid stress) and revenue is the money they obtain from the EV owners (charging the EV) and the consumers (transportation).

$$Grid_{profit} = AP_{cg} + AP_{evg} - AP_{gev} - AP_{cpg} \tag{4.35}$$

where, AP_{cpg} is the cost price of the energy which is sold by the grid operators to the EV. Using Eq. (4.15), Eq. (4.25), Eq. (4.26) and Eq. (4.30), the profit gained by the EV is shown in Fig. 4.10.

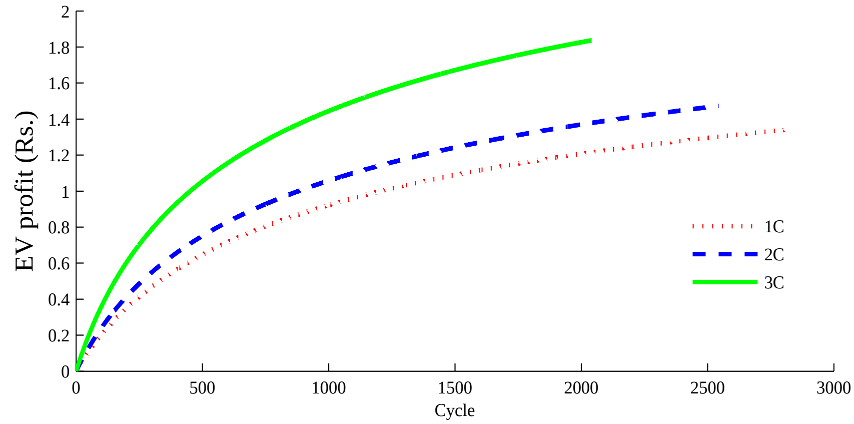

Figure 4.10: Profit Obtained by EV per day for transportation and V2G interaction.

Using Eq. (4.5), Eq. (4.15) and Eq. (4.29), the profit gained by the grid operators is shown in Fig. 4.11.

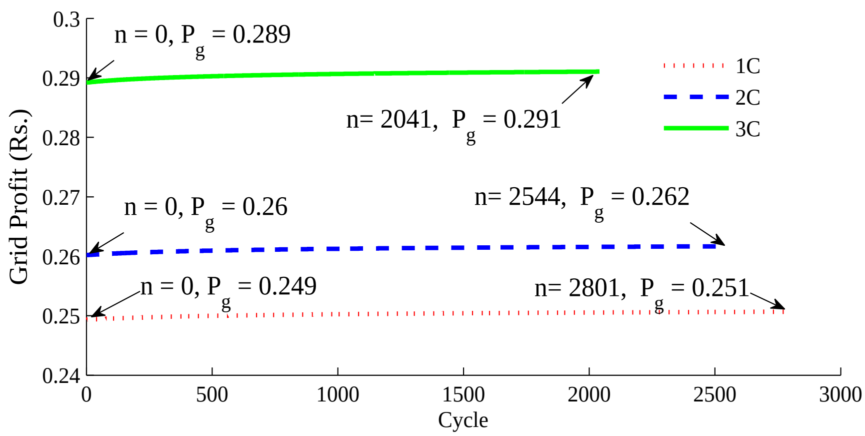

Figure 4.11: Profit obtained by the grid operators per day in V2G interaction.

While EV profit increases with battery cycle, grid operators' profit is almost constant for the complete battery cycle. This is due to the fact that while the EV owners receives the compensation money for the CL, the grid operators does not receives any such financial benefits. Also the profit gained in both the cases are extremely small. The profits can be desirably increased by manipulating x_2. Here the least possible value of x_2 was considered such that the consumers had to pay the least possible amount. when compared $3C_r$-$3D_r$ proves to be a better option for the EV owners and the grid operators. In this model the battery has been assumed to reach its zero depreciated value when its capacity reaches 10.66 kWh or 46.65 (Ah). In reality this battery can again be used for different purposes. So this depreciated battery is also worth money which varies locally. This turns to be added profit to the EV owners. Also the consumers pays for the energy during grid stress. So this energy is available to the grid as zero cost energy, which it sells to get an extra profit.

Using the above data (Fig. 4.5 to Fig. 4.11) the average values of the parameters are listed in Table 4.2. It is observed that the money paid by the EV to the grid operators is same for $1C_r$-$1D_r$, $2C_r$-$2D_r$ and $3C_r$-$3D_r$. Ideally the EV should be penalized for fast charging. Any penalty for the EV will result in a higher tariff for the grid operators, which will force the consumers to pay more. To avoid financial burden to the consumers, the EVs are not penalized. Table 4.2 also shows the cost per km for different C_r and D_r. $1C_r$-$1D_r$ is the most favorable case for consumers. Also, it can be seen that the average energy required during grid stress is 5.41 kWh and the EV uses 10.66 kWh of energy for transportation. So the passengers (consumers) pays for 50.75% of the net energy used for transportation. This will prompt the consumers to willingly pay for the grid support energy.

Table 4.2: Average values of the financial and energy transaction.

	$1C_r$ - $1D_r$	$2C_r$ - $2D_r$	$3C_r$ - $3D_r$
Battery reaches its critical level	2801^{th} cycle	2544^{th} cycle	2041^{th} cycle
z_{min} ($Rs.$)	0.97	1.06	1.32
Energy obtained by Grid (kWh)	5.41	5.41	5.41
A^p_{gev} ($Rs.$)	250.54	261.52	290.82
A_{veg} ($Rs.$)	142.223	142.223	142.223
A_{cg} ($Rs.$)	250.30	261.12	290.53
x_2 ($Rs.$)	46.31	48.36	53.73
EV profit ($Rs.$)	0.97	1.12	1.32
Grid profit ($Rs.$)	0.25	0.26	0.29
Cost/Per km ($Rs.$)	3.34	3.49	3.88

Using Table 4.1 and Table 4.2, it can be seen that the EV supporting the grid during peak hour has a higher average per km transportation cost when compared to an EV, which is not supporting with the grid. But still integration of the EV with the grid is more useful, as stated by the following points:

- It supports the grid when required.
- The consumers pays for almost half the energy (it had used for transportation) at an escalated price. With technology development this price is expected to be lower.

With technological development, this is also going to be financially beneficiary. Also in grid supporting scheme, only one-third of the total energy is used for transportation. In the other scheme, all the energy was utilized for transportation. This is the main cause for the higher per km cost of transportation for the EV integrated with the grid. Integration of the EV with the grid is desired, as this will enable an option for grid support when required.

4.6 Summary

- In this Chapter, a mathematical model for economic evaluation of EV to grid interaction taking into account the capacity fading/losses of EV battery is presented.
- The economic evaluation of the bidirectional energy transfer from V2G and G2V was formulated.
- The bidirectional energy transfer between EV battery and grid has been discussed at different charge and discharge rate.
- The capacity wear (loss) model was used to study the performance of battery during V2G interaction.
- The energy transfer between EV battery and grid, the money exchanged among the grid and EV owners was determined such that all are benefitted.
- The objective of this work is to determine the optimal cost of electricity so that both,the grid and the EVs owner are beneficiary.

In the next chapter, conclusions of the present work and the motivation of future research based on the grid support during the peak power demand and store the energy during the off-peak hours have been presented.

Note: This work, Mathematical Modeling for Economic Evaluation of Electric Vehicle To Smart Grid Interaction has been published in IEEE Transaction on Smart Grid.

5

Conclusion and Future Works

Contents

5.1 Summary of the Present Work

The objective of the work presented in this thesis is to mitigate the peak power demand and store the excess amount of energy in EVs' batteries during peak and off-peak hours. To address this issue, electrical equivalent circuit based mathematical model for EVs' batteries has been developed, which estimate the performance characteristics of EVs' batteries. The validation of the model has been carried out by comparing the simulated results with the real-time battery data obtained from four manufacturers' data sheets. Further, an SCS has been developed based on the battery model and fuzzy logic controllers, which control the power flow between EVs' batteries and grid. Also, this thesis focuses to predict the capacity fade at different charge and discharge rate and beneficiary model of EVs owners and grid operator for vehicle-to-grid interaction.

In Chapter 2, an accurate electric circuit based BM and CFM has been proposed. The BM parameters are extracted by using genetic algorithm. The developed BM and CFM performance characteristics are compared with battery manufacturers' catalogue such as voltage, power, energy, total processed energy and capacity fade. Four different battery manufacturers' data are used for validating the result. The proposed battery and capacity fade models are simple and it accurately represents the charge and discharge curves of the manufacturers' data sheets. The simulated values of capacity fade were found to be in good agreement with the manufacturers' data at different cycle numbers.

The multi-point SCS has been proposed in Chapter 3. The SCS has three main units: CCU, the CS aggregator and the BCCS unit. The CCU together with the CS aggregator has the ability to decide and distribute the power flow between EVs' batteries and the grid. Thus, this approach does not require extensive off-line optimization or driving pattern, except the real-time information of grid and the EVs' batteries. The BCCS unit modeled has 10 charging points, which is accessible for EVs of different battery ratings. Each charging point of BCCS unit is designed for a maximum peak power handling capacity of 50kW. The complete multi-point SCS is verified with a real-time grid data of Guwahati city. The control algorithm proposed in this work considers the limits preferred by EV battery owner regarding the battery; SOC_{cr} and C_{rate}. It is observed that EVs' batteries are not charged/discharged beyond the SOC limit and maximum C_{rate} prescribed by the EV owner, which proves the effectiveness of the proposed system.

In the last part of this thesis work, a mathematical modeling for economic evaluation of the vehicle-to-grid has been presented. During the peak hour, grid requires extra energy to fulfill the energy demand. The EVs would supply energy to the grid during peak hour and recharge itself during the off-peak hour. This will enable the EVs to act as a distributed energy source. Hence, a mathematical model has been developed for economic evaluation of the bidirectional energy transfer between EVs and grid. The bidirectional energy transfer has been discussed at different charge/discharge rate. The CFM model has been used to study the performance of the EV battery during vehicle-to-grid interaction. The total energy exchanged between the grid and the vehicle has been analyzed. On the basis of energy transfer, the money exchanged among the grid, EV and the consumers (EV users) has been determined such that all are benefited. In Chapter 4, a financial model for integrating the vehicle into the grid has been developed. This model can be used in any given scenario of the vehicle-to-grid interactions.

In all the works presented in this thesis, fuzzy based smart charging station has been implemented for the peak power shaving and valley filling. To analyze the energy transfer between EV battery and grid, an EEC based mathematical model for EV battery has been developed. This battery model predicts the charge and discharge rate characteristic of the EV battery and capacity losses at different charge and discharge rate. Moreover, an economic beneficiary model has been developed for EV battery and grid operator. This mathematical model can estimate the optimal cost required to charge the EV battery during the off-peak hours and support the grid during the peak hours.

5.2 Complete V2G System and Control Architecture

In this thesis, Chapter 2 discusses about the electric equivalent circuit based mathematical model of EVs' batteries. This Chapter, GA is used to extract the battery parameters and gives optimum value. The C_r and D_r characteristics are calculated using the parameters of the BM which are obtained from the GA and it compared with the different types of battery manufacturers' data. The results from BM and data given by the different types of battery manufacturers' are in good agreement.

In Chapter 3, discuss about the multi-point BCCS unit present in a SCS connected with the DN of the grid by using the developed battery model. A multi-point BCCS unit has various charging points, which are accessible to multiple EVs.

In this thesis, Chapter 4 discusses about the economical beneficiary calculation for EVs owners, grid operators and consumers. This chapter lacks discussion about the per km cost for consumers, beneficiary cost for EVs' owners and grid operators based on the energy transfer between EVs' and grid.

It has been observed that, each Chapter of this thesis presented a real time implementation of battery modeling, coordination of multiple EVs in the SCS to mitigate peak power demand during peak and off-peak hours and economic evaluation based on the energy transfer between EVs' batteries and the grid. If, all the works of V2G presented in this thesis is combined together, the complete system can solve the peak power demand of the distribution node as well as maintain the voltage profile of the grid throughout a day. The complete V2G system along with the control architecture is shown in Fig. 5.1.

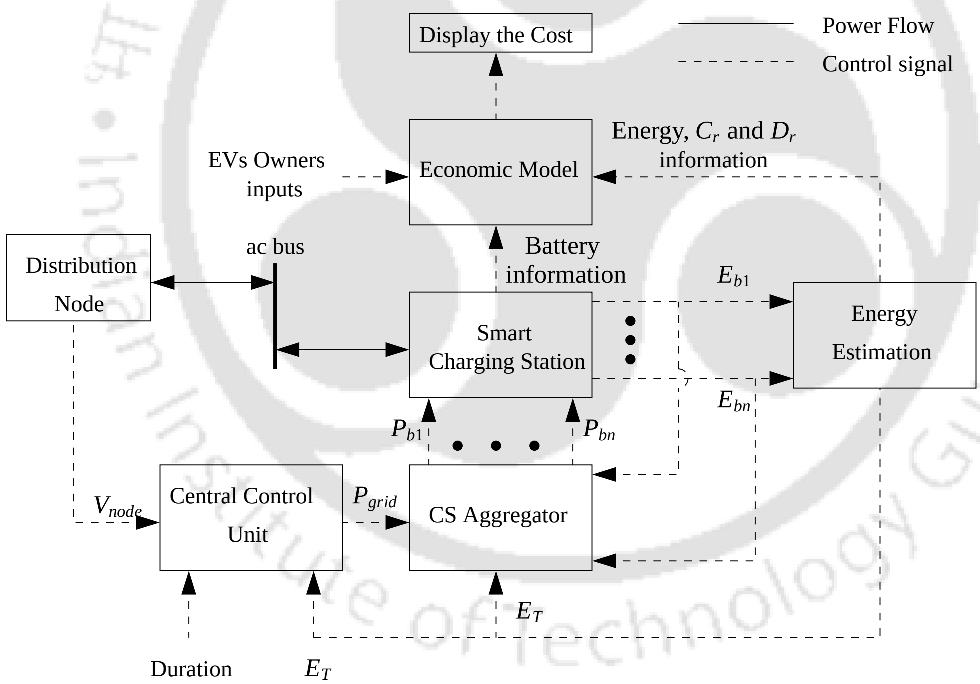

Figure 5.1: Complete V2G system along with the control architecture.

5.3 Contributions of the Present Work

The important contribution of this research work reported in this thesis is the implementation of the SCS for EVs' batteries based on the fuzzy logic controller. The main contributions are given below:

(i) An EEC based mathematical model (battery model) has been developed for EVs' batteries to analysis the performance (charge or discharge rate) characteristics.

(ii) Polynomial equation with exponential function is formulated to represent the EEC parameters, this is because of battery performance characteristics are exponentially increasing or decreasing nature.

(iii) GA has been used to optimize the BM polynomial coefficient.

(iv) Capacity fade model has been developed based on the SOC_{cr}/DOD_{cr}, C_r/D_r and processed energy for charging/discharging scenario.

(v) A closed-loop control algorithm has been developed, which can estimate the charge rate, charging time and SOC_{cr} for charging scenario and discharge rate, discharging time and DOD_{cr} for discharging scenario.

(vi) User defined charge/discharge rate, SOC/DOD limits are considered while developing the BM. Moreover, the closed-loop control logics are not allowed to charge/discharge beyond the user defined charge/discharge rate and SOC/DOD limits.

(vii) An FLC based SCS has been developed to mitigate the peak power demand and store the excess amount of energy in the ESS.

(viii) FLC based CCU has been used to control the total power flow between grid and SCS.

(ix) An aggregator has been designed for SCS which coordinate multiple EVs present in the SCS and distribute the reference power signal to each EV battery based on the updated values of the energy status of each individual EV battery, total energy availability of the SCS and total power generated from CCU.

(x) Bidirectional converter and inverter are used to transfer the power in either direction.

(xi) Contactless charging systems are used due to elimination of direct electric contacts, heating of the sockets, burning of cables, risk of fire and electrical injuries.

(xii) An FLC based control techniques are developed for bidirectional converter and inverter, which can control the battery charging current, maintain constant dc-link voltage and power angle.

(xiii) FLC based synchronization controller has been used to synchronize the BCCS unit with grid.

(xiv) Mathematical model for economic evaluation of energy transfer between EVs' batteries and grid has been developed, which can estimate the financial benefit for EV owners, grid operators and consumers.

5.4 Scope for Future Research

In this section some important scope for future research work is presented.

(i) The battery parameters are optimized with less number of polynomial coefficients.

(ii) A general battery model can be developed for other types of batteries (lead acid, lithium-ion and alkaline battery, etc.) based on the manufacturer's data.

(iii) An optimization method can be developed to predict the pre-exponential and adjustable factor at different charge and discharge rate.

(iv) The implementation of reactive power control for voltage regulation can be studied to analyze the impacts in the distribution system.

(v) Multi SCS has to be modeled for BCCS unit, which can supply/inject the active or reactive or both active and reactive power for voltage regulation. This multi SCS can be connected in the multi node of the Guwahati city distribution system. This methodology would solve the peak power demand of city.

(vi) The power transfer between grid and EVs battery can be studied by using the DC bus which has to be placed between the three-phase ac to dc and dc to high-frequency ac conversion. In this case, the synchronization time gets reduces because the BCCS unit having only one bidirectional converter.

(vii) The integration of both renewable-energy source and EV battery can be implemented in the SCS. The impact of the distribution node due to interaction of RES and EVs' can also be analyzed.

(viii) The effect of the coupling variations (misalignments of the coil or changes in the dimensions of the air gap) in contactless coil can also be analyzed.

(ix) A suitable FLC based controller can be designed for the misalignment of primary and secondary side coil. This controller maintains the voltage constant with respect of the misalignments in the coils by controlling the resonant frequency of the system.

(x) The economic evaluation model for V2G interaction can also be developed by using the driving pattern of EVs. This will be more accurate and convincing for beneficiary calculation of EV owners and grid operators.

A

Battery Sample Calculation, Initial Population and Solution Set

A.1 Sample Calculation for Battery Model

In this section, the detail calculation for C_r, SOC_{cr}, PE_c, E_{total}, etc. during charging the battery has been shown. Similarly, the values can be calculate for discharging scenario.

A.1.1 Current SOC (SOC_{cr}) and Charge rate (C_r) Calculation

The example of Chapter 2 has taken and the following values are considered for sample calculation: Battery type - EIG, Q=8, SOC_{ini}=70, I_c=1, $V^C_{c_1 00}$=2.2723, SOC_{ini}=100, SOC_{min}=0, $V^C_{d_j}$ =2.1596, T_s=37 and C^{lmt}_r=8.

The calculated value of C^{crt}_r is given in Eq. (A.1).

$$C_r = C^{crt}_r = \frac{8}{8} = 1 \tag{A.1}$$

The EIG battery calculated values of t_c and SOC_{cr} is given in Eq. (A.2) - Eq. (A.3).

$$t_c = \frac{\left((3600 \times 8) - \left(\frac{70}{100}\right) \times 3600 \times 8\right)}{8} + (37 - 36) = 1081 \tag{A.2}$$

$$SOC_{cr} = 70 + \left(\frac{8 \times (1081 - 1045)}{8 \times 3600}\right) = 70.01 \tag{A.3}$$

Similarly, t_d, DOD_{cr}, D_r and I_d can obtained by using Eq. (2.6) - Eq. (2.16).

A.1.2 Battery Power and Processed Energy

The P_c and P_d for charging and discharging scenario is given in Eq. (A.4).

$$\begin{aligned} P_c &= 2.2723 \times 8 = 18.1784 \\ P_d &= 2.1596 \times 8 = 17.2768 \end{aligned} \tag{A.4}$$

The amount of stored and available energy during charging and discharging process at 70% of SOC_{cr} and DOD_{cr} is given in Eq. (A.6).

$$\begin{aligned} E_{stor} &= 2.2723 \times 8 \times \left(\tfrac{70-69}{100}\right) = 0.18184 \\ E_{avail} &= 2.1596 \times 8 \times \left(\tfrac{70-69}{100}\right) = 0.172552 \end{aligned} \tag{A.5}$$

The processed energy for charging and discharging case is calculated form Fig. A.1

$$\begin{aligned} PE_c &= 17.8942 \\ PE_d &= 17.4297 \end{aligned} \tag{A.6}$$

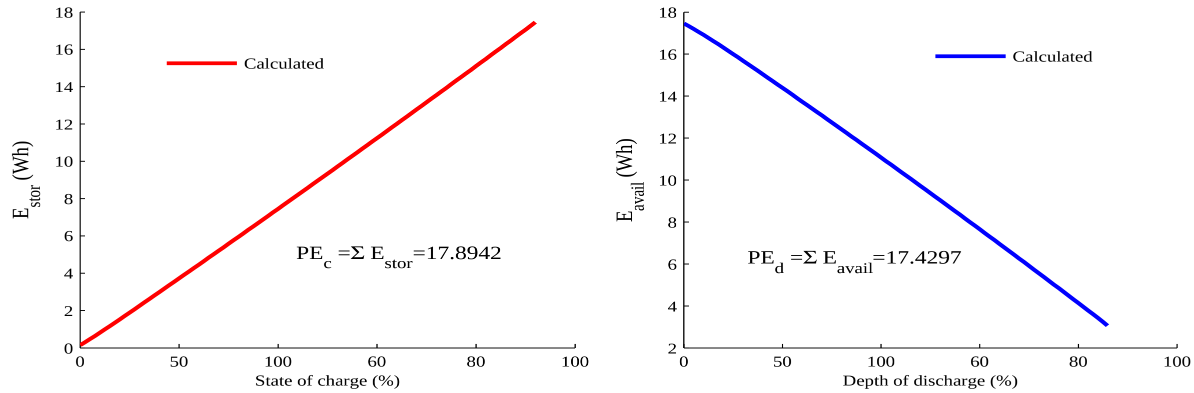

Figure A.1: Process energy for charging and discharging scenario at $1C_r$ and $1D_r$.

The total processed energy is calculated by substitute the values of PE_c and PE_d in Eq. 2.17.

$$E_{total} = (17.8942 + 17.4297) = 35.3239 \tag{A.7}$$

A.2 Capacity Fade Model

A sample calculation of the capacity fade at different charge and discharge rate is given in Eq. (A.8).

$$\begin{aligned} Q^{C}_{l_k} &= 0.09051 \times \exp\left(-\frac{24.9872\times0.000073\times17.8942\times8\times1\times0.7}{8.01499\times298.16}\right) + 7.8995 \times \exp\left(-\frac{24.9872\times7.9812^{-4}\times8\times17.4297\times1\times0.7}{8.01499\times298.16}\right) \\ Q^{C}_{l_k} &= 7.8936 \end{aligned} \tag{A.8}$$

where, 24.9872 is the dimensional analysis constant. The capacity fade characteristic is optimized by the fitness function ($F'(x)$). The $F'(x)$ is maximized, when the difference between $Q^{M}_{l_k}$ and $Q^{C}_{l_k}$ capacity loss is minimized. The value of $F'(x)$ is given in Eq. (A.9), where n=1, $\sum Q^{M}_{l_1}$ is 7.9998.

$$F'(x) = \frac{1}{1 + (7.9998 - 7.8936)} = 0.903996 \tag{A.9}$$

A.3 Genetic Algorithm

To solve the battery parameter extraction problem, the optimum solution set process typically involves modeling of the system, objective function for the optimization problem which give optimal solution. The objective function to be minimized may be non-convex and have several local minima values. Then, a global optimization method is needed to prevent the local minimum. Therefore, in the recent years, there has been a great deal of interest in developing methods for solving global optimization problems. A Genetic Algorithm (GA) is used for solving the parameter extraction problem which gives the global optimum values. The population is the main element of GA and the genetic operators such as reproduction, crossover and mutation are manipulating the population for next generation if the system is not optimized. The final optimal solution has a ”close to optimal” solution set.

A.3.1 Initial Population

The first step in GA is to generate random number of initial population with having upper (x_i^U = 163.835) and lower (x_i^L = 0) boundary. In this problem, the population size has been taken as matrix size of 300×465. The length of the each string is 15 which are given in Table A.1. Then, the string should be decoded by using the Eq. (2.20).

Example, let take first string from Table A.1 $a_{m_i,n}$=110000110101000

$S_1 = 2^0(0) + 2^1(0) + 2^2(0) + 2^3(1) + 2^4(0) + 2^5(1) + 2^6(0) + 2^7(1) + 2^8(1) + 2^9(0) + 2^{10}(0) + 2^{11}(0) + 2^{12}(0) + 2^{13}(1) + 2^{14}(1)$

$S_1 = 0 + 0 + 0 + 8 + 0 + 32 + 0 + 128 + 256 + 0 + 0 + 0 + 0 + 8192 + 16384$

$S_1 = 25000$

Then, the decoded values should convert into real values. The corresponding real of the S_1 is given below:

$a_1 = a_i{}^L + \frac{a_i{}^U - a_i{}^L}{2^l - 1} \times S_i$

$a_1 = 0 + \frac{163.835-0}{32767} \times 25000$

$a_1 = 125$

The initial value os the polynomial coefficient a_1 is 125.00 which is given in Table A.2. Let take second string from Table A.1:

$a_{m_i,n}$ = 000100110001011

$S_1 = 2^0(1) + 2^1(1) + 2^2(0) + 2^3(1) + 2^4(0) + 2^5(0) + 2^6(0) + 2^7(1) + 2^8(1) + 2^9(0) + 2^{10}(0) + 2^{11}(1) + 2^{12}(0) + 2^{13}(0) + 2^{14}(0)$

$S_1 = 0 + 0 + 0 + 8 + 0 + 32 + 0 + 128 + 256 + 0 + 0 + 0 + 0 + 8192 + 16384$

$S_1 = 2443$

Then, the decoded values should convert into real values. The corresponding real of the S_1 is given below:

$a_2 = 0 + \frac{163.835-0}{32767} \times 2443$

$a_2 = 12.215$

The initial value os the polynomial coefficient a_2 is 12.22 which is given in Table A.2. Similarly, the corresponding real values is calculated for remaining values of the Table A.1.

A.4 Polynomial Coefficients ($a_1 - a_{31}$)

The performance characteristics of the battery model depends on the parameters (R_1, R_2, C and V_0) of the electrical equivalent circuit. The battery parameters is obtained based on the optimized value of the polynomial coefficients ($a_1 - a_{31}$). The initial polynomial coefficients are given in Table A.2 which is calculated from Eq. (2.21).

A.5 Battery Parameters

A simple electric equivalent circuit based BM has shown in Fig. 2.3, which consists open-circuit voltage (V_0) with a series resistance (R_1) and the parallel resistance and capacitance (R_2C) circuit as shown in Fig. 2.3. Ideally, the battery model parameters are dependent on multi-variable functions like SOC, DOD, C_r, D_r, temperature and cycle number. The parameters V_0, R_1 with parallel R_2C characterizes the usable capacity, instantaneous voltage drop and self discharge energy loss. The R_2C network in the model is similar to that in Thevenin based model, which simulates the transient response. The battery parameters' R_1, R_2, V_0 and C have an exponential nature [194] and are represented as a function of SOC, DOD, C_r and D_r for charging and discharging scenarios in terms of polynomial equations. Therefore, the general polynomial equation for denoting the battery charge and discharge rate characteristics has given in Eq. (2.1) - Eq. (2.6).

Thus, R_1, R_2, C and V_0 are represented in terms of polynomial equations using coefficients from a_1 to a_{31}. The detailed extraction method to find the polynomial coefficient is based on GA based optimization approach. The optimized polynomial coefficients for EIG battery by using GA is shown in Table A.3. Similarly, the battery parameters of SONYUS18650, PANASONIC and SANYO at different C_r and D_r also can extract from GA.

Table A.1: Initial population matrix

Initial population from a_1 to a_8								
	String - a_1	String - a_2	String - a_3	String - a_4		String - a_{29}	String - a_{30}	String - a_{31}
1	110000110101000	000100110001011	111100010001000	101001101100110	…	111001000001111	101111111011100	010011101110111
2	111110011111000	011000011110001	011000011111100	011100011101111	…	000010111100011	001111111101001	111011111100010
3	111001001100101	011011110011000	010111100001010	001001111010011	…	111110110100101	001101010010101	011011011000100
4	110010101011101	101111110110101	101111101100100	100011100011010	…	001010100011011	011000010110011	111001001000100
5	000000100110111	111111001000111	001011010100000	110011110110110	…	011000000001111	011000101111111	110011001101111
6	011011101000100	001010110101000	000011011000000	010111000101011	…	011010100111110	110010011010001	001010101100000
7	111010111000100	011000100001101	010011010010100	111110001000100	…	000011101011100	111000101100001	100010001100010
8	101010000011010	000010110001111	101001011111100	100101100100010	…	000010111100101	011110110110000	000100001010000
9	001011110010011	011100110011010	001001100101010	100111110100001	…	000101000011010	011101010111001	100101100101011
10	001000000100011	000111101100111	010000001011011	110000001111011	…	001010010101010	001011001001100	100001010111111
11	010101101100010	110111000100000	001000011101101	011100100010111	…	101010010011001	000011101011110	011000101111110
12	110101110010100	111101000101011	101000101001111	110111111001111	…	111110111111111	011000100001101	010010010100011
13	111110101011001	111000010010100	011100111110000	111000010100110	…	001101100000100	001110101001111	000010000011111
14	100111111100101	101001001001110	001000010001110	101101001010100	…	011000100111100	100101111001001	010100111000001
15	001000111001001	110111001000110	100010111100000	100000000010010	…	100011000010111	101101001111010	000111110011100
16	101110000100001	111001100110000	000100110010101	110011101101011	…	001110000001000	011101100111011	101111100110100
17	000100101001011	011100010110000	100010000101010	100001101111101	…	010000011000100	011111001001110	100111111000111
18	011111110101110	010010010110011	111110110110010	001001111100001	…	110111100110100	001101001111001	000100010111111
19	010101101100011	110111000100000	001000011101101	011100100010111	…	000111111001001	001010010001101	110001101001011
20	111010011111111	101100111001000	011010100100010	011000011000100	…	101010010011001	000011101011110	011000101111110
21	011000010100110	110111001000100	110110110000010	110001010011011	…	101100011001100	000011100110100	011100100001000
22	101100000110001	101110100100111	101001010010010	111010001001000	…	000110111011001	101010000011101	100110111001110
23	100111011010011	010011010001000	001111010010100	111001011011100	…	110111011101111	001011101001101	001100000110001
24	110001010000011	100000100110110	001111000111010	011111011100101	…	010001010111101	110011000110101	000110001001101
25	000110111110100	000000011000001	011001110011011	010100001001110	…	010100101001011	101000000000111	101001000101011
26	110101110010100	111101000101011	101000101001111	110111111001111	…	111110111111111	011000100001101	010010010100011
27	101110101010110	101001100011011	111101010011000	111111010100111	…	110000001101100	010110010101000	101111001111001
28	111100100011001	110111111011111	101001111101011	010111001001001	…	110101010101001	101010110000001	110100001110010
29	010111001001110	001000001011001	101101001100001	010011101100111	…	000100101010011	000010101011110	011111111010001
30	110111110011110	101001100001110	010011101100011	111000111001100	…	011010111101011	010010110100111	111000011111010
31	011100011111101	000011110001100	100010110000111	111011001100100	…	110000001001001	101000010100011	100010100111100
32	111111110111001	111000111111100	100001111000001	001011100111110	…	100111001010001	101000001001000	110000000010001
33	101110010000100	001000110001100	111011001111000	100011101101111	…	101001010101101	000011110010000	111000001001000
34	001111010101010	001010001000000	001010110001001	010110001010110	…	000101011000111	101110001010010	111011010011100
35	011101100111100	001111000010100	011010101100011	001101111010011	…	001111100011110	001001010111110	100101000011001
36	101010100011000	001010111000000	001110100001011	101111110011000	…	010001111001010	100010011001001	001110101100000
37	001100011111111	001010001101010	011101101101111	101000110100100	…	000011001111110	100010110110000	011001101101101
38	000011110000001	000101001110100	001011010000111	011010010001001	…	011000000001110	001011010100111	011010001110100
39	010111111000111	110001001110110	010010000111100	111001111111000	…	100001110100111	101110110010010	000110110111101
40	100001110100110	111011110111101	101010111001100	001101100101101	…	010101101101010	110111110111111	101110111000110
	⋮	⋮	⋮	⋮		⋮	⋮	⋮
265	000110110110010	010110111001010	001001111001111	010010111100001	…	010011010010110	010111001011010	111100100111101
266	100110000001011	111100011110111	010010011011100	000010101010101	…	101100101110001	111010110011011	011111010111111
267	111001101011011	001101110010101	000100011111111	110101111010010	…	111111101001110	110110000101011	110100100101000
268	001100010111100	010001010001101	010000001000100	000001011011000	…	010100110001101	111111101110001	001011111101001
269	010011111000110	011100000100001	011111100100111	010100101110000	…	100100101011101	011000000110101	110000111011000
270	010000110100001	111010110101010	111001100010111	010110011110100	…	110001011100111	010010011100000	101110110011010
271	011011110011001	111110100011111	111101001011101	001011001010111	…	001110011011111	001111011000101	001001111100001
272	111101100011001	000100011001101	011110010100011	000110111000011	…	010011101010010	011011000010101	010110011000010
273	010111110001101	011101011001110	110100001010111	011011010000001	…	000001111001010	100010010001101	001110101100000
274	011101100111100	001111000010100	011010101100011	001101111010011	…	011100010000011	111000110001100	110011100111111
275	000110011001111	011001011100110	011101000111111	101011100011101	…	001010010101010	011011001001100	100001010111111
276	001000000100011	000111101100101	010000001001011	110000001111011	…	000000011100100	011111000100000	110010110100011
277	111001101011011	001101110010101	000100011111111	110101111010010	…	010100110001101	111111101110001	001011111101001
278	100100000011011	110111010101010	110110111011101	100100100100011	…	000100100100100	101111001110000	101101110110000
279	001000000100110	001010111001001	111111101011011	001000100010110	…	001000101101110	000101010000011	011111100001111
280	110110101000001	000000010101110	111101110011101	110000001001101	…	111001000001111	101111111101001	111011111100010
281	110000110101000	000100110001011	111100010001000	101001101100110	…	000011001111110	100010110110000	011001101101101
282	000011110000001	000101001110100	001011010000111	100000110100100	…	010100110001101	111111101110001	001011111101001
283	111001101011011	001101110010101	000100011111111	110101111010010	…	111110000101010	100010010010111	001100000001101
284	110000001101110	101110100000111	110000010010101	110010001000100	…	001000000000101	111000010100001	110111110001111
285	010001010100001	101011001010011	010110101101101	101010001110001	…	011000000001110	001011010100111	011010001110100
286	001100011111111	001010001101010	011101101101111	011010010001001	…	011000000001111	011000101111111	110011001101111
287	011011101000100	001010110101000	000011011000000	010111000101011	…	100011000010111	101101001111010	000111110011100
288	101110001100001	111001100110000	000100111100000	100000000010010	…	010001010111101	110011000110101	000110001001101
289	110001010000011	100000100110110	001111000111010	011111011100101	…	001101110001001	110101001101000	000101110101011
290	110000001101110	101100010111110	011111010001100	000000110110000	…	000111101101000	001010000000110	010110100011111
291	110100110110001	001001010000100	010011111100101	100100010010111	…	000111111001001	001110010001101	110001101001011
292	111010011111111	101100111001000	011010100100010	011000011000100	…	011010111101011	010010110100111	111000011111010
293	010111001001110	001000001011001	101101001100011	111000111001100	…	100001010100111	101110110010010	000110110000110
294	010111111000111	110001001110110	010010000111100	111001111111000	…	110100111000011	100011110111111	100111110001100
295	100000101000110	010101000011101	010101011000100	111011110110111	…	001111100011110	001001010111110	100101000011001
296	101010100011000	001010111000010	001110100001011	101111110011000	…	110111100110100	011111001001110	100111111000111
297	011111110101110	010010010110011	111110110110010	011001111100001	…	010001111001010	100010011001101	001110101100000
298	011101100111100	001111000010100	011010101100011	001101111010011	…	011110100000011	001000000111000	100010001001100
299	110011100100010	000011111001010	100000111010101	011000101101101	…	101100011001100	000011100110100	011100100001000
300	101100000110001	101110100100111	101001010010010	111010001001000	…	101100011001100	000011100110100	011100100001000

Table A.2: Initial set of polynomial coefficients

	Initial solution set														
	a_1	a_2	a_3	a_4	a_5	a_6	a_7		a_{25}	a_{26}	a_{27}	a_{28}	a_{29}	a_{30}	a_{31}
1	125	12.215	154.28	106.75	38.665	145.19	66.18	…	146.04	34.61	43.37	38.69	146	122.7	50.515
2	159.96	62.645	62.7	72.875	65.535	18.245	75.46	…	136.42	12.965	97.46	39	7.535	40.845	153.45
3	146.43	71.16	60.21	25.375	132.07	163.6	96.795	…	64.115	120.3	6.355	43.52	160.83	34.025	70.1
4	129.75	122.51	122.1	91.01	36.24	151.36	105.74	…	151.49	88.205	155.33	54.885	27.015	62.335	146.26
5	1.555	161.64	28.96	132.75	135.48	71.2	69.67	…	33.955	74.68	129.91	132.21	61.515	63.355	131.12
6	70.74	27.72	8.64	59.095	11.86	103.88	22.335	…	32.825	156	133.05	58.475	68.15	129.05	27.36
7	150.74	62.785	49.38	159.06	103.13	47.755	30.795	…	97.33	110.54	127.37	135.93	9.42	145.13	87.53
8	107.65	7.115	106.22	96.17	0.03	46.16	134.45	…	91.47	161.5	156.63	142.13	7.545	78.96	10.64
9	30.175	73.73	24.53	101.93	28.55	58.005	121.88	…	6.12	29.705	55.15	61.785	12.93	75.165	96.215
10	20.655	19.715	41.415	123.5	100.68	135.94	52.65	…	112.04	11.58	84.5	74.975	26.45	28.54	85.435
11	55.53	140.96	21.665	73.075	25.56	139.81	63.74	…	23.145	76.35	87.085	96.085	108.29	9.43	63.35
12	137.7	156.38	104.08	143.12	58.17	80.43	90.18	…	126.19	69.71	8.12	29.19	162.56	62.785	46.895
13	160.45	144.1	74.16	144.19	95.44	9.77	16.16	…	152.68	117.39	37.505	61.545	34.58	37.515	5.275
14	102.27	105.35	21.19	115.62	44.61	95.03	106.3	…	94.765	146.27	143.34	159.23	63.02	97.005	53.445
15	22.765	141.15	89.44	82.01	47.525	2.545	19.795	…	5.955	152.25	39.48	15.485	89.715	115.81	19.98
16	117.93	147.44	12.265	132.38	37.3	135.73	39.81	…	108.76	49.415	105.92	104.7	35.88	75.815	121.86
17	11.895	72.56	87.25	86.385	21.325	103.86	132.8	…	1.71	136.54	2.825	30.285	41.94	79.75	102.12
18	81.51	46.975	160.89	25.445	30.715	148.37	31.59	…	125.1	11.025	90.255	60.365	142.34	33.885	11.195
19	55.535	140.96	21.665	73.075	25.56	139.81	63.74	…	10.895	74.215	89.055	109.83	20.205	26.305	127.1
20	149.76	114.92	68.01	62.42	24.575	71.965	130.29	…	23.145	76.35	87.085	96.085	108.29	9.43	63.35
21	62.27	141.14	140.17	126.22	7.3	29.12	159.51	…	126.52	117.04	103.93	100.17	113.66	9.22	73
22	112.89	119.24	105.69	148.84	116.84	50.555	18.985	…	15.81	122.66	87.27	36.25	17.725	107.67	99.59
23	100.9	49.32	39.14	147.02	142.23	69.955	81.32	…	79.465	68.21	95.155	115.69	142	29.825	30.965
24	126.1	83.47	38.69	80.505	15.255	162.7	7.72	…	131.89	115.95	98.9	5.12	44.465	130.83	15.745
25	17.86	0.965	66.055	51.59	36.25	110.11	133.44	…	74.615	5.245	80.08	79.19	52.855	102.44	105.18
26	137.7	156.38	104.08	143.12	58.17	80.43	82.5	…	126.18	69.71	8.08	29.19	162.56	62.785	46.895
27	119.47	106.38	156.92	162.12	118.02	32.045	29.285	…	61.265	71.65	53.04	84.73	123.42	57.16	120.93
28	155.01	143.2	107.42	59.245	141.58	60.465	40.25	…	153.05	6.355	25.435	31.555	136.53	109.45	133.69
29	59.27	20.925	115.69	50.435	29.665	125.14	115.96	…	128.7	27.27	128.75	41.495	11.935	6.87	81.685
30	142.87	106.31	50.415	145.66	40.43	23.245	151.24	…	138.78	107.54	5.46	117.67	69.015	48.195	144.61
31	72.945	9.66	88.995	151.54	105.9	133.11	36.47	…	66.495	123.83	109.67	55.68	123.25	103.22	88.62
32	163.49	145.9	86.725	29.75	129.32	124.29	160.56	…	97.28	115.67	33.015	122.86	100.25	102.76	122.97
33	118.42	22.46	151.64	91.435	90.18	161.97	8.36	…	33.765	24.965	51.72	91.68	105.83	9.68	143.72
34	39.25	25.92	27.565	56.75	24.695	93.57	56.205	…	57.785	162.31	132.02	40.845	13.795	118.17	151.82
35	75.82	38.5	68.335	35.615	122.55	19.935	85.22	…	68.105	103.92	115.9	54.405	39.83	23.99	94.845
36	108.92	27.84	37.175	122.36	35.345	92.9	55.43	…	104.36	57.695	15.45	85.09	45.81	88.045	37.6
37	31.995	26.13	76.075	104.5	156.8	155.3	7.445	…	81.35	37.125	135.19	26.425	8.31	89.2	65.825
38	9.605	13.38	28.835	67.245	136.37	135.86	88.25	…	110.12	57.215	127.55	5.205	61.51	28.995	67.14
39	61.155	126.03	46.38	148.44	149.34	93.01	109	…	113.47	144.88	65.36	51.845	86.595	119.77	17.585
40	86.59	153.27	109.82	34.785	94.74	25.055	64.215	…	139.42	144.77	132.12	115.54	55.57	143.04	120.03
41	16.945	118.1	103.22	8.185	12.89	104.05	129.36	…	3.935	45.34	114.57	69.325	79.735	72.59	72.5
42	22.965	110.48	32.705	159.93	138.06	88.155	150.62	…	47.51	134.11	139.16	130.72	19.185	66.995	133.06
43	81.51	46.975	160.89	66.405	30.715	148.36	31.59	…	113.47	144.88	65.36	51.845	85.315	119.77	17.31
	⋮	⋮	⋮	⋮	⋮	⋮	⋮		⋮	⋮	⋮	⋮	⋮	⋮	⋮
259	108.260	63.715	5.505	50.755	13.210	24.095	157.690	…	22.415	40.290	102.410	142.515	78.415	13.805	6.760
260	58.430	75.710	127.575	69.775	27.735	121.025	124.395	…	154.930	87.370	27.395	31.760	12.090	123.610	89.300
261	108.920	27.850	37.175	122.280	35.345	92.900	55.410	…	126.515	117.040	24.565	100.165	113.660	9.220	73.000
262	112.885	119.235	105.690	148.840	116.820	29.120	159.510	…	27.145	103.915	115.900	54.405	39.830	23.990	94.845
263	100.135	43.190	75.010	72.975	162.145	21.630	127.580	…	79.465	68.210	95.155	115.690	141.995	29.825	30.965
264	100.895	49.320	39.140	147.020	142.230	69.955	81.320	…	21.400	113.595	88.835	69.560	143.235	88.610	69.860
265	17.530	58.610	25.355	48.485	101.870	71.215	120.110	…	10.815	136.265	39.710	76.525	49.390	59.330	155.185
266	97.335	154.835	47.180	6.825	75.930	121.375	12.210	…	134.000	63.010	142.915	13.820	114.485	150.535	80.315
267	147.655	35.305	11.515	138.010	129.655	15.010	50.070	…	34.975	149.985	7.040	152.325	162.950	138.455	134.600
268	31.660	44.225	41.300	3.640	50.160	163.265	114.770	…	50.835	149.955	25.005	70.910	53.185	163.125	30.605
269	50.910	71.845	80.835	53.040	157.350	64.155	105.650	…	97.410	147.675	124.095	123.235	93.905	61.705	125.240
270	43.045	150.610	147.315	57.540	127.185	77.765	23.550	…	50.290	28.345	75.650	48.145	106.260	5.625	118.325
271	71.165	160.155	156.625	28.595	81.150	30.105	15.230	…	40.000	121.145	23.575	144.730	126.595	47.200	119.810
272	157.565	11.265	77.615	17.615	94.425	70.055	10.865	…	7.480	75.505	48.880	81.000	36.955	39.385	25.445
273	60.865	75.270	133.555	69.765	113.550	132.125	141.725	…	106.955	148.625	38.485	40.960	50.330	69.225	57.290
274	75.820	38.500	68.335	35.615	122.545	60.885	85.220	…	104.355	57.695	15.450	85.090	4.850	87.745	37.600
275	16.395	65.150	74.555	111.505	67.565	74.260	42.055	…	119.495	16.525	110.065	14.475	72.335	145.340	132.155
276	20.655	19.705	41.335	123.495	100.680	135.940	52.650	…	112.035	11.580	84.500	74.975	26.450	69.500	85.435
277	147.655	35.305	11.515	138.010	129.655	11.895	73.780	…	59.800	104.615	61.565	30.120	1.140	79.520	130.095
278	92.295	141.650	140.625	93.615	37.065	61.090	50.070	…	50.825	149.945	25.005	70.910	53.185	163.125	30.605
279	20.670	27.885	163.015	21.870	42.145	142.320	57.375	…	101.110	99.750	157.470	111.390	11.700	120.880	117.360
280	139.845	0.870	158.225	123.265	41.125	162.545	67.810	…	54.105	84.665	105.865	46.905	22.310	13.455	80.715
281	125.000	12.215	154.280	106.750	38.665	145.190	66.180	…	146.040	34.610	43.360	38.690	145.995	122.765	153.450
282	9.605	13.380	28.835	84.020	156.800	155.295	7.445	…	80.070	37.125	135.185	5.945	8.310	89.200	65.825
283	147.655	35.305	11.515	138.010	129.655	15.010	50.070	…	50.825	149.955	25.005	70.910	53.185	163.125	30.605
284	123.430	119.075	123.625	128.340	98.700	102.295	55.980	…	92.460	160.790	15.705	111.085	158.930	87.795	30.785
285	44.325	110.495	58.145	108.085	155.420	79.015	78.430	…	152.275	31.510	122.660	142.960	20.505	144.165	142.795
286	31.995	26.130	76.075	67.245	136.365	135.855	88.250	…	110.120	57.215	127.545	5.205	61.510	28.995	67.140
287	70.740	27.720	8.640	59.095	11.860	21.960	22.335	…	33.955	74.680	129.905	132.205	61.515	63.355	131.115
288	118.245	147.440	12.640	82.010	47.525	2.545	19.795	…	5.955	152.245	39.480	15.480	89.715	115.810	19.980
289	126.095	83.470	38.690	80.505	15.255	162.700	7.720	…	131.885	115.950	98.900	5.120	44.465	130.825	15.745
290	123.430	113.590	80.060	2.160	159.985	159.530	87.835	…	68.820	18.495	56.170	131.560	35.245	136.200	14.935
291	135.285	23.700	51.065	92.915	119.825	155.100	146.815	…	50.805	82.610	157.450	102.450	19.720	25.630	57.755
292	149.755	114.920	68.010	62.420	24.575	71.965	130.290	…	10.895	74.215	89.055	109.825	20.205	36.545	127.095
293	59.270	20.925	115.695	145.660	40.430	23.245	151.235	…	138.775	107.540	5.460	117.670	69.015	48.195	144.610
294	61.155	126.030	46.380	148.440	149.340	93.010	103.880	…	113.470	144.880	65.360	51.845	85.315	119.770	17.310
295	83.550	53.905	54.740	153.235	68.620	16.700	48.725	…	35.560	35.820	9.715	126.245	135.375	91.835	101.820
296	108.920	27.850	37.175	122.360	35.345	92.900	55.430	…	68.105	103.915	115.900	54.405	39.830	23.990	94.845
297	81.510	46.975	160.890	66.405	30.715	148.370	31.590	…	125.095	11.025	90.255	60.365	142.340	79.750	102.115
298	75.820	38.500	68.335	35.615	122.545	60.885	85.220	…	104.355	57.695	15.450	85.090	45.810	88.065	37.600
299	132.010	9.970	84.265	63.265	135.735	139.020	81.515	…	69.110	84.100	12.840	15.415	78.095	20.760	87.420
300	112.885	119.235	105.690	148.840	116.820	29.120	159.510	…	126.515	117.040	24.565	100.165	113.660	9.220	73.000

Table A.3: EIG battery parameters at $0.5C_r$ (charge rate).

Charge rate at 0.5 C_r												
R_1	R_2	C	V_0	$V_{c_i}^C$	SOC_{cr}		R_1	R_2	C	V_0	$V_{c_i}^C$	SOC_{cr}
0.091554	0.030567	0.398065	2.94854	1.971578	0		0.041648	0.010449	1.506431	2.632624	2.215846	51
0.079745	0.027253	0.54597	2.877689	2.021709	1		0.041648	0.010449	1.506481	2.635492	2.218715	52
0.069871	0.024206	0.687286	2.812934	2.060315	2		0.041648	0.010449	1.506523	2.638374	2.221598	53
0.062556	0.021712	0.807817	2.760305	2.086156	3		0.041648	0.010448	1.506559	2.64127	2.224495	54
0.057137	0.019671	0.91062	2.717607	2.103144	4		0.041648	0.010448	1.50659	2.64418	2.227406	55
0.053123	0.017999	0.998303	2.683043	2.11407	5		0.041648	0.010448	1.506616	2.647104	2.23033	56
0.050149	0.01663	1.073089	2.655143	2.120912	6		0.041648	0.010448	1.506639	2.650041	2.233268	57
0.047946	0.015509	1.136875	2.632702	2.125061	7		0.041648	0.010448	1.506658	2.652992	2.236219	58
0.046314	0.014592	1.19128	2.614733	2.127489	8		0.041648	0.010448	1.506674	2.655956	2.239183	59
0.045104	0.013841	1.237682	2.60043	2.128868	9		0.041648	0.010448	1.506688	2.658933	2.24216	60
0.044209	0.013226	1.27726	2.589131	2.129655	10		0.041648	0.010448	1.5067	2.661923	2.24515	61
0.043545	0.012722	1.311017	2.580295	2.130156	11		0.041648	0.010448	1.50671	2.664925	2.248153	62
0.043053	0.01231	1.339808	2.573479	2.13057	12		0.041648	0.010448	1.506719	2.667941	2.251169	63
0.042689	0.011973	1.364365	2.568319	2.131025	13		0.041648	0.010448	1.506726	2.670968	2.254197	64
0.042419	0.011696	1.38531	2.56452	2.131594	14		0.041648	0.010448	1.506732	2.674009	2.257237	65
0.04222	0.01147	1.403174	2.561837	2.13232	15		0.041648	0.010448	1.506738	2.677061	2.260289	66
0.042072	0.011285	1.418411	2.560071	2.133221	16		0.041648	0.010448	1.506742	2.680125	2.263354	67
0.041962	0.011133	1.431407	2.55906	2.1343	17		0.041648	0.010448	1.506746	2.683202	2.26643	68
0.041881	0.011009	1.442491	2.558669	2.135553	18		0.041648	0.010448	1.506749	2.68629	2.269519	69
0.04182	0.010907	1.451945	2.55879	2.136968	19		0.041648	0.010448	1.506752	2.68939	2.272619	70
0.041776	0.010824	1.460009	2.559332	2.138533	20		0.041648	0.010448	1.506755	2.692502	2.275731	71
0.041743	0.010756	1.466886	2.560223	2.140234	21		0.041648	0.010448	1.506757	2.695625	2.278854	72
0.041718	0.0107	1.472752	2.561402	2.142055	22		0.041648	0.010448	1.506759	2.69876	2.281988	73
0.0417	0.010654	1.477756	2.56282	2.143983	23		0.041648	0.010448	1.50676	2.701906	2.285134	74
0.041687	0.010617	1.482023	2.564437	2.146007	24		0.041648	0.010448	1.506761	2.705063	2.288291	75
0.041677	0.010586	1.485663	2.56622	2.148114	25		0.041648	0.010448	1.506762	2.708231	2.291459	76
0.041669	0.010561	1.488767	2.568141	2.150295	26		0.041648	0.010448	1.506763	2.711409	2.294638	77
0.041664	0.010541	1.491415	2.570179	2.152541	27		0.041648	0.010448	1.506764	2.714599	2.297828	78
0.04166	0.010524	1.493673	2.572315	2.154844	28		0.041648	0.010448	1.506765	2.717799	2.301028	79
0.041657	0.01051	1.495599	2.574535	2.157198	29		0.041648	0.010448	1.506765	2.72101	2.304239	80
0.041655	0.010499	1.497242	2.576825	2.159596	30		0.041648	0.010448	1.506766	2.724231	2.30746	81
0.041653	0.01049	1.498643	2.579177	2.162035	31		0.041648	0.010448	1.506766	2.727463	2.310691	82
0.041652	0.010482	1.499838	2.581582	2.16451	32		0.041648	0.010448	1.506767	2.730704	2.313933	83
0.041651	0.010476	1.500858	2.584033	2.167018	33		0.041648	0.010448	1.506767	2.733956	2.317185	84
0.04165	0.010471	1.501727	2.586525	2.169556	34		0.041648	0.010448	1.506767	2.737218	2.320446	85
0.04165	0.010467	1.502469	2.589053	2.17212	35		0.041648	0.010448	1.506767	2.740489	2.323717	86
0.041649	0.010463	1.503101	2.591613	2.17471	36		0.041648	0.010448	1.506768	2.74377	2.326999	87
0.041649	0.010461	1.50364	2.594202	2.177324	37		0.041648	0.010448	1.506768	2.747061	2.330289	88
0.041649	0.010458	1.504101	2.596818	2.17996	38		0.041648	0.010448	1.506768	2.750361	2.333589	89
0.041649	0.010456	1.504493	2.599458	2.182616	39		0.041648	0.010448	1.506768	2.75367	2.336899	90
0.041649	0.010455	1.504828	2.602121	2.185292	40		0.041648	0.010448	1.506768	2.756989	2.340217	91
0.041649	0.010454	1.505113	2.604805	2.187987	41		0.041648	0.010448	1.506768	2.760316	2.343545	92
0.041649	0.010453	1.505357	2.607509	2.1907	42		0.041648	0.010448	1.506768	2.763653	2.346881	93
0.041648	0.010452	1.505564	2.610233	2.19343	43		0.041648	0.010448	1.506768	2.766998	2.350227	94
0.041648	0.010451	1.505742	2.612974	2.196177	44		0.041648	0.010448	1.506768	2.770353	2.353581	95
0.041648	0.010451	1.505893	2.615733	2.198941	45		0.041648	0.010448	1.506768	2.773715	2.356944	96
0.041648	0.01045	1.506021	2.618509	2.20172	46		0.041648	0.010448	1.506768	2.777087	2.360315	97
0.041648	0.01045	1.506131	2.621301	2.204515	47		0.041648	0.010448	1.506769	2.780466	2.363695	98
0.041648	0.010449	1.506225	2.624109	2.207326	48		0.041648	0.010448	1.506769	2.783854	2.367083	99
0.041648	0.010449	1.506305	2.626932	2.210151	49		0.041648	0.010448	1.506769	2.78725	19116.21	100
0.041648	0.010449	1.506373	2.62977	2.212991	50		-	-	-	-	-	-

Table A.4: EIG battery parameters at $0.5D_r$ (discharge rate).

Discharge rate at 0.5 D_r											
R_1	R_2	C	V_0	$V_{d_j}^C$	DOD_{cr}	R_1	R_2	C	V_0	$V_{d_j}^C$	DOD_{cr}
0.0416	0.0104	1.5068	2.7869	2.3701	0	0.0416	0.0104	1.5063	2.6269	2.2102	51
0.0416	0.0104	1.5068	2.7839	2.3671	1	0.0416	0.0104	1.5062	2.6241	2.2073	52
0.0416	0.0104	1.5068	2.7805	2.3637	2	0.0416	0.0104	1.5061	2.6213	2.2045	53
0.0416	0.0104	1.5068	2.7771	2.3603	3	0.0416	0.0105	1.506	2.6185	2.2017	54
0.0416	0.0104	1.5068	2.7737	2.3569	4	0.0416	0.0105	1.5059	2.6157	2.1989	55
0.0416	0.0104	1.5068	2.7704	2.3536	5	0.0416	0.0105	1.5057	2.613	2.1962	56
0.0416	0.0104	1.5068	2.767	2.3502	6	0.0416	0.0105	1.5056	2.6102	2.1934	57
0.0416	0.0104	1.5068	2.7637	2.3469	7	0.0416	0.0105	1.5054	2.6075	2.1907	58
0.0416	0.0104	1.5068	2.7603	2.3435	8	0.0416	0.0105	1.5051	2.6048	2.188	59
0.0416	0.0104	1.5068	2.757	2.3402	9	0.0416	0.0105	1.5048	2.6021	2.1853	60
0.0416	0.0104	1.5068	2.7537	2.3369	10	0.0416	0.0105	1.5045	2.5995	2.1826	61
0.0416	0.0104	1.5068	2.7504	2.3336	11	0.0416	0.0105	1.5041	2.5968	2.18	62
0.0416	0.0104	1.5068	2.7471	2.3303	12	0.0416	0.0105	1.5036	2.5942	2.1773	63
0.0416	0.0104	1.5068	2.7438	2.327	13	0.0416	0.0105	1.5031	2.5916	2.1747	64
0.0416	0.0104	1.5068	2.7405	2.3237	14	0.0416	0.0105	1.5025	2.5891	2.1721	65
0.0416	0.0104	1.5068	2.7372	2.3204	15	0.0417	0.0105	1.5017	2.5865	2.1696	66
0.0416	0.0104	1.5068	2.734	2.3172	16	0.0417	0.0105	1.5009	2.584	2.167	67
0.0416	0.0104	1.5068	2.7307	2.3139	17	0.0417	0.0105	1.4998	2.5816	2.1645	68
0.0416	0.0104	1.5068	2.7275	2.3107	18	0.0417	0.0105	1.4986	2.5792	2.162	69
0.0416	0.0104	1.5068	2.7242	2.3075	19	0.0417	0.0105	1.4972	2.5768	2.1596	70
0.0416	0.0104	1.5068	2.721	2.3042	20	0.0417	0.0105	1.4956	2.5745	2.1572	71
0.0416	0.0104	1.5068	2.7178	2.301	21	0.0417	0.0105	1.4937	2.5723	2.1548	72
0.0416	0.0104	1.5068	2.7146	2.2978	22	0.0417	0.0105	1.4914	2.5702	2.1525	73
0.0416	0.0104	1.5068	2.7114	2.2946	23	0.0417	0.0106	1.4888	2.5681	2.1503	74
0.0416	0.0104	1.5068	2.7082	2.2915	24	0.0417	0.0106	1.4857	2.5662	2.1481	75
0.0416	0.0104	1.5068	2.7051	2.2883	25	0.0417	0.0106	1.482	2.5644	2.146	76
0.0416	0.0104	1.5068	2.7019	2.2851	26	0.0417	0.0107	1.4778	2.5628	2.144	77
0.0416	0.0104	1.5068	2.6988	2.282	27	0.0417	0.0107	1.4728	2.5614	2.1421	78
0.0416	0.0104	1.5068	2.6956	2.2789	28	0.0417	0.0108	1.4669	2.5602	2.1402	79
0.0416	0.0104	1.5068	2.6925	2.2757	29	0.0418	0.0108	1.46	2.5593	2.1385	80
0.0416	0.0104	1.5068	2.6894	2.2726	30	0.0418	0.0109	1.4519	2.5588	2.137	81
0.0416	0.0104	1.5067	2.6863	2.2695	31	0.0419	0.011	1.4425	2.5587	2.1356	82
0.0416	0.0104	1.5067	2.6832	2.2664	32	0.042	0.0111	1.4314	2.5591	2.1343	83
0.0416	0.0104	1.5067	2.6801	2.2634	33	0.0421	0.0113	1.4184	2.5601	2.1332	84
0.0416	0.0104	1.5067	2.6771	2.2603	34	0.0422	0.0115	1.4032	2.5618	2.1323	85
0.0416	0.0104	1.5067	2.674	2.2572	35	0.0424	0.0117	1.3853	2.5645	2.1316	86
0.0416	0.0104	1.5067	2.671	2.2542	36	0.0427	0.012	1.3644	2.5683	2.131	87
0.0416	0.0104	1.5067	2.6679	2.2512	37	0.0431	0.0123	1.3398	2.5735	2.1306	88
0.0416	0.0104	1.5067	2.6649	2.2482	38	0.0435	0.0127	1.311	2.5803	2.1302	89
0.0416	0.0104	1.5067	2.6619	2.2452	39	0.0442	0.0132	1.2773	2.5891	2.1297	90
0.0416	0.0104	1.5067	2.6589	2.2422	40	0.0451	0.0138	1.2377	2.6004	2.1289	91
0.0416	0.0104	1.5067	2.656	2.2392	41	0.0463	0.0146	1.1913	2.6147	2.1275	92
0.0416	0.0104	1.5067	2.653	2.2362	42	0.0479	0.0155	1.1369	2.6327	2.1251	93
0.0416	0.0104	1.5066	2.65	2.2333	43	0.0501	0.0166	1.0731	2.6551	2.1209	94
0.0416	0.0104	1.5066	2.6471	2.2303	44	0.0531	0.018	0.9983	2.683	2.1141	95
0.0416	0.0104	1.5066	2.6442	2.2274	45	0.0571	0.0197	0.9106	2.7176	2.1031	96
0.0416	0.0104	1.5066	2.6413	2.2245	46	0.0626	0.0217	0.8078	2.7603	2.0862	97
0.0416	0.0104	1.5065	2.6384	2.2216	47	0.0699	0.0242	0.6873	2.8129	2.0603	98
0.0416	0.0104	1.5065	2.6355	2.2187	48	0.0797	0.0273	0.546	2.8777	2.0217	99
0.0416	0.0104	1.5064	2.6326	2.2158	49	0.0931	0.031	0.3803	2.9573	1.5649	100
0.0416	0.0104	1.5064	2.6298	2.213	50	-		-	-	-	

B

Fuzzy Logic Controller

B.1 Introduction

In this section, the fuzzification and defuzzification method of the fuzzy central controller is discussed, which has used in Chapter 3. Similarly, the explanation can be suitable for other controllers such as the fuzzy based synchronization controller, dc-link voltage controller and charging current controller. The uncontrolled charging or discharging of the EVs causes voltage fluctuation in the DN at which the SCS has been connected. Therefore, there is a need of coordinating the EVs at the SCS to control the power flow between the EVs and the DN. The charging and discharging of the EVs' batteries have been controlled using a Fuzzy Logic Controller (FLC). For example, the input parameters of the CCU are taken as the available energy in the CS, voltage profile at the DN and duration to support the grid. For a low energy and high node voltage, EV will charge while for a high SOC and low node voltage, EV will discharge. However, there may also be cases where both the available energy and node voltages are high or both are low. For such situations, low charging or discharging needs to be employed. Thus, the FLC has been fine tuned to take care of such situations as well, so as to keep the node voltage fluctuations within the permissible limits.

Fuzzy logic is another class of artificial inelegance but the history and its applications are more recent than those of expert system [165]. Fuzzy logic derived from fuzzy set theory which can deal with uncertainties in systems. Fuzzy logic incorporates a simple, IF-THEN rule based approach to solve a control problem rather than attempting to mathematically model a system. Fig. B.1 shows the functional block diagram of a fuzzy logic controller. Unlike binary logic, Fuzzy Logic is a many-valued logic where the fuzzy logic variables may have truth values ranging in different degrees between 0 and 1. Fuzzy Logic can deal with the uncertainties in the system through a simple IF-THEN rule based approach, thereby eliminating the need for a mathematical model of the system. This is very much useful for complex system where the complete mathematical model representation may not be possible. It consists of fuzzification, knowledge system, inference engine and defuzzification, which is shown in Fig. B.1. The crisp input is converted or translates into crisp values by using the fuzzification. The rule or knowledge base collects the control rules which describe expert's knowledge and experience in the fuzzy set. Based on the rule base and fuzzification output, the fuzzy control values have been generated in the inference engine. Then, the fuzzy values are converted into crisp values by using the defuzzification method.

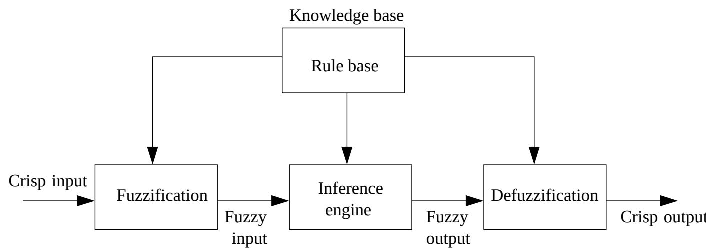

Figure B.1: Functional block diagram of fuzzy logic controller.

The following steps are required to implement fuzzy logic technique:

- Fuzzification convert real value or crisp data into fuzzy data or Membership Functions (MFs).
- Inference Engine combine membership functions with the control rules to derive the fuzzy output.
- Defuzzification is a process which convert fuzzy quantities into crisp quantities.

Mamdani type inference is used here for the implication of rules. In order to achieve a fast and accurate result, center of gravity method is chosen for defuzzification process. Three fuzzy subsets such as Low (L), Medium (M) and High (H) have been chosen as the input variables. Negative High (NH), Negative Medium (NM), Negative Low (NL), Positive Low (PL), Positive Medium (PM) and Positive High (PH) are chosen as output in order to obtain the required control action. The triangular membership function has been used in this work because the calculations and implementation are easy, which is given in Fig. B.1. It is very difficult to calculate the arithmetic operations in case of Bell, Sigmoidal, Asymmetric and Guassian. The rule base for CCU-FLC is given in Table B.1.

B.1.1 Fuzzification

Fuzzification is the first step to apply a fuzzy inference system. Most variables existing in the real world are crisp or classical variables. One needs to convert those crisp variables to fuzzy variables. Then apply fuzzy inference to process those data to obtain the desired output. Generally, fuzzification process involves deriving the MFs for input and outputting variables and representing them with linguistic variables such as Low, Medium, etc,. The triangular MFs have been used in this work.

Table B.1: Rule base for CCU-FLC.

V_{node}	E_T	D	P_{grid}	V_{node}	E_T	D	P_{grid}
L	L	L	NH	M	M	H	NL
L	L	M	NM	M	H	L	NH
L	L	H	NL	M	H	M	NM
L	M	L	NH	M	H	H	NL
L	M	M	NM	H	L	L	PH
L	M	H	NL	H	L	M	PM
L	H	L	NH	H	L	H	PL
L	H	M	NM	H	M	L	PH
L	H	H	NL	H	M	M	PM
M	L	L	PL	H	M	H	PL
M	L	M	PL	H	H	L	PH
M	L	H	PL	H	H	M	PM
M	M	L	NH	H	H	H	PL
M	M	M	NM	-	-	-	-

B.1.2 Defuzzification

Defuzzification is a method which converts fuzzy output into crisp output. The generated fuzzy outputs are not possible to use. Hence, it is necessary to convert the fuzzy output into crisp output. This can be archived by using defuzzification process. Several methods of defuzzification are used in practice such as center of area (also called as center of gravity), maxima, mean of maxima, height and modified height methods. The most popular method is center of area which estimate the center of gravity of the fuzzy set. The general expression for the center of area is given below:

$$P_{grid} = \frac{\sum_{i=1}^{n} P_{grid_i}\mu\left(P_{grid_i}\right)}{\sum_{i=1}^{n} \mu\left(P_{grid_i}\right)} \tag{B.1}$$

Detailed fuzzy logic process is explained with numerical example of the CCU-FLC.

(i) ***Step - 1:*** The rule base for CCU-FLC has been decided based on the total available energy of the CS, distribution node voltage and duration to support or inject the power. If the node voltage is low, total energy availability of the CS is high, the duration is medium then the CS support the grid with very high power value. The distribution node voltage (V_{node}) is 0.965, the total energy availability (E_T) is 0.9 and the duration (D) is 0.9.

(ii) ***Step - 2:*** Estimate the Degree of Membership Function (DOF) of $\mu(V_{node}(p.u))$, $\mu(E_T(p.u))$ and $\mu(D(p.u))$ for the equal fuzzy sets. $\mu_M(V_{node}) = 0.9$, $\mu_H(V_{node}) = 0.1$, $\mu_M(E_T) = 0.2$,

$\mu_H(E_T) = 0.8$, $\mu_M(D) = 0.1$ and $\mu_H(D) = 0.9$.

(iii) ***Step - 3:*** The rule base for the CCU-FLU is given in Table B.1. Identify the eight rules from this Table for M, H values of $\mu(V_{node}(p.u))$, $\mu(E_T(p.u))$ and $\mu(D(p.u))$.

- Rule 1: If $\mu(V_{node}) = M$ AND $\mu(E_T) = M$ AND $\mu_H(D) = M$ THEN $\mu(P_{grid}) = NM$.
- Rule 2: If $\mu(V_{node}) = M$ AND $\mu(E_T) = M$ AND $\mu_H(D) = H$ THEN $\mu(P_{grid}) = NL$.
- Rule 3: If $\mu(V_{node}) = M$ AND $\mu(E_T) = H$ AND $\mu_H(D) = M$ THEN $\mu(P_{grid}) = NM$.
- Rule 4: If $\mu(V_{node}) = M$ AND $\mu(E_T) = H$ AND $\mu_H(D) = H$ THEN $\mu(P_{grid}) = NL$.
- Rule 5: If $\mu(V_{node}) = H$ AND $\mu(E_T) = M$ AND $\mu_H(D) = M$ THEN $\mu(P_{grid}) = PM$.
- Rule 6: If $\mu(V_{node}) = H$ AND $\mu(E_T) = M$ AND $\mu_H(D) = H$ THEN $\mu(P_{grid}) = PL$.
- Rule 7: If $\mu(V_{node}) = H$ AND $\mu(E_T) = H$ AND $\mu_H(D) = M$ THEN $\mu(P_{grid}) = PM$.
- Rule 8: If $\mu(V_{node}) = H$ AND $\mu(E_T) = H$ AND $\mu_H(D) = H$ THEN $\mu(P_{grid}) = PL$.

Then, estimate the DOF of each rules sing the min or AND operator.

- DOF_1: min $\{\mu_M(V_{node}), \mu_M(E_T), \mu_M(D)\} = min\{0.9, 0.2, 0.1\} = 0.1$.
- DOF_2: min $\{\mu_M(V_{node}), \mu_M(E_T), \mu_H(D)\} = min\{0.9, 0.2, 0.9\} = 0.2$.
- DOF_3: min $\{\mu_M(V_{node}), \mu_H(E_T), \mu_M(D)\} = min\{0.9, 0.8, 0.1\} = 0.1$.
- DOF_4: min $\{\mu_M(V_{node}), \mu_H(E_T), \mu_H(D)\} = min\{0.9, 0.8, 0.9\} = 0.8$.
- DOF_5: min $\{\mu_H(V_{node}), \mu_M(E_T), \mu_M(D)\} = min\{0.1, 0.2, 0.1\} = 0.1$.
- DOF_6: min $\{\mu_H(V_{node}), \mu_M(E_T), \mu_H(D)\} = min\{0.1, 0.2, 0.9\} = 0.1$.
- DOF_7: min $\{\mu_H(V_{node}), \mu_H(E_T), \mu_M(D)\} = min\{0.1, 0.8, 0.1\} = 0.1$.
- DOF_8: min $\{\mu_H(V_{node}), \mu_H(E_T), \mu_H(D)\} = min\{0.1, 0.8, 0.9\} = 0.1$.

(iv) ***Step - 4:*** Estimate the total power flow between in either direction μP_{grid_i} for corresponding rules in the above Table.

- $\mu(P_{grid_1}) := -0.6$ for NM corresponding to DOF_1=0.1.

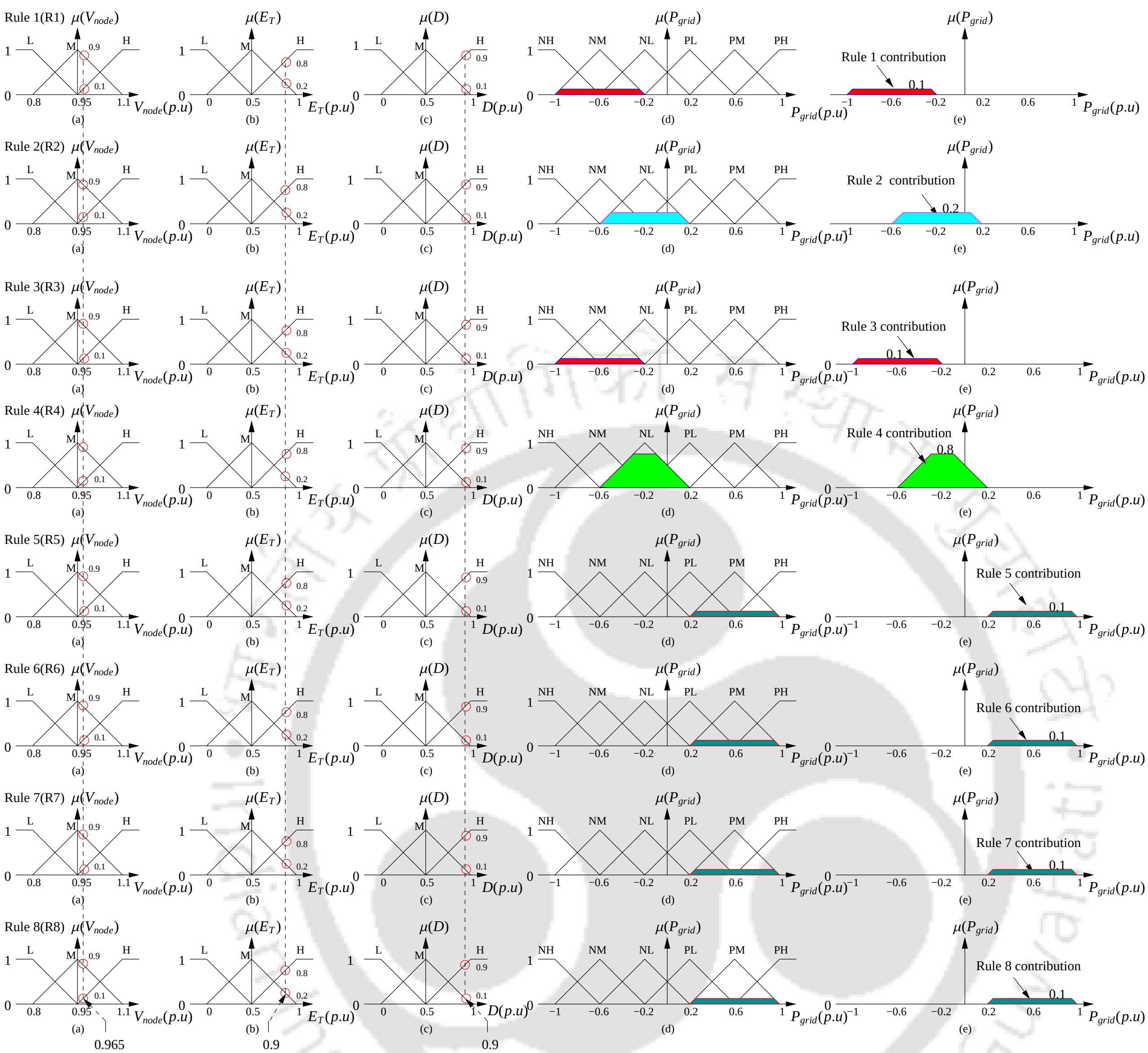

Figure B.2: Membership functions for CCU controller (a) $V_{node}(p.u)$, (b) E_T(p.u), (c) D, (d) P_{grid} and (e) rules contribution.

- $\mu(P_{grid_2}) := -0.2$ for NL corresponding to DOF_1=0.2.
- $\mu(P_{grid_3}) := -0.6$ for NM corresponding to DOF_1=0.1.
- $\mu(P_{grid_4}) := -0.2$ for NL corresponding to DOF_1=0.8.
- $\mu(P_{grid_5}) := 0.6$ for PM corresponding to DOF_1=0.1.
- $\mu(P_{grid_6}) := 0.6$ for PL corresponding to DOF_1=0.1.
- $\mu(P_{grid_7}) := 0.6$ for PM corresponding to DOF_1=0.1.
- $\mu(P_{grid_8}) := 0.6$ for PL corresponding to DOF_1=0.1.

(v) ***Step - 5:*** Estimate the crisp output μP_{grid} by the center of area method.

$$P_{grid} = \frac{(0.1\times -0.96) + (0.1\times -0.56) + (0.2\times -0.52) + (0.8\times -0.28) + (0.8\times -0.12) + (0.2\times 0.12) + (0.1\times 0.16) + (0.1\times 0.24) + (0.1\times 0.56)}{0.1 + 0.1 + 0.2 + 0.8 + 0.8 + 0.2 + 0.1 + 0.1 + 0.1} \tag{B.2}$$

$$P_{grid} = -0.1824. \tag{B.3}$$

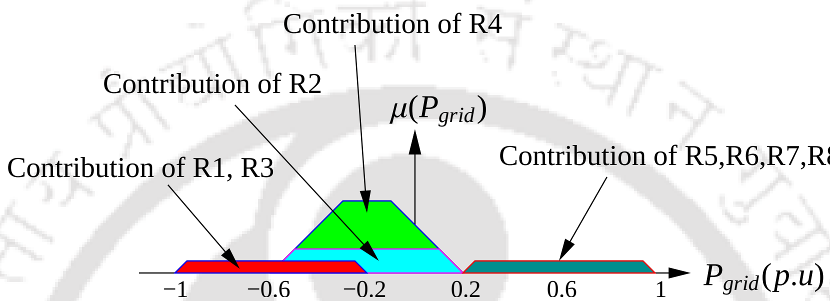

Figure B.3: Crisp value of the P_{grid}.

From Eq. (B.2), the crisp value of the output power is shown in Fig. B.3. The defuzzified value of the total power flow in either direction is value is $-0.1824p.u.$ The controller has decide the negative sign and low value of P_{grid} which means the power will plow from CS to grid and the grid voltage near to unity. Therefore, the CS support the grid with low power level.

Detailed fuzzy logic process is explained with another numerical example:

(i) ***Step - 1:*** The distribution node voltage (V_{node}) is 1.05, the total energy availability (E_T) is 0.3 and the duration (D) is 0.5.

(ii) ***Step - 2:*** Estimate the Degree of Membership Function (DOF) of $\mu(V_{node}(p.u))$, $\mu(E_T(p.u))$ and $\mu(D(p.u))$ for the equal fuzzy sets. $\mu_M(V_{node}) = 0.5$, $\mu_H(V_{node}) = 0.5$, $\mu_L(E_T) = 0.4$, $\mu_M(E_T) = 0.6$ and $\mu_M(D) = 1$.

(iii) ***Step - 3:*** The rule base for the CCU-FLU is given in Table B.1. Identify the eight rules from this Table for M, H values of $\mu(V_{node}(p.u))$, $\mu(E_T(p.u))$ and $\mu(D(p.u))$.

- Rule 1: If $\mu(V_{node}) = M$ AND $\mu(E_T) = L$ AND $\mu_H(D) = M$ THEN $\mu(P_{grid}) = PL$.
- Rule 2: If $\mu(V_{node}) = M$ AND $\mu(E_T) = M$ AND $\mu_H(D) = M$ THEN $\mu(P_{grid}) = NM$.

- Rule 3: If $\mu(V_{node}) = H$ AND $\mu(E_T) = L$ AND $\mu_H(D) = M$ THEN $\mu(P_{grid}) = PM$.
- Rule 4: If $\mu(V_{node}) = H$ AND $\mu(E_T) = M$ AND $\mu_H(D) = M$ THEN $\mu(P_{grid}) = PM$.

Then, estimate the DOF of each rules sing the min or AND operator.

- DOF_1: min $\{\mu_M(V_{node}), \mu_L(E_T), \mu_M(D)\} = min\,\{0.5, 0.4, 1\} = 0.4$.
- DOF_2: min $\{\mu_M(V_{node}), \mu_M(E_T), \mu_M(D)\} = min\,\{0.5, 0.6, 1\} = 0.5$.
- DOF_3: min $\{\mu_H(V_{node}), \mu_L(E_T), \mu_M(D)\} = min\,\{0.5, 0.4, 1\} = 0.4$.
- DOF_4: min $\{\mu_H(V_{node}), \mu_M(E_T), \mu_M(D)\} = min\,\{0.5, 0.6, 1\} = 0.5$.

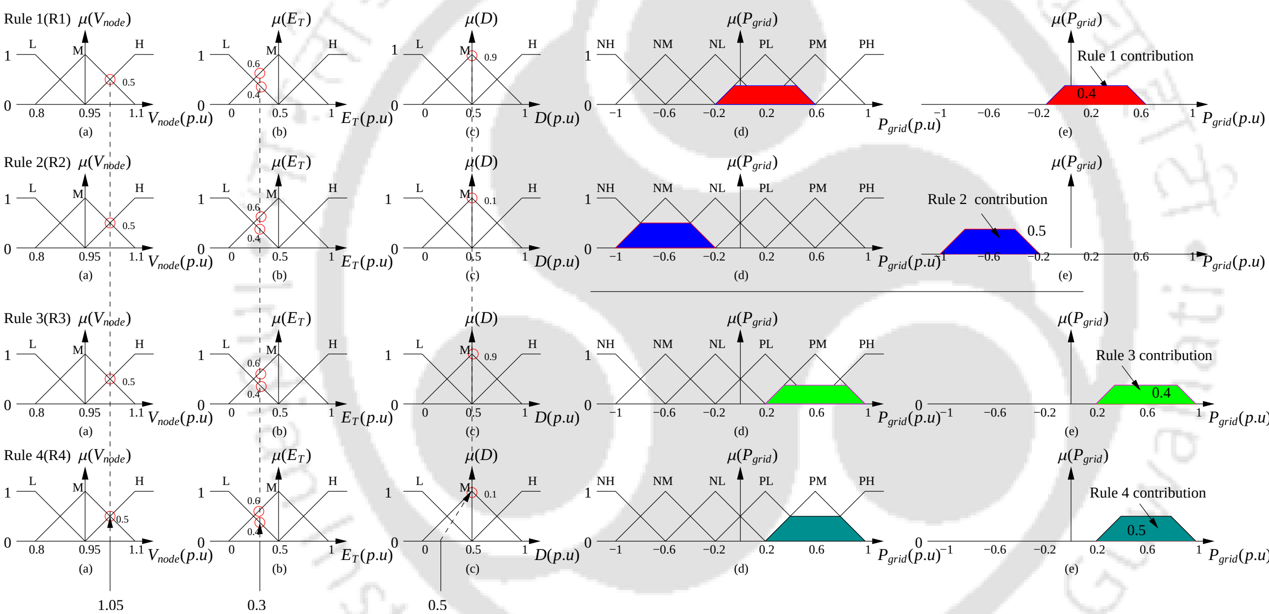

Figure B.4: Membership functions for CCU controller (a) $V_{node}(p.u)$, (b) E_T(p.u), (c) D, (d) P_{grid} and (e) rules contribution.

(iv) ***Step - 4:*** Estimate the total power flow between in either direction μP_{grid_i} for corresponding rules in the above Table.

- $\mu(P_{grid_1}) := 0.2$ for NM corresponding to DOF_1=0.4.
- $\mu(P_{grid_2}) := -0.6$ for NL corresponding to DOF_1=0.5.
- $\mu(P_{grid_3}) := 0.6$ for NM corresponding to DOF_1=0.4.
- $\mu(P_{grid_4}) := 0.6$ for NL corresponding to DOF_1=0.5.

(v) ***Step - 5:***Estimate the crisp output μP_{grid} by using Eq. B.1.

$$P_{grid} = 0.2896. \tag{B.4}$$

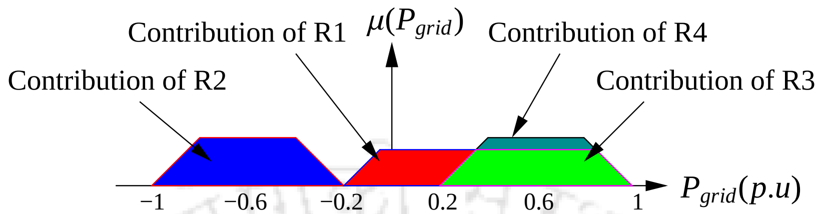

Figure B.5: Crisp value of the P_{grid}.

From Eq. (B.2), the crisp value of the output power is shown in Fig. B.5. The defuzzified value of the total power flow in either direction is value is $0.2896 p.u.$ The controller has decide the positive sign and medium value of P_{grid} which means the power will plow from grid to CS and the grid voltage greater than unity. Therefore, the CS inject the power from grid.

C

Filter Design

C.1 dc-dc Converter Design

There are different types of circuit topologies has been reported for bidirectional dc to dc Buck-Boost (BB) converter [195–199]. A simple dc-dc converter topology is used in the BCCS unit. Fig. C.1 (a) shows the circuit diagram for bidirectional BB converter with two switches (S_{13} and S_{14}) and two diodes (D_{13} and D_{14}). This circuit diagram has the ability to provide an output voltage higher or lower than the input voltage and also it can transfer power in both directions. Moreover, this circuit diagram has few number of switches are used for bidirectional power flow. This circuit topology selected due to its simple structure, well-known dynamic behavior, pulse by pulse currant limitation and instantaneous shutdown. The output voltage is controlled in either direction by controlling the duty (D) ratio of the S_{13} or S_{14}.

C.1.1 Modes of Operation

During G2V operation the switch S_{13} and diode D_{14} will conduct and V2G operation switch S_{14} and diode D_{14} would conduct.

The BB converter operates by storing the energy in the inductor (L_b) during the interval of Switch S_{13} in turned *on* (t_{on}). The stored energy is transferred to load or distributed energy source when the switch S_{13} is turned off (t_{off}). During this operating interval, the L_b provides a least resistance path. Hence, the maximum current flows through the L_b. The capacitor C_{b2} is used to remove the ripples in the output voltage. Fig. C.1(b) and Fig. C.1 (c) shows the equivalent circuit diagram for G2V modes operation and corresponding waveforms. When the S_{13} is turned *on*, the energy is stored into the L_b, the inductor current (I_{b1}) is reaching to the maximum (I_{max}) after a time interval kT which is shown in Fig C.1 (c). The voltage across the switch S_{13} is low and the current provided from the source (I_{dc}) to load is maximum. The switch S_{13} is turned off, then the current falls to zero but the I_{b2} starts to flow through the load and diode D_{14}. The stored energy in the L_b will transfer to the load. The I_{b2} is decreased, then the switch S_{13} would be turned *on* again in the next cycle.

The net impedance (Z_{net}) of the output side is calculated from Eq. (C.1).

$$Z_{net} = \frac{V_{c/d}^2}{P_{cs}} \tag{C.1}$$

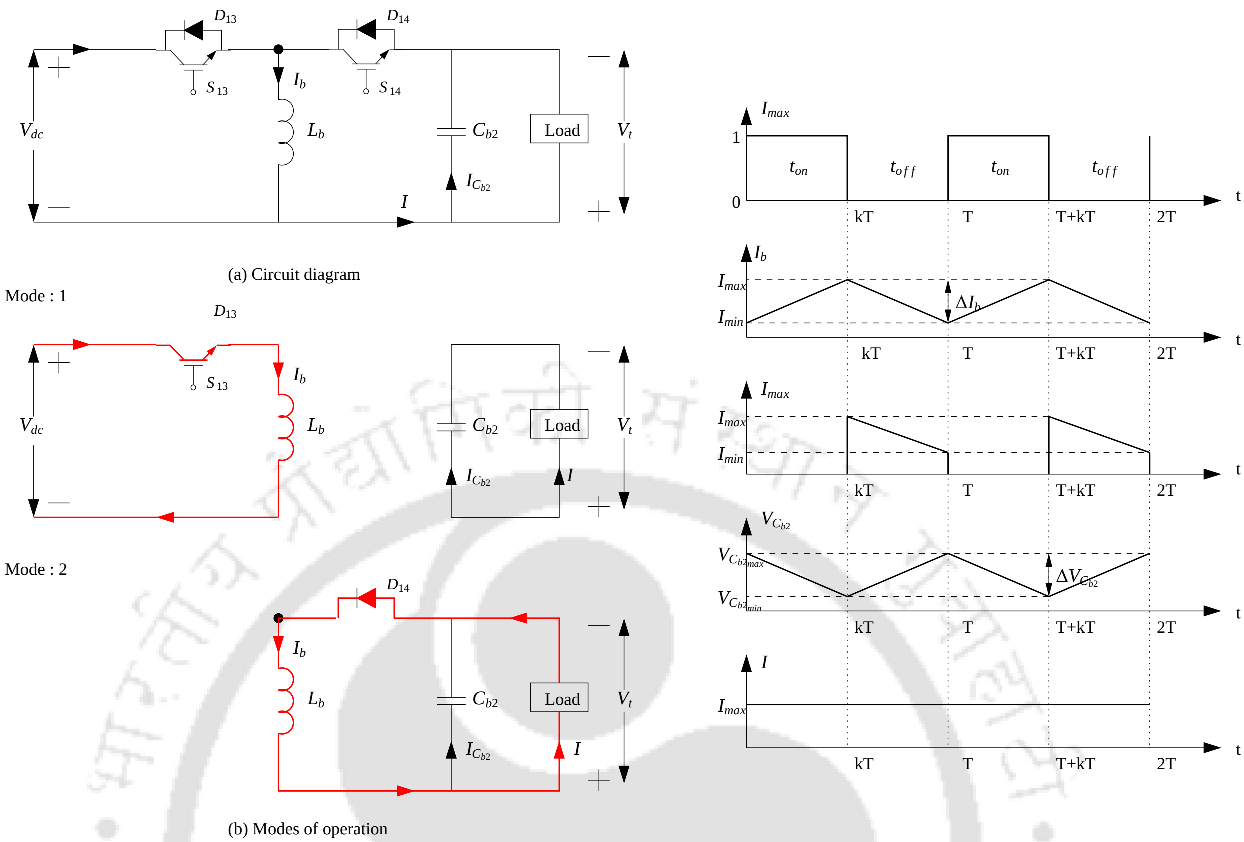

Figure C.1: Buck-boost converter circuit diagram, modes of operation and waveforms.

where $V_{c/d}$ is the battery terminal voltage or output voltage of the dc-dc converter and P_{cs} is the maximum power handling capacity of the BCCS unit. The peak to peak ripple current (ΔI_b) is calculated from Eq. (C.2).

$$\Delta I_b = \frac{V_{dc}}{fL_b} \tag{C.2}$$

where V_{dc} is the supply voltage or input voltage of the BB converter and f is the switching frequency. The peak to peak ripple voltage ($\Delta V_{C_{b2}}$) is calculated from Eq. (C.3).

$$\Delta V_{C_{b2}} = \frac{Ik}{fC_{b2}} \tag{C.3}$$

where k is the duty cycle. The output voltage of the BB converter is given in Eq. (C.4).

$$V_{c/d} = -\frac{V_{dc}k}{1-k} \tag{C.4}$$

The equation for L_b and C_{b2} is derived from Eq. (C.2) and Eq. (C.3) which is given below. Assume the peak to peak ripple voltage is 3% of the maximum voltage and the ripple current is 3% of the rated current.

$$L_b = \frac{V_{dc}k}{f\Delta I_b} \tag{C.5}$$

$$C_{b2} = \frac{Ik}{f\Delta V_{C_{b2}}} \tag{C.6}$$

C.2 Contactless Power Transfer System

The inductive power transfer (IPT) system consists of the primary and the secondary sides. Primary side consists of a converter that converts dc supply into high-frequency ac signal and passes on to the primary coil. The primary coil is coupled with the secondary coil. The high-frequency current passing through the primary coil induces a voltage into the secondary coil and hence the power is transferred.

C.2.1 Self and Mutual Inductance Calculation

Although spiral circular geometry is the one having better coupling [94], the geometry used here is square or rectangular with planar coil distribution. They show better tolerance to misalignment, which is one of the important characteristics for EV applications. The calculation of L_1 and L_2 for rectangular winding and planar coil distribution can be approximated using neuman's formula, which is given in Eq. (C.7). The rectangular winding with N_1 and N_2 turns and their equivalent radius r is given by

$$L = \frac{\mu_o}{4\pi} N^2 \oint_{r_1} \oint_{r_2} \frac{dl.dl'}{r} \tag{C.7}$$

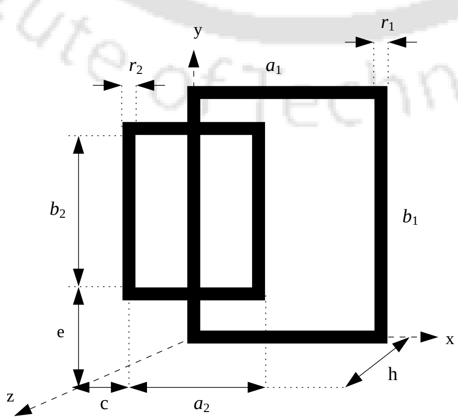

Figure C.2: Parameters of the rectangular coils for any dimension and any relative position between them [2]

The Eq. (C.7), applied to the system shown in Fig. C.2, gives

$$L = \frac{\mu o}{\pi} N_i^2 \left[\begin{array}{l} a_i . \ln \frac{2a_i b_i}{r_i(a_i + \sqrt{a_i^2 + b_i^2})} + b_i . \ln \frac{2a_i b_i}{r_i(b_i + \sqrt{a_i^2 + b_i^2})} \\ -2(a_i + b_i - \sqrt{a_i^2 + b_i^2}) + 0.25(a_i + b_i) \end{array} \right] \tag{C.8}$$

Where r_i is the equivalent radius of the winding, defined as

$$r_i = \sqrt{\frac{N_i S_i}{\pi}} \tag{C.9}$$

Winding resistance R_i is given by the following expression:

$$R_i = \rho CuNi \frac{2(a_i + b_i)}{S_i} \tag{C.10}$$

Where in Eq. (C.8) - Eq. (C.10), $i = 1$ should be used for the primary winding and $i = 2$ for the secondary winding. To consider the possibility of having winding of different sizes and significant misalignment can occur while transferring the power from primary side to secondary side via contactless coil. Therefore, an general expression for mutual inductance of the primary and secondary side coil is given in Eq. (C.11).

$$M = \frac{\mu_0}{4\pi} N_1 N_2 \oint_{r_1} \oint_{r_2} \frac{dl.dl'}{r} \tag{C.11}$$

Fig. C.3 shows the induced and reflected voltages, which are specified in terms of mutual inductance M, the operational frequency ω_o and I_p, I_s, V_p, V_s are the primary and secondary current and voltages. The mutual inductance is related to the magnetic coupling coefficient, k and is given by

$$k = \frac{M}{\sqrt{L_p L_s}} \tag{C.12}$$

C.2.2 Electrical Circuit Parameter Calculation

Fig. C.3 shows the series-series compensation circuit topology and mutual inductance coupling model of a series compensated contactless coil.

The voltage induced at the secondary side of the contactless coil is given in Eq. (C.13).

$$V_s = j\omega M I_p \tag{C.13}$$

Reflected impedance at the primary side can be expressed as the ratio of the reflected voltage and

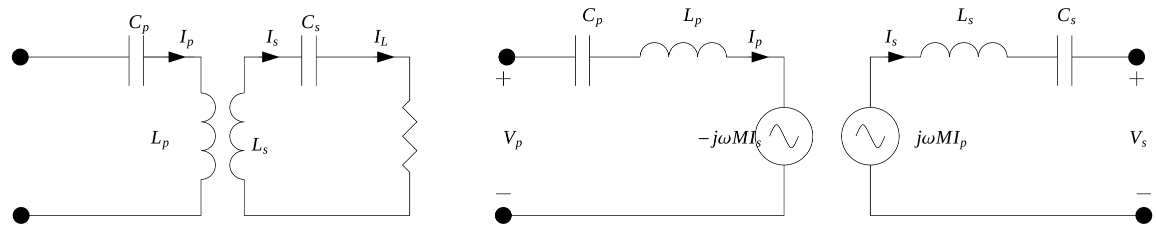

(a) Baisc circuit topology (b) Mutual inductance coupling model

Figure C.3: Circuit topology and mutual inductance coupling model.

the primary current.

$$Z_r = \frac{j\omega MI_s}{I_p} \tag{C.14}$$

The secondary current can be expressed as the ratio of the secondary voltage (reflected upon by primary coil) and secondary impedance (Z_s).

$$I_s = \frac{j\omega MI_p}{Z_s} \tag{C.15}$$

Hence, the general expression reflected impedance Z_r from the secondary to the primary is found by dividing the reflected voltage by the primary current resulting in

$$Z_r = \frac{{\omega_o}^2 M^2}{Z_s} \tag{C.16}$$

where Z_s is the impedance of the secondary network and depends on the selected compensation topology. Assuming load resistance to be R, the secondary side reflected impedances for the is given below.

$$Z_s = j\omega L_s + \frac{1}{j\omega C_s} + R_s + R \tag{C.17}$$

where ω is the angular frequency which is $\omega = \frac{1}{\sqrt{L_s C_s}}$. The load impedance ($Z_t$) seen by the power supply can be found by combining the primary impedance and the reflected impedance. In the case of series-compensated primary,

$$Z_t = \frac{1}{j\omega C_p} + j\omega L_p + R_p + Z_r \tag{C.18}$$

The power transferred from the primary to the secondary is given by

$$P = (\text{Re}Z_r){I_p}^2 \tag{C.19}$$

Where the operator *Re* represents the real component of corresponding variable. The current flowing through the secondary winding is given by

$$I_s = \frac{j\omega_o M I_p}{Z_s} \tag{C.20}$$

The voltages across the primary and secondary windings is given in Eq. (C.21) and Eq. (C.22).

$$V_p = j\omega_o L_p I_p - j\omega_o M I_s \tag{C.21}$$

$$V_s = j\omega_o M I_p - j\omega_o L_s I_s \tag{C.22}$$

Efficiency of the system (ignoring switching losses) can be determined by

$$\eta = \frac{RI_2^2}{R_1 I_p^2 + R_2 I_s^2 + RI_2^2} \tag{C.23}$$

C.2.3 Operating Frequency

The primary side and secondary side operating frequency should be same. The change in primary operating frequency is mainly to attain zero phase angle (ZPA) operations by nullifying or minimizing the reactive impedance as seen by the power supply. This is done to minimize the VA rating of the power supply. However, the ZPA frequency must be within a certain range of the resonant frequency, else it would affect the power transfer capability of the system. Also, the operation frequency may be changed to control power flow from primary to secondary. By detuning the system, the power transfer capability of the system is reduced. This method is often used to control the secondary side voltage or current from primary side.

C.2.4 Compensation Level

There are four basic compensation topology has been reported in literature such as series-series (SS), series-parallel (SP), parallel-series (PS) and parallel-parallel (PP). Although, series-series compensation has been used for in this work because, its require less copper mass and lower current. Compensation of the primary and secondary coil is a very important element of the IPT system. Firstly, operation at or near to resonance points help in maximizing power transfer capability. Secondly, compensation helps in reducing VA rating of the power supply. In the absence of compensation, a higher magnitude of current would be needed to sustain the system. This would result in greater resistive losses in wires and also during switching. Hence, the primary compensation is necessary to minimize the VA rating of the supply. In the secondary compensation, it is essential for maximizing power transfer capability, which is normally low due to lose coupling.

Selection of topology is based on various theoretical as well as practical considerations. The series compensated secondary resembles a voltage source while parallel compensated secondary resembles a current source. Assuming secondary coil resistance to be zero, the reflected resistances (real part of impedance) comes out to be $\frac{\omega^2 M^2}{R}$ and $\frac{\omega^2 M^2}{L_s^2}$, respectively and then using Eq. (C.19), one can see the validity of the statement. A series compensated primary is used to keep primary coil voltage and current at manageable levels while parallel compensated secondary is used for generating high current. Hence, the selection of the circuit topology is based on the application. Moreover, there are more factors that vary along with the circuit topology and affect the selection of primary operation frequency and primary capacitance.

The series resonant circuit shown in Fig. C.2 is formed by compensation capacitors C_p and C_s, and leakage inductance L_p and L_s. The approximate resonant frequency of the resonant circuit is given by

$$\omega_o = \frac{1}{\sqrt{(L_p + n^2 L_s).(C_p + \frac{C_s}{n^2})}} \tag{C.24}$$

where, $n = \frac{N_p}{N_s}$ is the turn's ratio of the transformer. Therefore, the required compensation, C_{comp} of the series capacitor is given by

$$C_{comp} = \frac{1}{\omega_o{}^2 L_{leak}} \tag{C.25}$$

A usual method of design is to select the primary operation frequency as the nominal frequency (secondary resonant frequency). In this case, it is assumed that the load and the magnetic coupling don't vary much. The ZPA frequency is made the same as the nominal frequency by selecting the primary capacitance such that it nullifies the reactive impedance as seen by the power source at the nominal frequency. The choice of primary capacitance depends on the topology selected.

- Series compensated secondary reflects only real impedance on the primary side at nominal frequency. Hence, in series-series topology, primary capacitance can be tuned independent of coupling and load.
- In parallel-series topology, the imaginary part of the impedance as seen by the source and hence primary capacitance tuning depends on load as well coupling.
- Parallel compensated secondary reflects the load independent capacitive reactance on the primary side. In series-parallel topology, primary capacitance tuning depends on the magnetic coupling but not load.
- In parallel-parallel topology, tuning depends on both magnetic coupling and load.

Hence, after selection of the primary capacitance for fixed frequency operation in PP and PS topology, it has to be ensured that the load and coupling variation is within limits and doesn't lead to significant shift in ZPA frequency and hence increase VA rating. Similarly in the case of SP topology, variation of load must be in limits. Theoretically, SS topology can be considered to be most desirable as its primary capacitance tuning is independent of magnetic coupling or load. However, due to practical considerations, it may be preferable to use parallel compensation on one of the sides.

C.3 Filter Design for Bidirectional Converters

The converters are used to convert one form electrical energy into another form of electrical energy based on the switching operations. Fig. C.4 shows the circuit diagram of bidirectional 3Φ and 1Φ ac-dc converter with filter. These converters are used in the industrial application, variable speed control and voltage regulator, etc. These converters are act as a rectifier and inverter during G2V and V2G operating modes, respectively.

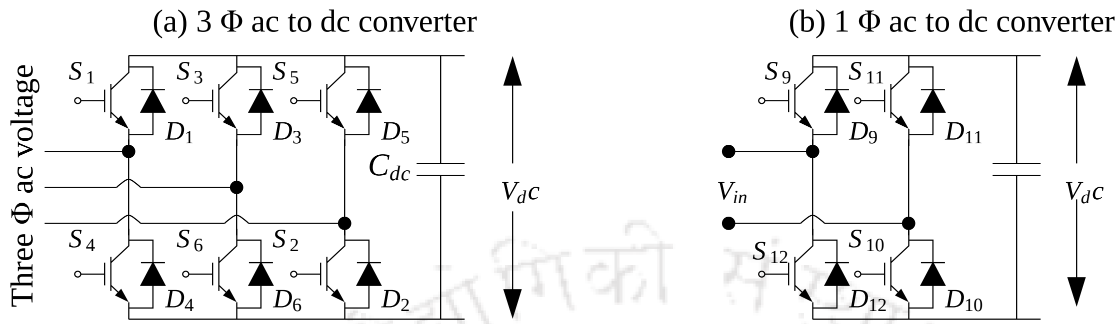

Figure C.4: Circuit diagram of bidirectional 3Φ and 1Φ ac-dc converter with filter.

In the G2V operation, the electric grid supplies the excess amount of energy to store in the EVs' batteries during off-peak hours. Then, the 3Φ ac voltage is converted into dc voltage by using the switches' S_1 to S_6. Further, the 1Φ high-frequency voltage is converted into dc voltage. The output voltage of this converter is not a pure dc voltage, some ac component also raiding in the top of the dc voltage. Therefore, filter circuit is required to remove the harmonics in the dc output voltage. The filter circuit has been design based on the net reflected impedance seen from the source, which is given in Eq. (C.26).

$$Z_{net} = \frac{V_{dc}^2}{P_{cs}} \tag{C.26}$$

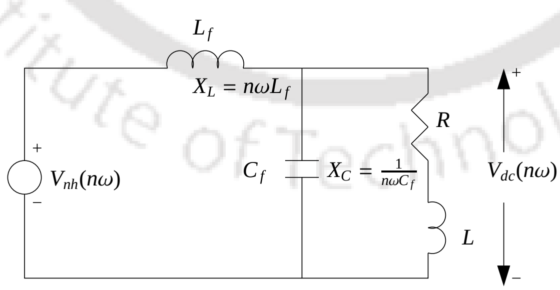

(a) Circuit diagram

Figure C.5: Equivalent circuit diagram for n^{th} order harmonics.

The equivalent circuit of the harmonics is shown in Fig. C.5. The n_{th} harmonic ripple current to pass through the filter capacitance. Therefore, the load impedance, much greater than the filter capacitance [200].

$$\sqrt{R^2 + (n\omega L)^2} >> \frac{1}{n\omega C_f} = \frac{10}{n\omega C_f} \tag{C.27}$$

The root-mean-square (rms) value of the n_{th} harmonic component appearing on the output of the ac to dc converter, which is given in Eq. (C.28).

$$V_{on} = \frac{\frac{-1}{n\omega C_f}}{n\omega L_f - \frac{1}{n\omega C_f}} V_{nh} \tag{C.28}$$

$$V_{on} = \frac{-1}{(n\omega)^2 C_f L_f - 1} V_{nh} \tag{C.29}$$

The ripple voltage due to harmonic is given in Eq. (C.31)

$$V_{ac} = \left(\sum_{n=2,4,6,...}^{\infty} V_{on}^2 \right)^{\frac{1}{2}} \tag{C.30}$$

The Fourier series for ac to dc converter is given in Eq. (C.32).

$$V_o(t) = V_{dc} + \sum_{n=2,4,6,...}^{\infty} (a_n \cos n\omega t + b_n \sin n\omega t) \tag{C.31}$$

The output voltage of the ac to dc converter, a_n and b_n are given below:

$$\begin{aligned} V_{dc} &= \frac{1}{2\pi} \int_0^{2\pi} V_0(t)\, d\omega t \\ V_{dc} &= \frac{2}{2\pi} \int_0^{\pi} V_m \sin \omega t d\omega t = \frac{2V_m}{\pi} \end{aligned} \tag{C.32}$$

$$\begin{aligned} a_n &= \frac{1}{\pi} \int_0^{2\pi} V_0 \cos n\omega t d\omega t = \frac{2}{\pi} \int_0^{\pi} V_m \sin \omega t \cos n\omega t d\omega t \\ a_n &= \sum_{n=2,4,6,...}^{\infty} \frac{-1}{(n-1)(n+1)} \text{for} n = 2, 4, 6, .. \\ & 0 \text{for} n = 1, 3, 5, ... \end{aligned} \tag{C.33}$$

$$\begin{aligned} b_n &= \frac{1}{\pi} \int_0^{2\pi} V_0 \sin n\omega t d\omega t = \frac{2}{\pi} \int_0^{\pi} V_m \sin \omega t \sin n\omega t d\omega t \\ b_n &= 0 \end{aligned} \tag{C.34}$$

Substitute the values of V_{dc}, a_n and b_n in Eq. (C.31).

$$b_n = \frac{1}{\pi}\int_0^{2\pi} V_0 \sin n\omega t \mathrm{d}\omega t = \frac{2}{\pi}\int_0^{\pi} V_m \sin \omega t \sin n\omega t \mathrm{d}\omega t$$
$$b_n = 0 \tag{C.35}$$

$$V_0(t) = \frac{2V_m}{\pi} + \sum_{n=2,4,6,...}^{\infty} \frac{4V_m}{\pi} \frac{-1}{(n-1)(n+1)} \cos n\omega t$$
$$V_0(t) = \frac{2V_m}{\pi} - \frac{4V_m}{3\pi}\cos 2\omega t - \frac{4V_m}{15\pi}\cos 4\omega t - \frac{4V_m}{35\pi}\cos 6\omega t - -\frac{4V_m}{62\pi}\cos 8\omega t... \tag{C.36}$$

From Eq. (C.36), the second order harmonic is the dominant and the rms value is given in Eq. (C.38).

$$V_{2h} = \frac{4V_m}{3\sqrt{2}\pi} \tag{C.37}$$

Substitute $n = 2$ in Eq. (C.29)

$$V_{02} = \frac{-1}{(2\omega)^2\left(L_f C_f - 1\right)} V_{2h} \tag{C.38}$$

The value of the filter capacitance (C_f) is given in below equation

$$\sqrt{R^2 + (2\omega L)^2} = \frac{10}{2\omega C_f} \tag{C.39}$$

Simplifying the above equation,

$$C_f = \frac{10}{4\pi f \sqrt{R^2 + (4\pi f L)^2}} \tag{C.40}$$

The value of the filter inductance can be calculated from ripple factor (rf) which is defined as the ratio between the input and output voltage of the converter.

$$rf = \frac{V_{ac}}{V_{dc}} = \frac{V_{02}}{V_{dc}} = \frac{V_{2h}}{V_{dc}} \frac{1}{(4\pi f)^2 L_f C_f - 1} \tag{C.41}$$

Assume, 5% of the ripples in the output voltage,

$$L_f = \frac{10.428}{(4\pi f)^2 C_f} \tag{C.42}$$

Similarly, the value of the filter capacitance and inductance for 3Φ ac to dc converter is given below,

$$C_f = \frac{10}{(12\pi f)^2 \sqrt{R^2 + (12\pi f L)^2}} \tag{C.43}$$

$$L_f = \frac{1.0082}{(12\pi f)^2 C_f} \quad \text{(C.44)}$$

C.4 LCL Filter Design

Fig. C.6 shows the equivalent circuit of three-phase inverter connected to the grid. The switching frequency effects in the inverter can inject harmonics from the charging station to the grid. These harmonics requires the connection of filter between the inverter and the grid. The filter attenuates most low order harmonics in the output.

The inductor (L) determines the ripple on the current and reduces the low-frequency harmonic components. The voltage across the inductor (V_L) with respect to the switching frequency (f_{sw}) and ripple current (ΔI_L) is given by Eq. (C.45).

$$V_L = L\frac{\Delta I_L}{f_{sw}} \quad \text{(C.45)}$$

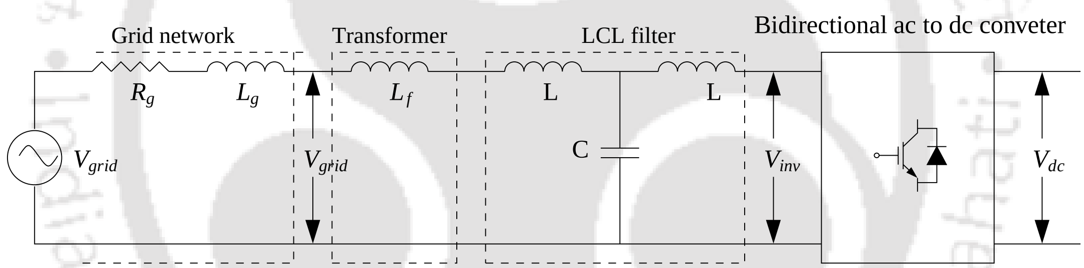

Figure C.6: Equivalent circuit of grid connected inverter.

According to the harmonic standards, 15-20% of the rated ripple current is allowable; 20% is assumed. The maximum ripple depends on the inductance, dc voltage (V_{dc}) and f_{sw}. The dc link voltage and switching frequency is constant and the inductance can be calculated from Eq. (C.46).

$$L = \frac{1}{8}\frac{V_{dc}}{\Delta I_L f_s} \quad \text{(C.46)}$$

The high-frequency components have to be eliminated from the inductor current when connected to the grid. This must be performed by the shunt impedance which is low at high frequencies. Assuming, V_{inv} is the inverter voltage, V_c is the capacitor voltage and Z_c, Z_t, Z_g and Z_L are the impedances of the capacitor, transformer, grid network and inductor respectively. Let, L is the total inductance of the filter circuit. The L_1 is designed based on the current ripple and L_2 is assumed to be a fraction of L_1

or greater than or less than of L_1. Therefore, the total inductance of the filter circuit is defined as the sum of filter inductance L_1 and L_2 ($L = L_1 + L_2$). The relationship between the L_1 and L_2 is $L_1 = aL_2$. The transfer function of the Fig. C.6 is given in Eq. (C.47).

$$\frac{I_o(s)}{V_{inv}(s)} = \frac{Z_c(s)(Z_t(s) + Z_g(s))}{Z_c(s)(Z_t(s) + Z_g(s) + Z_{L1}(s)) + Z_{L1}(s)(Z_t(s) + Z_g(s))} \tag{C.47}$$

The LCL filter transfer function which affects the closed loop system bandwidth in grid connected mode of operation is

$$\frac{i_o(s)}{V_{inv}(s)} = \frac{1}{s^3LC\left(L_g + L_t\right) + s^2LR_gC + s\left(L + L_t + L_g\right) + R_g} \tag{C.48}$$

The filter capacitance value has been obtained from the above equation.

$$C = -\frac{sk\left(L + L_t + L_g\right) + kR_g - 1}{Lks^2\left(s\left(L_g + L_t\right) + R_g\right)} \tag{C.49}$$

where, $k = \frac{i_o}{V_{inv}}$. Consider a charging system have 80kW peak power handling capacity and the three-phase inverter connected to a grid network through an isolation transformer 11kV/440V Δ/Y. The dc-link voltage is 650V and switched frequency of the three-phase inverter is 4kHz. From Eq. (C.46), the filter inductance will be $0.000008548845451H$. The standards state that the harmonic orders greater than 35 must not exceed 0.2% rated current [201]. Thus, the calculated value of the filter capacitance is $C = 0.5343028409e-5F$. The grid network impedance L_g and R_g vary depending on where CS is connected to the grid. The grid impedance used in the analysis is $L_g = 6.422 \times 10^-5$ and $Rg = 0.08064$. The maximum current flow from inverter to grid is given below,

$$i_o = \frac{P_{cs}}{\sqrt{3}V_{grid}} \tag{C.50}$$

The simplified equation for the filter capacitance by substituting the values in Eq. (C.49) and $s = In\omega$,

$$C = \frac{6399.99\,(1.1949e6s - 0.9869)}{s2\,(7.3987e6s + 0.08064)} \tag{C.51}$$

D

Synchronization

D.1 Sample Calculation

The detail sample calculation for CS aggregator is described in this section. Assume, V_{node} is 0.89 p.u and the D is 0.95 p.u. Then, the calculation for the individual energy of the EV battery is given below. The calculations are performed considering 10 EVs batteries of different ratings. The specifications of EVs batteries are given in Table 3.7. To avoid the repetition of similar type of calculation, only five EVs' batteries calculations are shown.

$$\begin{aligned} E_{b1} &= (250 \times 32 \times (0.7 - 0.25)) = 3.6kWh \\ E_{b2} &= (250 \times 40 \times (0.5 - 0.3)) = 2kWh \\ E_{b3} &= (400 \times 40 \times (0.85 - 0.3)) = 6.4kWh \\ E_{b4} &= (400 \times 50 \times (0.6 - 0.3)) = 6kWh \\ E_{b5} &= (500 \times 48 \times (0.8 - 0.25)) = 13.2kWh \end{aligned} \tag{D.1}$$

The total energy of the CS is given in Eq. (D.2) which is calculated from in Eq. (2.17).

$$\begin{aligned} E_T &= E_{b1} + E_{b2} + E_{b3} + E_{b4} + E_{b5} \\ E_T &= 2 \times 31.2 = 62.4kWh \end{aligned} \tag{D.2}$$

The fuzzy based CCU is decide the amount of power flow between the CS and grid based on the V_{node}, D and the energy of the CS. The CS aggregator distribute the reference power. The BCCS unit reference signals are given in Eq. (D.3).

$$\begin{aligned} P_{b1} &= \tfrac{7.2}{62.4} \times -170 = -9.8077kW \\ P_{b2} &= \tfrac{4}{62.4} \times -170 = -5.4487kW \\ P_{b3} &= \tfrac{12.8}{62.4} \times -170 = -17.4359kW \\ P_{b4} &= \tfrac{6}{62.4} \times -170 = -16.3462kW \\ P_{b5} &= \tfrac{13.2}{62.4} \times -170 = -35.9615kW \end{aligned} \tag{D.3}$$

The total power flow from CS to grid is given below.

$$\begin{aligned} P_{grid} &= P_{b1} + P_{b2} + P_{b3} + P_{b4} + P_{b5} \\ P_{grid} &= 2 \times -85 = -170kW \end{aligned} \tag{D.4}$$

The real power control between EVs' batteries and the DN is regulated by controlling the δ. The values of power angles are given in Eq. (D.5).

$$\begin{aligned} \delta_1 &= \sin^{-1}\left(\tfrac{-9807.7 \times 2.894}{440 \times 440}\right) = -8.43046^\circ \\ \delta_2 &= \sin^{-1}\left(\tfrac{-5448.7 \times 2.894}{440 \times 440}\right) = -4.67186^\circ \\ \delta_3 &= \sin^{-1}\left(\tfrac{-17435.9 \times 2.894}{440 \times 440}\right) = -15.1079^\circ \\ \delta_4 &= \sin^{-1}\left(\tfrac{-16346.2 \times 2.894}{440 \times 440}\right) = -14.1433^\circ \\ \delta_5 &= \sin^{-1}\left(\tfrac{-35961.5 \times 2.894}{440 \times 440}\right) = -32.518^\circ \end{aligned} \tag{D.5}$$

D.2 Synchronization Operation

Fig. D.1 shows the functional block diagram of the synchronization controller. It mainly consists of discrete three-phase PLL units, which extract the synchronization parameters (frequency and phase sequence) of the DN and V_{prim}, three-phase to two phase transformation and vice versa, LA-FLC and power estimator. three-phase V_{node} is the input for $abc - dq0$ transformation unit and discrete three-phase PLL.

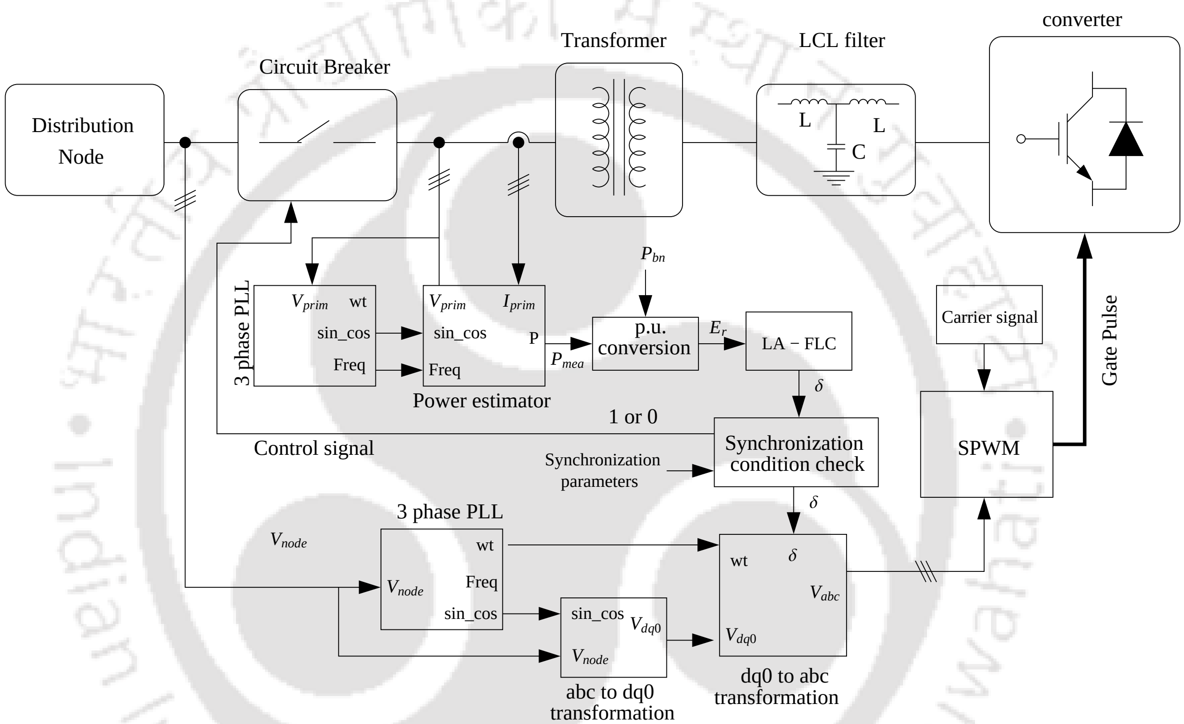

Figure D.1: Detailed block diagram of the FLC based synchronization controller.

One of the important conditions for synchronizing any Distributed Energy Resource (DER) with the grid is the line voltage of the DER system which must be equal or slightly greater than the line voltage of the grid. To satisfy this condition, the EVs batteries arrive at the charging station would discharge some energy initially for synchronizing with the grid. The system will be in floating condition for some period and no power transfer occurs. After synchronization operation, the direction of power transfer is decided. This must be satisfied for all EVs in the charging station arriving with high and low values of SOC. The buck-boost converter present in the EV battery system handles this operation. The duty ratio of the buck-boost converter is controlled and does the necessary operation and maintains the voltage level in the grid side. Initially, the EVs batteries have to discharge its energy to perform the synchronization operation. The control process is briefly described here.

D.2.1 Control Process

The objective of the control system is to control the charging/ discharging process of EVs' batteries, which mainly depend on DN voltage, energy status of the EVs' batteries and duration to support the grid (V_{node}, E_T and D). These inputs are given to Central Control Unit (CCU) and Charging Station (CS) aggregator, from which P_{bn} is fed inside the BCCS unit to control the charging/discharging states of EVs' batteries.

The input from the CS aggregator (P_{bn}) is the main control signal for the controllers in the BCCS unit. The P_{bn} is fed into the LA-FLC, which determines the amount and direction of power flow from/to the DN for both G2V and V2G operation. P_{bn} is also fed into the charging current control of the buck-boost converter in the battery side; which determines the reference current signal for the inner CC-FLC, as we required controlling the charging rate of the battery.

When EVs arrive at the CS, the BCCS unit will get connected with the DN and when it leaves the CS, the BCCS unit will get disconnected. However, the cases of charging/discharging operation of EVs; the initial synchronization process with the grid is necessary; without which the real power transfers in any direction cannot be controlled. The importance of synchronization of any power converters connected to the grid is explained in [168] and synchronization of BCCS unit has been described in reference [158]. For achieving this synchronization operation and to control the real power flow, we have load/power angle control in our work shown in Fig. 3.8. The LA-FLC provides the required δ to cause the power flow in any direction. The amount and direction of real power transfer take place, when the voltage produced by the BCCS unit leads or lags the voltage of the DN. This process is done by controlling the load angle of the BCCS unit. Thus, the charging/discharging process of EVs are controlled through appropriate control of the power converter based on the control signal from the CS aggregator.

During the synchronization period, the system is controlled and there is no power transfer between DN and EVs' batteries. However, the EVs arrive at the CS will have some initial discharge of energy. There will be a small negative flow of current during the synchronization period. This is because, the

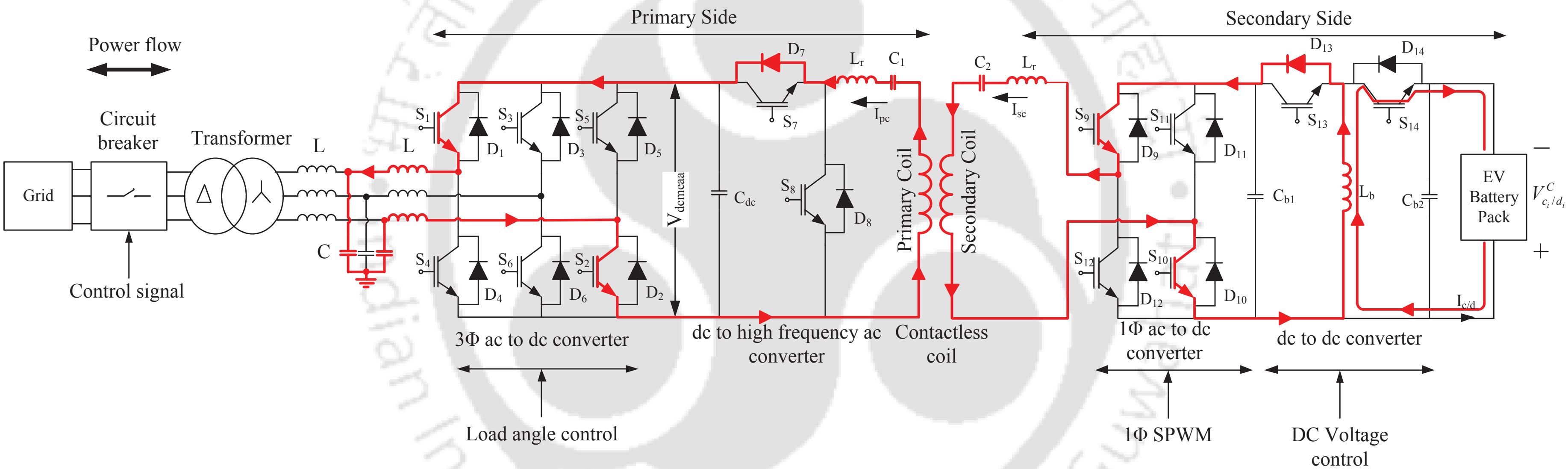

Figure D.2: Detailed circuit topology of individual BCCS unit

EVs' arrive at the CS will make a closed path through converter switches having low resistance and there is some initial current flow through LCL filter and this consumes very less power. The detailed circuit topology of individual BCCS unit with current flow direction at the initial synchronization period is shown in Fig. D.2.

E

Economic Beneficiary Calculation for EVs Owners, Grid Operators and Consumers

E.1 Sample Calculation

In this Section, sample calculation for economic beneficiary of EV owners and grid operators is described. Let, capacity of the battery is 80.025 after 332 (n') cycle. The following data's are obtained from battery and capacity fade model: $PE_{c/d} = 56.05kWh$, $E_q = 3.392kWh$, $E_{stor} = 25.61kWh$, $E_{transpor} = 10.67$ and $E_{rem} = E_{stor} - E_{transpor} = 25.61 - 10.67 = 14.94kWh$.

Also, the following assumptions are made: $c = 0$ (energy supplied by the grid to EVs' batteries during peak hours), $s' = 0$ (energy obtained by the grid during peak hours), total life of the battery ($n = 2801$), $D = 1$, $M =$Rs.$3,00,000$ and $x' = 4$.

The input energy to the battery provided by the grid has been calculated from Eq. (4.4).

$$\begin{aligned} E_{ib}^{G} &= 32 \times \left(\tfrac{100}{90}\right) \\ E_{ib}^{G} &= 35.55kWh \end{aligned} \tag{E.1}$$

The total amount of money paid by the EV owners to grid operators during a complete day is given in Eq. (4.5).

$$\begin{aligned} AP_{evg} &= \mathrm{cx} + \mathrm{c'x'} = 0x + c'x' \\ AP_{evg} &= 35.55 \times 4 = Rs.142.222. \end{aligned} \tag{E.2}$$

The actual amount of energy that the grid obtains from the EV is calculated from Eq. (4.13).

$$E_{trans} = \left(\frac{90}{100}\right) 14.94 = 13.446kWh \tag{E.3}$$

The amount paid by the grid operators to EV owner is obtained from Eq. (4.15).

$$\begin{aligned} AP_{gev} &= \mathrm{sx_2{+}s'x_2{}'} = sx_2 + 0x_2' \\ AP_{gev} &= sx_2 \end{aligned} \tag{E.4}$$

The x_2 is relative quantity, it can be determined from Eq. (4.27).

$$\begin{aligned} &\Rightarrow \mathrm{cx} + \mathrm{c'x'} + \tfrac{z+\frac{nM}{n'}}{D} = \mathrm{sx_2{+}s'x_2{}'} \\ &cx + c'x' + \tfrac{z+\frac{nM}{n'}}{D} = sx_2 + s'x_2 \\ &0 + \tfrac{32\times4}{0.9} + \tfrac{z+\frac{332\times300000}{2801}}{2801} = 13.446x_2 + 0x_2' \\ &142.22 + \tfrac{z+35558.73}{2801} = 13.446x_2 \\ &x_2 = 11.5214 + \tfrac{z}{37662.246} \end{aligned} \tag{E.5}$$

The value of z can be determined by using Eq. (4.21) and Eq. (4.22).

$$\begin{aligned} z &\geq \frac{3M_{dep}E_q}{2E_{avail}nPE_{c/d}} \\ z &\geq \frac{3M_{dep}E_q}{2E_{avail}nPE_{c/d}} \\ z &\geq \frac{3\times300000\times6.392}{2\times14.94\times2801\times56.05} \geq 1.226 \\ z &= 1.23 \end{aligned} \tag{E.6}$$

Substitute the value of z in Eq. (E.5),

$$\begin{aligned} x_2 &= 11.5214 + \frac{1.23}{37662.246} \\ x_2 &= Rs.11.52 \end{aligned} \tag{E.7}$$

The total amount of money paid by the grid operators to the EV owners during a complete day is calculated from Eq. (4.15).

$$\begin{aligned} AP_{gev} &= sx_2 + s'x_2 = sx_2 + 0x_2 \\ AP_{gev} &= sx_2 = 13.446 \times 11.52 \\ AP_{gev} &= Rs.145.89792 \end{aligned} \tag{E.8}$$

Profit for EV owners is calculated from Eq. (4.28)

$$x_2' \geq x'x_2 \geq x' \geq 4 \tag{E.9}$$

The total amount of money paid by the consumers to the grid operators during a complete day is calculated from Eq. (4.29).

$$\begin{aligned} A_{cg} &= sx_1 + s'x_1 = sx_1 \\ A_{cg} &= 13.446 \times 11.53 \\ A_{cg} &= Rs.155.03 \end{aligned} \tag{E.10}$$

Profit for grid operators is calculated from Eq. (4.30).

$$x_1 \geq x_2 \geq Rs.11.52 \tag{E.11}$$

Total energy consumed per kilometer is $\frac{225km}{40kWh} = 5.625km/kWh$. To charge the EVs' battery from grid, the consumers pay Rs. 154.056 per day. Therefore, cost per km is Rs. 3.34.

Bibliography

[1] EIG, "Battery Charge Rate Characteristics," http://www.eigbattery.com/.

[2] J. Sallan, J. Villa, A. Llombart, and J. Sanz, "Optimal design of ICPT systems applied to electric vehicle battery charge," *IEEE Trans. Ind. Electron.*, vol. 56, no. 6, pp. 2140–2149, June 2009.

[3] "Electricity Generation in India and Power Sector at a Glance "ALL INDIA"," http://en.wikipedia.org/wiki/Electricity_sector_in_Indiaandhttp://www.powermin.nic.in/indian_electricity_scenario/introduction.htm.

[4] "Indian Energy Sector: An Overview," http://http://en.wikipedia.org/wiki/Electricity_sector_in_India.

[5] "Energy Calculation per Capita," http://www.indexmundi.com/g/r.aspx?v=81000.

[6] "Electricity Generation in India," http://www.teriin.org/events/docs/Cop14/mitigation.pdf.

[7] "Peak power demand in assam," http://articles.economictimes.indiatimes.com/2012-12-27/news/36022094_1_power-projects-power-allocation-free-power.

[8] AERC, "Assam Electricity Regulatory Commission," http://aerc.nic.in/.

[9] M. Singh, P. Kumar, and I. Kar, "Analysis of vehicle to grid concept in indian scenario," 14^{th} *Int. Power Electron. and Motion Control Conf. (EPE/PEMC'10)*, pp. T6–149–T6–156, Sept. 2010.

[10] "Design Department of Assam Electricity Grid Corporation Ltd. [online]." Available:http://www.aegclsldc.org/1024.html,2010.

[11] "Battery (electricity)," Available:http://en.wikipedia.org/wiki/Battery_28electricity29 and http://batteryuniversity.com/learn/article/charging_lithium_ion_batteries.

[12] S. Buller, E. Karden, D. Kok, and R. De Doncker, "Modeling the dynamic behavior of supercapacitors using impedance spectroscopy," *IEEE Trans. Ind. Appl.*, vol. 38, no. 6, pp. 1622–1626, Nov./Dec. 2002.

[13] D. Cericola, P. Ruch, R. KÁJtz, P. NovÁk, and A. Wokaun, "Simulation of a supercapacitor/Li-ion battery hybrid for pulsed applications," *J. of Power Sources*, vol. 195, no. 9, pp. 2731–2736, May 2010.

[14] W. Hassenzahl, "Superconducting magnetic energy storage," *in Proc. of IEEE*, vol. 71, no. 9, pp. 1089–1098, Sept. 1983.

[15] W. Buckles and W. Hassenzahl, "Superconducting magnetic energy storage," *IEEE Power Engineering Review*, vol. 20, no. 5, pp. 16–20, May 2000.

[16] H. Louie and K. Strunz, "Superconducting magnetic energy storage (SMES) for energy cache control in modular distributed hydrogen-electric energy systems," *IEEE Trans. Appl. Supercond.*, vol. 17, no. 2, pp. 2361–2364, 2007.

[17] D. Wang, Z. hui Wu, G. Xu, D. da Wang, M. Song, and X. tao Peng, "Real-time power control of superconducting magnetic energy storage," *IEEE Int. Conf. on Power Syst. Technol. (POWERCON'12)*, Oct./Nov. 2012.

[18] M. Komori and Y. Uchimura, "Improving the dynamics of two types of flywheel energy storage systems with SMBs," *IEEE Trans. Appl. Supercond.*, vol. 15, no. 2, pp. 2261–2264, June 2005.

[19] A. Buchroithner, I. Andrasec, and M. Bader, "Optimal system design and ideal application of flywheel energy storage systems for vehicles," *IEEE Int. Energy Conf. and Exhibition (ENERGYCON'12)*, pp. 991–996, Sept. 2012.

[20] "Flywheel," http://advantage-environment.com/framtid/energy-storage-with-flywheel-technology/.

[21] R. Hein, P. R. Kleindorfer, and S. Spinler, "Valuation of electric vehicle batteries in vehicle-to-grid and battery-to-grid systems," *Technological Forecasting and Social Change*, vol. 79, no. 9, pp. 1654–1671, Nov. 2012.

[22] J. Tomić and W. Kempton, "Using fleets of electric-drive vehicles for grid support," *J. of Power Sources*, vol. 168, no. 2, pp. 459–468, June 2007.

[23] W. Kempton and J. Tomić, "Vehicle-to-grid power implementation: From stabilizing the grid to supporting large-scale renewable energy," *J. of Power Sources*, vol. 144, no. 1, pp. 280–294, June 2005.

[24] S. Deilami, A. Masoum, P. Moses, and M. A. S. Masoum, "Real-time coordination of plug-in electric vehicle charging in smart grids to minimize power losses and improve voltage profile," *IEEE Trans. Smart Grid*, vol. 2, no. 3, pp. 456–467, Sept. 2011.

[25] C. Quinn, D. Zimmerle, and T. Bradley, "An evaluation of state-of-charge limitations and actuation signal energy content on plug-in hybrid electric vehicle, vehicle-to-grid reliability, and economics," *IEEE Trans. Smart Grid*, vol. 3, no. 1, pp. 483–491, Mar. 2012.

[26] C. K. Ekman, "On the synergy between large electric vehicle fleet and high wind penetration - an analysis of the danish case," *Renewable Energy*, vol. 36, no. 2, pp. 546–553, Feb. 2011.

[27] J. M. L. Camila Fernandes, Pablo Frías, "Impact of vehicle-to-grid on power system operation costs: The spanish case study," *Applied Energy*, vol. 96, no. 0, pp. 194–202, Aug. 2012.

[28] J. Barton and D. Infield, "Energy storage and its use with intermittent renewable energy," *IEEE Trans. Energy Convers.*, vol. 19, no. 2, pp. 441–448, June 2004.

[29] C.-S. Wang, O. Stielau, and G. Covic, "Design considerations for a contactless electric vehicle battery charger," *IEEE Trans. Ind. Electron.*, vol. 52, no. 5, pp. 1308–1314, Oct. 2005.

[30] Y. Ma, T. Houghton, A. Cruden, and D. Infield, "Modeling the benefits of vehicle-to-grid technology to a power system," *IEEE Trans. Power Syst.*, vol. 27, no. 2, pp. 1012–1020, May 2012.

[31] Y. Ota, H. Taniguchi, T. Nakajima, K. Liyanage, J. Baba, and A. Yokoyama, "Autonomous distributed V2G (vehicle-to-grid) satisfying scheduled charging," *IEEE Trans. Smart Grid*, vol. 3, no. 1, pp. 559–564, Mar. 2012.

[32] L. Pieltain Fernandez, T. Roman, R. Cossent, C. Domingo, and P. Frias, "Assessment of the impact of plug-in electric vehicles on distribution networks," *IEEE Trans. Power Syst.*, vol. 26, no. 1, pp. 206–213, Feb. 2011.

[33] Z. Darabi and M. Ferdowsi, "Aggregated impact of plug-in hybrid electric vehicles on electricity demand profile," *IEEE Trans. Sustain. Energy*, vol. 2, no. 4, pp. 501–508, Oct. 2011.

[34] M. Singh, P. Kumar, and I. Kar, "A multi charging station for electric vehicles and its utilization for load management and the grid support," pp. 1026–1037, June 2013.

[35] Y. Ma, T. Houghton, A. Cruden, and D. Infield, "Modeling the benefits of vehicle-to-grid technology to a power system," *IEEE Trans. Power Syst.*, vol. 27, no. 2, pp. 1012–1020, May 2012.

[36] K. Qian, C. Zhou, M. Allan, and Y. Yuan, "Modeling of load demand due to EV battery charging in distribution systems," *IEEE Trans. Power Syst.*, vol. 26, no. 2, pp. 802–810, May 2011.

[37] G. Joos, M. De Freige, and M. Dubois, "Design and simulation of a fast charging station for PHEV/EV batteries," *IEEE Electric Power and Energy Conf. (EPEC'10)*, pp. 1–5, Aug. 2010.

[38] C. Alaoui, "Solid-state thermal management for lithium-ion EV batteries," *IEEE Trans. Veh. Technol.*, vol. 62, no. 1, pp. 98–107, Jan. 2013.

[39] M. Chen and G. Rincon-Mora, "Accurate electrical battery model capable of predicting runtime and I-V performance," *IEEE Trans. Energy Convers.*, vol. 21, no. 2, pp. 504–511, June 2006.

[40] T.-K. Lee, B. Adornato, and Z. Filipi, "Synthesis of real-world driving cycles and their use for estimating PHEV energy consumption and charging opportunities: Case study for Midwest/U.S." *IEEE Trans. Veh. Technol.*, vol. 60, no. 9, pp. 4153–4163, Nov. 2011.

[41] RicardoFariaandPedroMouraandJoaquimDelgadoandAnibalT.deAlmeida, "A sustainability assessment of electric vehicles as a personal mobility system," *Energy Conversion and Management*, vol. 61, pp. 19–30, Sept. 2012.

[42] "Electric vehicle battery," http://en.wikipedia.org/wiki/Electric_vehicle_battery.

[43] P. H. Andersen, J. A. Mathews, and M. Rask, "Integrating private transport into renewable energy policy: The strategy of creating intelligent recharging grids for electric vehicles," *Energy Policy*, vol. 37, no. 7, pp. 2481–2486, July 2009.

[44] J. Mullan, D. Harries, T. Bráunl, and S. Whitely, "The technical, economic and commercial viability of the vehicle-to-grid concept," *Energy Policy*, vol. 48, no. 0, pp. 394–406, Sept. 2012.

[45] Y. A. R. I. Mohamed and E. El-Saadany, "Hybrid variable-structure control with evolutionary optimum-tuning algorithm for fast grid-voltage regulation using inverter-based distributed generation," *IEEE Trans. Power Electron.*, vol. 23, no. 3, pp. 1334–1341, May 2008.

[46] H. Sepahvand, J. Liao, and M. Ferdowsi, "Investigation on capacitor voltage regulation in cascaded h-bridge multilevel converters with fundamental frequency switching," *IEEE Trans. Ind. Elect.*, vol. 58, no. 11, pp. 5102–5111, Nov. 2011.

[47] H. Fujita and H. Akagi, "Voltage-regulation performance of a shunt active filter intended for installation on a power distribution system," *IEEE Trans. Power Electron.*, vol. 22, no. 3, pp. 1046–1053, May 2007.

[48] E. Demirok, P. Casado Gonzaález, K. Frederiksen, D. Sera, P. Rodriguez, and R. Teodorescu, "Local reactive power control methods for overvoltage prevention of distributed solar inverters in low-voltage grids," *IEEE Journal of Photovoltaics*, vol. 1, no. 2, pp. 174–182, Oct. 2011.

[49] F. Wang, J. Duarte, and M. A. M. Hendrix, "Pliant active and reactive power control for grid-interactive converters under unbalanced voltage dips," *IEEE Trans. Power Electron.*, vol. 26, no. 5, pp. 1511–1521, May 2011.

[50] J. Escudero-Garzas, A. Garcia-Armada, and G. Seco-Granados, "Fair design of plug-in electric vehicles aggregator for V2G regulation," *IEEE Trans. Veh. Technol.*, vol. 61, no. 8, pp. 3406–3419, Oct. 2012.

[51] G. Liu and K. Tomsovic, "Quantifying spinning reserve in systems with significant wind power penetration," *IEEE Trans. Power Syst.*, vol. 27, no. 4, pp. 2385–2393, Nov. 2012.

[52] N. Chowdhury and R. Billinton, "Export/import of spinning reserve in interconnected generation systems," *IEEE Trans. Power Syst.*, vol. 6, no. 1, pp. 43–50, Feb. 1991.

[53] A. Abiri-Jahromi, M. Fotuhi-Firuzabad, and E. Abbasi, "Optimal scheduling of spinning reserve based on well-being model," *IEEE Trans. Power Syst.*, vol. 22, no. 4, pp. 2048–2057, Nov. 2007.

[54] M. Q. Wang and H. Gooi, "Spinning reserve estimation in microgrids," *IEEE Trans. Power Syst.*, vol. 26, no. 3, pp. 1164–1174, Aug. 2011.

[55] N. Chowdhury and R. Billinton, "Assessment of spinning reserve in interconnected generation systems with export/import constraints," *IEEE Trans. Power Syst.*, vol. 4, no. 3, pp. 1102–1109, Aug. 1989.

[56] ——, "Export/import of spinning reserve in interconnected generation systems," *IEEE Trans. Power Syst.*, vol. 6, no. 1, pp. 43–50, Feb. 1991.

[57] E. Sortomme and M. El-Sharkawi, "Optimal scheduling of vehicle-to-grid energy and ancillary services," *IEEE Trans. Smart Grid*, vol. 3, no. 1, pp. 351–359, March 2012.

[58] H. Khayyam, H. Ranjbarzadeh, and V. Marano, "Intelligent control of vehicle to grid power," *J. of Power Sources*, vol. 201, no. 0, pp. 1–9, Mar. 2012.

[59] S. Han, S. Han, and K. Sezaki, "Effects of electric vehicles on power systems in northern europe," *Energy*, vol. 48, no. 1, pp. 356–368, Dec. 2012.

[60] Bessa, R. J., and M. A. Matos, "The role of an aggregator agent for ev in the electricity market," 7^{th} *Mediterranean Conf. and Exhibition on Power Gener. Transm. Distrib. and Energy Convers. (Med-Power'10)*, Nov. 2010.

[61] S. Han, S. Han, and K. Sezaki, "Estimation of achievable power capacity from plug-in electric vehicles for V2G frequency regulation: Case studies for market participation," *IEEE Trans. Smart Grid*, vol. 2, no. 4, pp. 632–641, Dec. 2011.

[62] S.-K. Kim, J.-H. Jeon, C.-H. Cho, J.-B. Ahn, and S.-H. Kwon, "Dynamic modeling and control of a grid-connected hybrid generation system with versatile power transfer," *IEEE Trans. Ind. Electron.*, vol. 55, no. 4, pp. 1677–1688, Apr. 2008.

[63] M. De Freige, G. Joos, and M. Dubois, "Energy management & scheduling in a fast charging station for PHEV batteries," *IEEE Power and Energy Society General Meeting (PES'11)*, pp. 1–5, July 2011.

[64] Y. He, B. Venkatesh, and L. Guan, "Optimal scheduling for charging and discharging of electric vehicles," *IEEE Trans. Smart Grid*, vol. 3, no. 3, pp. 1095–1105, Sept. 2012.

[65] E. Sortomme and M. El-Sharkawi, "Optimal charging strategies for unidirectional vehicle-to-grid," *IEEE Trans. Smart Grid*, vol. 2, no. 1, pp. 131–138, March 2011.

[66] K. Clement-Nyns, E. Haesen, and J. Driesen, "The impact of charging plug-in hybrid electric vehicles on a residential distribution grid," *IEEE Trans. Power Syst.*, vol. 25, no. 1, pp. 371–380, Feb. 2010.

[67] G. Li and X.-P. Zhang, "Modeling of plug-in hybrid electric vehicle charging demand in probabilistic power flow calculations," *IEEE Trans. Smart Grid*, vol. 3, no. 1, pp. 492–499, March 2012.

[68] J. Lopes, F. Soares, and P. Almeida, "Integration of electric vehicles in the electric power system," *in Proc. of IEEE*, vol. 99, no. 1, pp. 168–183, Jan. 2011.

[69] S. S. Raghavan and A. Khaligh, "Impact of plug-in hybrid electric vehicle charging on a distribution network in a smart grid environment," *IEEE PES Innovative Smart Grid Technol. (ISGT'12)*, pp. 1–7, Jan. 2012.

[70] E. Sortomme, E. Doheny, and M. El-Sharkawi, "The effect of electric vehicle drive efficiency on bidding vehicle-to-grid services," *IEEE Int. Electric Machines Drives Conf. (IEMDC'11)*, pp. 1288–1293, May 2011.

[71] M. Khan, I. Husain, and Y. Sozer, "Integrated electric motor drive and power electronics for bidirectional power flow between electric vehicle and DC or AC grid," *IEEE Energy Convers. Congress and Exposition (ECCE'12)*, pp. 3403–3410, Sept. 2012.

[72] L. Hui-ling, B. Xiao-min, and T. Wen, "Impacts of plug-in hybrid electric vehicles charging on distribution grid and smart charging," *IEEE Int. Conf. on Power Syst. Technol. (POWERCON'12)*, pp. 1–5, Oct. 2012.

[73] S. Han, S. Han, and K. Sezaki, "Development of an optimal vehicle-to-grid aggregator for frequency regulation," *IEEE Trans. Smart Grid*, vol. 1, no. 1, pp. 65–72, June 2010.

[74] M. Singh, P. Kumar, and I. Kar, "Implementation of vehicle to grid infrastructure using fuzzy logic controller," *IEEE Trans. Smart Grid*, vol. 3, no. 1, pp. 565–577, Mar. 2012.

[75] D. Steen, L. Tuan, O. Carlson, and L. Bertling, "Assessment of electric vehicle charging scenarios based on demographical data," *IEEE Trans. Smart Grid*, vol. 3, no. 3, pp. 1457–1468, Sept. 2012.

[76] J. Xu and V. Wong, "An approximate dynamic programming approach for coordinated charging control at vehicle-to-grid aggregator," *IEEE Int. Conf. on Smart Grid Communications (SmartGridComm'11)*, pp. 279–284, Oct. 2011.

[77] D. Wu, D. Aliprantis, and L. Ying, "Load scheduling and dispatch for aggregators of plug-in electric vehicles," *IEEE Trans. Smart Grid*, vol. 3, no. 1, pp. 368–376, March 2012.

[78] C. Wu, H. Mohsenian-Rad, and J. Huang, "Vehicle-to-aggregator interaction game," *IEEE Trans. Smart Grid*, vol. 3, no. 1, pp. 434–442, Mar. 2012.

[79] L. Gao, S. Liu, and R. Dougal, "Dynamic lithium-ion battery model for system simulation," *IEEE Trans. Comp. Packag. Technol.*, vol. 25, no. 3, pp. 495–505, Sept. 2002.

[80] J. Dogger, B. Roossien, and F. Nieuwenhout, "Characterization of li-ion batteries for intelligent management of distributed grid-connected storage," *IEEE Trans. Energy Convers.*, vol. 26, no. 1, pp. 256–263, Mar. 2011.

[81] S. Beer, T. Gomez, D. Dallinger, I. Momber, C. Marnay, M. Stadler, and J. Lai, "An economic analysis of used electric vehicle batteries integrated into commercial building microgrids," *IEEE Trans. Smart Grid*, vol. 3, no. 1, pp. 517–525, Mar. 2012.

[82] U. Madawala and D. Thrimawithana, "A bidirectional inductive power interface for electric vehicles in V2G systems," *IEEE Trans. Ind. Electron.*, vol. 58, no. 10, pp. 4789–4796, Oct. 2011.

[83] ——, "A single controller for inductive power transfer systems," *IEEE* 35th *Annual Conf. of Ind. Electron. (IECON '09)*, pp. 109–113, Nov. 2009.

[84] D. Thrimawithana and U. Madawala, "A three-phase bi-directional IPT system for contactless charging of electric vehicles," *IEEE Int. Symp. on Ind. Electron. (ISIE'11)*, pp. 1957–1962, June 2011.

[85] M. Budhia, G. Covic, and J. Boys, "A new IPT magnetic coupler for electric vehicle charging systems," 36th *Annual Conf. on IEEE Ind. Electron. Society (IECON'10)*, pp. 2487–2492, Nov. 2010.

[86] M. Pinuela, D. Yates, S. Lucyszyn, and P. Mitcheson, "Maximizing DC-to-load efficiency for inductive power transfer," *IEEE Trans. Power Electronics*, vol. 28, no. 5, pp. 2437–2447, May 2013.

[87] C.-S. Wang, G. Covic, and O. Stielau, "Power transfer capability and bifurcation phenomena of loosely coupled inductive power transfer systems," *IEEE Trans. Ind. Electron.*, vol. 51, no. 1, pp. 148–157, Feb. 2004.

[88] S. Mohagheghi, B. Parkhideh, and S. Bhattacharya, "Inductive power transfer for electric vehicles: Potential benefits for the distribution grid," *IEEE Int. Electric Veh. Conf. (IEVC'12)*, pp. 1–8, March 2012.

[89] H. L. Li, A. Hu, and G. Covic, "A direct AC - AC converter for inductive power-transfer systems," *IEEE Trans. Power Electron.*, vol. 27, no. 2, pp. 661–668, Feb. 2012.

[90] T. Bieler, M. Perrottet, V. Nguyen, and Y. Perriard, "Contactless power and information transmission," *IEEE Trans. Ind. Appl.*, vol. 38, no. 5, pp. 1266–1272, Sept./Oct. 2002.

[91] J. Zhao, J. Jiang, and X. Yang, "AC-DC-DC isolated converter with bidirectional power flow capability," *IET Trans. Power Electron.*, vol. 3, no. 4, pp. 472–479, July 2010.

[92] G. Covic, J. Boys, M. Kissin, and H. Lu, "A three-phase inductive power transfer system for roadway-powered vehicles," *IEEE Trans. Ind. Electron.*, vol. 54, no. 6, pp. 3370–3378, Dec. 2007.

[93] U. Madawala, M. Neath, and D. Thrimawithana, "A power - frequency controller for bidirectional inductive power transfer systems," *IEEE Trans. Ind. Electron.*, vol. 60, no. 1, pp. 310–317, Jan. 2013.

[94] J. Hayes, M. Egan, J. M. D. Murphy, S. Schulz, and J. Hall, "Wide-load-range resonant converter supplying the SAE J-1773 electric vehicle inductive charging interface," *IEEE Trans. Ind. Appl.*, vol. 35, no. 4, pp. 884–895, Jul./Aug. 1999.

[95] J. Villa, J. Sallan, J. Sanz Osorio, and A. Llombart, "High-misalignment tolerant compensation topology for ICPT systems," *IEEE Trans. Ind. Electron.*, vol. 59, no. 2, pp. 945–951, Feb. 2012.

[96] D. Thrimawithana, U. Madawala, and M. Neath, "A synchronization technique for bidirectional IPT systems," *IEEE Trans. Ind. Electron.*, vol. 60, no. 1, pp. 301–309, Jan. 2013.

[97] D. Yazdani, A. Bakhshai, G. Joos, and M. Mojiri, "A nonlinear adaptive synchronization technique for grid-connected distributed energy sources," *IEEE Trans. Power Electron.*, vol. 23, no. 4, pp. 2181–2186, July 2008.

[98] Y. F. Wang and Y. W. Li, "Grid synchronization PLL based on cascaded delayed signal cancellation," *IEEE Trans. Power Electron.*, vol. 26, no. 7, pp. 1987–1997, July 2011.

[99] L. Zhang, L. Harnefors, and H.-P. Nee, “Power-synchronization control of grid-connected voltage-source converters,” *IEEE Trans. Power Syst.*, vol. 25, no. 2, pp. 809–820, May 2010.

[100] S. Z. Chen, N. Cheung, Y. Zhang, M. Zhang, and X.-M. Tang, “Improved grid synchronization control of doubly fed induction generator under unbalanced grid voltage,” *IEEE Trans. Energy Convers.*, vol. 26, no. 3, pp. 799–810, Sept. 2011.

[101] F. Blaabjerg, R. Teodorescu, M. Liserre, and A. Timbus, “Overview of control and grid synchronization for distributed power generation systems,” *IEEE Trans. Ind. Electron.*, vol. 53, no. 5, pp. 1398–1409, Oct. 2006.

[102] T. Sharma, B. Sen, and B. C. Babu, “Improved grid synchronization algorithm for DG system using DSRF PLL under grid disturbances,” *IEEE Students Conf. on Engg. and Syst. (SCES ’12)*, pp. 1–6, Mar. 2012.

[103] P. Rodriguez, A. Luna, R. Muoz-Aguilar, I. Etxeberria-Otadui, R. Teodorescu, and F. Blaabjerg, “A stationary reference frame grid synchronization system for three-phase grid-connected power converters under adverse grid conditions,” *IEEE Trans. Power Electron.*, vol. 27, no. 1, pp. 99–112, Jan. 2012.

[104] S. Golestan, M. Monfared, F. Freijedo, and J. Guerrero, “Design and tuning of a modified power-based pll for single-phase grid-connected power conditioning systems,” *IEEE Trans. Power Electron.*, vol. 27, no. 8, pp. 3639–3650, Aug. 2012.

[105] M. P. D. Yazdani and A. Bakhshai, “Three-phase grid synchronization techniques for grid connected converters in distributed generation systems,” *IEEE Int. Symp. on Ind. Electron. (ISIE’09)*, pp. 1105–1110, July 2009.

[106] ——, “Single-phase grid-synchronization algorithms for converter interfaced distributed generation systems,” *IEEE Canadian Conf. on Electrical and Computer Engineering (CCECE’09)*, pp. 127–131, May 2009.

[107] E. Wood, M. Alexander, and T. H. Bradley, “Investigation of battery end-of-life conditions for plug-in hybrid electric vehicles,” *J Power Sources*, vol. 196, no. 11, pp. 5147–5154, Feb. 2011.

[108] H.-K. Tseng, J. S. Wu, and X. Liu, “Affordability of electric vehicles for a sustainable transport system: An economic and environmental analysis,” *Energy Policy*, vol. 61, no. 0, pp. 441–447, June 2013.

[109] V. Marano and G. Rizzoni, “Energy and economic evaluation of PHEVs and their interaction with renewable energy sources and the power grid,” *in Proc. IEEE Int. Conf. on Vehicular Electron. and Safety (ICVES’08)*, pp. 84–89, Sept. 2008.

[110] B. M. Al-Alawi and T. H. Bradley, “Total cost of ownership, payback, and consumer preference modeling of plug-in hybrid electric vehicles,” *Applied Energy*, vol. 103, no. 0, pp. 488–506, Nov. 2013.

[111] B. Dietz, K. Ahlert, A. Schuller, and C. Weinhardt, “Economic benchmark of charging strategies for battery electric vehicles,” *IEEE Trondheim Power Tech. 2011*, pp. 1–8, June 2011.

[112] M. Fasugba and P. Krein, “Cost benefits and vehicle-to-grid regulation services of unidirectional charging of electric vehicles,” *in Proc. IEEE Energy Conversion Congress and Expo. (ECCE’11)*, pp. 827–834, Sept. 2011.

[113] A. De Los Rios, J. Goentzel, K. E. Nordstrom, and C. Siegert, “Economic analysis of vehicle-to-grid (V2G)-enabled fleets participating in the regulation service market,” *in Proc. IEEE PES Innovative Smart Grid Technol. (ISGT’12)*, pp. 1–8, Jan. 2012.

[114] M. Granovskii, I. Dincer, and M. A. Rosen, "Economic and environmental comparison of conventional, hybrid, electric and hydrogen fuel cell vehicles," *J Power Sources*, vol. 159, no. 2, pp. 1186–1193, Jan. 2006.

[115] M. Peng, L. Liu, and C. Jiang, "A review on the economic dispatch and risk management of the large-scale plug-in electric vehicles (phevs)-penetrated power systems," *Renewable and Sustainable Energy Reviews*, vol. 16, no. 3, pp. 1508–1515, Jan. 2012.

[116] M. Yilmaz and P. Krein, "Review of the impact of vehicle-to-grid technologies on distribution systems and utility interfaces," *IEEE Trans. Power Electron.*, vol. 28, no. 12, pp. 5673–5689, Dec. 2013.

[117] E. Sortomme and M. El-Sharkawi, "Optimal combined bidding of Vehicle-to-Grid ancillary services," *IEEE Trans. on Smart Grid*, vol. 3, no. 1, pp. 70–79, Mar. 2012.

[118] V. Agarwal, K. Uthaichana, R. DeCarlo, and L. Tsoukalas, "Development and validation of a battery model useful for discharging and charging power control and lifetime estimation," *IEEE Trans. Energy Convers.*, vol. 25, no. 3, pp. 821–835, Sept. 2010.

[119] C. Alaoui, "Solid-state thermal management for lithium-ion EV batteries," *IEEE Trans. on Vehicular Tech.*, vol. 62, no. 1, pp. 98–107, Jan. 2013.

[120] M. Singh, P. Kumar, and I. Kar, "Implementation of vehicle to grid infrastructure using fuzzy logic controller," *IEEE Trans. on Smart Grid*, vol. 3, no. 1, pp. 565–577, Mar. 2012.

[121] J. Dogger, B. Roossien, and F. Nieuwenhout, "Characterization of li-ion batteries for intelligent management of distributed grid-connected storage," *IEEE Trans. Energy Convers.*, vol. 26, no. 1, pp. 256–263, Mar. 2011.

[122] P. Ramadass, B. Haran, R. White, and B. N. Popov, "Mathematical modeling of the capacity fade of li-ion cells," *J Power Sources*, vol. 123, pp. 230–240, Mar. 2003.

[123] R. Spotnitz, "Simulation of capacity fade in lithium-ion batteries," *J Power Sources*, vol. 113, pp. 72–80, Jan. 2003.

[124] C. M. Shepherd, "Design of primary and secondary cells - part 2. an equation describing battery discharge," *J Electroche. Soc.*, vol. 112, pp. 657–664, Jul. 1965.

[125] O. Tremblay, L.-A. Dessaint, and A.-I. Dekkiche, "A generic battery model for the dynamic simulation of hybrid electric vehicles," *IEEE Int. Vehicle Power and Propulsion Conf. (VPPC'07)*, pp. 284–289, Sept. 2007.

[126] L. Gao, S. Liu, and R. Dougal, "Dynamic lithium-ion battery model for system simulation," *IEEE Trans. on Comp. Packag. Technol.*, vol. 25, no. 3, pp. 495–505, Sept. 2002.

[127] G. Ning, B. Haran, and B. N. Popov, "Capacity fade study of lithium-ion batteries cycled at high discharge rates," *J Power Sources*, vol. 117, pp. 160–169, Dec. 2003.

[128] R. Rao, S. Vrudhula, and D. Rakhmatov, "Battery modeling for energy aware system design," *Computer*, vol. 36, no. 12, pp. 77–87, Dec. 2003.

[129] S. Tian, M. Hong, and M. Ouyang, "An experimental study and nonlinear modeling of discharge I-V behavior of valve-regulated lead-acid batteries," *IEEE Trans. Energy Convers.*, vol. 24, no. 2, pp. 452–458, Jun. 2009.

[130] G. Capizzi, F. Bonanno, and G. Tina, “Recurrent neural network-based modeling and simulation of lead-acid batteries charge-discharge,” *IEEE Trans. Energy Convers.*, vol. 26, no. 2, pp. 435–443, Jun. 2011.

[131] Y.-H. Liu, C.-H. Hsieh, and Y.-F. Luo, “Search for an optimal five-step charging pattern for li-ion batteries using consecutive orthogonal arrays,” *IEEE Trans. Energy Convers.*, vol. 26, no. 2, pp. 654–661, Jun. 2011.

[132] T. Kim and W. Qiao, “A hybrid battery model capable of capturing dynamic circuit characteristics and nonlinear capacity effects,” *IEEE Trans. Energy Convers.*, vol. 26, no. 4, pp. 1172–1180, Dec. 2011.

[133] M. Jongerden and B. Haverkort, “Which battery model to use?” *IET Software*, vol. 3, no. 6, pp. 445–457, Dec. 2009.

[134] H. Duval, “Computer model of the lead/acid starter battery in automobiles,” *J Power Sources*, vol. 53, no. 2, pp. 351–357, Feb. 1995.

[135] P. M. Gomadam, J. W. Weidner, R. A. Dougal, and R. E. White, “Mathematical modeling of lithium-ion and nickel battery systems,” *J Power Sources*, vol. 110, no. 2, pp. 267–284, Aug. 2002.

[136] Z. Salameh, M. Casacca, and W. A. Lynch, “A mathematical model for lead-acid batteries,” *IEEE Trans. Energy Convers.*, vol. 7, no. 1, pp. 93–98, Mar. 1992.

[137] M. Chen and G. Rincon-Mora, “Accurate electrical battery model capable of predicting runtime and I-V performance,” *IEEE Trans. on Energy Conv.*, vol. 21, no. 2, pp. 504–511, Jun. 2006.

[138] M. Durr, A. Cruden, S. Gair, and J. McDonald, “Dynamic model of a lead acid battery for use in a domestic fuel cell system,” *J Power Sources*, vol. 161, no. 2, pp. 1400–1411, Oct. 2006.

[139] H. Blanke, O. Bohlen, S. Buller, R. W. D. Doncker, B. Fricke, A. Hammouche, D. Linzen, M. Thele, and D. U. Sauer, “Impedance measurements on lead-acid batteries for state-of-charge, state-of-health and cranking capability prognosis in electric and hybrid electric vehicles,” *J Power Sources*, vol. 144, no. 2, pp. 418 – 425, Jun. 2005.

[140] F. Huet, “A review of impedance measurements for determination of the state-of-charge or state-of-health of secondary batteries,” *J Power Sources*, vol. 70, no. 1, pp. 59 – 69, Jan. 1998.

[141] E. Kuhn, C. Forgez, P. Lagonotte, and G. Friedrich, “Modelling Ni-mH battery using cauer and foster structures,” *J Power Sources*, vol. 158, no. 2, pp. 1490–1497, Aug. 2006.

[142] T. F. F. M. Doyle and J. Newman, “Modeling of galvanostatic charge and discharge of the lithium/polymer/insertion cell,” *J. Electrochem. Soc.*, vol. 140, no. 6, pp. 1526–1533, Jun. 1993.

[143] P. Mauracher and E. Karden, “Dynamic modelling of lead/acid batteries using impedance spectroscopy for parameter identification,” *Journal of Power Sources*, vol. 67, no. 1-2, pp. 69–84, Jul.-Aug. 1997.

[144] Y.-S. Lee, W.-Y. Wang, and T.-Y. Kuo, “Soft computing for battery state-of-charge (BSOC) estimation in battery string systems,” *IEEE Trans. on Ind. Elect.*, vol. 55, no. 1, pp. 229–239, Jan. 2008.

[145] I.-H. Li, W.-Y. Wang, S.-F. Su, and Y.-S. Lee, “A merged fuzzy neural network and its applications in battery state-of-charge estimation,” *IEEE Trans. Energy Convers.*, vol. 22, no. 3, pp. 697–708, Sept. 2007.

[146] M. Einhorn, F. Conte, C. Kral, and J. Fleig, “Comparison, selection, and parameterization of electrical battery models for automotive applications,” *IEEE Trans. Power Electron.*, Mar. 2013.

[147] K. Deb, "Optimization for engineering design: Algorithms and examples," *Prentice Hall, India*, 1998.

[148] R. Escarela-Perez, T. Niewierowicz, and E. Campero-Littlewood, "Synchronous machine parameters from frequency-response finite-element simulations and genetic algorithms," *IEEE Trans. Energy Convers.*, Jun. 2001.

[149] P. Ramadass, B. Haran, R. White, and B. N. Popov, "Capacity fade of sony 18650 cells cycled at elevated temperatures Part I. cycling performance," *J Power Sources*, vol. 112, pp. 606–613, Aug. 2002.

[150] B. Y. Liaw, R. G. Jungst, G. Nagasubramanian, H. L. Case, and D. H. Doughty, "Modeling capacity fade in lithiumion cells," *J Power Sources*, vol. 140, pp. 157–161, Aug. 2005.

[151] P. Ramadass, B. Haran, R. White, and B. N. Popov, "Capacity fade of sony 18650 cells cycled at elevated temperatures Part II. capacity fade analysis," *J Power Sources*, vol. 112, pp. 614–620, Aug. 2002.

[152] SONY-US18650, "Lithium Ion Rechargeable Batteries - Technical Handbook," http://www.sony.com.cn/products/ed/battery/download.pdf.

[153] PANASONIC, "Lithium Ion Batteries - Individual Data Sheet," http://www.batteryspace.com/prod-specs/4666.pdf.

[154] SANYO, "Battery specification," http://www.manualslib.com/manual/148360/Sanyo-Ur18500f.html and http://www.sanyoindia.com/index.aspx.

[155] M. Chen and G. Rincon-Mora, "Dynamic lithium-ion battery model for system simulation," *IEEE Trans. on Energy Conver.*, vol. 21, no. 2, p. 504511, Jun. 2006.

[156] P. Kumar, "A framework for multi-objective optimization and multi-criteria decision making for design of electrical drives," *Ph.D Thesis*, pp. 47–99, Oct. 2008.

[157] L. Zhang, H. Chang, and R. Xu, "Equal-width partitioning roulette wheel selection in genetic algorithm," *in Proc. Conf. on Tech. and Appl. of Artificial Intelligence (TAAI'12)*, pp. 62–67, Nov. 2012.

[158] D. J. Thrimawithana, U. K. Madawala, M. Neath, and T. Geyer, "A sense winding based synchronization technique for bi-directional IPT pick-ups," *in Proc. IEEE Energy Convers. Congress and Exposition (ECCE'11)*, pp. 1405–1410, Sept. 2011.

[159] R. M. Miskiewicz, A. J. Moradewicz, and M. P. Kazmierkowski, "Contactless battery charger with bi-directional energy transfer for plug-in vehicles with vehicle-to-grid capability," *in Proc. IEEE Int. Symp. on Ind. Electron. (ISIE'11)*, pp. 1969–1973, Jun. 2011.

[160] A. Masoum, S. Deilami, P. Moses, M. Masoum, and A. Abu-Siada, "Smart load management of plug-in electric vehicles in distribution and residential networks with charging stations for peak shaving and loss minimisation considering voltage regulation," *IET Gener. Transm. and Distrib.*, vol. 5, no. 8, pp. 877–888, Aug. 2011.

[161] P. Stroehle, S. Becher, S. Lamparter, A. Schuller, and C. Weinhardt, "The impact of charging strategies for electric vehicles on power distribution networks," *in Proc.* 8^{th} *Int. Conf. on European Energy Market (EEM'11)*, pp. 51–56, May 2011.

[162] C. Camus and T. Farias, "Impacts of electric vehicles' charging strategies in the electricity prices," *in Proc.* 8^{th} *Int. Conf. on Energy Market (EEM'11)*, pp. 833–838, May 2011.

[163] P. Rodriguez, A. Luna, I. Candela, R. Mujal, R. Teodorescu, and F. Blaabjerg, "Multiresonant frequency-locked loop for grid synchronization of power converters under distorted grid conditions," *IEEE Trans. Ind. Electron.*, vol. 58, no. 1, pp. 127–138, Jan. 2011.

[164] K. Ahmed, S. Finney, and B. Williams, "Passive filter design for three-phase inverter interfacing in distributed generation," *in Proc. Compatibility in Power Electronics (CPE '07)*, pp. 1–9, June 2007.

[165] B. K. Bose, "Modern power electronics and AC drives," *Prentice Hall PTR*, 2002.

[166] C.-S. Wang, G. Covic, and O. Stielau, "General stability criterions for zero phase angle controlled loosely coupled inductive power transfer systems," *IEEE* 27^{th} *Annual Conf. on Ind. Electron. Society (IECON'01)*, vol. 2, pp. 1049–1054, Dec. 2001.

[167] H. L. Li, A. Hu, and G. A. Covic, "Development of a discrete energy injection inverter for contactless power transfer," *in Proc.* 3^{rd} *IEEE Conf. on Ind. Electron. and Appl. (ICIEA'08)*, pp. 1757–1761, Jun. 2008.

[168] B. Bouneb, D. M. Grant, A. Cruden, and J. R. McDonald, "Grid connected inverter suitable for economic residential fuel cell operation," *European Conf. on Power Electron. and Appl. (ECPEA'05)*, Sept. 2005.

[169] S. C. Rho, S. H. kim, Y. H. Ahn, and B. Kim, "A study on power transmission system using resonant frequency tracking method and contactless transformer with multiple primary winding," *in Proc. Int. Conf. on Electrical Machines and Syst. (ICEMS'07)*, pp. 1635–1639, Oct. 2007.

[170] T. M. Blooming and D. J. Carnovale, "Application of IEEE STD 519-1992 harmonic limits," *Pulp and Paper Ind. Tech. Conf.*, pp. 1–9, June 2006.

[171] Rony Argueta, "The Electric Vehicle," http://www.writing.ucsb.edu/faculty/holms/Writing_2E-_EV_Technical_Research_Report.pdf.

[172] N. Bhat, "Advantages and Disadvantages," http://library.thinkquest.org/C008050/ecars4.html.

[173] G. Stoeckl, R. Witzmann, and J. Eckstein, "Analyzing the capacity of low voltage grids for electric vehicles," *IEEE Electrical Power and Energy Conf. (EPEC'11)*, vol. 3, no. 1, pp. 415–420, Oct. 2011.

[174] U. Reiner, C. Elsinger, and T. Leibfried, "Distributed self organising electric vehicle charge controller system: Peak power demand and grid load reduction with adaptive ev charging stations," *IEEE Int. Electric Vehicle Conf. (IEVC'12)*, vol. 3, no. 1, pp. 1–6, March 2012.

[175] J. A. P. Lopes, "Demystifying the smart grid boston," *Electric vehicle grid integration*, Nov. 2009.

[176] S. I. Inage, "Modelling load shifting using electric vehicles in a smart grid environment," https://www.iea.org/publications/freepublications/publication/load_shifting.pdf,.

[177] G. Ning, B. Haran, and B. N. Popov, "Capacity fade study of lithium-ion batteries cycled at high discharge rates," *J. Power Sources*, vol. 117, pp. 160–169, Dec. 2003.

[178] P. Ramadass, B. Haran, R. White, and B. N. Popov, "Mathematical modeling of the capacity fade of li-ion cells," *J. Power Sources*, vol. 123, pp. 230–240, March 2003.

[179] T. Ali, A. Awami, and E. Sortomme, "Coordinating vehicle-to-grid services with energy trading," *IEEE Trans. Smart Grid*, vol. 3, no. 1, pp. 453–462, Mar. 2012.

[180] P. Ramadass, B. Haran, R. White, and B. N. Popov, "Capacity fade of sony 18650 cells cycled at elevated temperatures Part I. cycling performance," *J. Power Sources*, vol. 112, pp. 606–613, Aug. 2002.

[181] A. T. Stamps, C. E. Holland, R. E. White, and E. P. Gatzke, "Analysis of capacity fade in a lithium ion battery," *J. of Power Sources*, vol. 150, pp. 229–239, Oct. 2005.

[182] S. Shao, M. Pipattanasomporn, and S. Rahman, "Grid integration of electric vehicles and demand response with customer choice," *IEEE Trans. Smart Grid*, vol. 3, no. 1, pp. 543–550, Mar. 2012.

[183] T. Morgan, "Smart Grids and Electric Vehicles: Made for Each Other," http://www.internationaltransportforum.org/jtrc/DiscussionPapers/DP201202.pdf.

[184] S. Han and S. Han, "Economics of V2G frequency regulation in consideration of the battery wear," 3^{rd} *IEEE PES Int. Conf. and Exhibition on Innovative Smart Grid Technologies (ISGT'12)*, pp. 1–8, Oct. 2012.

[185] D. Trowler and B. Whitaker, "Bi-directional inverter and energy storage system," *Texas Instruments Analog Design Contest*, May 2008.

[186] Indian Express, "Different power rates for peak and off-peak hours," http://www.indianexpress.com/news/soon-different-power-rates-for-peak-offpeak-hours/917100.

[187] M. Singh, P. Kumar, and I. Kar, "Designing a multi charging station for electric vehicles and its utilization for the grid support," *IEEE Power and Energy Society General Meeting (PESGM'12)*, pp. 1–8, Jul. 2012.

[188] Nlukin, "Battery losses," http://www.teslamotors.com/forum/forums/battery-charging-and-discharging-losses.

[189] W. Luo, C. Lv, L. Wang, and C. Liu, "Study on impedance model of Li-ion battery," *in Proc.* 6^{th} *IEEE Conf. on Ind. Electron. and Applications (ICIEA'11)*, pp. 1943–1947, June 2011.

[190] U. Department Of Energy, "Electric Vehicles: Compare Side-by-Side," http://www.fueleconomy.gov/feg/evsbs.shtml.

[191] Battery University, "Electric Vehicle," http://www.batteryuniversity.com/learn/article/electric_vehicle.

[192] B. Berman, "The Hybrid Car Battery: A Definitive Guide," http://www.hybridcars.com/hybrid-car-battery.

[193] Center for Transportation Research Argonne National Laboratory, "Costs of Lithium-Ion Batteries for Vehicles," http://www.transportation.anl.gov/pdfs/TA/149.pdf/.

[194] Simanaitis, "EV Glossary," http://simanaitissays.com/2012/12/04/ev-glossary/.

[195] H.-H. Chung, W. C. Chow, S. Hui, and S. Lee, "Development of a switched-capacitor DC-DC converter with bidirectional power flow," *IEEE Trans. Circuits and Systems I: Fundamental Theory and Applications*, vol. 47, no. 9, pp. 1383–1389, Sept. 2000.

[196] Y. Du, S. Lukic, B. Jacobson, and A. Huang, "Review of high power isolated bi-directional DC-DC converters for phev/ev dc charging infrastructure," *IEEE Energy Conver. Congress and Expo. (ECCE'11)*, pp. 553–560, Sept. 2011.

[197] N. Wong and M. Kazerani, "A review of bidirectional on-board charger topologies for plugin vehicles," 25^{th} *IEEE Canadian Conf. on Electrical Computer Engg. (CCECE'12)*, pp. 1–6, 2012.

[198] D. Gunasekaran and L. Umanand, "Integrated magnetics based multi-port bidirectional DC-DC converter topology for discontinuous-mode operation," *IET Power Electron.*, vol. 5, no. 7, pp. 935–944, Aug. 2012.

[199] D. Xu, C. Zhao, and H. Fan, "A pwm plus phase-shift control bidirectional DC-DC converter," *IEEE Trans. Power Electron.*, vol. 19, no. 3, pp. 666–675, may 2004.

[200] M. H. Rashied, "Power electronics: Circuit, devices and applications," *Third Edition, Dorling Kindersley (India) pvt. Ltd.,*, 2009.

[201] I. S. 519-1992, "Recommended practices and requirements for harmonic control in electric power systems," 1992.

List of Publications

Journal Publications

1. **Kannan Thirugnanam**, Ezhil Reena Joy T.P, Mukesh Singh, "**Mathematical Modeling of Li-Ion Battery using Genetic Algorithm Approach for V2G Applications**," *IEEE Trans. on Energy Convers.*, vol. 29, Issue. 2, pp. 332 - 343, June 2014.

2. **Kannan Thirugnanam**, Ezhil Reena Joy .T. P, Mukesh Singh and Praveen Kumar, "**Modeling and Control of Contactless based Smart Charging Station in V2G Scenario**," *IEEE Trans. on Smart Grid*, vol. 5, No. 1, pp. 377-348, Jan. 2014.

3. Rajib Das, **Kannan Thirugnanam**, Praveen Kumar, Rajender Lavudiya and Mukesh Singh, "**Mathematical Modeling For Economic Evaluation Of Electric Vehicle To Smart Grid Interaction**," *IEEE Trans. on Smart Grid,* Vol. 5, Issue. 2, pp. 712-721, Feb. 2014.

4. Mukesh Singh, **Kannan Thirugnanam**, Praveen Kumar, and Indrani Kar, "**Real Time coordination of Electric Vehicles to Support the Grid at the Distribution Substation Level**," *IEEE Systems Journal*, vol. PP, No. 99, pp. 1-12, Sept. 2013.

Submitted:

1. Ezhil Reena Joy T.P, **Kannan Thirugnanam**, Mukesh Singh and Praveen Kumar, "**Impact of Electric Vehicle Charging Station on Industrial Load Area Network**," Manuscript has been submitted in IEEE Transaction on Energy Conversion.

Conference Publications

National:

1. **Kannan Thirugnanam**, Mohammed Nasir Ansari and Praveen Kumar, "**Selection and Requirements of Hybrid Electric Drivetrain Based on Energy Storage Devices**," National Round Table Meet on Hybrid Renewable Energy Sources for public transportation systems, IIT Guwahati, Oct. 2010.

International:

1. **Kannan Thirugnanam**, Himanshu Saini and Praveen Kumar, "**Mathematical Modeling of Li-Ion Battery for Charge/Discharge rate and Capacity fading Characteristics using Genetic Algorithm Approach**," *IEEE Transportation Electrification Conf. and Expo (ITEC'12)*, pp. 1-6, Jun., 2012.

2. **Kannan Thirugnanam**, Ezhil Reena Joy T.P, and Praveen Kumar, "**A Novel Fuzzy based Phase Angle Estimation Scheme for Grid Connected Bidirectional Contactless Power Transfer System suitable for EVs and PHEVs**," *IEEE Int. Conf. on Adv. Research in Engg. and Tech. (ICARET'13)*, Jan., 2013.

3. **Kannan Thirugnanam**, Ezhil Reena Joy T.P, and Praveen Kumar, "**A Fuzzy Based Frequency Control Technology for Bidirectional Contactless Charging System**," *IEEE Int. Conf. on Adv. Research in Engg. and Tech. (ICARET'13)*, Jan., 2013.

4. Kannan Thirugnanam, Swati Shukla, Mukesh Singh and Praveen Kumar, "**Synchronization of Grid Connected Vehicle-to-Grid System with Bidirectional Contactless Charging**," *IEEE PES Innovative Smart Grid Technologies Conference (ISGT'13)*, pp. 1-6, Nov. 2013.

5. Ezhil Reena Joy T.P, **Kannan Thirugnanam** and Praveen Kumar, "**A New Concept for Bidirectional Inductively Coupled Battery Charging System based on Direct AC-AC Converter for HEV's and EV's using Fuzzy Logic Approach**," *IEEE Transportation Electrification Conf. and Expo (ITEC'12)*, pp. 1-6, Jun., 2012.

6. Ezhil Reena Joy T.P, **Kannan Thirugnanam** and Praveen Kumar, "**Bidirectional Contactless Charging System using Li-Ion Battery Model**," 7^{th} *Int. Conf. on Ind. and Information Sys. (ICIIS'12)*, Aug., 2012.

7. Ezhil Reena Joy .T .P, **Kannan Thirugnanam** and Praveen Kumar, "**A Multi-Point Bidirectional Contactless Charging System in a Charging Station Suitable for EVs and PHEVs Applications**," Presented in INDICON 2013, Dec. 2013.

8. Ezhil Reena Joy T.P, **Kannan Thirugnanam** and Praveen Kumar, "**Novel Reduced Switch Count Bidirectional Contactless Charging System for EVs and PHEVs Applications**," *IEEE Students Conf. on Engg. and Syst. (SCES'13)*, pp. 1-6, Apr., 2013.

9. Himanshu Saini, **Kannan Thirugnanam** and Praveen Kumar, "**Mathematical Modeling for Economic Evaluation of Electric Vehicle to Smart Grid Interaction**," *IEEE Int. Conf. on Adv. Research in Engg. and Tech. (ICARET'13)*, Jan., 2013.

10. Mohammed Nasir Ansari, **Kannan Thirugnanam**, Ezhil Reena Joy .T .P and Praveen Kumar, "**Power-train Selection for Electric City Bus Based on the Multi-criteria Decision Making**," *IEEE* 14th *Int. Power Elect. and Motion Control Conf. (EPE/PEMC'10)*, pp. T6-140 - T6-148, Sept., 2010.

11. Mukesh Singh, **Kannan Thirugnanam**, S. Swami, Praveen Kumar and Indrani Kar, "**Coordination of Electric Vehicles in Charging Stations Connected at Different Nodes of a Distribution Substation**," *Annual IEEE India Conf. (INDICON'12)*, pp.1260-1265, Dec., 2012.

12. Venkata Ramana Kasi, **Kannan Thirugnanam**, Praveen Kumar and Somanath Majhi, "**Node Identification for Placing EVs and PAs in a Distribution Network**," *Manuscript has been accepted in IEEE Power & Energy Society General Meeting 2014 (IEEE PES GM'14).*

Bio-Data

1	Name:	Kannan T.
2	Date of Birth:	1 June 1983
3	Educational Qualifications:	April - 2005 (B.E.), June - 2009 (M.E.), June - 2014 (Ph.D.),
4	Permanent Address:	S/O A. Thirugnanam, 63, Thottakkadu, Kamaraj Nagar, Ramapuram - Post, Thanjavur (District), Tamil Nadu, India, Pin code - 613 003.
5	Contact Address:	Room No B-121, Barak Hostel, Indian Institute of Technology Guwahati, Guwahati - 781 039, Assam, India.
6	Contact Number	0(+91)-4362-250456